UNIVERSIDAD DE CANTABRIA
&
PAVOL JOZEF ŠAFÁRIK UNIVERSITY

PROGRAMA DE DOCTORADO EN Ciencia y Tecnología

TESIS DOCTORAL

Estudio experimental sobre el comportamiento del estado fundamental en el sistema $RENi_5$ (RE = Ce, Yb, Gd)

PHD THESIS

Experimental study of emergent ground state behaviour in $RENi_5$ (RE = Ce, Yb, Gd) system

Andrea DŽUBINSKÁ

Directores:
Marián Reiffers
Jesús Rodríguez Fernandéz

Escuela de Doctorado de la Universidad de Cantabria

Santander 2020

PAVOL JOZEF ŠAFÁRIK UNIVERSITY IN KOŠICE

&

UNIVERSITY OF CANTABRIA

EXPERIMENTAL STUDY OF EMERGENT GROUND STATE BEHAVIOUR IN $RENi_5$ (RE = Ce, Yb, Gd) SYSTEM

DISSERTATION THESIS

Ing. RNDr. Andrea DŽUBINSKÁ **2020**

PAVOL JOZEF ŠAFÁRIK UNIVERSITY IN KOŠICE

FACULTY OF SCIENCE

&

UNIVERSIDAD DE CANTABRIA

FACULTAD DE CIENCIAS

DISSERTATION THESIS

Presented to obtain

THE DEGREE OF DOCTOR OF PHILOSOPHY

at the

UNIVERSITY OF PAVOL JOZEF ŠAFÁRIK IN KOŠICE

and at the

UNIVERSITY OF CANTABRIA

by

ANDREA DŽUBINSKÁ

Subject:

EXPERIMENTAL STUDY OF EMERGENT GROUND STATE BEHAVIOUR IN $RENi_5$ (RE = Ce, Yb, Gd) SYSTEM

Univerzita P. J. Šafárika v Košiciach
Prírodovedecká fakulta

36100138881611268

ZADANIE ZÁVEREČNEJ PRÁCE

Meno a priezvisko študenta:	Ing. RNDr. Andrea Džubinská
Študijný program:	Progresívne materiály (Jednoodborové štúdium, doktorandské III. st., denná forma)
Študijný odbor:	Fyzika
Typ záverečnej práce:	Dizertačná práca
Jazyk záverečnej práce:	anglický
Sekundárny jazyk:	slovenský

Názov: Experimental study of emergent ground state behaviour in RENi5 (RE = Ce, Yb, Gd) system

Názov SK: Experimentálne štúdium neobvyklého chovania základného stavu v systéme na báze RENi5 (RE = Ce, Yb, Gd)

Cieľ: The main aim of thesis is the experimental study of emergent behaviour of ground state yielding to possible quantum criticality of system on a base of RENi5 (RE = Ce, Yb, Gd). Next important parameter influencing the behaviour of the system is the study of influence of sample quality of crystals (polycrystalline samples), structure and dimension (microcrystalline samples) on the ground state.
CeNi5 is well known as Stoner enhanced paramagnet, which is characterized by the existence of spin fluctuations SF in paramagnetic state. Spin fluctuations origin from Ni-atoms. Except that the mixed valence with different intensity was observed in dependence of the experimental technique.
On the other hand GdNi5 is known as a ferromagnetic compound with crystalline electric field (CEF) influence on its properties. Therefore, we want to study the influence of Gd on the appearance or disappearance of magnetism in Gd1-xCexNi5 system and its influence on the ground state.
Moreover, it is known that Ce and Yb presence in systems could produce very interesting behaviour like quantum criticality.
Therefore, the basic aims are the preparation and structural characterisation of polycrystalline samples on the base of (RE11-xRE2x)Ni5 (RE1, RE2 = Ce, Yb, Gd) system. Next aim is the study of the chemical pressure influence on the physical properties of systems on the YbNi5 base in order to correct the quantum critical point position.
All these results will give us new knowledge of the ground state behaviour of this system.

Literatúra:
1. B. Barbara, D. Gignoux, C. Vettier: Lectures on modern magnetism. (Springer-Verlag Berlin Heildelerg 1988) ISBN 3-540-17558-X.
2. V.M.T.S. Barthem, D. Gignoux, A. Nait-Saada, D. Schmitt, G. Creuzet, Phys. Rev. B37, 1733 (1988).
3. Yu.G.Naidyuk, M. Reiffers, A.G.M. Jansen, I.K. Yanson, P. Wyder, D. Gignoux, D. Schmitt, Int. J. Mod. Phys.B7, 222 (1993).
4. B.L. Nordstrom, M.S.S. Brooks, B. Johansson, Phys.Rev. B 46, 3458 (1992).

Kľúčové slová: spin fluctuations, thermal properties, magnetic properties, transport properties, quantum criticality

Univerzita P. J. Šafárika v Košiciach
Prírodovedecká fakulta

Školiteľ:	prof. RNDr. Marian Reiffers, DrSc.
Školiteľ:	prof. Jesús Maria Rodríguez Fernandez
Konzultant:	prof. RNDr. Rastislav Varga, DrSc.
Oponent:	prof. RNDr. Peter Bury, CSc.
Oponent:	Dr. Noelia Marcano Agudo, PhD.
Ústav :	ÚFV - Ústav fyzikálnych vied
Riaditeľ ústavu:	prof. RNDr. Peter Kollár, DrSc.

Dátum schválenia: 01.09.2016

ACKNOWLEDGEMENT

This thesis was created in cooperation between Pavol Jozef Šafárik Univerisity in Košice, Slovakia and University in Cantabria, Santander, Spain within the frame of cotutelle agreement. During my doctoral study, I have spent one academic year at the University of Cantabria. The rest of my PhD. study I have spent at the Pavol Jozef Šafárik Univerisity.

I express my thanks to my Slovak supervisor prof. Marián Reiffers and my Spanish supervisor prof. Jesús Rodríguez Fernandéz, whose giving me guidance and necessary advice during PhD. study in the field of investigation and also with administrative work.

My special thanks belong to prof. Rastislav Varga for his care, support and consultation. I would like to thank Dr. José Ignacio Espeso for his help. I cannot forget to say my deep thanks to prof. Mauro Giovannini and prof. Julian Sereni for their quick and constructive answers to my questions.

I want to thank special people for me dña. Mercedes H., Arun K., Andrea K., Alena G., Alena K., Daniel C., Katarína Š. and F&E, they were the right people in the right place.

My gratitude belongs to my colleagues from CPM TIP UPJŠ and my colleagues from DCITIMAC UNICAN, for their support, help and daily small things, which make agreeable hard scientific work.

I would like to thank my family and friends because without their support this work cannot be accomplished.

In the end, I thank to following grants and agencies for financial support:
University Science Park TECHNICOM for Innovation Applications Supported by Knowledge Technology, ITMS: 26220220182; VEGA 1/0164/16; VEGA 1/0611/18; VEGA 1/0053/19; VVGS-PF-2018-798; APVV-16-0079; the Spanish MINECO MAT2017-83631-C3-R and the grant from Slovak Academic Information Agency (SAIA) under National Scholarship program.

… and thank to everyone who have contributed to this work…

DECLARATION

I declare that this PhD. dissertation thesis entitled **"Experimental study of emergent ground state behaviour in $RENi_5$ (RE = Ce, Yb, Gd)"** is my own work under guidance of my supervisors' prof RNDr. Marián Reiffers, DrSc. and prof. Jesús Rodríguez Fernandéz, PhD. The results reported here are the accomplishment obtained during my PhD.

Košice 23th June 2020 .....

TABLE OF CONTENTS

List of Figures

gains within the ordered phase S_{MO} and the temperature of the dome T_D. Continuous green curve is a guide to the eyes for the $T_{cr}(B) = 0$ T and the ellipse represents an extrapolated point at $B = 1$ T. The dash-dot line at $T = 65$ mK indicates the thermal experimental limit. Continuous red line in $S_{MO}(B)$ covers the second-order-type transitions while the dashed segment extrapolates to the first-order one. On the right axis, the temperature of the maximum of $C_m/T(T_{max})$ is shown. The extrapolation of $T_{max}(B)$ to $B < 1$ T (dashed-dot blue line) is compared with the $T_D(B)$ using the left axis scale as indicated by the left pointing blue arrow [158].....147

List of Tables

Introduction

The study of intermetallic compounds has a long history. These alloys and compounds consist of billions of microscopic elementary particles: electrons, neutrons, protons, quantized lattice vibrations known as phonons, and many others. The physical properties of macroscopic intermetallic compounds cannot be explained completely only by simple extrapolation of the behavior of mentioned individual elementary particles even on the basis of statistical physics. Interesting and new properties emerge from a quantum arrangement of particles. This is what attracts scientists to explore condensed matter physics, which is the most active field related to strongly correlated electron systems (SCES).

In the early years of the 20th century, the study of physical properties in the low temperature range has started to develop. It is related to the emergent behaviour of matter due to the laws of quantum mechanics.

When the temperature approaches zero kelvin, the highly correlated state of electron system arises. This is usually caused by the enhanced electronic density of electron levels close to the Fermi energy in metals, especially in sharp 4*f* electronic states in rare earth elements. The emerging field of study is arising due to undergoing quantum phase transitions. A fascinating variety of temperature values and magnetic field properties can be observed in the vicinity of quantum phase transition. Therefore, a new physics has appeared. This is one of the reasons, why we decided to study such a system in condensed matter physics.

The mentioned phenomena, which can arise at the level of quantum mechanics effects, leads our group to study the selected intermetallic systems. These materials belong to a group of advanced materials and potential magnetics actuators.

This work deals with rare earth materials such as cerium, gadolinium and ytterbium. In all prepared samples attractive physical properties could be found by using different scientific method. Moreover, these rare earth materials may become a possible basis for future applications.

Thesis consists of five chapters including several subchapters. Theoretical part describes main theory, effects and interactions, which are important for our studied systems. The second chapter offers a description of motivation, why the chosen systems were prepared and analysed. The third chapter explains the main aims of the thesis. Next

chapter deals with the experimental techniques and procedures, which are used for sample preparations and measurements of their physical properties. The last part is the experimental part, which is focused on explanation of collected data and their interpretation in agreement with current knowledge of condensed matter physics.

My personal contribution is following: I have prepared all samples except for $YbPd_2In$ and I carried out all the measurements of physical properties except the very low temperatures measurement in TRITON. I performed data processing. I participated on discussion of results interpretations and writing of manuscripts, which have already been published or manuscripts are under preparation.

The results of this work have been presented on several international conferences and some papers related to it have already been published under the sponsorship of scientific projects from different grant agencies. The list of presentations and publications is summarized at the end of thesis.

1 THEORETICAL CONCEPTS

The study of theoretical concepts has a very important role in every experimental work. Knowledge of the theory leads to successful execution of the experiment. When we study the ground state properties we can possibly observe very interesting physical properties based on quantum mechanics, which are very often difficult to be described and understood. For example, we can mention a situation in the systems based on lanthanides and actinides. Because of the special properties of cerium (Ce) and ytterbium (Yb) and strongly correlated electron systems, new emergent anomalous behaviour such as e.g. heavy fermion behaviour [1], superconductivity [2] or quantum criticality e.g. [3, 4] has been observed. In order to understand the physics beyond effects, it was necessary to develop new theoretical concepts. Therefore, to describe and to explain them we have to start with a concept using Fermi liquid theory.

1.1 The Fermi Liquid Theory

Fermi liquid theory, represents the easiest way of understanding a Fermion - collection ”box” with their mutual interactions taken into consideration. Defining this theory stands at the understanding of the new experimentally observed emergent behaviour of condensed matter. This theory covers the gaseous phase of the quantum fermion system. We have to consider that one mole of a metal has at least 10^{23} electrons. In order to describe their behaviour, it is impossible to calculate the wave functions of each particle following the theory. Therefore, one attempt was to handle the electrons in a statistical manner. First step was the Drude’s theory [5], which treated the electrons as a gas of non-interacting classical particles. One example of successful outputs based on this theory was Boltzmann transport equation used for explanation of electrical transport [6]. Next step was the application of quantum mechanical framework into it. It was done by Sommerfeld under assumption that electrons are fermions and they obey the Fermi-Dirac statistics [7]. This model describes a well-defined Fermi surface, a linear dependence of specific heat on temperature T and a temperature independent magnetic susceptibility. All mentioned dependences have been experimentally verified.

Later, the experimentally observed deviations from behaviour proposed by the Fermi gas model have been reported. This was the situation when strong interactions between electrons and other particles occurred. The first system with such a behaviour was liquid ^{3}He. In order to understand its behaviour, it was necessary to suppose the existence of interactions between ^{3}He and its neighbouring particles. Basic concept says that ground state is formed as a Fermi gas, while temperature is increasing; the interactions between electrons are gradually turning on. Landau introduced the term quasi-particles. They are elementary excitations of the Fermi liquid which have a one-to-one correspondence to the excitations of the Fermi gas, although now with a finite lifetime [7]. In this case, quasiparticles represent a renormalized version of their non-interacting counter parts. This renormalization yields to the different mass as for "free" particle mass. It is called effective mass m^*. The renormalization is described by Landau parameters (F_l^a and F_l^s) [8], which explain the observed mass enhancement:

$$m^* = m\left(1 + \frac{F_l^s}{3}\right), \tag{1}$$

where m^* is the effective mass of the quasiparticle and m is the free electron mass. Landau parameters are the spin- asymmetric (F_l^a) and spin-symmetric (F_l^s) terms of expansion (l = 0, 1, …). They are responsible for enhanced effective mass of conduction electrons.

Therefore, the standard description of metals physical properties at low temperatures relies on the Fermi-liquid (FL) theory of Landau based on the quasi-particle concept [7]. The main predictions of the FL theory are that well below a characteristic temperature, T_F, the resistance should exhibit quadratic temperature dependence, the heat capacity should show a linear temperature dependence and the magnetic susceptibility should be temperature independent. This concept can be applied to a number of different systems ranging from ^{3}He to simple metals like copper or gold to even more complicated compounds like $CeCu_6$ [9] where the Coulombic interactions in strongly localized f-electron shells results to an enormous interaction effects and a gigantic increase of the effective electron mass [10]. Landau FL theory thus predicts the low temperature properties of the Fermi liquid to obey the same laws as the Fermi gas with a renormalized effective mass m^*. In the limit of $T = 0$ K, the density of states (DOS) at the Fermi level is given by formula 2, where k_F represents the Fermi wavevector and $\hbar$ is the Planck constant:

$$N(E_F) = \left(\frac{m^* k_F}{\pi^2\,\hbar^2}\right), \tag{2}$$

where

$$E_F = \left(\frac{p_F^2}{2m}\right), \tag{3}$$

is the maximum energy of the lowest state of free electrons which is in accordance with Pauli's rule. The ground state contains the filled Fermi sea of occupied states in momentum space with a sharp limit at the level of Fermi energy.

The p_F is the momentum of the electron expressed by:

$$p_F = \hbar k_F = \hbar\left(3\pi \frac{N(E_F)}{V}\right)^{\frac{1}{3}}, \tag{4}$$

where $N(E_F)$ stands for the number of electrons on Fermi surface and V is the volume of Fermi surface in reciprocal space. The supply of energy (increasing temperature T) will create the low energy excited states from just below Fermi surface and their movement to states above Fermi surface. This process of electron-hole excitation causes an increase of DOS. Then the heat capacity of the electrons is given:

$$c_{electron} = {}^1\!/_3\,\pi^2 N(E_F) k_B^2 T = \gamma T. \tag{5}$$

Here k_B is Boltzmann constant and γ is the Sommerfeld coefficient. One could see immediately that there is a linear dependence of heat capacity on T and a dependence of γ on effective mass of electron.

Magnetic susceptibility $\chi(T)$ for Fermi liquid is temperature independent and it is enhanced over Fermi gas by a factor of $1/(1 + F_0^a)$, where μ_B is the Bohr magneton:

$$\chi(T) = \frac{\mu_0 \mu_B m^* k_F}{\pi^2 \hbar^2}\left(\frac{1}{1 + F_0^{\alpha}}\right), \tag{6}$$

Main difference between a Fermi gas and a Fermi liquid model is the existence of a new term AT^2 in the temperature dependence of electrical resistivity, which arises from the electron-electron scattering. Then:

$$\rho(T) = \rho_0 A T^2, \tag{7}$$

where ρ_0 is the residual resistivity due to the scattering on static defects and A is a constant [11].

These predictions for systems without broken symmetries have been borned out in many metals and heavy fermion systems (systems with very high effective mass of electrons) and seemed ubiquitous until the previous decades of the last century.

1.2 Mechanisms Affecting Electrons in Intermetallic Compounds

The study of scattering mechanisms in rare earth alloys and compounds is the most important for knowing their ground state. In this introductory part, we will describe the mechanisms which have a certain influence in studied intermetallic systems on the quantum level.

1.2.1 The Crystalline Electric Field Effect

The first type of mechanism is important because it refers to the influence of neighbouring atoms on the electron wave functions and therefore it depends also on the lattice symmetry. Knowing the parameters of the crystalline electric field (CEF) is very important for many reasons. The theory of CEF was formulated by Hans Bethe in 1929 [12]. He pointed out that the eigen values of Hamiltonian's characteristics of unoccupied electron levels of crystal atom can be qualified in terms of irreducible representations of the group given by its position. Later, this theory was modified considering the levels of unfilled 4*f* shells. This theory was improved by Stevens [13], Elliott [14] and Judd [15]. Experiments supporting these claims were done by the group of Hellweg, Blaney, and Dieke [16].

From the physics point of view, the CEF play a very important role in studying the rare earths physical properties, because it has a huge influence on magnetic properties (e.g. susceptibility anisotropy), heat capacity, magnetization processes, complex magnetic phase diagrams, singlet ground state effects or influence of CEF levels splitting, which are observed in many studied rare-earth systems. It is also necessary to know quantitatively the CEF parameters, because they represent a force, which together with a bilinear exchange coupling affects the rare-earth ions. The CEF effect is indispensable to define other contributions, namely the quadrupole interaction or magnetoelastic coupling. Their intensities are at least one order of magnitude smaller than the intensity of CEF. The comparison of CEF parameters with the theoretically determined values is very good for testing the ability of the applied model. In the Figure 1.1, a comparison of CEF and spin orbit coupling energies for 3*d* and 4*f* ions is plotted [17].

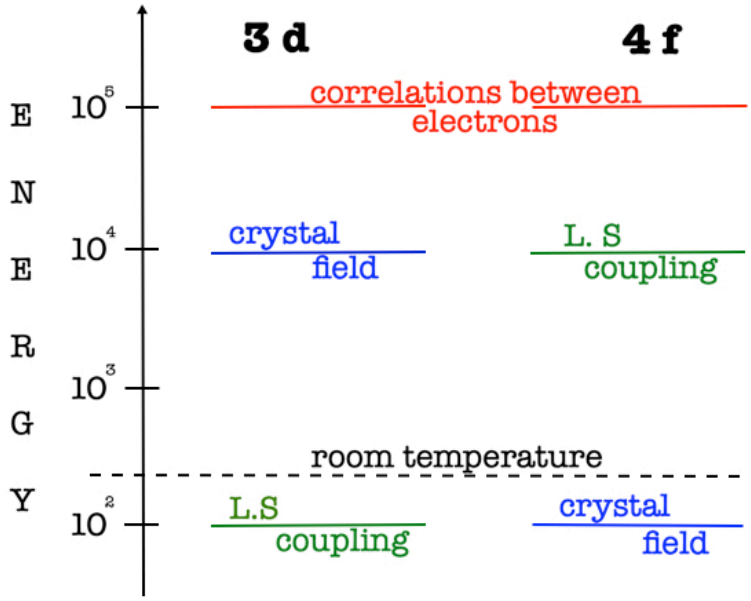

Figure 1.1 Schematic description of the energy of the CEF and spin-orbital (LS) coupling in 3d and 4f ions.

In the intermetallic compounds of the rare earths, two types of electron states exist. Delocalized electron states in *s* or *d* shells of the conduction electrons are responsible for heating, electric transport and other critical phenomena mentioned above and they are the first type. The second type is represented by localized states with low energy in *f* shells (4*f* lanthanides and 5*f* actinides). These define the thermodynamic properties and

apparently, they do not contribute to the charge transport. Localized states are influenced by neighbouring rare earth lattice ions with the charge eZ_i in the position $\overrightarrow{R_i}$. It is possible to use the following approximation: the influence of individual surrounding charges will be substituted by point charges. Then it will have an interaction of point charges and final potential will be:

$$V(\vec{r}) = \sum_i \frac{eZ_i}{|\vec{r}-R_i|}, \tag{8}$$

where V is potential and $\vec{r}$ is vector describing the position of the point charge in the space. The interpretation of the potential represents CEF model, which is the model of point charges [18].

The main difference between rare earths (important 4*f* electrons) and 3*d* elements is the magnitude of CEF splitting. For *d* elements the total CEF splitting is bigger than the splitting of the electron multiplet. Contrary, in rare earths the mutual influence of electron multiplet could be neglected in comparison with CEF splitting influence. Except for europium (Eu) and samarium (Sm), in which this effect could have an important role. A number of levels, created as a consequence of CEF splitting depends on symmetry. Effect of CEF is expressed by Hamiltonian:

$$\mathrm{H}_{CEF} = \sum_{l,m} B_l^m O_l^m, \tag{9}$$

where O_l^m represent equivalent Stevens CEF operators and B_l^m are CEF parameters characteristic for every metal [19].

The occupation of CEF levels by 4*f* electrons depends on temperature. This probability p_i is expressed by equation (10), which is Boltzmann relation [20], where E_i is the energy of i-state and k_B is the Boltzmann constant. In the denominator (10), there is a is statistic sum Σ_j and j is changing from 1 to the total number of CEF states in the studied material:

$$p_i = \frac{exp\left(-E_i/k_BT\right)}{\sum_j exp\left(-E_i/k_BT\right)}, \tag{10}$$

If it is possible to excite 4*f* electron from its ground state, the excitation will probably move through the lattice of rare earth ions. In quantum mechanics, this state of moving excitation is considered as a quasiparticle called magnetic exciton [21].

From the measurement of heat capacity, it is possible to adjust CEF parameters in an indirect way. Different levels contribute to the Schottky contribution of the heat capacity in the paramagnetic phase. In order to illustrate this, a two-component system being in the ground state is used. Here, the energy is $E_0 = 0$ with degeneracy q_0 and with the first excited state, having the energy E_1 with degeneracy q_1. Average energy of N particle system is determined by the following formula:

$$E = \frac{N q_1 E_1 e^{E_1/k_B T}}{q_0 + q_1 e^{E_1/k_B T}}. \tag{11}$$

It follows from this equation (11), that mentioned Schottky contribution to the heat capacity can be expressed by [22]:

$$\mathrm{C}_{Schottky} = \frac{\partial \mathrm{E}}{\partial \mathrm{T}} = N k_B \left(\frac{E_1}{T}\right)^2 \frac{q_0}{q_1} \frac{e^{E_1/k_B T}}{\left(1 + \frac{q_0}{q_1 e^{E_1/k_B T}}\right)^2}. \tag{12}$$

1.2.2 Indirect Exchange Interaction

An indirect exchange interaction is a type of interaction that has an important role in many physics' problems. It involves interaction with the localized moments in metal via polarization of conduction electrons. It dominates in metals, where only small or beyond-the-reach overlaps of wave functions of neighbouring atoms in the lattice exist. Comparisons of the distance ranging from 0.04 nm to 0.06 nm [23] with the dimension of 4*f* electron layer, show that a direct exchange interaction at 4*f* electrons is not possible. An exchange interaction at 4*f* electrons is then possible only via polarization of conduction electrons.

In 1956 Kasuya came with an explanation, about magnetic indirect effect. This theory was described in detail in works of Ruderman and Kittel [24], Kasuya [25] and Yosida [26]. Because of this fact, indirect exchange interaction is known as Ruderman – Kittel – Kasuya – Yosida interaction (RKKY interaction).

Conduction electrons are the carriers of RKKY interaction and therefore, the Fermi surface has a connection with this indirect interaction. The energy of RKKY interaction diminishes with the distance more slowly than a direct exchange interaction does. Moreover, its dependence on distance is more complicated. Because of that, it is important to take interactions among farther atoms into consideration. Magnetic properties of rare earth materials depend on RKKY interaction and CEF. The final bound between two spins S_i and S_j localized in the distance r_{ij} is done by the formula [27]:

$$J_{RKKY}^{ij} = 6\pi J^2 Z N(E_F) \left[\frac{\sin(2k_F r_{ij})}{(2k_F r_{ij})^4} - \frac{\cos(2k_F r_{ij})}{(2k_F r_{ij})^3}\right], \tag{13}$$

where Z parameter designates the number of induction electrons per atom, k_F is an electron wave vector and J is assigned as:

$$J = -\frac{|V_{sf}|^2}{|E_{4f} - E_F|}. \tag{14}$$

The exchange integral $J \propto V_{sf}$ is a hybridization matrix of elements between the f shell and electrons. $|V_{sf}|^2$ is characterized as hybridization among localized electrons and delocalized bonding. E_{4f} *is* the energetic location of $4f$ electron level [11].

At distances equivalent to distances between rare-earth's magnetic moments, the antiferromagnetic long-range order has been observed. The ferromagnetic behaviour [28] and the energy of RKKY is:

$$k_B T_{RKKY} \approx J^2 N(E_F). \tag{15}$$

In the compounds based on Ce, the energetic states are close to the Fermi surface and to some extent lead to heavy fermion systems. Close to the room temperatures, f

moments in the sublattice have properties, reminding weakly interacting magnetic moments. When the temperature decreases, conduction electrons screen magnetic moments and the effective mass is 10^3 times higher than the mass of free electrons [29]. The physical properties of heavy fermion compounds are considered as reason for additional effects of RKKY interaction.

1.2.3 The Itinerant System – Spin Fluctuations and Stoner Model

An elementary itinerant model of band ferromagnetism is expressed by Stoner's criterion [30]:

$$\hat{I} = IN(E_F) \geq 1, \tag{16}$$

which leads to division of compounds into two separate groups. $\hat{I}$ is an affective Stoner parameter and I represents exchange energy, which is connected with interaction responsible for the growing number of electrons with parallel spins. For ferromagnetic systems $\hat{I} \geq 1$ and for Pauli's paramagnetic compounds $\hat{I} < 1$. This criterion is valid only for spin systems and it is based on paramagnetic density of states, where two identical bands are separated into spin up and spin down.

Articles [31] and [32] deal with one particle excitation, where the temperature influence and magnetic field influence are the function of form and band structure close to the Fermi surface. Authors of the mentioned works supposed that there exists two intermediate states between paramagnetic and ferromagnetic states. One of them is collective electron metamagnetism [33] and other one is known as a spontaneous magnetization [32]. Close to the Stoner criterion, this behaviour is affected by spin fluctuations. It has no influence on qualitatively observed properties in the system but it has to be considered in the analysis.

If the value is close to the limit of Stoner criterion in the paramagnetic state (ferromagnetic instability for $\hat{I} = 1$), the total change of magnetic susceptibility χ will be enhanced in comparison to Pauli's paramagnetic susceptibility χ_0 by so-called Stoner factor $S = (1 - \hat{I})^{-1}$ and the final magnetization will have a form:

$$\hat{I} = S\chi_0 = \left(1 - \hat{I}\right)^{-1}\chi_0 \,. \tag{17}$$

The systems with these properties are called Stoner enhanced paramagnet. This effect is necessarily connected with the existence of spin fluctuations – low energy excitations – paramagnons, which can be conceptualized as heavy damping spin fluctuations of paramagnetic state.

Spin fluctuations can be defined as the characteristic marks of dynamic susceptibility $\chi(\vec{q},\ \omega_e)$ [34], representing the response of an interacting system to a small electromagnetic field with the wave vector $\vec{q}$ and with frequency ω_e. As well as the static susceptibility in the equation (17), is also enhanced in regard to statistic susceptibility $\chi_0(\vec{q},\ \omega_e)$ of non-integrate system:

$$\chi(\vec{q},\omega_e) = \chi(\vec{q},\omega_e)[1 - Im\chi_0(\vec{q},\omega_e)]^{-1}. \tag{18}$$

The imaginary part of magnetic susceptibility $Im\chi_0(\vec{q},\omega_e)$ for a small constant $\vec{q}$ as a function of ω could be expressed as $Im\chi_0(\vec{q},\omega_e) = A(\omega)/a$, where a is a constant. The $A(\omega)$ has a form:

$$A(\omega) = \frac{\widetilde{\omega}}{1 + \widetilde{\omega}^2}, \tag{19}$$

where $\widetilde{\omega} = \omega/k_B T_{SF}$. T_{SF} is a characteristic spin fluctuation temperature. The distinct effect in systems with spin fluctuations is scaling with spin fluctuation temperature T_{SF}. It is expressed by:

$$T_{SF} = \frac{T_F}{S}, \tag{20}$$

where $T_F = E_F/k_B$ is the Fermi temperature and S represents Stoner factor.

In Figure 1.2 the dependence of the imaginary part of susceptibility $Im\chi_0(\vec{q},\omega_e) = A(\omega)/a$ for a small constant $\vec{q}$ as a function of ω is plotted. The curve in this figure represents a density of paramagnon states [35]. This dependence can be measured by means of inelastic neutron scattering or a point-contact spectroscopy. From

the historical point of view, the first spin fluctuations were observed experimentally in liquid ^{3}He [36]. Density of paramagnons states has a characteristic shape with a maximum at energy $k_B T_{SF}$.

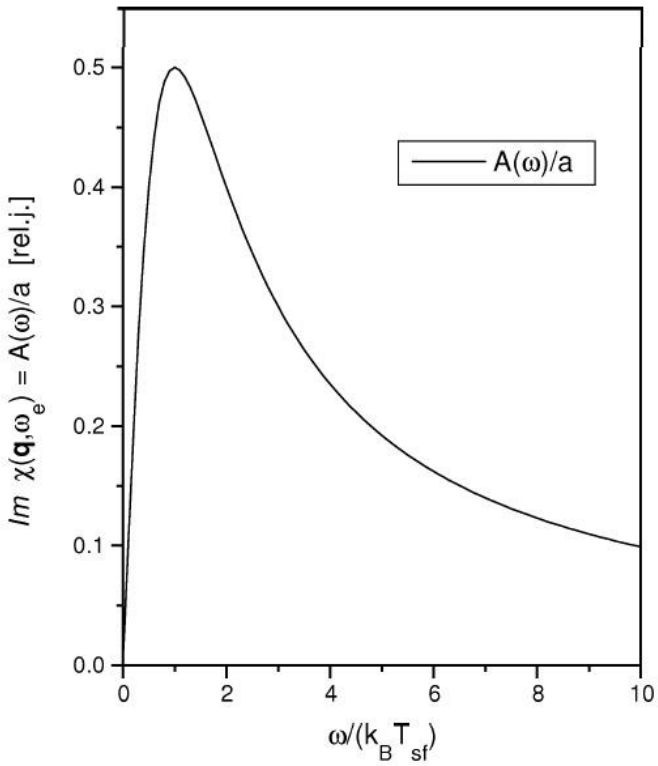

Figure 1.2 Dependence of density of paramagnon states [34].

Paramagnons are collective excitations and have measurable consequences on physical properties of bulk samples. Electrical resistivity is a very good example for observation of spin fluctuations. In the work [37], an electron-electron interaction term AT^2 in electrical resistivity was defined. It is known as a spin fluctuation effect. The A is proportional to $(T_{SF})^{-2}$, which was observed and theoretically demonstrated. This behaviour of the electrical resistivity was seen for $CeNi_5$ [38].

Other studies which deal with the existence of spin fluctuations are articles [39, 40], where the application of high magnetic fields depress their existence.

1.2.4 A Heavy Fermion System

Due to the presence of *4f*-electrons in Cerium and Ytterbium-based compounds, the electronic states are relatively close to the Fermi level. Due to hybridisation these states in the vicinity of Fermi surface can create an Abrikosov-Suhl resonance, which has a large impact on physical properties of such materials, causing for instance a very high effective mass of conduction electrons. This gives a terminological origin to the heavy-fermion (HF) systems. Close to room temperature values, the *f*-moment sublattice has properties resembling those of weakly (Curie-Weiss) interacting magnetic moments. As temperature decreases, the conduction electrons progressively screen the magnetic moments. It results in effective masses as large as 10^3 times that one of a free electrons. This is the reason why," heavy-fermion" were created. Heavy fermion (HF) materials can be canonically described on the basis of the existence of two temperature regimes. One of them is a high temperature regime characterised by weak interactions of local magnetic moments and conduction electrons. The other regime is characterised by strongly interacting particles (electrons), which at low temperatures show behaviour of particles having Landau-Fermi liquid-like character [41]. The intermetallic compounds containing rare earths shows a wide spectrum of physical phenomena at low temperatures, such as the formation of unconventional metallic and magnetically ordered states and a strong violation of Landau-Fermi liquid theory. It is the exchange interaction of the localized *4f* electrons with the conduction electrons having an itinerant character that gives rise to such phenomenon. The physical properties of HF compounds are usually considered to result from the competing effect of the intrasite Kondo and intersite Ruderman-Kittel-Kasuya-Yosida (RKKY) interactions. This model is characterised by both, Kondo and RKKY energies:

$$k_B T_K \propto -exp\left(\frac{-1}{|J_{ij}|}\right), \tag{21}$$

and

$$k_B T_{RKKY} \propto J_{ij}^2, \tag{22}$$

Both quantities are dependent on exchange coupling J_{ij} between the local 4*f*-moment and the conduction electrons. Here T_K denotes Kondo temperature and T_{RKKY}

denotes RKKY characteristic temperature. This yields to conclusion that for very small values of J_{ij} the RKKY interaction dominates and the system is expected to order magnetically at $T_M \approx T_{RKKY}$ (T_M means magnetic ordering temperature). As exchange interaction J_{ij} increases, the local moments become more affected by conduction electrons, and for a large value of J_{ij}, T_M falls down to zero as a result of $T_M >> T_{RKKY}$. In the region where the system shows a transition from a magnetically ordered to a non-magnetically ordered state, there is an occurrence of enhanced density of electronic states at the Fermi energy $N(E_F)$, revealing the HF properties [42].

The competition of Kondo effect and RKKY interaction is well illustrated in well-known Doniach diagram shown as example in the Figure 1.3.

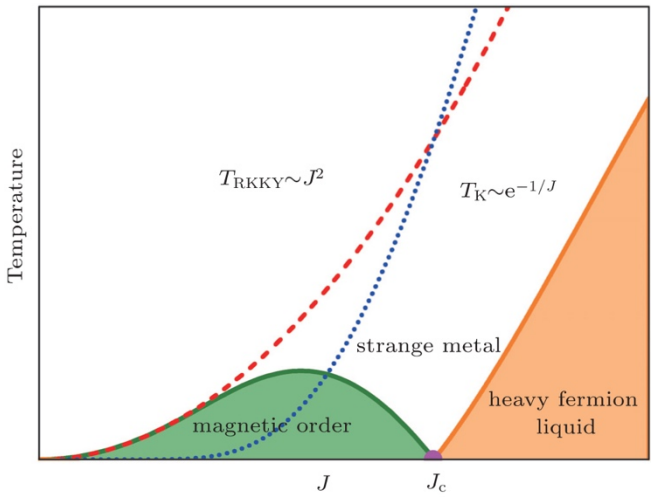

Figure 1.3 A schematic illustration of the Doniach phase diagram [43].

We could briefly describe various characteristic behaviours seen in the figure and defined as e.g. [4, 44]:

a) MAGNETIC MATERIALS - When the magnitude of exchange integral J_{ij} between the local moments and the conduction electrons is small then the Kondo interaction between them is almost negligible. As a result, due to the dominating RKKY interaction, the magnetically ordered ground state arises.

b) KONDO MAGNETICS - If the exchange integral J_{ij} increases, the intensity of Kondo interaction increases, too. However, when the temperatures are low

enough, the magnetic ordering is observed. This is due to stronger RKKY interaction.

c) HEAVY FERMIONS - In the region where the Kondo interaction is of the same order of magnitude as RKKY interaction, the heavy-fermion behaviour arises. As a matter of fact, the exchange integral J_{ij} is further increasing in intensity, the magnetic ordering temperature is being lowered to a final value of zero kelvin. Therefore, no ordering occurs at T = 0 K. If one is able to drive such transition by control parameter, the quantum critical point (QCP) is observed. Close to a QCP, unconventional or non-Fermi liquid behaviour arises. It will be briefly explained in next chapter.

d) VALENCE FLUCTUATING COMPOUNDS - in this region, the J_{ij} increases even more and thus it yields to rise of the Kondo energy scale. Kondo energies are comparable to the order of CEF-excitation energies. As a result, the valence fluctuating behaviour is observed.

1.3 Phase Transitions

1.3.1 Classical Phase Transitions

Classical phase transitions are characterized by thermal fluctuations of the ordered parameter in an energy window $k_B T_c$ around critical temperature T_c, which is called the classical critical region. It can occur in a first order or in the continuous level (second ordered state or higher). Fluctuations mentioned above are growing as T is approaching to T_c and the correlation length of thermal fluctuations (ξ) diverges as:

$$\xi = |t|^{-a}, \tag{23}$$

where $t \equiv \left|\frac{T-T_c}{T_c}\right|$ represents the reduced temperature and a is the critical exponent [45]. When the system is close to the T_c, the divergence of the correlation length implies that the spatial fluctuations extend through the whole system. On the other hand, fluctuations

of the order parameter also exist inside the time domain. Consequently, τ_c is what represents the correlation time. It diverges as it follows from equation (24), where the parameter z is known as the dynamic critical exponent:

$$\tau_c = \xi^z = |t|^{-az}, \tag{24}$$

From equations (23) and (24) it yields that the critical behaviour is described in observed physical properties through a power law. Described information leads to the universality classes, which are determined by spatial dimensionality and the symmetry of the order parameter. There are no relevant details of the microscopic interactions of the system [44].

1.3.2 Quantum Phase Transitions

As temperature approaches to zero K, the thermal fluctuations are no longer relevant as quantum fluctuations arising due to Heisenberg uncertainty principle, which is the driving force in normal phase transitions. Although at any finite temperature quantum fluctuations are negligible. Then quantum fluctuations have an energy scale:

$$\hbar\omega_c = \frac{\hbar}{\tau_c}|t|^{az}, \tag{25}$$

where t, a and z have the same definitions as for classical phase transitions [45]. From this follows that if we are able to tune the temperature to the vicinity of zero K then the classical phase transition will change to quantum phase transition (QPT). However, we could also use another proper tuning parameter (e.g. pressure or magnetic field) and we would be able to tune the phase transition to so called quantum critical point (QCP) [10] as it is presented in the Figure 1.4.

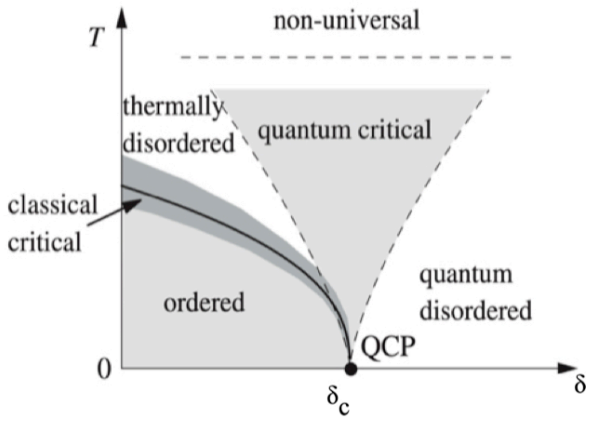

Figure 1.4 Schematic phase diagram in the vicinity of a continuous quantum phase transition. The control parameter δ_c tunes the system through the QCP [45].

Experimental observations of such situation, e.g. [10] yielded to many new discoveries of unexpected behaviour. We can mention e.g. logarithmic behaviour of heat capacity, divergences of some physical properties in the vicinity of QCP and many others. It was not possible to use Fermi-liquid theory or heavy fermion description any more. Therefore, a new name came into a practice – the non-Fermi liquid (NFL) behaviour, which is described in more details in next section.

1.3.3 Non-Fermi Liquid Behaviour

The above-mentioned situations yielded to observation of highly correlated systems where the heavy fermion model could not explain observed deviations from Fermi liquid theory, even considering corrections of very high effective masses. Due to the enormous effective masses of electrons, the metallic systems and intermetallic compounds have exposed a number of new phases in condensed matter so-far. They indicated reconsideration and remodelling of our understanding of metallicity, of the metallic ground states of matter, and of the many-body problem in physics in general. When a magnetic phase transition is suppressed very close to 0 K, a highly exotic state of matter arises with typically logarithmic divergences in ordinary thermal properties such as the specific heat and magnetic susceptibility. The physical properties are found to be as follows:

$$\frac{C(T)}{T} \propto -\frac{1}{T_0}\ln\left(\frac{T}{T_0}\right), \tag{26}$$

$$\frac{C(T)}{T} \propto T^{-n}, \tag{27}$$

$$\frac{C(T)}{T} \propto T^{n}, \tag{28}$$

where $1 < n < 2$ at low temperatures. These power laws can have many origins and it often happens that non-Fermi liquid behaviour is observed close to a magnetic instability, and close to a magnetic quantum critical point. We mentioned several examples [3, 46-49] as well as some explanations of the observed effects in order to point out the importance of highly correlated matter and quantum phase transitions, which have been attending scientist during the recent decades. However, experiments have demonstrated that exceptions do exist in some heavy fermion compounds, transition metal alloys and oxides, including high-T_c superconductors, quantum dots and organic charge-transfer systems [4, 50, 51].

As a result of NFL mechanism, many of these systems have the same physical property of being in the proximity of a quantum phase transition (QPT) or a quantum critical point (QCP) [52]. Alternative approaches to the QPT scenario, propose to explain NFL features by the theory of specific disordered systems and of multi-channel or quadrupolar Kondo models [53]. At present, there are two theoretical scenarios available neither of which is able to explain the experiment. The Hertz-Millis-Moriya model assumes that quasi-particles undergo singular scattering at the QCP point due to the abundance of low-lying magnetic fluctuations [54, 55]. In the Table 1, a summary of theoretical findings of different theories is presented.

Table 1 The summary of main results of three selected theories is: (a) - [54] and [55]; (b) - [56]; and (c) - [57]. The symbol d represents the dimensionality of the system.

THEORY	QUANTITY	AFM d = 3	AFM d = 2	FM d = 3	FM d = 2
(a)	C/T	$\gamma_0 - aT^{1/2}$	$\log(T_0/T)$	$\log(T_0/T)$	$T^{-1/3}$
	ρ	$T^{3/2}$	T	T	-
	χ	$T^{3/2}$	$\chi_0 - dT$	-	-
(b)	C/T	$\gamma_0 - aT^{1/2}$	$\log(T_0/T)$	$\log(T_0/T)$	$T^{-1/3}$
	ρ	$T^{3/2}$	T	$T^{5/3}$	$T^{4/3}$
	χ	$T^{-3/2}$	$-\log(T)/T)$	$T^{-4/3}$	$-\log(T)/T$
(c)	C/T	$\gamma_0 - aT^{1/2}$	-	$\log(T_0/T)$	$T^{-1/3}$
	ρ	$T^{3/2}$	-	$T^{5/3}$	$T^{4/3}$
	χ	$T^{-3/2}$	-	$T^{-4/3}$	T^{-1}

The other model postulates a break-down of the quasi-particle concept altogether at the QCP, emphasizing their composite nature due to the local hybridization of the 4f-electrons and the conduction electrons [58, 59]. The detailed discussions on this subject (also the classification of different models following critical exponents), are presented in the review work by G. R. Stewart [4].

Due to the fact that this behaviour is still not fully explained, it is one of the forefronts studying problems in physics of condensed matter.

1.3.4 The Pressure Response of Rare-Earth Ions

As one could see from Figure 1.4, one of the possible tuning parameters is pressure. It is important for many reasons: pressure influences the physical properties also in Fermi liquid model. In addition, it is important because of the crystal electric field, which plays an important role in determining the physical properties of rare-earth intermetallic compounds. As it was mentioned in section 1.2.1, CEF depends on crystal symmetry. Special situation arises in Ce and in Yb. Due to 4*f* electron levels arrangement

and occupancy the pressure could substantially modify the electron wave function [12]. Therefore, the overwhelming number of different strongly correlated electrons effects is found in Ce, Yb and U-based compounds and alloys. They could be referred to as the instabilities of the electronic configuration of the ground state.

The mentioned effects originate usually from symmetry between Ce ($4f^1$) and Yb ($4f^{13}$) electron configurations. Here, $4f^1$ Ce-electrons behave mirror-like to the holes, which are associated with the $4f^{13}$ electrons. Then, if we apply the pressure to such system based on Yb or Ce, we can observe that the magnetism of Ce ions is suppressed. It is because of the fact that, $4f^1$ electron is squeezed out of the $4f$ shell. This situation is presented in the Figure 1.5.

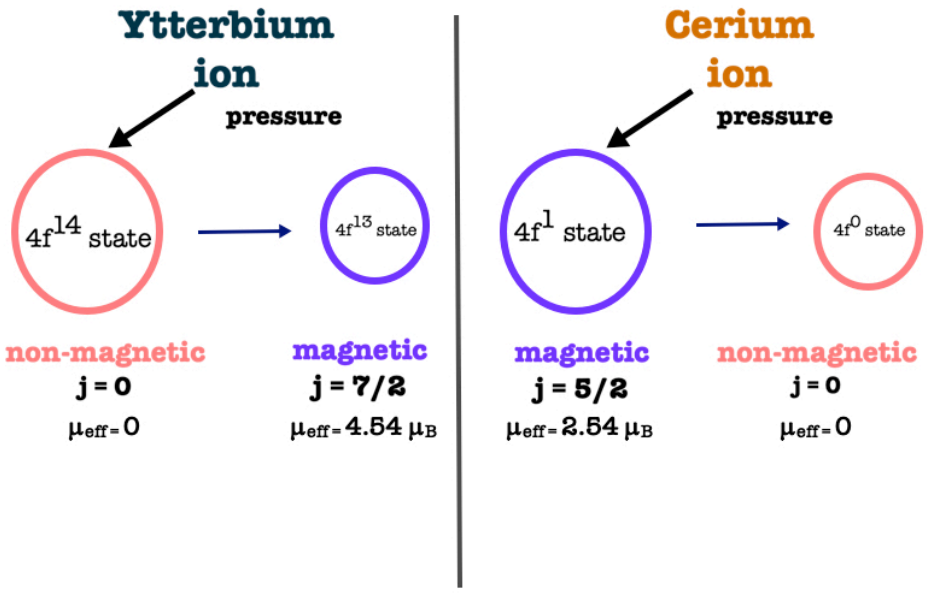

Figure 1.5 An illustration of the pressure response of Ytterbium ion and Cerium ion.

However, the situation is different in Yb ion where, magnetic state is stabilized with applied pressure. This electron-hole analogy has been observed in many of such systems. The variety of control parameters like substitution, pressure, chemical pressure, magnetic field or valency enable us to change the relevant interactions and thus modify the ground state. This yields to modification of J_c parameter in the Doniach diagram Figure 1.3 or $J.N(E_F)$. In case of Ce compounds the characteristic temperatures are increasing and in case of Yb decreasing. One could illustrate here the works on isostructural series of $CeCu_{5-x}Al_x$ [60] and $YbCu_{5-x}Al_x$ [61].

2 MOTIVATION FOR THE STUDY OF $RENi_5$ SYSTEM

The principal parameter for this class of compounds is the rare earth - RE. This work deals with three RE elements – Cerium, Gadolinium and Ytterbium. Gadolinium belongs to heavy-rare-earth element group. Its Curie temperature for ferromagnetic ordering is T_c = 293 K. Only Yb is from yttrium subclass where the antiferromagnetic structure has not been observed, yet. On the other hand, Gd shows a change of spin orientation. It was evidenced by the measurements of magnetic anisotropy and neutron diffraction, where in the temperature interval ranging from 293 K to 232 K the moments are parallel to crystallographic axis *c* and down to 232 K the angle in regard of *c* axis grows to the maximum value of 75° at T = 180 K. Then, an angle is decreases to 32° at T = 4.2 K. The saturated magnetic moment for Gd is 7.55 μ_B [62]. Ytterbium, as well as lutetium, are metals from rare earth elements, which are paramagnetic up to the lowest temperatures. Both of them have 4*f* electron shell totally occupied [63, 64]. From a magnetic point of view, cerium is the most interesting material. In polycrystalline cerium, an antiferromagnetic transition at T_N = 12.5 K has been observed in the hexagonal *dhcp* crystal structure. In this type of system inside in hexagonal structure, a ferrimagnetic ordering exists. However, both planes together form antiferromagnetic ordering. Magnetic moments are parallel with *c* axis and their value is 0.62 μ_B per atom [63, 65].

Motivation for the study of $RENi_5$ (RE = Ce, Yb, Gd) system is the knowledge of ground state evolution among 3 different systems. One could expect the emergent behaviour arising due to existence of different physical interactions which could be connected with e.g. spin fluctuations, quantum criticality, Kondo effect or magnetocaloric effect. Their mutual competing can be tuned by magnetic field or pressure. It is already well-known how they influence Yb and Ce atoms. Magnetic field as well as pressure effects their physical properties in an opposite way by changing their state properties. Furthermore, nobody has studied their nonstoichiometric composition. Only the binary systems of $CeNi_5$, $YbNi_5$ and $GdNi_5$ have been investigated.

On the other hand, we are working with other systems, where Ni atom is substituted by Cu, Pd or In. Prepared compounds are good candidates for the study of physical properties at low temperature regime, where emergent behaviour due to quantum mechanics effects should be observed. The reason, why those were chosen, will be explained latter.

2.1 $CeNi_5$ Binary Compound

The first investigations of $CeNi_5$ binary system were done 50 years ago. The first research paper dealt with the valency of Ce. However, the question, standing in the centre of scientists' attention was not only about the valency of Ce, but also its relation to the possibility of migration of 5*d* electrons to 3*d* conduction band. The reason for this movement from 5*d* to 3*d* is the difference in a Fermi surfaces for Ce and Ni. This band is splitted and the final state is formed at the bottom of 5*d* and in the top of 3*d* band. Fermi surface can move to "lower" position in regard to 4*f* shells, but one condition must be fulfilled: the number of Ni atoms has to be higher than of Ce atoms. Figure 2.1 shows schematic representation of the density of states $N(E_F)$ metals of Ce and Ni metals (a) and in system Ce-Ni (b) [66].

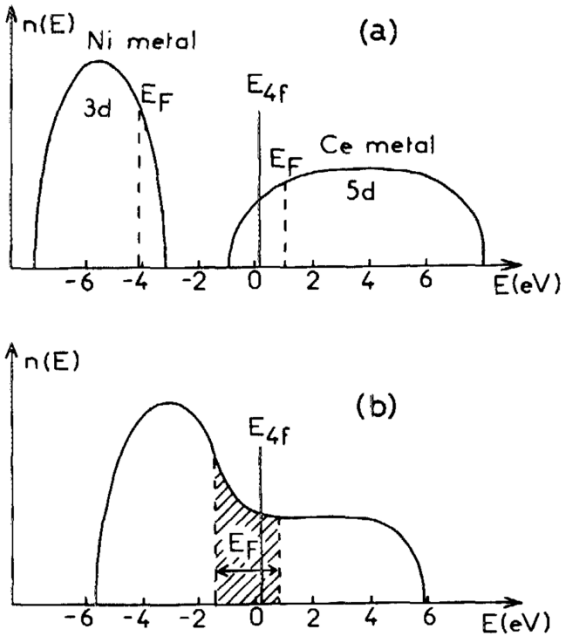

Figure 2.1 Graphic representation of density of states (a) for Ce atom and Ni atom; (b) for system Ce-Ni [66].

The different size of Ni and Ce atoms causes that dominantly between them itinerant ferromagnetism is created. The location of 4*f* electrons plays an important role there. This behaviour is related to Stoner criterion (see in relation 16). $CeNi_5$ is a well-

known Stoner enhanced paramagnet, where an itinerant ferromagnetic correlation can appear. However, it has not been confirmed experimentally yet. From the crystallographic point of view, $CeNi_5$ crystallizes in hexagonal $CaCu_5$ type of structure with *P6/mmm* space group. In the temperature range from 4 K to room temperature, it is a paramagnetic material. Nevertheless, the measurement of a magnetic susceptibility $\chi(T)$ shows a broad maximum (Figure 2.2) in a temperature region near 100 K [67].

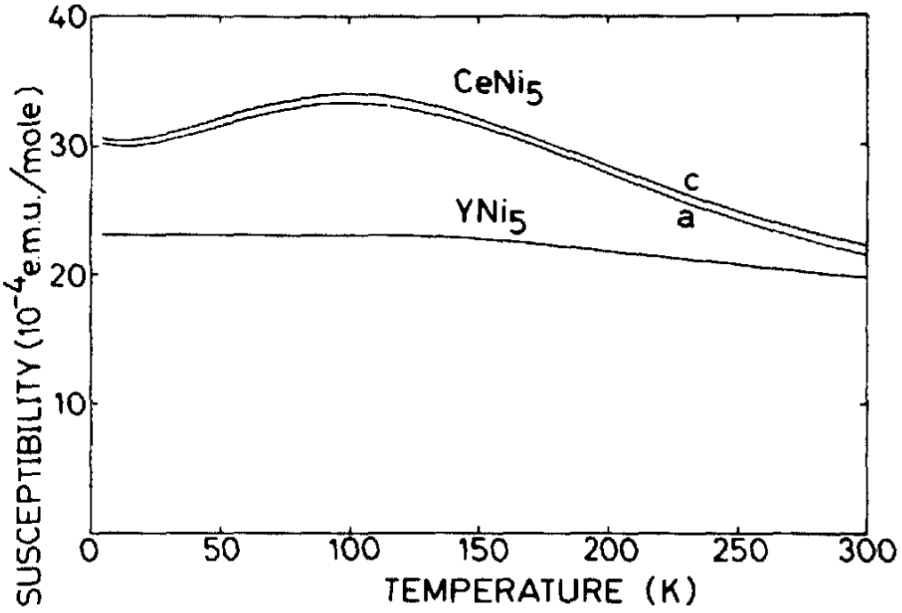

Figure 2.2 The temperature dependence of magnetic susceptibility for single crystal of $CeNi_5$ along a and c crystallographic axis [67].

Interpretations of this anomaly were different. One of them talks about the existence of gradual change of Ce ions valency from Ce^{4+} at T = 0 K to noninteger valency, when the material is at room temperature. It is a consequence of thermal excitation to Ce^{3+} states. This process is described in the published paper [68].

Another analysis of this broad maximum says that, in the whole temperature range, Ce is ion nonmagnetic and its valency is close to 4+ [67], which was confirmed by several experiments. In another part of Ce investigations, it was found out that the temperature dependence of cell parameters did not have any influence on Ce valency from 4.2 K to 300 K. The X-ray diffraction defines the valency of Ce close to 4+, but this is not consistent with the results in paper [69], where authors used the same experimental

techniques and their results for Ce valency were 3.3+. Next experiment of thermal expansion confirmed an analogy with other $RENi_5$ compounds. With changing temperature, the experiment did not show the change of valency state. Appealing to [70], the Ce in $CaCu_5$ structure should have been bigger than other atoms to show three-valency.

The subject of the study of Ce valency was also very important for the work [71], dealing with neutron diffraction. With the use of neutron diffraction, Gignoux et al. were able to separate the contributions to magnetic susceptibility from a certain location of atoms. It should not be from Ce, because if it were, it would be connected with the change of Ce valency. Because of that, this maximum has an origin in thermally smeared density of states of *d* electrons on Fermi surface, which is enhanced by the effect of spin fluctuations.

$CeNi_5$ is an attractive material not only for experimental study. Theoretical works deal with the electron structure. These calculated results confirmed experimental results, where the Fermi surface is localized in 3*d* band of Ni atoms (Figure 2.3). The hybridization of the 4*f* state with 3*d* state of Ni changes the electron structure in the studied material. This causes a maximum created on the Fermi surface, which becomes evident in Stoner conjunction $IN(E_F)$ for $CeNi_5$. Based on the ground state it is magnetically unstable, thus in this interesting system spin fluctuations occur [72].

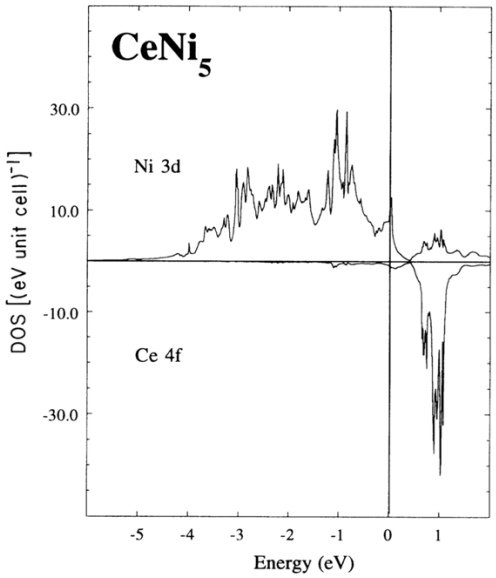

Figure 2.3 Calculation of density of states for $CeNi_5$ at the Fermi energy [72].

Other authors [67] focused on the study of electrical resistivity in the temperature range, from 4.2 K to 300 K along the two main crystallographic axes *a* and *c*. In the low temperature regime, the electrical resistivity follows AT^2 dependence, where the A coefficient along *c*-axis is equal 7.10^{-10} ΩcmK^{-2} and along *a*-axis grows and its value is 11.10^{-10}ΩcmK^{-2}. From those results it is evident, that $CeNi_5$ belongs to Pauli's enhanced paramagnets occurring close to Stoner criterion. This analysis of electrical resistivity agrees with confirmation of noninteger valency of Ce.

The first experiment on $CeNi_5$ was done 50 years ago. Authors of [73] studied heat capacity in very low temperature range, where they were able to determine a Sommerfeld coefficient γ = 37 mJ/mol^{-1}K^{-2}. An increased γ had its origin in Ce atoms because atoms of Ni were situated in the electron configuration $3d^{10}$ and then 4*f* band of Ce was very closed to Fermi surface.

The theoretical study [72] established a Sommerfeld coefficient γ = 24.8 mJ/molK^{-2}. This value is still higher than value for simple metals. Here, the difference is explained by contribution of paramagnons derived from spin fluctuations.

Mentioned spin fluctuations of $CeNi_5$ were proven with point contact spectroscopy [74], whereby applied magnetic fields depressed the presence of paramagnons from 3*d* band.

2.2 $YbNi_5$ Binary Compound

There is not so many information about $YbNi_5$ compound. The main reason could be the problem with preparing the samples because of evaporation of Yb during the melting process. Currently, only few papers exist about it. Paper [75] deals with physical properties as Mösbauer spectroscopy, magnetic and electrical resistivity measurement of binary $YbNi_5$. DC magnetic susceptibility measurement made in the low temperature range is shown in Figure 2.4.(a). The upturn of susceptibility shows an ordering temperature at T_c = 0.55 K and it has an origin of ferromagnetic nature.

On the other hand, Mösbauer absorption spectra (Figure 2.4(b)) agree with magnetic measurements. Here, in the saturated state (in the top figure), there is an effective hyperfine field line shape observed. The authors of mentioned publication have found from Mösbauer's analysis, that the quadrupole hyperfine interaction plays a

dominant role in the contribution coming from 4*f* electron shell and the small contribution is coming from distribution of the lattice charges.

The investigation and evaluation of static and dynamic magnetic properties of $YbNi_5$ shows only a small contribution in comparison to other information about $RENi_5$ group.

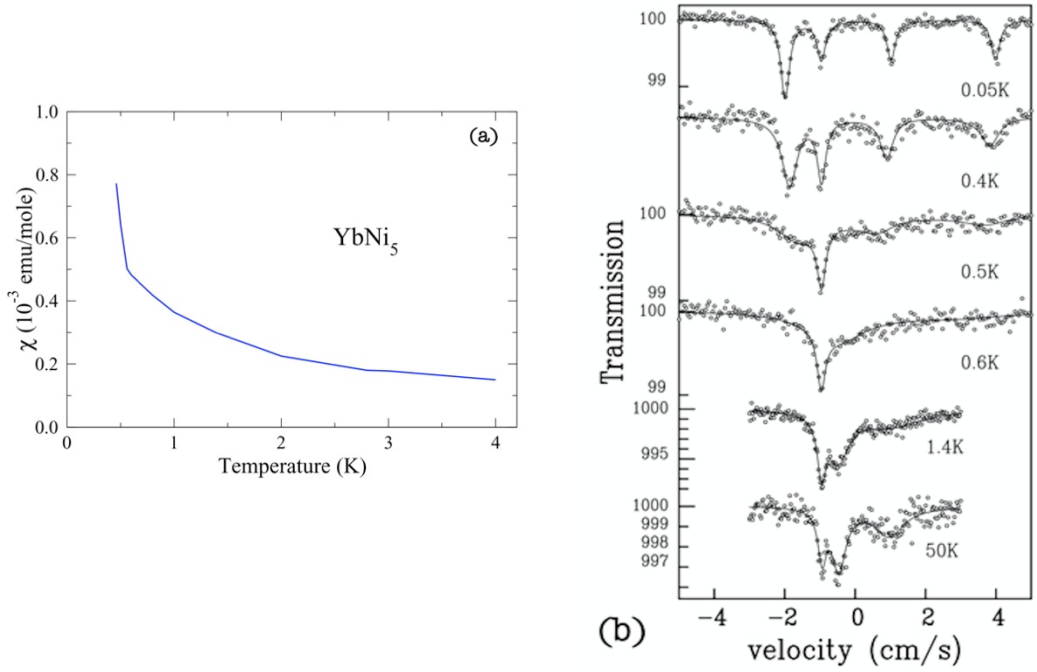

Figure 2.4 (a) Temperature dependence of magnetic susceptibility for $YbNi_5$, where the transition temperature can be seen near T_c = 0.55 K. (b) ^{170} Yb Mösbauer absorption spectra in $YbNi_5$. Critical temperature T_c is evident at 0.55 K [75].

2.3 $GdNi_5$ Binary Compound

The compound $GdNi_5$ is very interesting because of its physical properties. Orbital quantum number for ground state Gd^{3+} ($^8S_{7/2}$) is L = 0 and the crystalline electric field effect is therefore negligible [76].

The first paper about $GdNi_5$ appeared in 1970s, when authors studied magnetic properties with paramagnetic electron resonance. The sample was prepared by induction melting. Magnetic measurements were done in the temperature range from 4.2 K up to 700 K, where an extract method of domain ordering was used. Temperature dependence of magnetic susceptibility follows the Curie-Weiss law, where the paramagnetic Curie

temperature is θ_P = 31 K and effective paramagnetic moment μ_{eff} = 7.94 μ_B/f.u. An exchange interaction calculated from RKKY interaction gives a value of J = -0.011 eV [77].

Another group of authors [78] discussed about anomaly behaviour of $GdNi_5$, which crystallizes in hexagonal crystal structure $CaCu_5$ type with two non-equivalent positions for Ni atoms (Figure 2.5). The crystallographic axis *a* has the same direction as the light axis of magnetization.

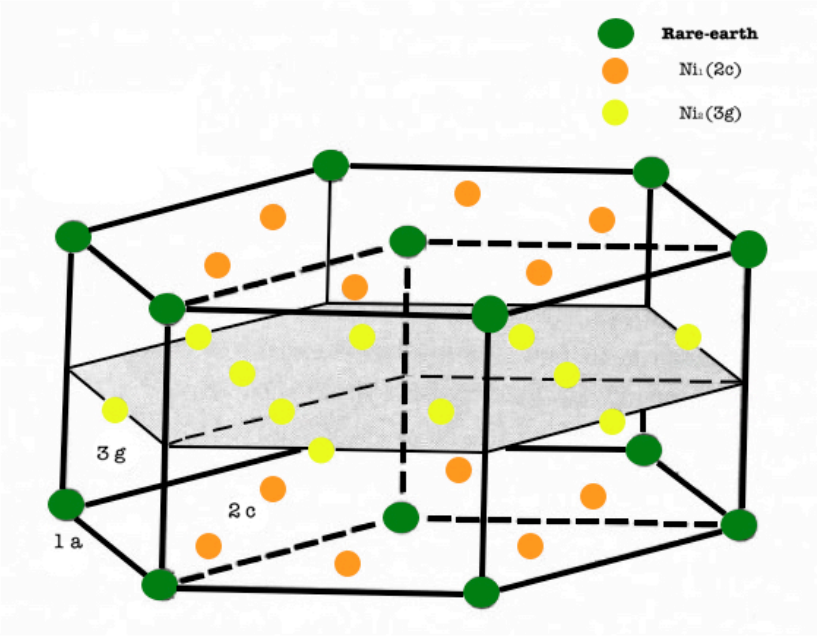

Figure 2.5 The Hexagonal crystal structure $CaCu_5$ type with two non-equivalent positions for Ni atoms.

AC susceptibility measurements shows a sharp maximum, which corresponds to Curie temperature for $GdNi_5$ T_c = 32 K [78]. It is worth mentioning, that in this publication $GdNi_5$ is not regarded as a simple ferromagnet without the influence of CEF. The reason for such an interpretation of the maximum comes from fast changes during the movement of domain walls at temperatures close to the Curie temperature. In [78] the magnetic properties were studied. They confirm ferromagnetically ordered state with Curie temperature of T_c = 32 K [79].

The heat capacity measurements (Figure 2.6) were performed in the temperature range from 1.3 K to 48 K and with the applied magnetic fields up to 5 T. Total heat

capacity consists of several contributions – electron contribution γT, phonon contribution and magnetic contribution. The Sommerfeld coefficient was determined from the extrapolation of the dependence of C/T *vs* T^2, obtaining a value $\gamma = (36 \pm 3)$ mJ/mol^{-1}K^{-2}. The magnetic contribution, was determined after fitting the heat capacity with a Debye function above the critical temperature, from this fitting was obtained a Debye temperature $\theta_D = (296 \pm 2)$ K. Obtained results agree with theoretical calculations [76].

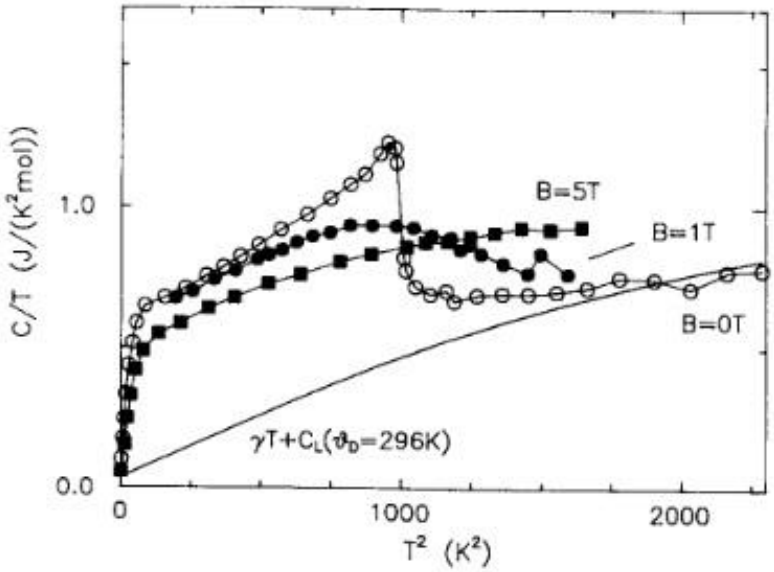

Figure 2.6 C/T vs T^2 dependence for $GdNi_5$ at zero applied magnetic field [76].

2.4 Physical Properties of Similar $RENi_5$ Systems

The selected group of compounds for more detail study is based on rare-earths which have already been studied for several decades. Structural characterization displays in the whole family of $RENi_5$ system hexagonal crystal structure $CaCu_5$ type with *P6/mmm* space group. Its physical properties are influenced by exchange interaction and CEF. In the low temperature range, these alloys and compounds show magnetically ordered state except for $PrNi_5$, which is Van Vleck paramagnet [80]. $CeNi_5$ compound is an exception because it is significant by the influence of spin fluctuations, as it has already been described. Ni atoms contribute to the magnetism only in $CeNi_5$ compound.

One of the aims of this work is to study the physical properties of $RENi_5$ (RE = Ce, Yb, Gd). Although it is a new system, a few works do already exist. These works study the basic physical properties of $RENi_5$ [81, 82]. Here, the authors investigate

theoretical calculations. A research paper about $Yb_xGd_{1-x}Ni_5$ belongs to this group [83]. It motivated us to prepare the samples, perform the physical measurements and analyse of experimental data.

For detailed research, it is important to have information about the possible existence of materials in which the influence of spin fluctuations has been observed. These systems were investigated few decades ago. Temperature dependence of magnetic susceptibility shows a shoulder (Figure 2.7), where the specified effect was presented [84].

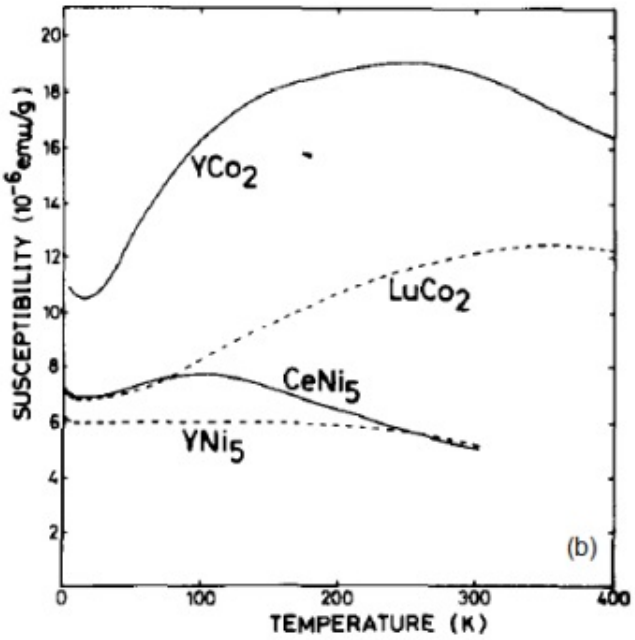

Figure 2.7 χ(T) for YCo_2, $LuCo_2$, $CeNi_5$ and YNi_5 with specific shoulder [84].

The observed maximum in every compound is imputed as the influence of spin fluctuations, but the temperature is notably lower as Stoner model predicted.

The other similar system is $Gd_xLa_{1-x}Ni_5$. In [85] the electron structure and magnetic properties are analysed. Conclusions yield to the result that the average value of an effective paramagnetic moment of Ni decreases with the increase of Gd quantity. Described behaviour suppose the damping of spin fluctuations in the itinerant mechanism.

Selected publications inform about the same behaviour as the systems investigated in this thesis have. For this reason, they were chosen to be characterized.

2.5 Substitution of Ni by Cu, Pd and In

The main aim of this subchapter is to describe the reason to study substitution of Ni by Cu, Pd and In. Expected changes are due to the application of chemical pressure. This yields to observation of the interesting physical properties like e. g. quantum criticality, heavy fermion behaviour superconductivity.

2.5.1 $YbCu_4Ni$ System

In recent decades, $YbCu_{5-x}M_x$ (M = transition metal) system has been studied. This interest was caused by experimental research of binary $YbCu_5$, which crystallizes in $CaCu_5$ type [86]. It is the same crystal structure as in $RENi_5$ compounds. When the $YbCu_5$ was prepared by arc melting techniques, the sample contained several crystalline phases and it was characterized as paramagnetic with fully occupied 4*f* level.

After this study, $YbCu_5$ was prepared by another way, which brought interesting results such as observation of cubic structure $AuBe_5$ type [87]. Next research showed, that cubic compound belonged to heavy fermion family with formation of Kondo lattice and trivalent magnetic state [88]. Calculations of Sommerfeld coefficient [89] also confirmed heavy fermion character with $\gamma = 470\text{m mJ/mol.K}^2$.

Later works [90-92] about $YbCu_5$ and [93-95] about $YbCu_4Ni$ were done. In a recent work [95], where sample was prepared by induction furnace, the structural analysis showed *fcc* structure of $MgCu_4Sn$ type (Figure 2.8), being a derivative of $AuBe_5$ type.

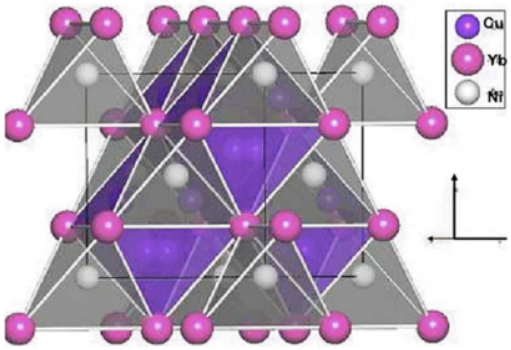

Figure 2.8 Crystal structure of $YbCu_4Ni$ [95].

From the magnetic measurements, they calculated (Figure 2.9) an effective paramagnetic moment with the value of $\mu_{eff} = 4.42\ \mu_B$, which is close to free ion value for Yb^{3+}. By a applying the Curie-Weiss law, the authors obtained θ_P = -19 K, which indicated presence of antiferromagnetic state at low temperatures. In magnetization measurements a strong curvature at $T = 2$ K has been observed. It can be fitted with a usual Brillouin function $B_J(x)$ with $x = B/T$ and effective $J = ½$ [95].

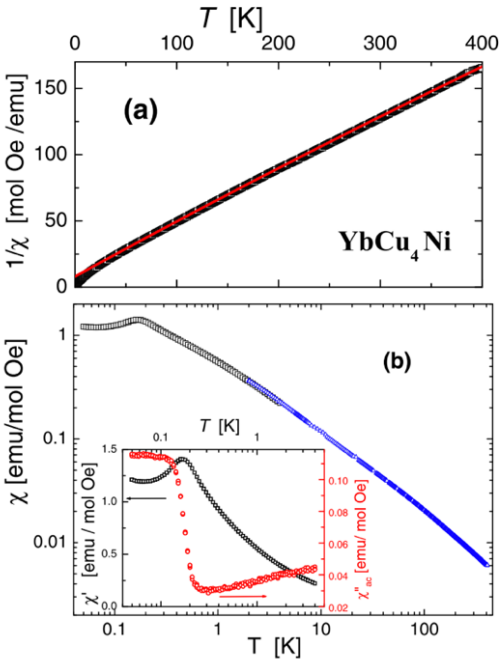

Figure 2.9 (a) The temperature dependence of the inverse magnetic susceptibility. (b) Low-temperature inductive component of ac susceptibility scaled with high-temperature dc susceptibility in a double logarithmic representation. Inset shows inductive and dissipative components of ac susceptibility [95].

The characterization of the thermal properties of $YbCu_4Ni$ was done in [94]. In Figure 2.10 (a) the temperature dependence of the magnetic heat capacity is shown and a possible magnetic transition can be seen at the lowest temperatures. Schottky maximum is also observed around 60 K and it is connected with CEF on the Yb ion. In the Figure 2.10 (b) the magnetic entropy $S(T)$/Rln8 ratio from $C_{mag}(T)$ is presented. R represents the gas constant and 8 is the total degeneracy of the ground state with $J = 7/2$ for Yb^{3+} ion. Entropy $S = R\ln 2$ has value corresponding to partial thermally populated system at about

T = 32 K. This behaviour is in the agreement with other publication [96], where the $YbCu_4X$ (X = Ag, Au and Pd) system was studied [94].

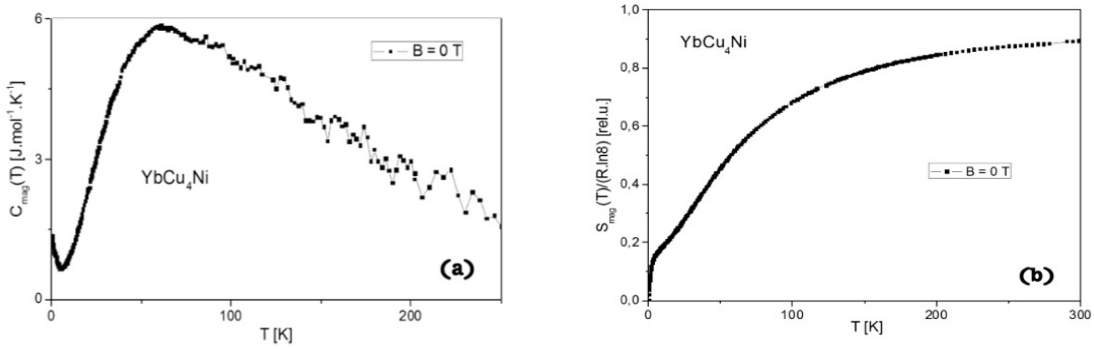

Figure 2.10 (a) $C_{mag}(T)$ of the heat capacity of $YbCu_4Ni$ at B = 0 T. (b) $S_{mag}(T)$ of $YbCu_4Ni$ at B = 0 T [94].

Measurements of electrical resistivity reported in [93] are plotted in Figure 2.11. It is evident, that at very low temperatures electrical resistivity decreases with increase of temperature. Authors also present, below 10 K there is a $\rho(T)$ dependence for zero applied magnetic field and the compound behaves as a Kondo system. The maximum has not been confirmed below the very low temperature of T = 0.4 K.

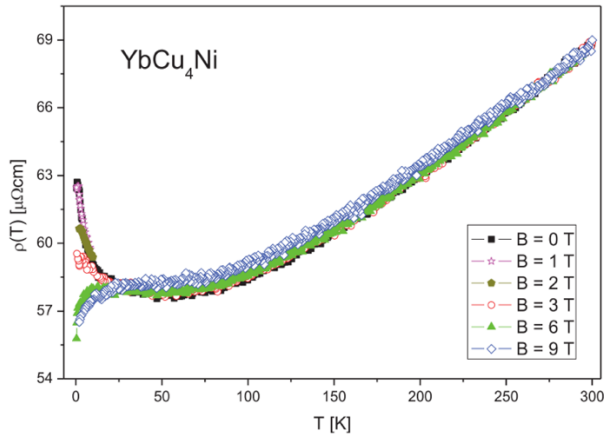

Figure 2.11 Temperature dependence of the electrical resistivity measured in different magnetic fields [93].

Thus, when Cu is substituted in the $YbCu_{5-x}M_x$ system, a curious and attractive physical properties can be found. It depends on the type of M element. Some works have

already been reported [88, 97] and this is one of our motivations for preparing samples, where these properties could arise.

2.5.2 Yb-Pd-In System

Before the Yb-Pd-In ternary system was created, single binary compounds were studied. The first Yb-Pd compound was investigated by Iandelli and Palenzona [98] and the next one by Okamato [99]. The $YbPd_7$ is formed during peritectoid reaction at T = 449 °C (it is also published in the work [100]).

Another binary system, Pd-In, was published by Okamato [101] on the basis of experimental work of Knight and Rhys [102], where six compounds were studied. Four of them showed only one phase. Two of them, Pd_2In and Pd_3In, occurred in a low and a high temperature modification.

The last possible modification of binary system consisting of those elements is Yb-In. Here the two works are reported by Palenzona [103] and McMasters [104]. After research devoted to combination of Yb-based binary compounds, a ternary system was investigated. Only five ternary phases were studied in [105, 106] works, in which the main results were described.

The first study, was the study of ternary phase YbPdIn, which crystallizes in *hP9-ZrNiAl* type structure [105]. The ground state physical properties were measured and published in [107]. Another phase, the tetragonal Yb_2Pd_2In crystallizes in *tP10-*Mo_2FeB_2 structure. A long-range magnetic order down to 0.4 K was not observed. When mechanical pressure is applied, the observation of the system behaviour shows magnetic instability [108]. The monoclinic $Yb_2Pd_6In_{13}$, which crystallizes in *mS42-*$Yb_2Pd_6In_{13}$ was reported by Zaremba et. al [109]. The diamagnetic $YbPdIn_2$ crystallizes in *oS16 –* $MgCuAl_2$ structure and it is described in [110]. The last published paper from this series is about phase of $YbPdIn_4$ with orthorhombic *oS24 –* $YNiAl_4$ type structure. Here, it was concluded, that this compound consists of three-dimensional polyanions and Yb atoms are occupying the distorted pentagonal and hexagonal channels [111].

From the isothermal section of the phase diagram, phase relationships for Yb-Pd-In system at 600 °C is shown in Figure 2.12 in detail. It is evident, that for Pd ≤ 60 at. % the phases YbPdIn, Yb_2Pd_2In, Yb_2Pd_2In, $Yb_2Pd_6In_{13}$, $YbPdIn_2$ and $YbPdIn_4$ phases

suggest the existence of a liquid phase. In Figure 2.12, the dashed lines represent the areas, where the liquid phase is in coexistence with the two solid phases [105]. In this system the punctual phases were found, except $Yb_2Pd_6In_{13}$ from 50 to 53 at. % of In and $Yb_{12}Pd_{15}In_{73}$ from 15 to 25 at. % of In.

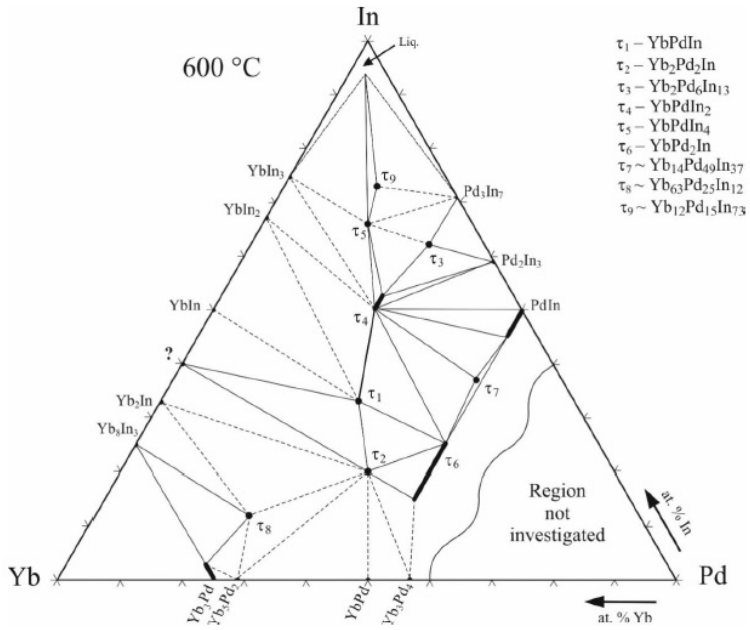

Figure 2.12 Yb-Pd-In system and its phase relationship at 600℃. Hypothetic phase equilibrium is indicated by dotted lines [112].

3 OBJECTIVES OF THE DISSERTATION THESIS

On the based previous study, the main objectives of this PhD. thesis consist of:

1) Preparation and structural characterization of polycrystalline $(RE1_{1-x}RE2_x)Ni_5$ (RE1, RE2 = Ce, Yb, Gd); $YbPd_2In$, $Yb_{0.8}Lu_{0.2}Cu_4Ni$, $Yb_{0.8}Sc_{0.2}Cu_4Ni$, $YbCu_{4.7}Ni_{0.3}$ and $YbCu_{4.2}Ni_{0.8}$.
2) The study of physical properties with the emphasis on competition between the effect of spin fluctuations and the possible existence of quantum criticality.
3) A dimension response of physical properties of $(RE1_{1-x}RE2_x)Ni_5$ (RE = Ce, Gd).
4) The response of chemical pressure on the physical properties of $Yb_{0.8}Lu_{0.2}Cu_4Ni$, $Yb_{0.8}Sc_{0.2}Cu_4Ni$, $YbCu_{4.7}Ni_{0.3}$ and $YbCu_{4.2}Ni_{0.8}$.
5) Ground state study and very low temperatures properties of a new $YbPd_2In$ compound.

The summary of aims is illustrated in the Figure 3.1.

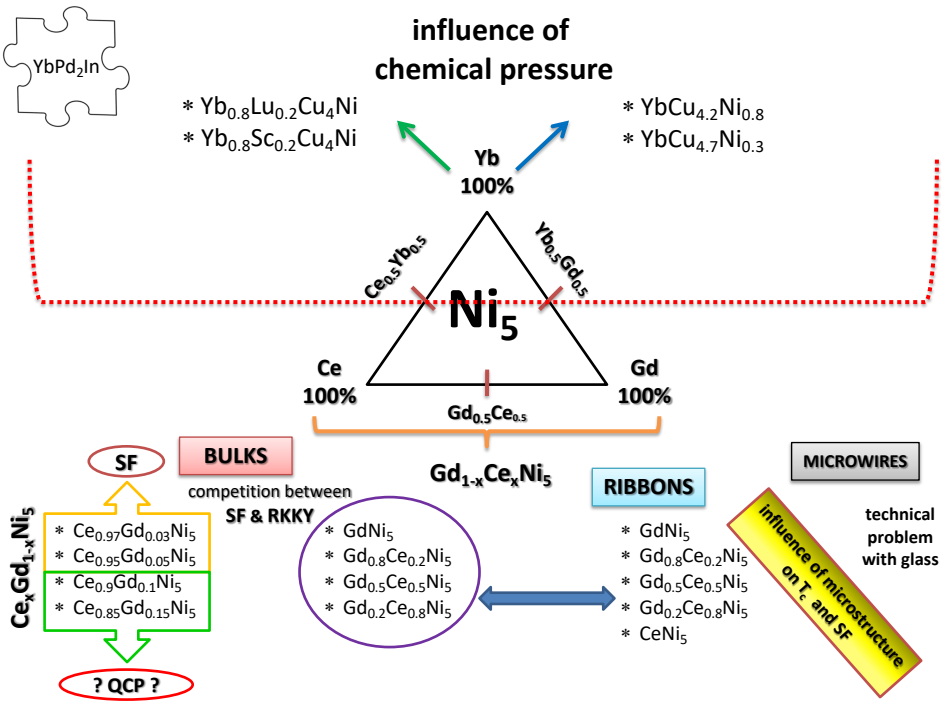

Figure 3.1 Summary of aims.

4 EXPERIMENTAL TECHNIQUES

In this part of the thesis, we will introduce several experimental techniques and procedures, which were used. The section 4.1 deals with preparation methods of studied samples. Other part is about structural and morphological characterization.

4.1 Sample Preparation

Studied samples were prepared in different ways. The effect on the properties of the diverse methods of sample preparation is one of the thesis objectives.

The procedure of sample preparation covers four different steps. The first one is an arc melting, by which bulk samples were obtained. Then a rapid quenching method could be used for ribbons production from the obtained ingot. Inducting furnace is the best solution for preparation of Yb materials because of Yb evaporation. The last method used for production of the glass-coated microwires, has two advantages – it is very fast and it is very suitable for many materials and their practical applications.

4.1.1 Arc Melting

Bulk samples of $RENi_5$ (RE = Ce and Gd) were prepared in two different departments. The first series of materials was made at the University of Cantabria, Spain ($Gd_{1-x}Ce_xNi_5$), while samples, containing more percentage of Ce were prepared at University of Pavol Jozef Šafárik, Slovakia.

First of all, every chemical element was of a high purity (99.999 %). Elements must have been without oxides on the surface to compose the material with no impurities. After that, the starting products were weighted according to the molar amounts.

An arc furnace (Figure 4.1), *Arc Melter MAM-1* includes a chamber, in which, an inert gas atmosphere produced by Ar – 99.99 % exists during a melting process. Inside the chamber - on the top of it, there is an electrode while bottom of the chamber is protected by copper crucible. The cooling is secured by flowing water. Using this technique, polycrystalline sample can be prepared. The maximum mass is 10 g per

fragment, and the melting temperature could reach 3300 °C. This temperature is limited because of cathode. It is made of tungsten and its melting temperature is 3410 °C [113].

Figure 4.1 The arc melter furnace. A detail shows the chamber, where sample is made.

The chamber, where the melting process runs is purged 3 times, to avoid an oxidation of the compounds and subsequently it is evacuated. The pressure of Ar atmosphere is kept at about 0.6 bar. The melting mechanism runs through inert atmosphere. After that, when applying the voltage, the current heats single elements and they are melted together. The melting action is repeated several times, at least 3 times to ensure a homogeneity of sample. The presented technique is exothermic and the prepared ingot usually weight from 1 g up to maximum mass. The obtained product belongs to polycrystalline materials.

4.1.2 High Frequency Induction Melting and Annealing Process

The best process for preparing a sample containing evaporating elements is probably a high frequency induction melting. In this type, the compounds belong to Yb-

based materials, which were prepared for studying an interesting physical problem. Elements are closed and sealed in tantalum crucible as it is shown in Figure 4.2.

Required stoichiometric amounts of metals were sealed in crucible and then situated in a coil, where current was applied during melting process. Due to the Joule heating of magnetic field, created by high frequency, an electric current was induced and the metallic sample got melted. To ensure the homogeneity, the crucible was shaking continuously. This method is also exothermic as arc melting is.

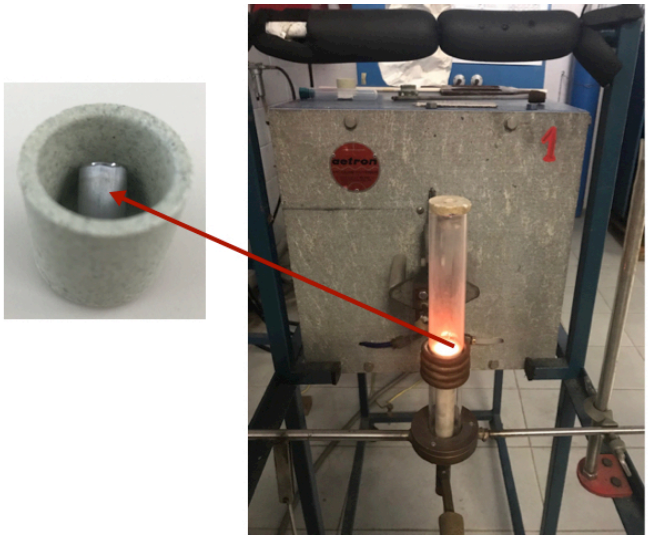

Figure 4.2 An induction furnace during melting procedure. The miniature shows sealed tantalum crucible prepared for melting.

Afterwards, the metallic samples based on Yb were closed into quartz ampule under argon pressure and annealed - the first series - 10 days at 700 °C ($YbNi_5$, $Yb_{0.5}Ce_{0.5}Ni_5$ and $Yb_{0.5}Gd_{0.5}Ni_5$) and the second series in two different periods - 10 days at 700 °C and 11 days at 600°C ($Yb_{0.8}Lu_{0.2}Cu_4Ni$, $Yb_{0.8}Sc_{0.2}Cu_4Ni$, $YbCu_{4.7}Ni_{0.3}$ and $YbCu_{4.2}Ni_{0.8}$).

After that, all the samples were quenched in cold water.

4.1.3 A Rapid Quenching Method

Samples prepared by rapid quenching method usually have a different physical properties in comparison to bulk samples. However, this will be described in next section.

Process starts with incoming bulk having the mass ~ 5g inside the tube and it is located into the thread. Before starting this preparation, a glass crucible is on its top covered with bohrium nitride (BN), which prevent the glass to be in contact with material. A certain alloy is put inside. The distance between copper cylinder and the tube has to be about 2 mm. After that, the chamber is closed, and evacuated. A vacuum pump ensures high vacuum. The next step is filling the chamber with He gas, which makes the atmosphere without oxidation. The tube is located in a high frequency field, created by the induction coil. The intensity of that field can rise by increasing the electrical current. Sample inside the tube is being heated until it starts melting. The melting temperature is observed on pyrometer. As soon as it is possible to see that the sample is a molten liquid, valves open and overpressure from He gas box is created in the tube. Described process causes that melt material is infixing on the rapid rotating copper cylinder. The result is a sample in a ribbon form. It is possible to change the parameter of ribbon by the following ways: the gap distance between copper cylinder and tube opening; the rotation velocity of the copper wheel and overpressure of helium gas. The speed of the quenching method is from10^5 to 10^6 K.s^{-1} [114]. Experimental arrangement is shown in Fig. 4.3.

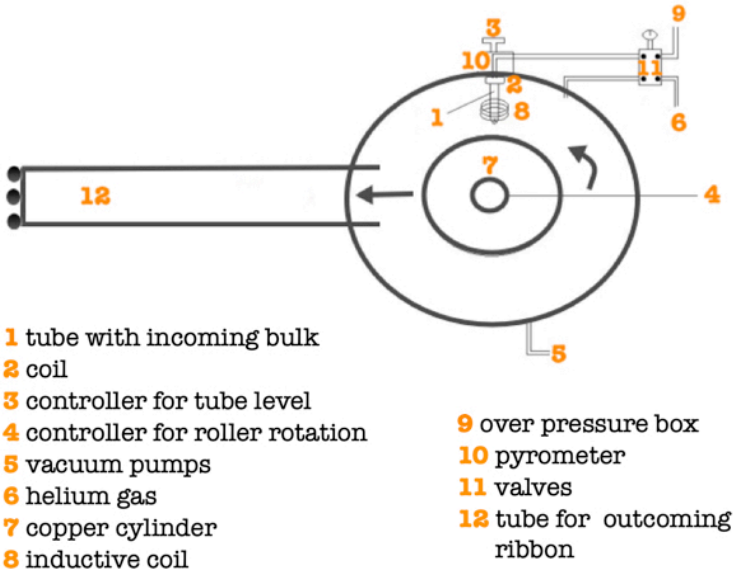

Figure 4.3 Schematic picture for melt spinner with legend.

4.2 Structural Characterization

After the sample preparation, the next step is the structural characterization. By these methods, it is possible to check if the prepared samples have required structures, stoichiometric composition and if other physical analysis can be applied.

4.2.1 X-ray Diffraction

In the field of Material Science, diffraction methods are techniques frequently used for structure characterization of a studied material. When working with crystalline materials, intensity arises at the points of coherent beams. Explained technique is based on scattering of X-ray beam and it is in detail explained in [5]. This effect is described by Bragg's law:

$$2d\sin\theta = n\lambda, \tag{29}$$

where d represents distance between crystallographic planes, θ is the angle of incidence, $n \in Z$ and λ means wavelength [115]. In order to calculate Bragg's law a Bragg's condition (see Figure 4.4) must be fulfilled.

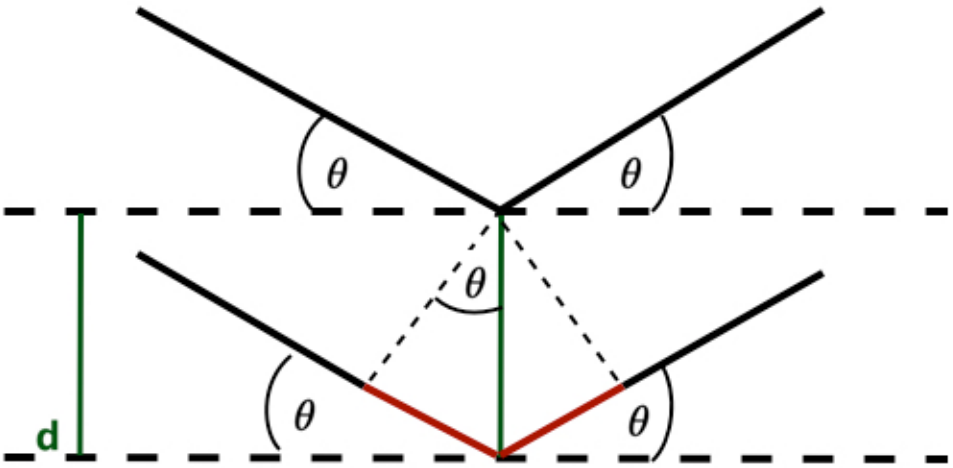

Figure 4.4 Schematic illustration of Bragg's condition.

In the structural analysis, several methods for sample preparation exist to measure the intensity of scattered X-ray beam. For bulk samples, Debye-Scherrer's powder analysis have been chosen. Its specification is explained in the work [116]. From technical point of view a small amount of sample is crushed to powder and installed in the room temperature sample holder, shown in Figure 4.5. For sample fixing, a vaseline or ethanol is used. Ribbon samples have not been prepared as a powder, only one piece of it was installed on the sample holder and fixed there.

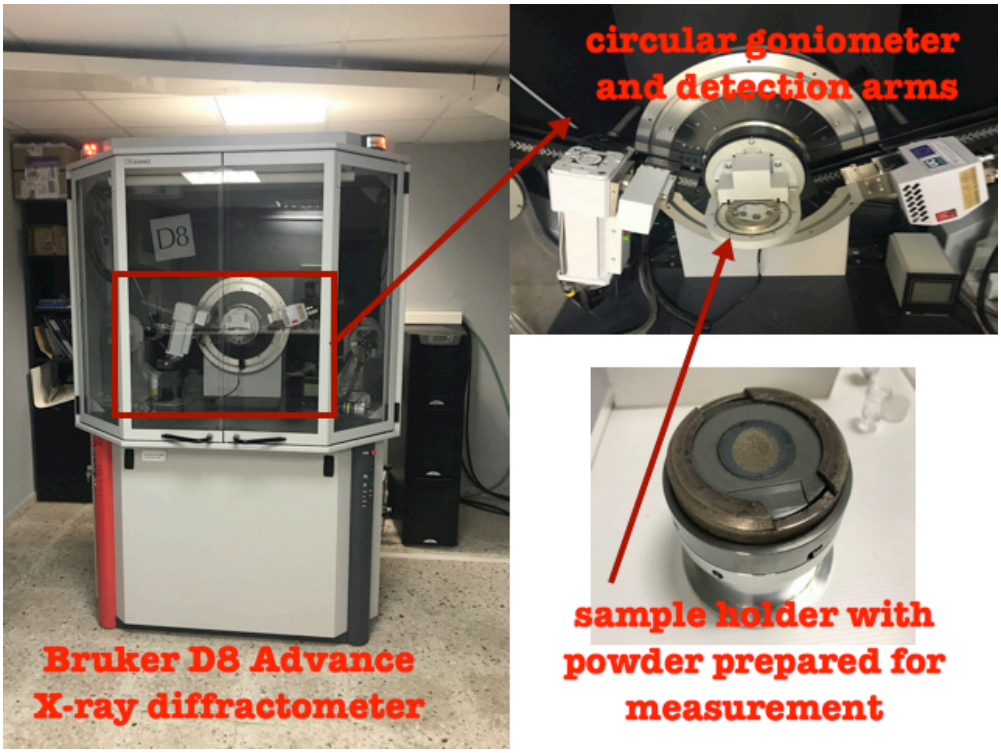

Figure 4.5 Bruker D8 Advance X-ray diffractometer.

In the laboratory of CITIMAC it is possible to measure from 5° to 140° (2θ angle) with a goniometer controlled with steps of $\Delta(\theta) = 0.0005°$. XRD patterns were collected from 20° until 100° of 2θ-angle range with 2θ-angle steps 0.02 and an integration time 0.5s per step with Cu-K_α = 0.7107Å in order to suppress K_β reflections.

In order to determine a crystal structure for samples, FullProf program [117] and PowderCell program have been used and cell parameters were obtained.

4.2.2 Scanning Electron Microscopy

Scanning electron microscopy (SEM) is one of the best techniques to get to know microstructural characteristics of solid states. Used SEM is shown in Figure 4.6 and it is installed at the University of Cantabria, Spain. Its popularity and high usage are caused by a relatively high resolution and quick sample preparation. Using SEM with EDX option, it is available to study the chemical composition and homogeneity of material. When we compare SEM to light microscopy the major difference is that SEM uses electron beams.

Sample for SEM has to be conductive. It is installed into the sample holder and fixed by carbon tape.

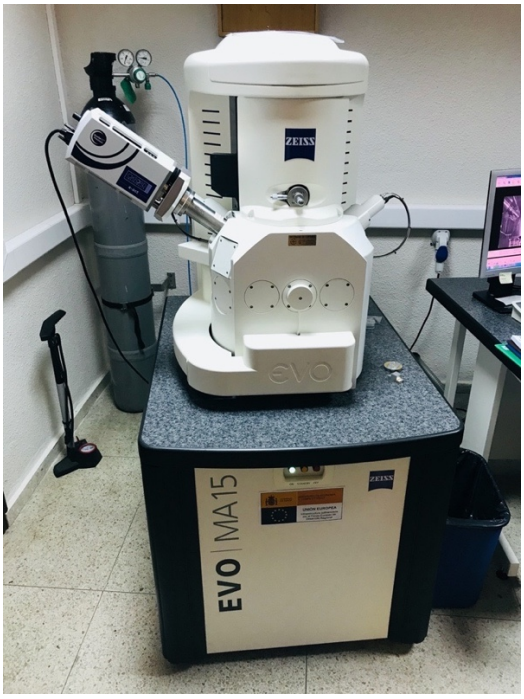

Figure 4.6 Scanning electron microscopy at the UNICAN.

Main structure of SEM consists of: electron beams, magnetic lenses, several detectors and PC, where the output data are shown. Type of signals produced by SEM in a sample are secondary electrons (SE) and backscattered electrons (BSE), which carry an information on sample morphology and its composition. The existing small deviation from real composition is about 2 %.

Detectors of SE and BSE are standard for scanning microscope. During the analysis process, a vacuum ~ 10^{-3} Pa is produced inside of the chamber [116, 118]. The working process of SEM is described Figure 4.7 [119].

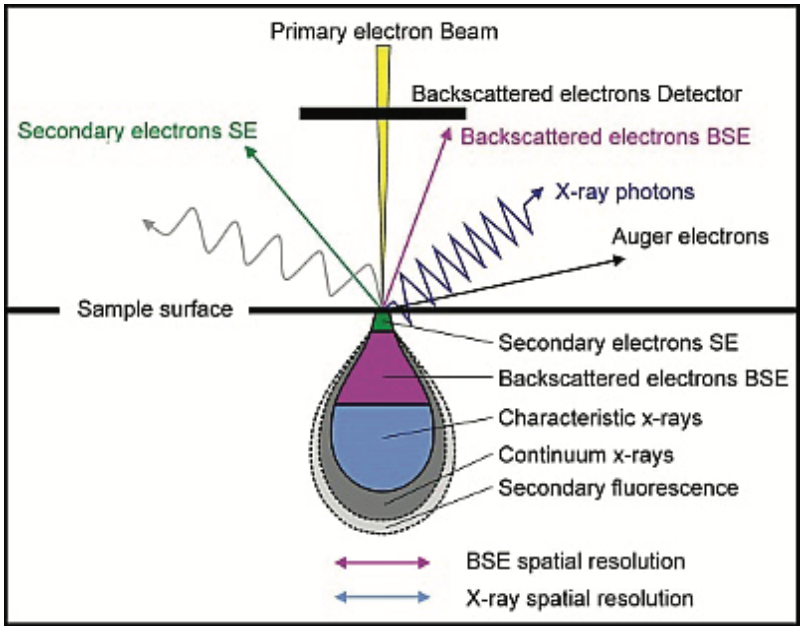

Figure 4.7 Schematic diagram of the interaction for electron beam with sample in SEM [119].

Using SEM, it is possible to study material in several ways. In a general way, it is a detection of SE emitted by atoms of excited electron beam. Number of electrons depends on angle between the primary electron beam and a sample surface. Topography of material is detected through scanning the surface, collecting the secondary electrons and thus creating the picture of sample surface. The second method is based on existing BSE. These electrons have lower energy than the incident electrons [118].

4.3 Experimental Devices for Physical Properties Measurement

One of the most important parts of this thesis are the experimental devices for studying the physical properties. Consequently, analysis and interpretation of the collected data were performed. Measurements were done mostly in Slovakia at the University of Pavol Jozef Šafárik, the University of Prešov and the Slovak Academy of

Sciences in Košice. Experiments on SQUID magnetometer were performed at University of Cantabria in Spain.

4.3.1 The PPMS DynaCool

The PPMS DynaCool (seen in Figure 4.8) belongs to the equipments of Quantum Design company. The measuring temperature range is from 1.8 K to 400 K and applied magnetic field is up to 9 T. The sample holder is installed into 12 pin connectors pre-wired to the system electronics control.

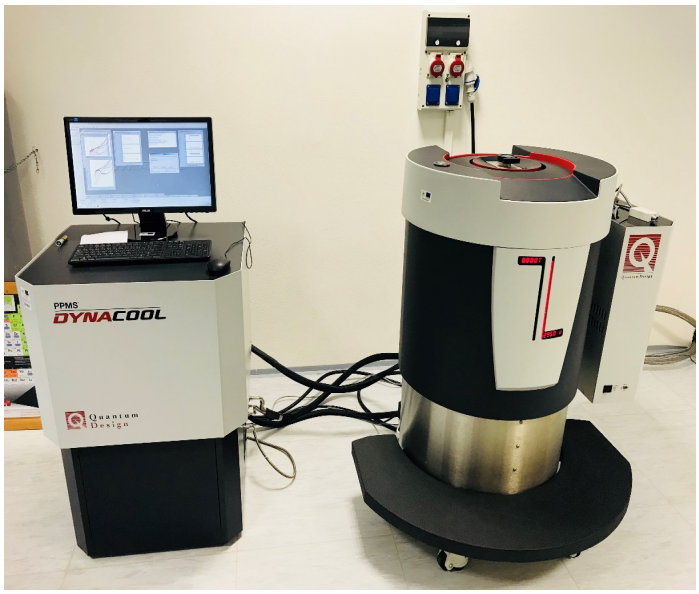

Figure 4.8 The PPMS DynaCool at the University of Prešov, Slovakia.

It is unique from the PPMS family group because of the small required amount of ^{4}He liquid for the cooling process of superconducting magnet and sample chamber. Main principle of cryostat working with individual parts is in detail described in Figure 4.9, where the main components of the control system: cryostat, magnetic field and temperature chamber are presented.

When compared to the more known PPMS device, DynaCool provides the user with all capabilities, as the PPMS does, and its hardware is fully compatible with another Quantum Design devices.

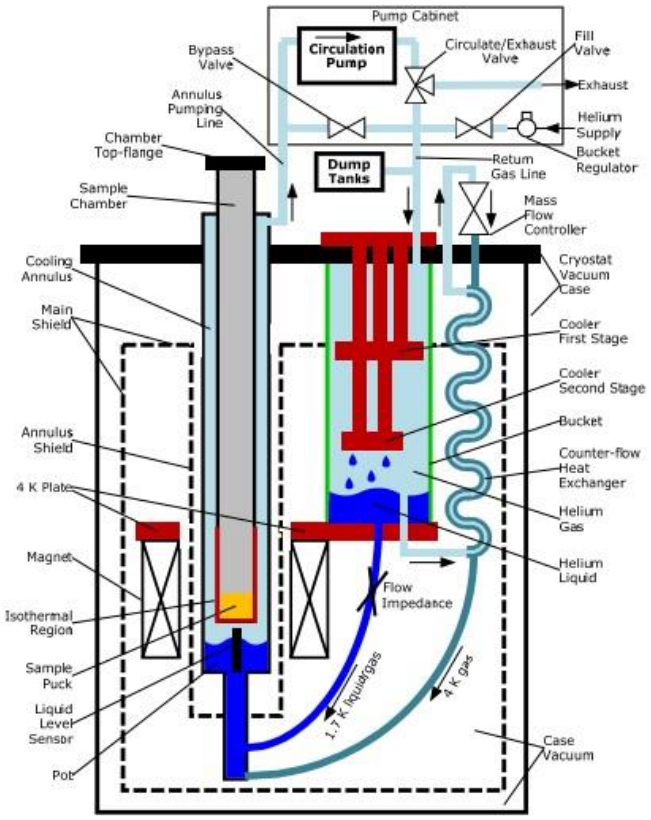

Figure 4.9 Schematic picture of DynaCool cryostat, where individual components are shown [120].

This type of measurement system has different type of options, which will be described in detail in the next section. They are namely:

A. Vibrating Sample Magnetometer (VSM) Option
B. Heat Capacity (HC) Option
C. Electrical Transport Option (ETO)
D. Thermal Transport & Thermopower and Electrical Resistivity Measurements option (TTO)

A. Vibrating Sample Magnetometer (VSM) Option

A very typical procedure for characterizing the magnetic properties of magnetic materials is the study of DC magnetization as a temperature dependence under an applied magnetic field. In general, magnetization is expressed as:

$$M = \frac{dm}{dV} \ [A.m^{-1}], \tag{30}$$

where *dm* express an element of elementary magnetic moment and *dV* represents the volume of material.

The measurement is characterized by the repetition of some sequences, as sample vibration and time detection of flux by induction coil along magnetization of sample. Usually zero field cooling (ZFC) and field cooling (FC) processes are applied. At ZFC procedure a material is cooled down without applied magnetic field. After that, when sample is cooled at low temperature, magnetic field is applied and stays constant during the measurement. The response of material inside of cryostat is recorded as a function of temperature during heating. On the other hand, FC represents a process in which the sample is cooling down under the presence of magnetic field. Here, the response of the system is measured as a function of temperature at constant applied field, during heating or even during subsequent cooling.

The VSM option uses sensitive DC magnetometer with possibility of cooling or heating to desired temperature. Generally, the measurements are provided with use if a pickup coil (oscillating sample) and detect the induced voltage. The oscillation amplitude is relatively large, from 1 to 3 mm, and frequency is of 40 Hz. The system is able to analyse magnetization changes lower than 10^{-6} emu [121].

Mentioned option consists of VSM linear motor transport head. This is where vibrations of the sample come from: electronics for driving the motor and arrestment of the response from the pickup coil and a coil set puck for detection. Through the measurement, a data collection of detection signal in coil (V_{coil}) is done by own software. Detection signal is time dependent and it is described by equation (31), where ϕ represents magnetic flux by the pickup coil, *t* is time and the vertical position respect to the coil is defined as *z*.

$$V_{coil} = \frac{\mathrm{d}\phi}{dt} = \left(\frac{\mathrm{d}\phi}{dz}\frac{\mathrm{d}z}{dt}\right). \tag{31}$$

The position of the sample is sinusoidally oscillating position. It is described by:

$$V_{coil} = 2\pi fCMA \cdot sin(2\pi ft), \tag{32}$$

where C represents coupling, M characterizes DC magnetic moment of a sample, A is amplitude and f means frequency of sinusoidal oscillating signal [122].

Typical scheme for VSM option of DynaCool is presented in

Figure 4.10. The sample position and amplitude of oscillation is controlled by the motor module which uses an optical linear signal. It is read back from VSM linear motor transport. The sample rod is fixed and moves sinusoidally. The signal from the pickup coil is induced by the voltage and then is amplified and lock-in detected in VSM module which uses the position coder signal (comes from VSM linear motor transport) just as a reference for synchronous detection. After that signals are averaged. The last step is sending a message (averaged signals) over the CAN electronics to VSM application, which is running on the PC [121].

VSM option is usually used for the systems with high magnetic moments. This is true for samples containing Gd. For a sample with a lower value of magnetic moment, a SQUID magnetometer is used. It will be described in the next part of the thesis.

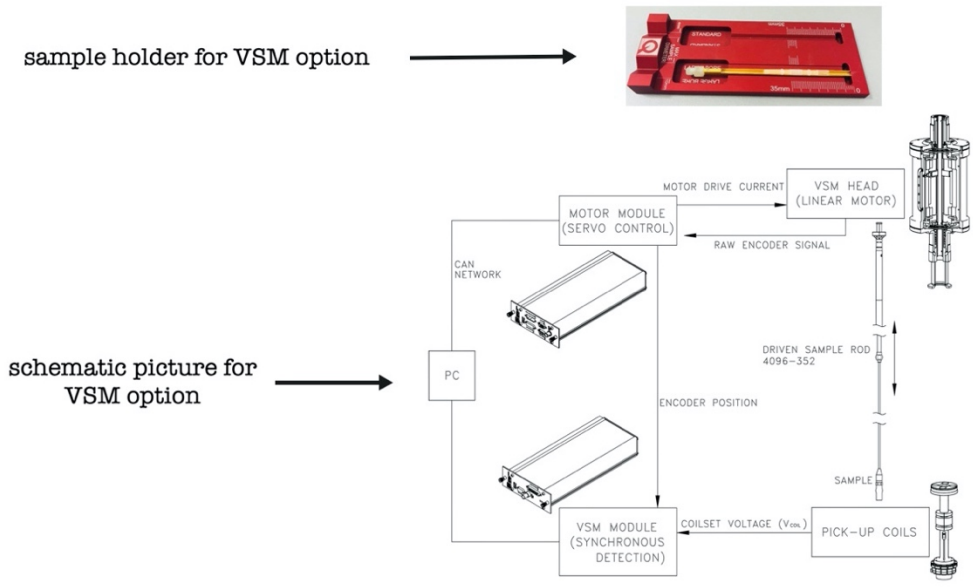

Figure 4.10 Sample holder for VSM option during preparing of measurement. Below it, there is a scheme for VSM option [121].

B. Heat Capacity (HC) Option

Heat capacity measurements give us a lot of information on magnetic and electronic and phonon contribution to the total heat capacity of the studied system. Heat capacity is defined by the following formula:

$$C_p = \left(\frac{\mathrm{dQ}}{dt}\right)_p. \tag{33}$$

An equation expresses the amount of thermal energy which must be added to a system to raise its temperature by 1 K.

From a technical point of view, C_p measurement is possible to provide in two models – simple model (τ) or 2-τ model. The system is self-contained and it chooses working mode on the basis of the thermal contact between the sample and a sample holder. When an equilibrium exists, it uses simple (τ) mode. If there is a heat difference, a 2-τ model is chosen [122]. More details about software work are in [123].

During the heat capacity measurement, PC monitors whole process. On the platform block, there are heater and thermometer connected by wires (see Figure 4.11), which carry an information about heat contact. Sample is fixed by a grease called Apiezon. This grease is responsible for heat contact also. The thermal connection between sample platform and the sample is shown in Figure 4.11.

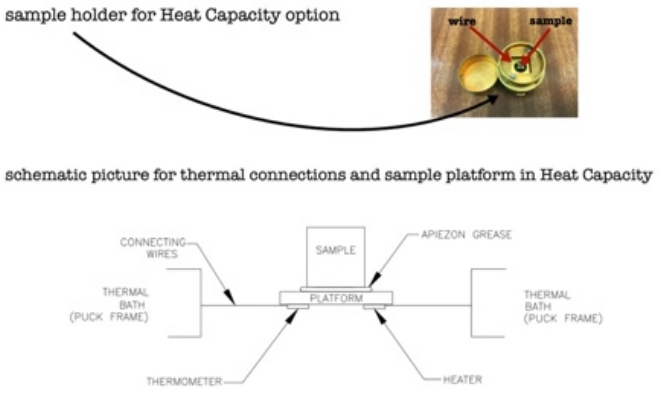

Figure 4.11 Operating scheme for thermal connections between sample and sample platform. Below is illustration for a sample holder.

C. Electrical Transport Option ETO

With measurements of electrical transport, it is possible to obtain the complex information about the nature of the physical properties. Sample is fixed on the special puck (Figure 4.12 (a)), which is covered with insulating layer of tape. On one puck, the electrical resistivity of 3 different samples can be measured independently. The wires (usually Ag wires) are installed in positions for every channel of mounted (Figure 4.12 (b)) voltage (V^+; V^-) and electrical current (I^+; I^-). Used 4-point contact method as a consequence yields to high ratio signal vs. noise [124]. When a puck with sample is prepared, it is electrically insulated inside of cryostat. Following the safety rules is very important because of contacts which are fragile.

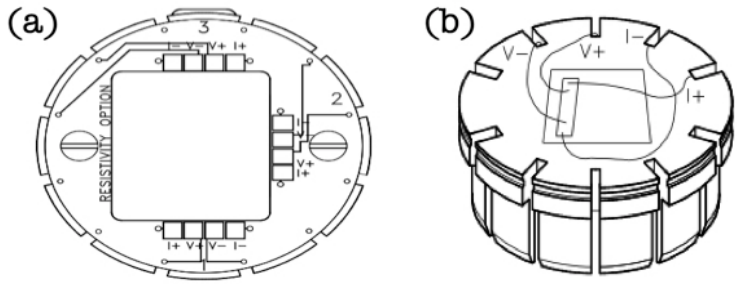

Figure 4.12 (a) Resistivity puck for 3 samples, which can be measured independently. (b) 4-probe technique scheme with sample ready for resistivity measurements [124].

The equation describing relation for electrical resistivity is:

$$\rho = \frac{V \cdot S}{I \cdot l}, \tag{34}$$

where V is the difference between potential contacts on the studied sample, S is cross section area of the sample, I is current and l is the length among voltage contacts. Thermometers on the puck are calibrated.

D. Thermal Transport & Thermopower and Electrical Resistivity Measurements Option (TTO)

To provide a measurement of thermal properties as thermal conductivity (in our case) κ or thermal power α(T) and electrical resistivity ρ(T), one could use the TTO option (see Figure 4.13). Thus it is possible to determine directly the figure of merit $ZT = (\alpha^2)T/\kappa\rho$. The measuring temperature range is 2 - 400 K in the applied magnetic fields 0 - 9 T. The measurements could be done in 2-contact-or 4-contact-technique, where one end is at bath temperature and second end is heated with defined heat flow. The created temperature gradient or voltage difference (depending on the measured physical property) is measured via 2 contacts. The used technique is steady state heat flow.

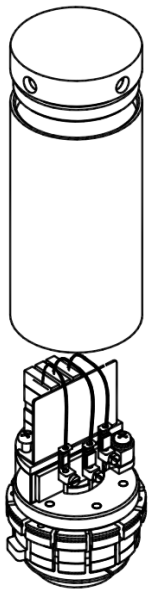

Figure 4.13 Thermal transport sample puck [125].

4.3.2 SQUID Magnetometer

As it was mentioned in the subchapter 4.3.1 A, for materials, which have lower magnetic moment, a different method for magnetic properties study is necessary. The physical principle is very similar as in VSM. SQUID magnetometer (Superconducting Quantum Interference Device) consists of superconducting coil with two parallel

Josephson junctions illustrated in detail in Figure 4.14. DC SQUID measures voltage oscillations while the magnetic flux is being changed. Continuous counting of oscillations allows us to evaluate the appeared flux change. The superconducting magnet works when the low temperatures are present and He liquid is necessary [126].

Preparation of the sample involves closing material into a capsule and putting it in straw and placing into the SQUID sensor on a carbon fiber sample rod.

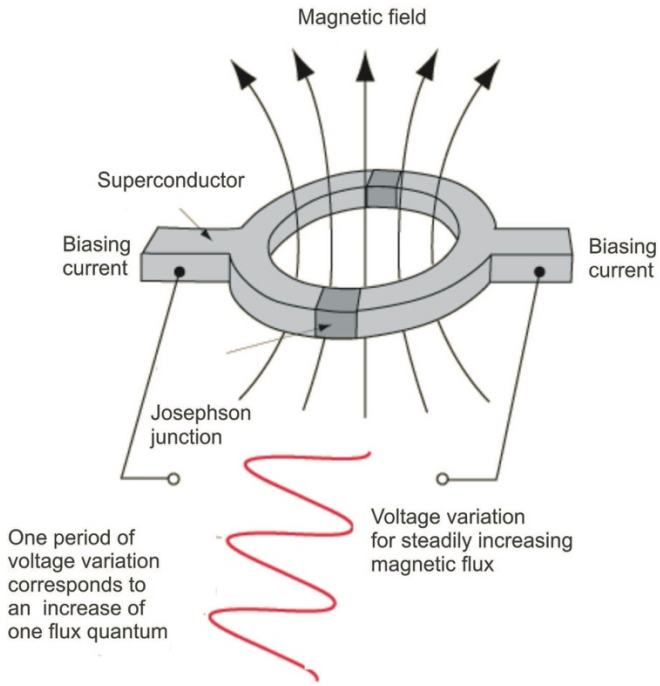

Figure 4.14 SQUID principle illustration [126].

For measurements under the pressure, SQUID magnetometer is one of the best choices. High-pressure technique offers the study of another variable magnetic state and modified structure. In this work, we used pressure cell – Easylab Mcell 10, which uses piston-cylinder cell.

Pressure cell – EasyLab Mcell 10

This system allows the use of hydrostatic pressure up to 1 GPa. A very important things is, that it can be used in the low temperature range (T = 1.8 K). This plays an important role to changing physical properties in rare-earth systems based on Yb or Ce.

Working idea is simple. The piston is getting tightened and therefore the screws rotate. In this manner the creating force is transmitted to the hydrostatic liquid through bits, which are made of ceramics. Material is inserted into capsule (capsule is made of teflon). The pressure is detected by a Sn piece, which is inside the teflon capsule. After that, the capsule is closed and inserted into the Be-Cu cylinder. The cell is closed with copper disk, pistons and ceramic plugs. The prepared pressure cell is shown in Figure 4.15(a). The pressure is applied by external hydraulic system (Figure 4.15(b)). The initial value of the pressure can be estimated by the pressure shown in manometer, the increase of the cell diameter and the number of turns on the top nut. The final (and real) pressure is calculated from the temperature of the Sn superconducting transition using an equation, which will be described in the experimental parts [127, 128].

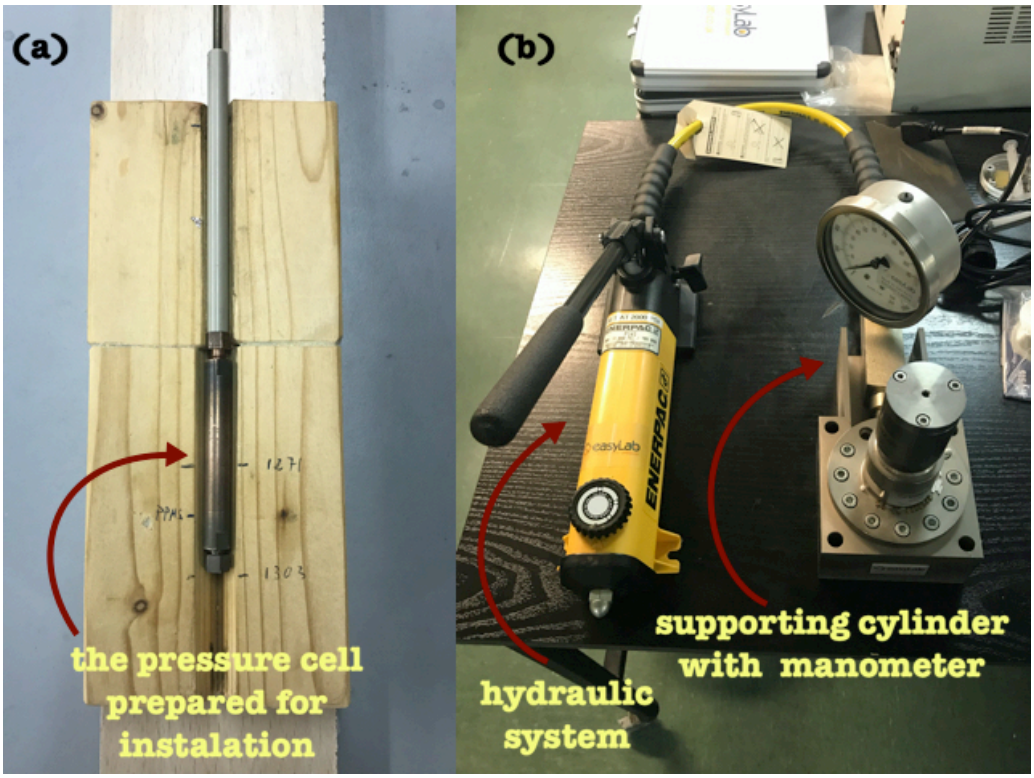

Figure 4.15 (a) EasyLab Mcell 10 - the pressure cell prepared for installation to SQUID. (b) Hydraulic system and supporting cylinder. Pressure system is located at the University of Cantabria, Santander.

4.3.3 The Physical Property Measurement System – ^{3}He Option

The PPMS ^{3}He option was used for measurements in a very low temperature range down to to 0.4 K. ^{3}Helium system is integrated into PPMS based platform. From detailed description of DynaCool follows that it is the cryogen free version of the PPMS. Because of this, it is not necessary to describe it here again. This option is compatible with PPMS AC transport, Resistivity and Heat capacity options. For the needs of this work, Heat capacity and Resistivity options were used. The sample for Heat capacity or Resistivity is prepared in the same way as it is in arrangement into a DynaCool. When a sample is installed on the ^{3}He, the next step is to insert it in the PPMS chamber. The temperature is controlled totally automatically with using the software for ^{4}He refrigerator [129].

The cooling process down to 0.4 K runs through by ^{3}He liquid pumping. The operating scheme is in Figure 4.16. The power cooling for condensed ^{3}He is given by the cold walls in the PPMS chamber. For cooling, it is necessary to lower the pressure. It is provided by turbo pumps. The sample chamber is thermally isolated keeping the sealing and the high vacuum system is safety provided by PPMS High Vacuum System. With the use of a small capillary, the continuous cooling process runs below 0.5 K.

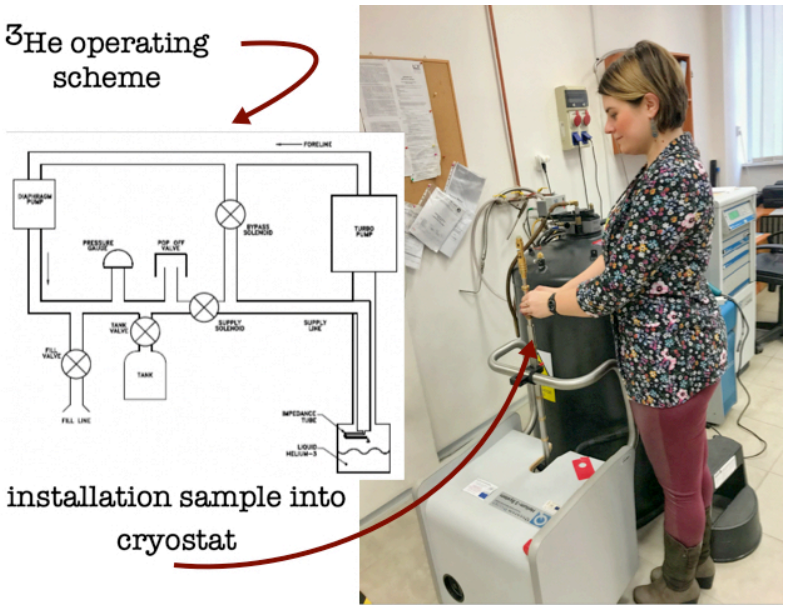

Figure 4.16 On the left - schematic picture for Helium-3 option. On the right, there is a process of sample installation into the PPMS chamber. PPMS is located in a laboratory shared by the University of Pavol Jozef Šafárik, Košice and the Institute of Experimental Physics SAS.

4.3.4 Triton - The ^{3}He-^{4}He Refrigerator

A very interesting in a condensed matter physics is the study of physical properties in millikelvin temperature range. In this work, we used cryogen free dilution ^{3}He -^{4}He refrigerator TRITON. It is installed in a laboratory of the Institute of Experimental Physics of Slovak Academy of Sciences in Košice. It is illustrated in Figure 4.17. Operational principle is explained in e. g. [130].

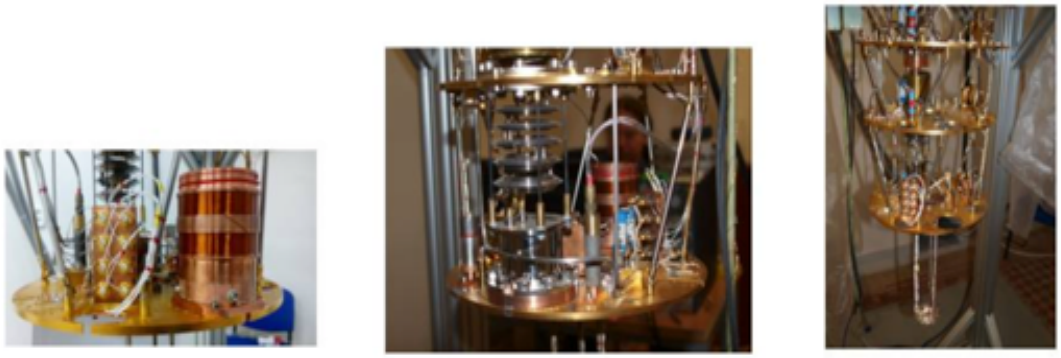

Figure 4.17 ^{3}He – ^{4}He dilution refrigerator belongs the Institute of Experimental Physics of Slovak Academy of Sciences in Košice, Slovakia [131].

TRITON consists of superconducting magnet, calibration thermometers and space for sample mounting. Working range for magnet is up to 8 T and for temperature from 0.01 K to 1 K. Software is analogous to other experimental devices running automatically. Moreover, ^{3}He – ^{4}He dilution refrigerator is compatible with specialised low eddy current design and piezo nanopositioning stage. A very important property of TRITON is low vibration. It is due to isolated coldhead in this system on the top and intermediate plate and also 4 K stage [131].

5 EXPERIMENTAL RESULTS AND DISCUSSION

This chapter of the thesis deals with the experimental data obtained during our research and their analysis. The samples were prepared in a polycrystalline form. After the preparation process, the samples were characterized by several analyses. Results are shown and discussed in this part.

The following systems have been prepared and studied:

1. bulk samples of $Gd_{1-x}Ce_xNi_5$ system, where x = 0; 0.2; 0.5 and 0.8.
2. ribbon samples of $Gd_{1-x}Ce_xNi_5$ system, where x = 0; 0.2; 0.5; 0.8 and 1.
3. bulk samples of $(Ce,Gd)Ni_5$ system.
4. bulk samples based on Yb.

The metals, which have been used as starting materials were namely: cerium (Ce) (pieces, 99.99 %); gadolinium (Gd) (pieces, 99.95 %); ytterbium (Yb) (pieces, 99.9 %); nickel (Ni) of two types (pieces and foil, 99.9 %); copper (Cu) (pieces, 99.9 %); scandium (Sc) (pieces, 99.9 %); lutecium (Lu) (pieces, 99.9 %); palladium (Pd) (foil, 99.95 %) and indium (bar 99.999 %).

The total weight of the samples varies from 1.2 g for $YbPd_2In$ and Yb-based samples through 2 g for $Gd_{1-x}Ce_xNi_5$ system up to 5 g for samples concerning $(Ce,Gd)Ni_5$ system. In Figure 5.1 the characteristic irregular shape of prepared ribbon is shown. Samples are very fragiles.

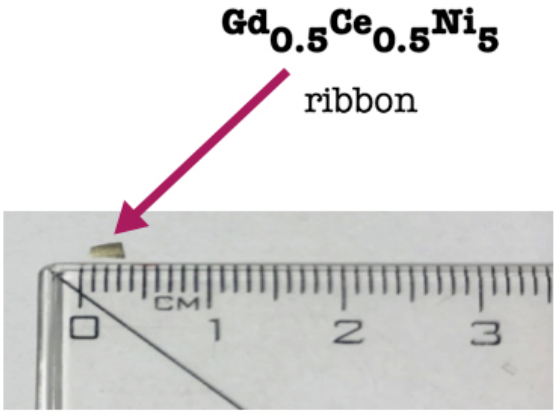

Figure 5.1 Ribbon next to the ruler.

5.1 Bulk Samples of $Gd_{1-x}Ce_xNi_5$ (x = 0; 0.2; 0.5 and 0.8) system

The polycrystalline samples of $Gd_{1-x}Ce_xNi_5$ system, where x = 0; 0.2; 0.5 and 0.8, have been prepared by arc melting method. Their total weight of each sample reached 2 g. The weight losses during the preparation were very low. The obtained results are described in this part of the thesis.

5.1.1 X-Ray Diffraction

Rietveld refinement of $Gd_{1-x}Ce_xNi_5$ system is plotted in the Figure 5.2. The indexed reflections refer to the hexagonal $CaCu_5$ type structure (see in Figure 2.5) with *P6/mmm* space group. Therefore, the Vegard's law [132] can be applied and it is shown in the Figure 5.3.

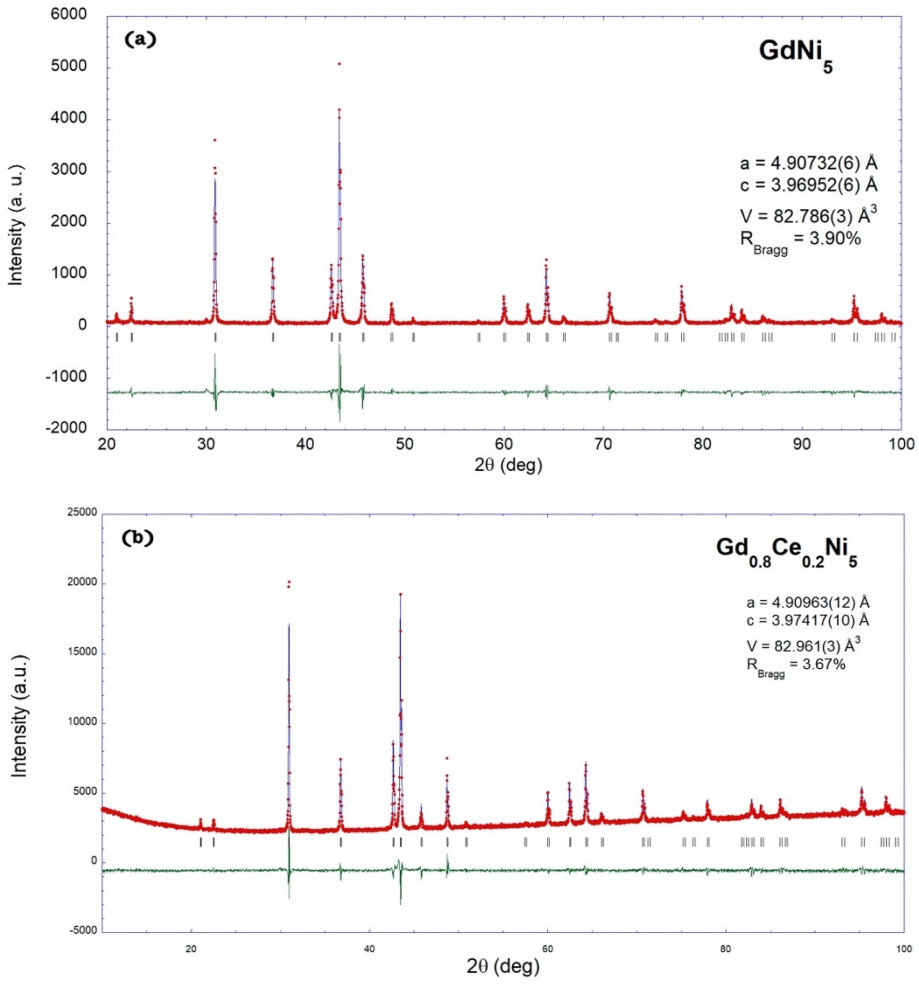

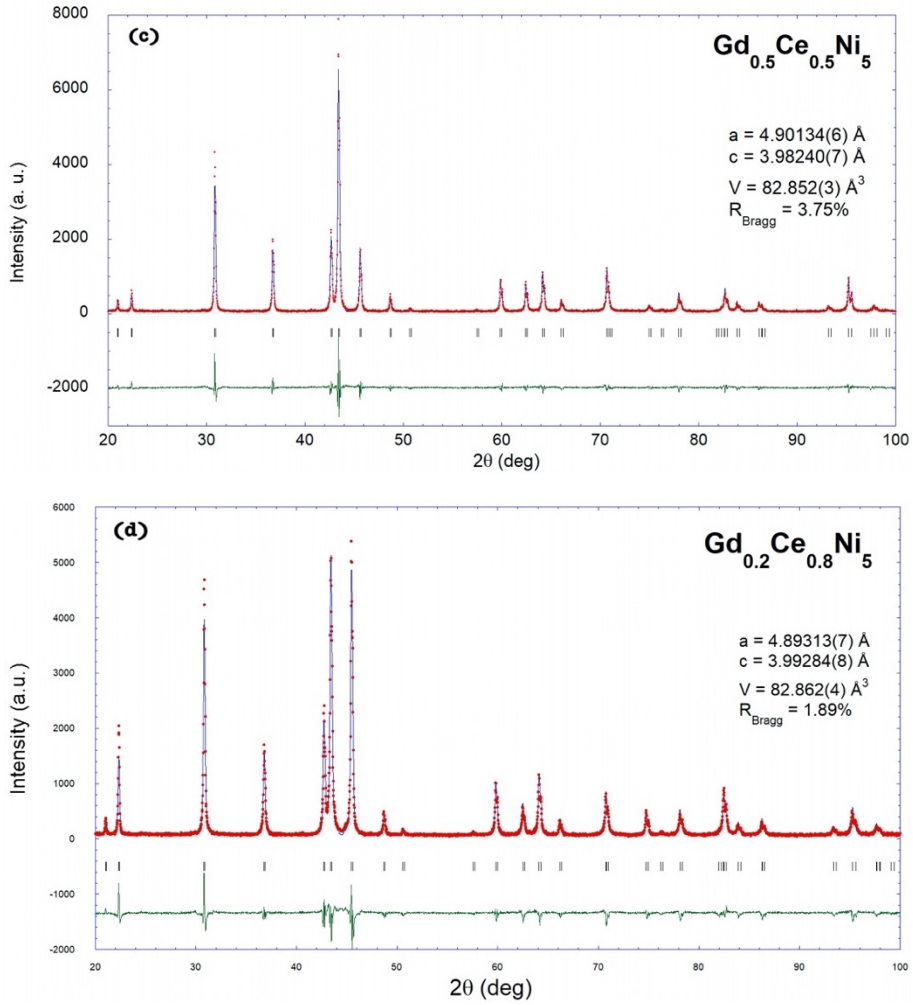

Figure 5.2 Rietveld refinement for bulk samples of $Gd_{1-x}Ce_xNi_5$ system. (a) $GdNi_5$ and obtained cell parameters; (b) $Gd_{0.8}Ce_{0.2}Ni_5$ and obtained cell parameters; (c) $Gd_{0.5}Ce_{0.5}Ni_5$ and obtained cell parameters; (d) $Gd_{0.2}Ce_{0.8}Ni_5$ and obtained parameters.

XRD data were collected at room temperature. The red circles represent the observed data. The blue line is a Rietveld fit of the data. The green line at the bottom of the figure is the difference between the fit and the data. The black vertical lines represent the Bragg positions. The results showed only a small decrease of *a* parameter and increase of *c* parameter with increase of Ce content, what has already been published [133]. This is caused by the fact, that the cell values (*a*) for $GdNi_5$ are slightly bigger than $CeNi_5$. The data for $GdNi_5$ are in agreement with previous study [79, 134-136]. The summarized and rounded values of cell parameters are shown in the Table 2.

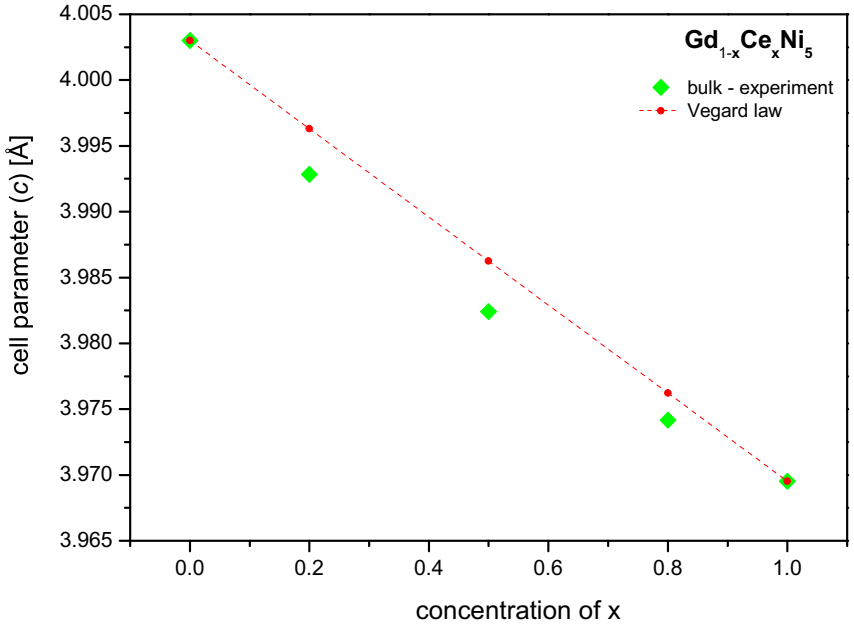

Figure 5.3 The comparison of Vegard's law (red symbols) and obtained experimental data (green symbols) for bulk compounds of $Gd_{1-x}Ce_xNi_5$ system.

Table 2 Summary of experimental values of parameters of bulk samples of $Gd_{1-x}Ce_xNi_5$ system.

$Gd_{1-x}Ce_xNi_5$ bulk	x = 0	x = 0.2	x = 0.5	x = 0.8
a [Å]	4.90732	4.90963	4.90134	4.8913
c [Å]	3.96952	3.97417	3.9824	3.99284
V [Å^3]	82.786	82.961	82.852	82.791

5.1.2 Electron Microscopy

Using the electron microscopy techniques, it is possible to provide a microstructural analysis and then to confirm or disconfirm the nominal composition of prepared samples. The first results are plotted in the Figure 5.4. One can see, that the surface structure is different. $GdNi_5$ looks like porous material, while samples consisting

of only a small amount of Ce, have totally different surfaces. On the other hand, surfaces of $Gd_{0.5}Ce_{0.5}Ni_5$ and $Gd_{0.2}Ce_{0.8}Ni_5$ are in a shape of a cascade, but $Gd_{0.8}Ce_{0.2}Ni_5$ surface is smooth. The photos from SEM and EDX analysis of samples, consisting of more Ce are shown in Figure 5.5.

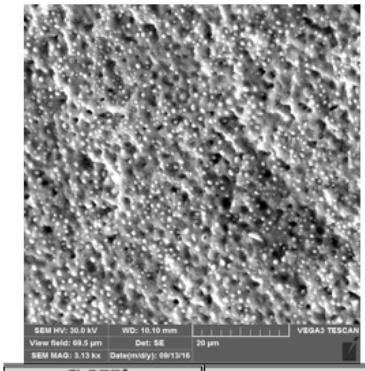

$GdNi_5$ bulk	Atomic %
Gd	16.54
Ni	83.46
TOTAL	100.00

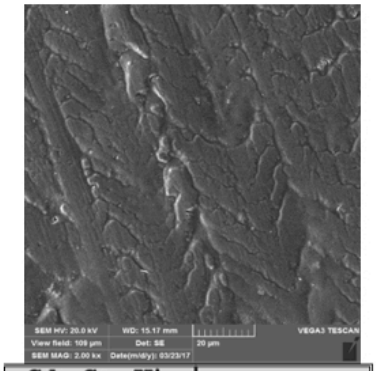

$Gd_{0.8}Ce_{0.2}Ni_5$ bulk	Atomic %
Gd	12.66
Ce	3.79
Ni	83.55
TOTAL	100.00

Figure 5.4 SEM photos and obtained compositions of polycrystalline samples $GdNi_5$ (on the left) and $Gd_{0.8}Ce_{0.2}Ni_5$ (on the right).

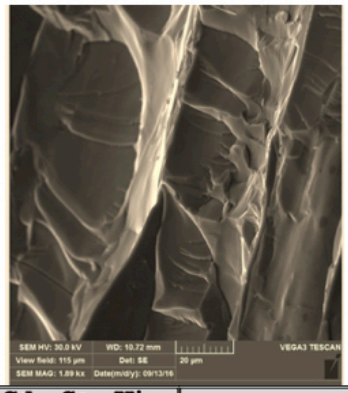

$Gd_{0.5}Ce_{0.5}Ni_5$ bulk	Atomic %
Gd	8.27
Ce	7.79
Ni	83.94
TOTAL	100.00

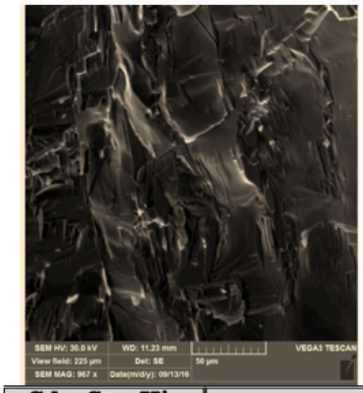

$Gd_{0.2}Ce_{0.8}Ni_5$ bulk	Atomic %
Gd	3.03
Ce	11.19
Ni	85.78
TOTAL	100.00

Figure 5.5 SEM photos and obtained compositions of polycrystalline samples $Gd_{0.5}Ce_{0.5}Ni_5$ (on the left) and $Gd_{0.2}Ce_{0.8}Ni_5$ (on the right).

Based on the EDX analysis, it is possible to conclude that all already confirmed compositions of all samples belonging to the studied $Gd_{1-x}Ce_xNi_5$ system were obtained. It is not possible to compare these results with literature because the SEM images have not been published before.

5.1.3 Magnetic Measurements

The magnetic measurements were done by DynaCool system installed at the University of the Prešov, described in detail in chapter 4.3.1. The series of magnetic measurements has been performed in a temperature range from 2 K up to 300 K and in the applied magnetic fields up to 9 T.

Figure 5.6 presents the temperature dependence of magnetization in ZFC-FC regime for $GdNi_5$ compound. When small magnetic fields were applied, a maximum with a small hysteresis is present at transition temperature. High magnetic fields smear the maximum as it is shown in this picture.

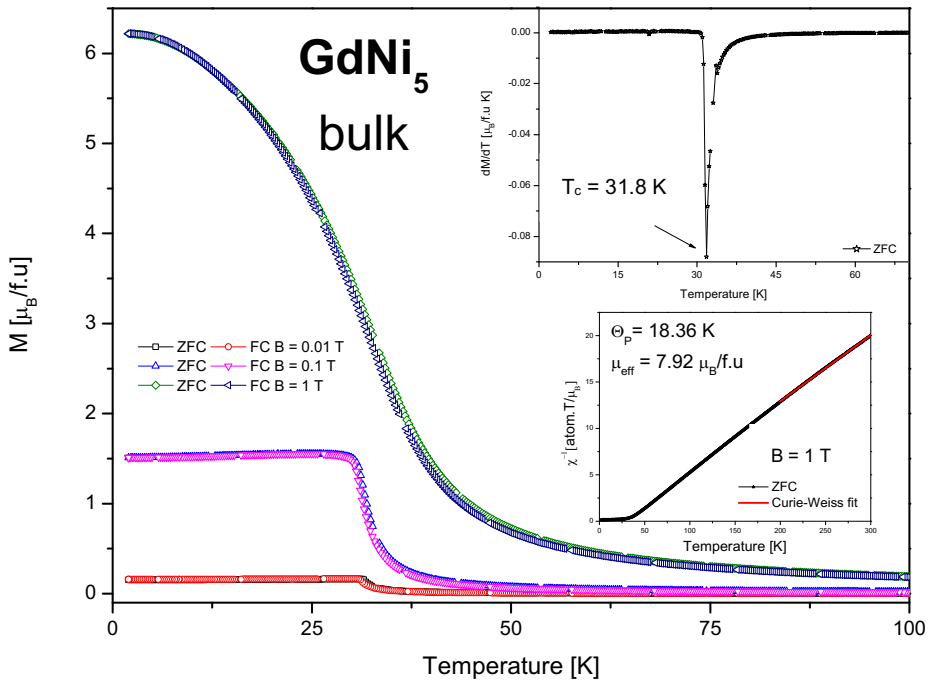

Figure 5.6 The temperature dependence of ZFC-FC magnetization at three different applied magnetic fields for $GdNi_5$. The inset (up) shows the dM/dT with calculation of T_c. The inset (down) shows, the inverse of the magnetic susceptibility fitted to a CW law.

Results show, that the critical temperature is 31.8 K and the behaviour is typical for ferromagnetic ordering. This agrees with previous study [79, 133, 134]. The inverse of the magnetic susceptibility follows a Curie-Weiss law in a high temperature region. From the fitting of $1/\chi$ it is possible to obtain the paramagnetic Curie temperature θ_P and the effective paramagnetic moment μ_{eff}. The positive value of paramagnetic Curie temperature supports the fact that $GdNi_5$ is a ferromagnet. Effective paramagnetic moment is of 7.92 μ_B/f.u, what is very close to the theoretical value for Gd^{3+} ion (7.94 μ_B/f.u).

In order to fulfil the aim of this work, we prepared samples containing Ce and we did measurements of magnetic properties. The similar trends for ZFC – FC measurements were observed just as in the previous samples. The applied magnetic field changes the position for maximum, even magnetic field $B = 1$ T smears it. This is plotted in the Figure 5.7.

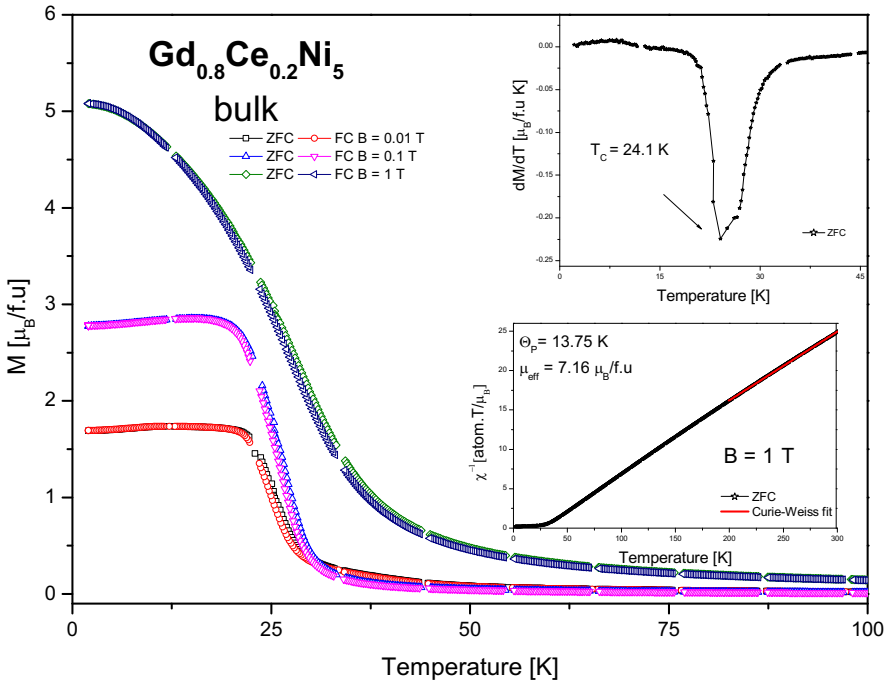

Figure 5.7 The temperature dependence of ZFC-FC magnetization at three different applied magnetic fields for $Gd_{0.8}Ce_{0.2}Ni_5$. The inset (up) shows the dM/dT with calculation of T_c. The inset (down) shows, the inverse of the magnetic susceptibility fitted to a CW law.

Transition temperature for $Gd_{0.8}Ce_{0.2}Ni_5$ is 29.1 K, what is in agreement with expectation, when the 20 % of Ce is implemented. This is caused by Ce properties. Calculated parameter θ_P is still positive, what is typical for ferromagnetic compounds. Effective paramagnetic moment is a little bit lower (7.16 μ_B/f.u) in regard to Gd^{3+}. In fact, it gives sense because of the presence of Ce atoms.

The concentration, where Gd and Ce has an equivalent representation, gives the following results (see Figure 5.8). Figure 5.8. For *M(T)*, a shoulder, corresponding with a transition temperature (T = 20.9 K) is present at B = 0.01 T, 0.1 T. For B = 1 T, no shoulder is visible.

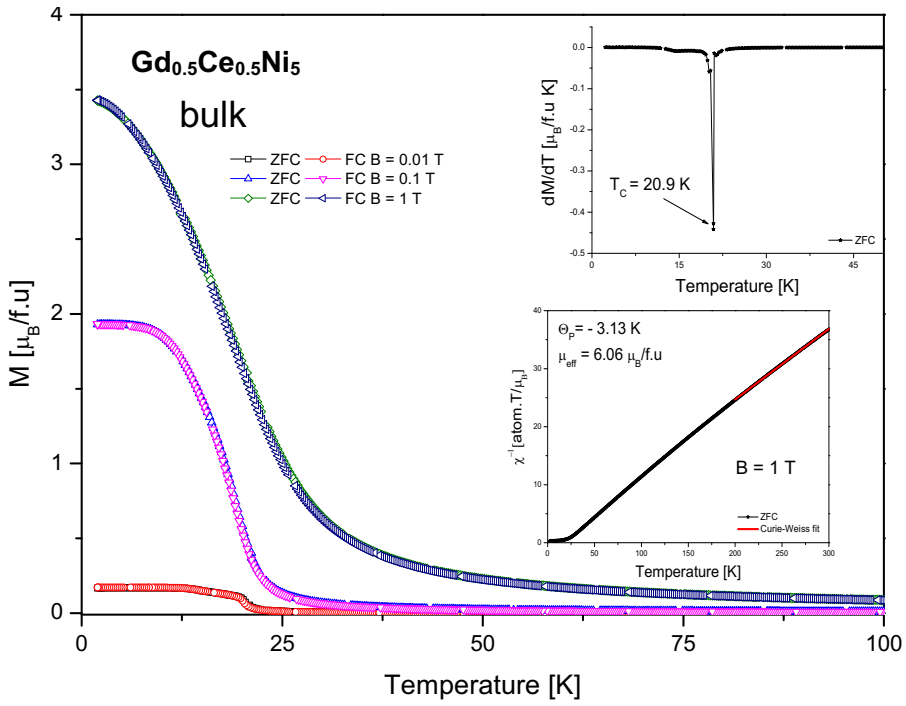

Figure 5.8 The temperature dependence of ZFC-FC magnetization at three different applied magnetic fields for $Gd_{0.5}Ce_{0.5}Ni_5$. The inset (up) shows the dM/dT with calculation of T_c. The inset (down) shows, the inverse of the magnetic susceptibility fitted to a CW law.

The situation is different, when the calculation for the paramagnetic Curie temperature is done. It is negative, which means that antiferromagnetic interaction starts

to dominate. Effective paramagnetic moment still decreases and for the $Gd_{0.5}Ce_{0.5}Ni_5$ is of 6.06 μ_B/f.u.

The last sample prepared in this group is $Gd_{0.2}Ce_{0.8}Ni_5$. Its experimental data are presented in the

Figure 5.9. Here, B = 0.1 T is just enough for smoothing the shoulder at $M(T)$. The ordering temperature markedly diminished, what is connected with physical properties of $CeNi_5$. An effective paramagnetic moment is negative. This indicates an antiferromagnetic interaction as in the previous sample.

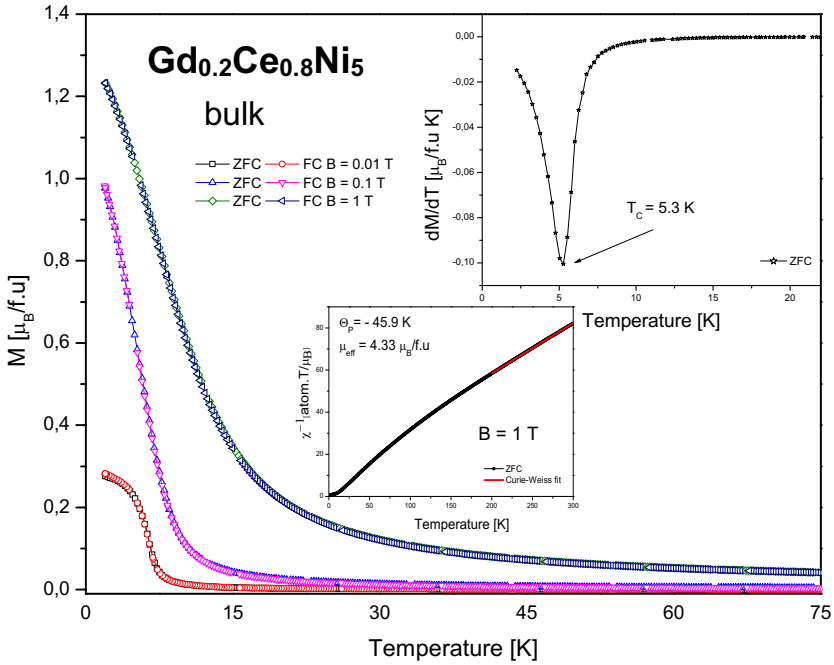

Figure 5.9 The temperature dependence of ZFC-FC magnetization at three different applied magnetic fields for $Gd_{0.2}Ce_{0.8}Ni_5$. The inset (up) shows the dM/dT with calculation of T_c. The inset (down) shows, the inverse of the magnetic susceptibility fitted to a CW law.

The Ce influence on the magnetization as a function of the applied magnetic field at different temperatures is shown in Figure 5.10. The isothermal magnetization curves as a function of magnetic field at T = 2 K are compared in Figure 5.11. However, no

maximum in the magnetic susceptibility at about 100 K, which could be connected with spin fluctuations effect was observed.

In $GdNi_5$, the value of saturation magnetization is in an agreement with the previous data [79, 136]. Generally, the saturation magnetization decreases with increasing Ce content. This fact could be explained as a result of substitution Gd/Ce. Ce has a lower contribution to total magnetization than Gd does have.

Table 3, presents the results of μ_{eff} and M_{SAT}. Increasing content of Ce decreases the value of M_{SAT}. However, the calculations taking the free ion values of Ce^{+3} and Gd^{+3} into account, gives the higher values than the experiment. In case of $CeNi_5$ there is no magnetic ordering and M_{SAT} does not exist. The possible explanation is that there are the non-magnetic Ce^{4+} ions in some positions presented. Experimentally determined valency of $CeNi_5$ varied from 3 to 3.5 [137].

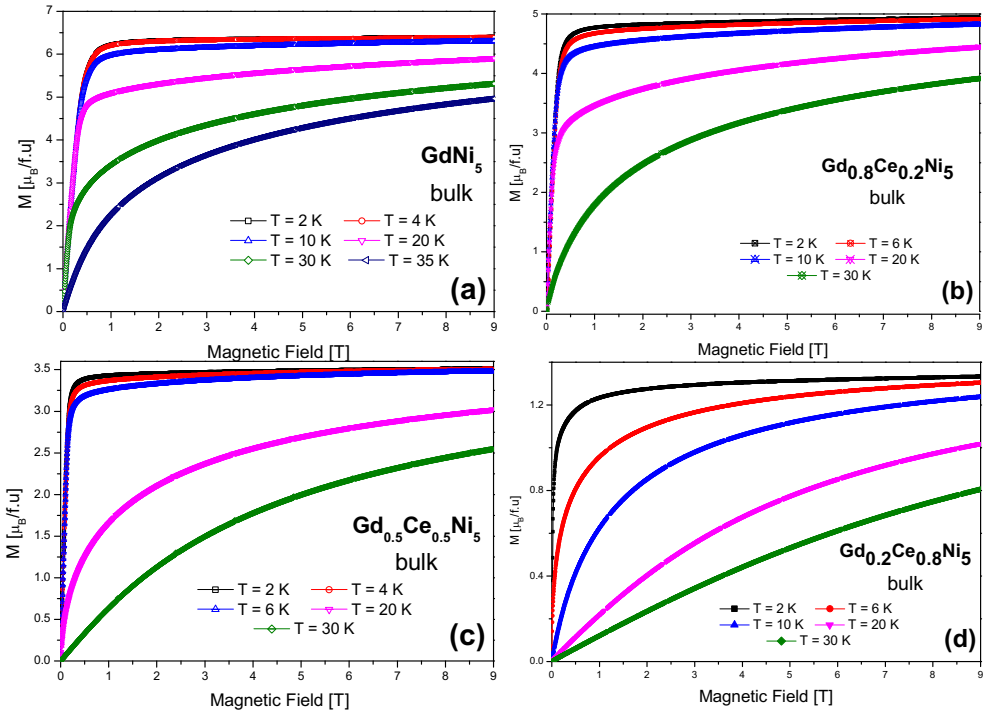

Figure 5.10 Isothermal magnetization as a function of magnetic fields for $Gd_{1-x}Ce_xNi_5$ (0; 0.2; 0.5 and 0.8) system at different temperatures.

Moreover, B_{SAT} is decreasing with Ce content, which could be connected with the shape anisotropy (see in Figure 5.11). From magnetic results we can conclude, that bulk samples are isotropic.

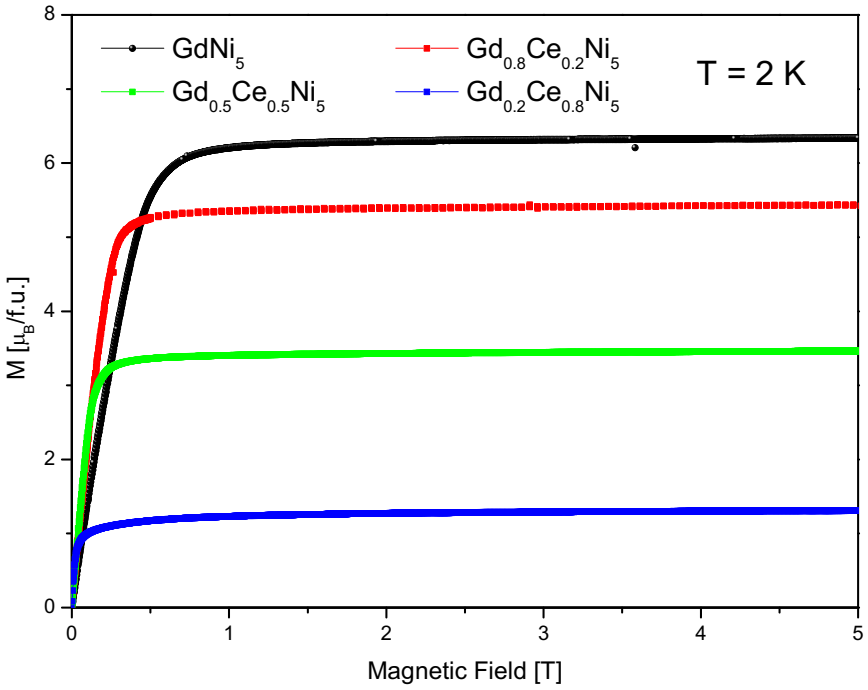

Figure 5.11 Characteristic behaviour of magnetic field dependence at T = 2 K of magnetization for $Gd_{1-x}Ce_xNi_5$ [133].

Table 3 The results of μ_{eff} and M_{SAT} of $Gd_{1-x}Ce_xNi_5$ system.

$Gd_{1-x}Ce_xNi_5$	x = 0	x = 0.2	x = 0.5	x = 0.8
EFFECTIVE MAGNETIC MOMENT Gd^{3+} = 7.94 μ_B and Ce^{3+} = 2.54 μ_B; Ce^{4+} = 0 μ_B				
theory	μ_{eff} = 7.94 μ_B/f.u.	μ_{eff} = 6.86 μ_B/f.u.	μ_{eff} = 5.24 μ_B/f.u.	μ_{eff} = 3.62 μ_B/f.u.
experiment	μ_{eff} = 7.92 μ_B/f.u.	μ_{eff} =7.16 μ_B/f.u.	μ_{eff} = 6.06 μ_B/f.u.	μ_{eff} = 4.33 μ_B/f.u.
SATURATION MAGNETIZATION M_{SAT} for B = 9 T Gd^{3+} = 7 μ_B and Ce^{3+} = 2.14 μ_B; Ce^{4+} = 0 μ_B				
theory	M_{SAT} = 7	M_{SAT} = 5.588	M_{SAT} = 5.865	M_{SAT} = 3.002
experiment	M_{SAT} = 6.397	M_{SAT} = 5.421	M_{SAT} = 3.513	M_{SAT} = 1.33

5.1.4 Heat Capacity Measurements

Thermal transport properties were measured by DynaCool PPMS on the same samples as magnetic measurements. The HC option is described in the part 4.3.3 HC option.

The obtained experimental data for $GdNi_5$ are shown in Figure 5.12. Low temperature detail confirms a transition temperature (T_c = 31 K), which is little lower than the temperature observed at magnetic measurements (T_c = 31.8 K). An applied magnetic field shifts maximum to higher temperatures and smears it, which is characteristic of ferromagnetic behaviour. The similar behaviour was published in [81].

Generally, total heat capacity consists of phonon, electron and magnetic contributions. In order to calculate the mentioned contributions, it is necessary to determine contributions excluding relation to magnetic origin. This method was done by following the procedure in [138] and results are plotted in Figure 5.12.

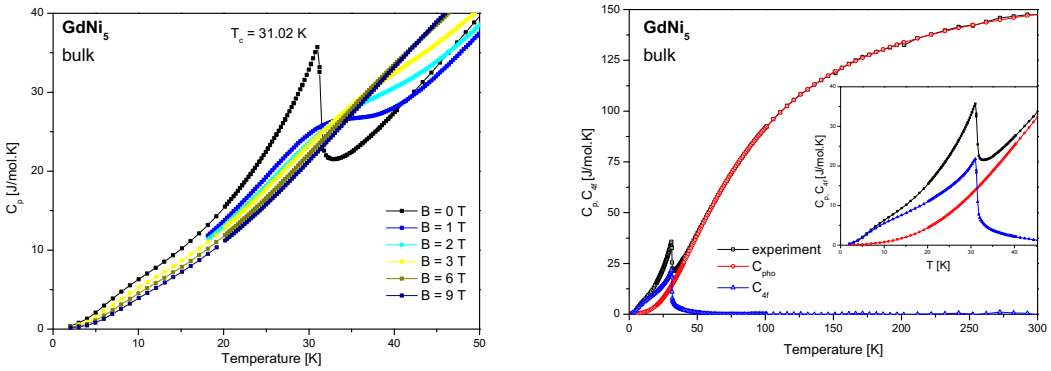

Figure 5.12 Low temperature detail of $C_p(T)$ measured at different applied magnetic fields for $GdNi_5$ with T_c (on the left) and calculated contributions to the total heat capacity (on the right).

When a small amount of Ce (20%) is substituted with Gd in the compound, transition temperature shifts to lower temperatures (T_c = 23.2 K). Even a small magnetic field moves this maximum to higher temperatures and the high magnetic field (B > 6 T) depresses it. Low temperature detail for $Gd_{0.8}Ce_{0.2}Ni_5$ is presented in Figure 5.13 (left). The calculation of contributions to the heat capacity is shown in Figure 5.13 (right). It is evident, that the maximum connected with transition temperature is broader.

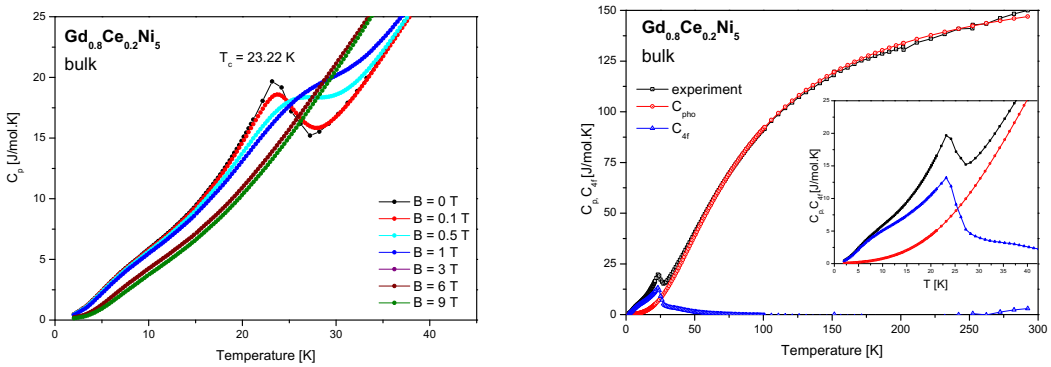

Figure 5.13 Low temperature detail of $C_p(T)$ measured at different applied magnetic fields for $Gd_{0.8}Ce_{0.2}Ni_5$ with T_c (on the left) and calculated contributions to the total heat capacity (on the right).

The situation is very similar for $Gd_{0.5}Ce_{0.5}Ni_5$ (Figure 5.14) and for $Gd_{0.2}Ce_{0.8}Ni_5$ Figure 5.15. In both compounds, transition temperatures are shifted to lower temperatures with increasing Ce content. A small shoulder observed at about 8 K could be attributed to the CEF effects [79]. It means possibility of increasing the thermal population of 8 levels of ground state multiplet levels for Gd^{3+}, when the temperature increases [79].

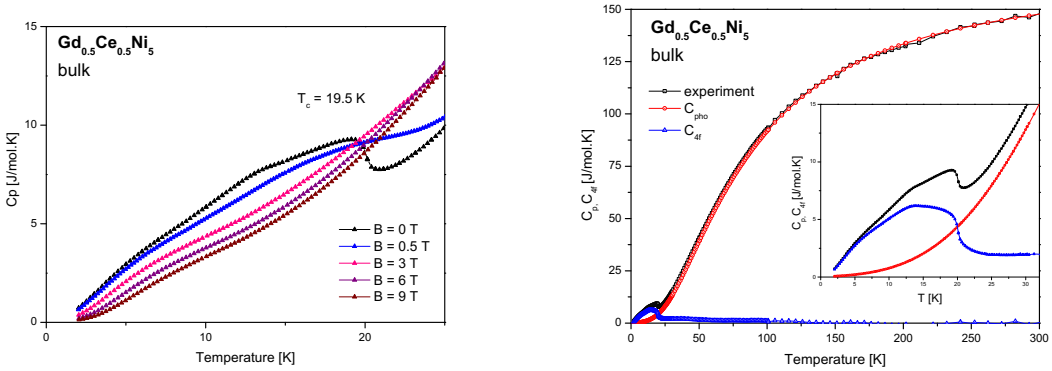

Figure 5.14 Low temperature detail of $C_p(T)$ measured at different applied magnetic fields for $Gd_{0.5}Ce_{0.5}Ni_5$ with Tc (on the left) and calculated contributions to the total heat capacity (on the right).

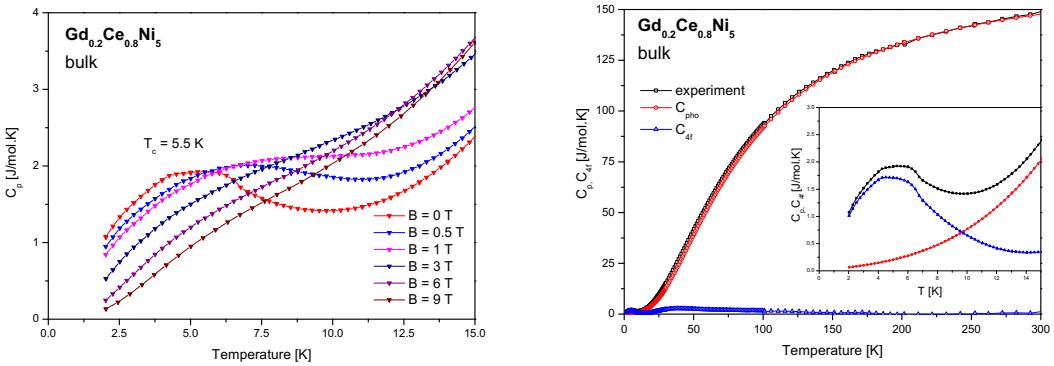

Figure 5.15 Low temperature detail of $C_p(T)$ measured at different applied magnetic fields for $Gd_{0.5}Ce_{0.5}Ni_5$ with T_c (on the left) and calculated contributions to the total heat capacity (on the right).

In order to manifest the influence of Ce substitution on C_p Figure 5.16 is plotted. At room temperature, $C_p(T)$ tends to the $3n$R value expected from the Dulong-Petit law, where n represents number of atoms in the formula unit and R is the gas constant. In the low temperature range maxima are visible, which corresponds with transitions temperatures. They are shifted to higher temperatures with the increase of Gd, which is in an agreement with magnetic measurements.

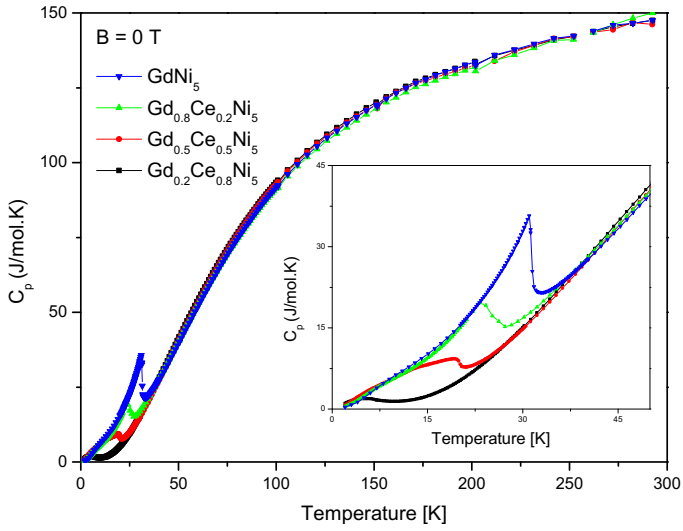

Figure 5.16 Temperature dependence of the heat capacity for different compositions at B = 0 T. Inset shows low temperature detail and transition temperatures are more visible [133].

Magnetic contribution to entropy $S_{mag}(T)$ was calculated by the formula:

$$S_{mag} = \int_0^T \frac{C_{mag}(T)}{T} dT. \tag{35}$$

The results are shown in Figure 5.17. As expected, the entropy has a tendency to saturate. Value for $GdNi_5$ is close to the $Rln(2J+1) = Rln8 = 17.28$ J/mol.K. It agrees with expected Hund`s rule octet ground state for $J = {}^{7}/_{2}$, where $J = 0$ inhibits the CEF effects independently of the point symmetry as it is the case for free Gd^{3+} ions. When Ce content increases, the magnitude of entropy saturation is decreases and, in addition the entropy value in the magnetic transition decreases with the respect of saturation value due to the effects of the CEF. The determined dependencies show the shoulders connected well with the transition temperatures into magnetically ordered state.

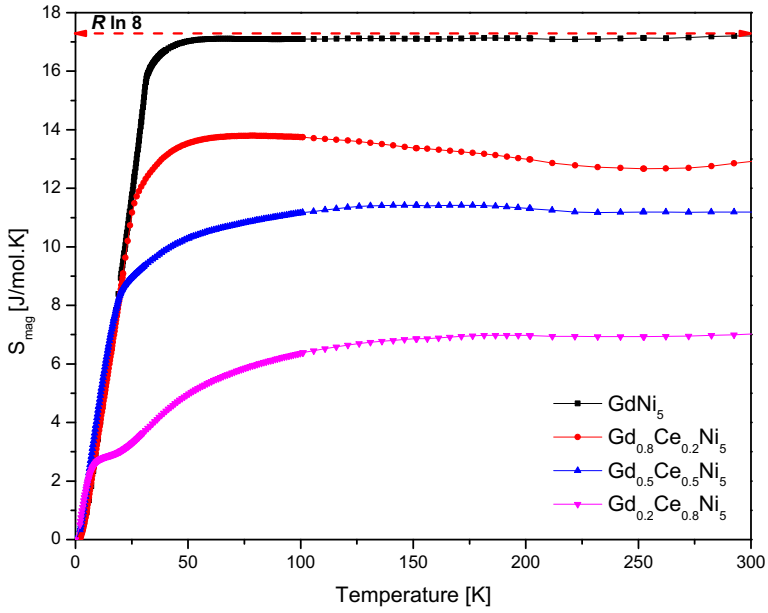

Figure 5.17 The temperature dependence of the magnetic entropy of $Gd_{1-x}Ce_xNi_5$ system.

The Sommerfeld coefficient was also calculated from the $Cp(T)vsT^2$ curves. We have used the data taken at the applied magnetic field 9 T, because in zero magnetic field the magnetic contribution is significant. Moreover, a heavy fermion behaviour is not present in this system. Therefore, magnetic field depresses these contributions.

Observations are reported in Table 4. and they are in an agreement with previous studies [79, 134, 136]. One can see the tendency of decreasing the coefficient with increasing Ce content. The higher values than values for simple metals are due to electron band structure.

Table 4 The electronic Sommerfeld coefficients for bulk samples of $Gd_{1-x}Ce_xNi_5$ system.

$Gd_{1-x}Ce_xNi_5$ bulk	x = 0	x = 0.2	x = 0.5	x = 0.8
γ_{9T} [mJ/mol.K^2]	43	31	28	26

5.1.5 Electrical Resistivity and Magnetoresistivity Measurements

All measurements of electrical resistivity and magnetoresisitivity have been done by 4-point method described in the previous chapter.

The temperature dependences of the electrical resistivities $\rho(T)$ with transition temperatures marked with arrows are shown in Figure 5.18. All compounds show a typical metallic behaviour. The residual resistivity ratio (RRR = $\rho_{300K}/\rho_{4.2K}$) for each sample have the following values: for $GdNi_5$ it is 2.43; for $Gd_{0.8}Ce_{0.2}Ni_5$ it is 4.33; for $Gd_{0.5}Ce_{0.5}Ni_5$ it is 4.2 and for $Gd_{0.2}Ce_{0.8}Ni_5$ it is 6. These values indicate a rather good quality of prepared samples.

The transition temperatures for magnetically ordered state, which are determined as the position of the small anomalies like shoulders, are in a good agreement with temperatures determined from magnetic properties and from heat capacity. When the magnetic field $B > 3$ T is applied, the shoulders are smeared out. We have not done the phonon etalon measurements of electrical resistivity like $LaNi_5$. Therefore, we could not use the direct subtraction method to determine magnetic contribution. In order to determine the magnetic contribution to the electrical resistivity, a fitting procedure described in detail in [138] was used.

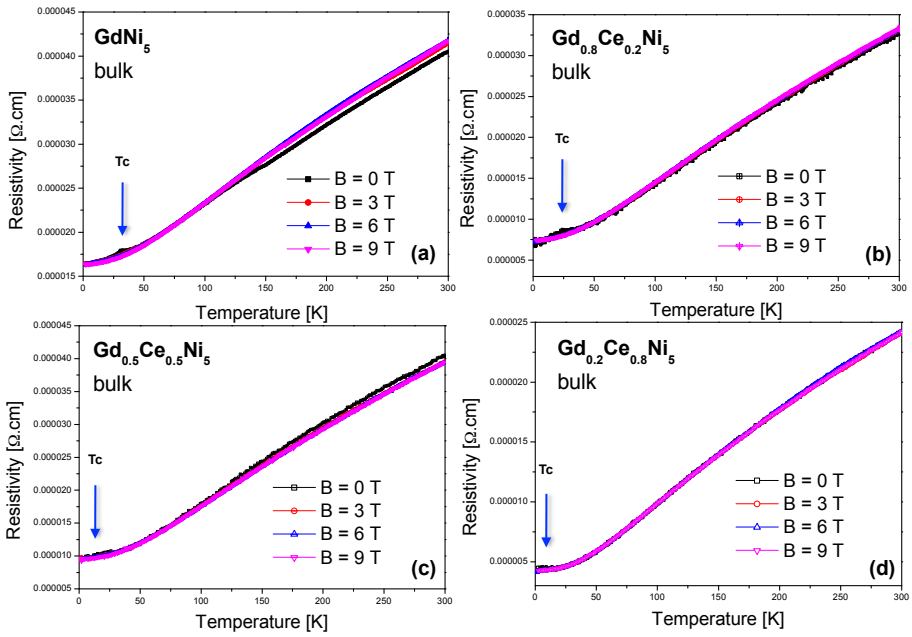

Figure 5.18 Temperature dependencies of the electrical resistivity of all compounds at different applied magnetic fields.

The results of such procedure for all compounds are presented in $B = 0$ T in Figure 5.19. For x = 0; 0.2 and 0.5, there is a clear abrupt slope change present at temperatures, which correlate well with transition temperatures determined from other methods. The behaviour is similar to the contribution of spin disorder resistivity like e.g. in [139]. This abrupt slope change is depressed for concentration x = 0.8. The main signature of this compound is a broad shoulder around $T = 200$ K, which is present at high temperatures, which is probably due to the CEF effects.

The magnetic field dependences of electrical magnetoresistivity (MR) for different temperatures for all samples are presented in Figure 5.20. The magnetoresistance has been calculated from the field dependence of the resistivity data using the formula:

$$\frac{\Delta\rho}{\rho}(\%) = \frac{[\rho(B) - \rho(0)]}{\rho(0)}.100, \qquad (36)$$

where $\rho(0)$ and $\rho(B)$ are the resistivities measured in various applied magnetic fields. All magnitudes are negative, except for $Gd_{0.8}Ce_{0.2}Ni_5$ compound at T = 2 K. Here, MR has a positive value.

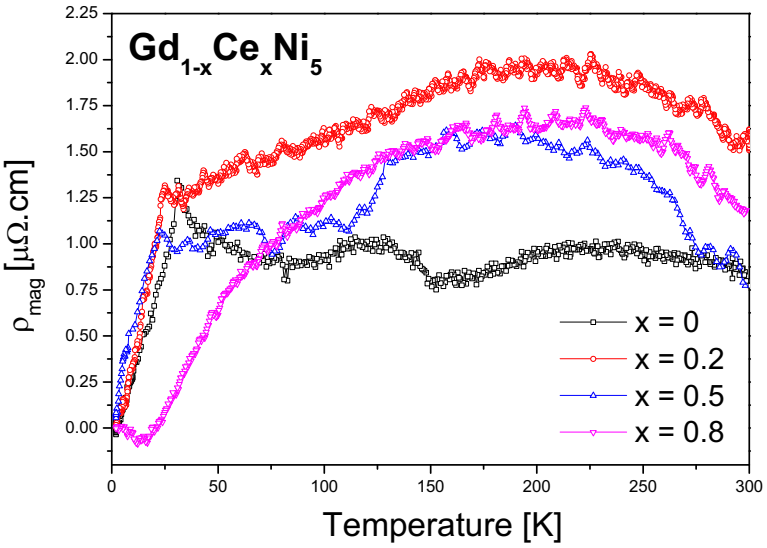

Figure 5.19 ρ_{mag}(T) of $Gd_{1-x}Ce_xNi_5$ *system at B = 0 T.*

The maximum magnitudes of magnetoresistivity are reached in the transition temperatures range, as it was theoretically calculated in [140]. An interesting experimental fact is that for higher concentrations of Ce (Ce 80%) up to B = 1 T, MR rapidly increases and then MR gets saturated. However, for other samples from this series MR increases gradually.

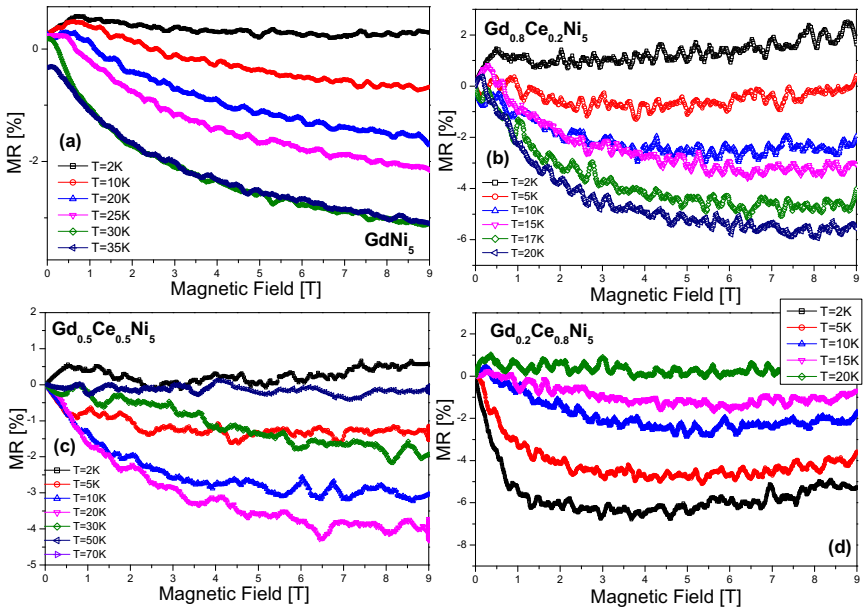

Figure 5.20 The magnetic field dependences of electrical magnetoresisistivity as a function of temperatures of $Gd_{1-x}Ce_xNi_5$ system.

5.1.6 Conclusion

The intermetallic samples of polycrystalline $Gd_{1-x}Ce_xNi_5$ (x = 0; 0.2; 0.5 and 0.8) system were prepared by arc melting method. Ground state physical properties were studied. Structural characterization and SEM analysis confirm single phase samples. Magnetic measurements indicate ferromagnetic transitions. Measurement of $C_p(T)$ and transport measurements support this scenario. The experimental results show, that magnetic ordering dominates and influence of spin fluctuation is not observed at these concentrations for x = 0; 0.2; 0.5 and 0.8.

5.2 Ribbon Samples of $Gd_{1-x}Ce_xNi_5$ (x = 0; 0.2; 0.5, 0.8 and 1) system

One of the aims of this thesis is to study the influence of the shape and dimension on the physical properties connected especially with spin fluctuations. The reason for this is also the reason to use the technique of microwires e.g. [141, 142] to prepare this system. It is known that such a method yields to very good crystallinity of a sample, which is like single crystals e. g. [143]. Therefore, we would like to study the ribbon form as a transition to prepare sample in a microwire form. For this reason, ribbon samples of Gd_{1-}

$_xCe_xNi_5$ (x = 0; 0.2; 0.5, 0.8 and 1) have been prepared. The obtained results are the objectives of this chapter.

5.2.1 X-Ray Diffraction

Analogically to bulk samples, the Rietveld refinement has been performed after the preparation and it is plotted in Figure 5.21. The results show, that with the increase of the Ce content, the unit cell is expanding. It is consistent with the larger Ce volume with regard to Gd. Prepared samples crystallize in the $CaCu_5$-type structure, so the Vegard's law [132] can be applied. The application is in Figure 5.22, where the comparison of the experimental data and Vegard's law is plotted. The presented results confirm the fact, that indexed peaks in every sample belong to this hexagonal structure. The peaks have sharp character and, in any case, it is not amorphous material, what could one expect due to preparation process. Cell parameters are summarized in Table 5.

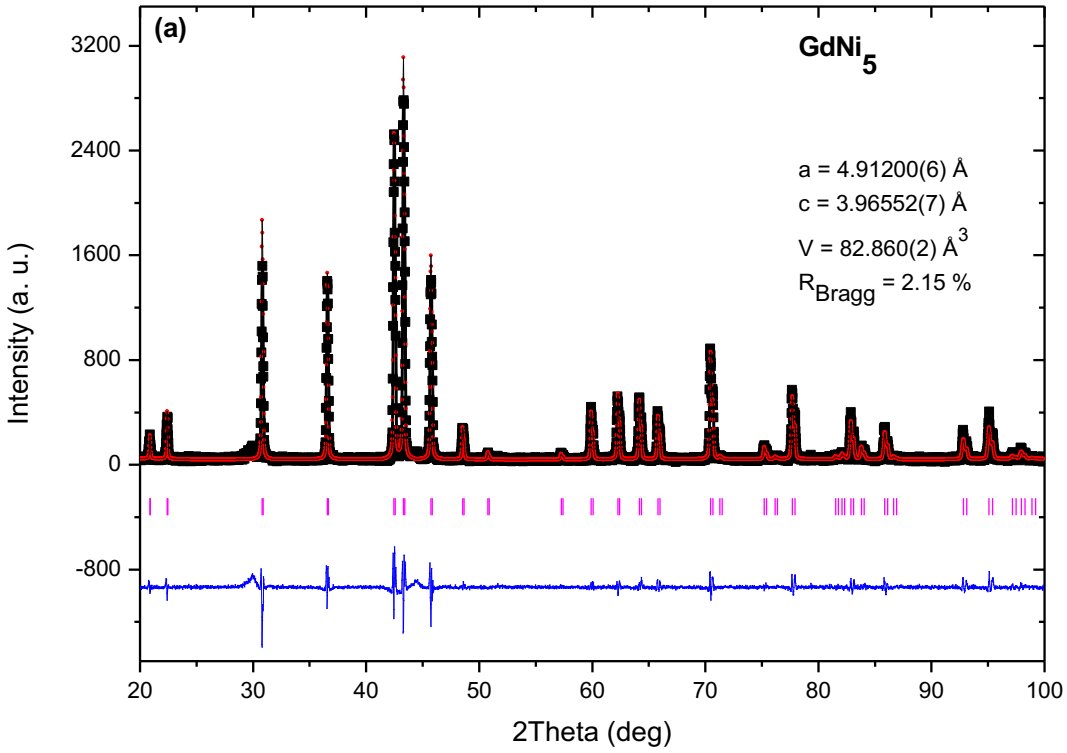

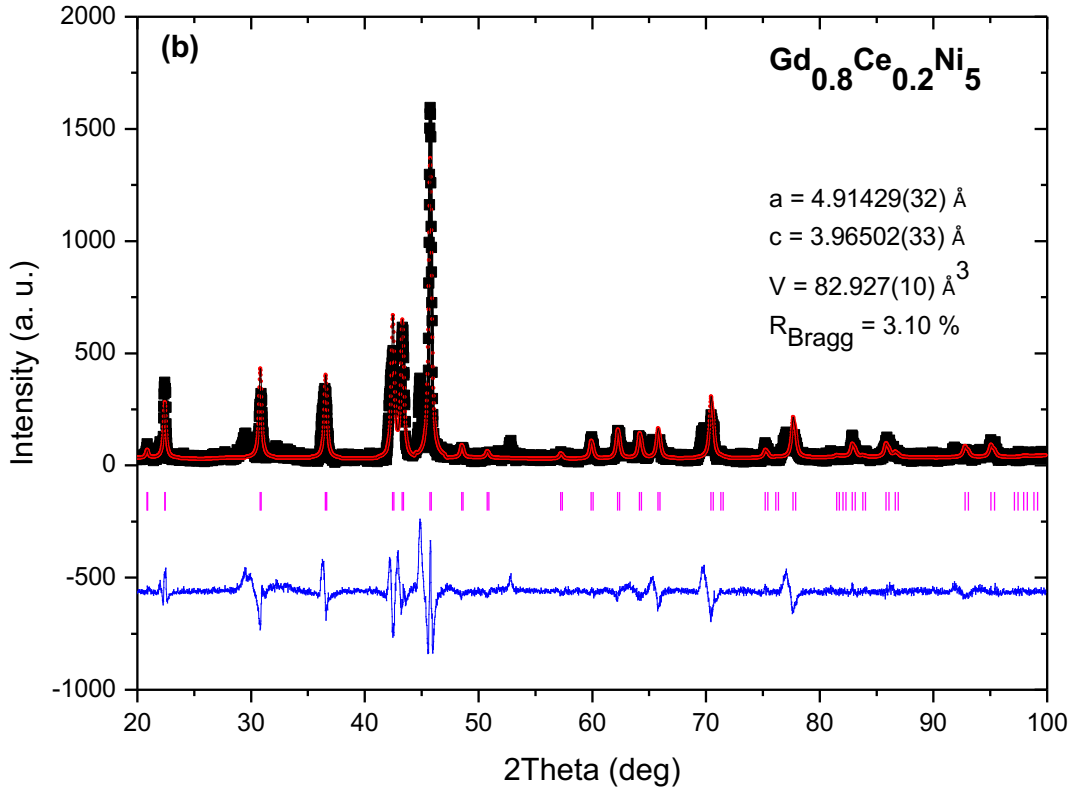
(b)
Gd0.8Ce0.2Ni5
a = 4.91429(32) Å
c = 3.96502(33) Å
V = 82.927(10) Å3
RBragg = 3.10 %
Intensity (a. u.)
2Theta (deg)

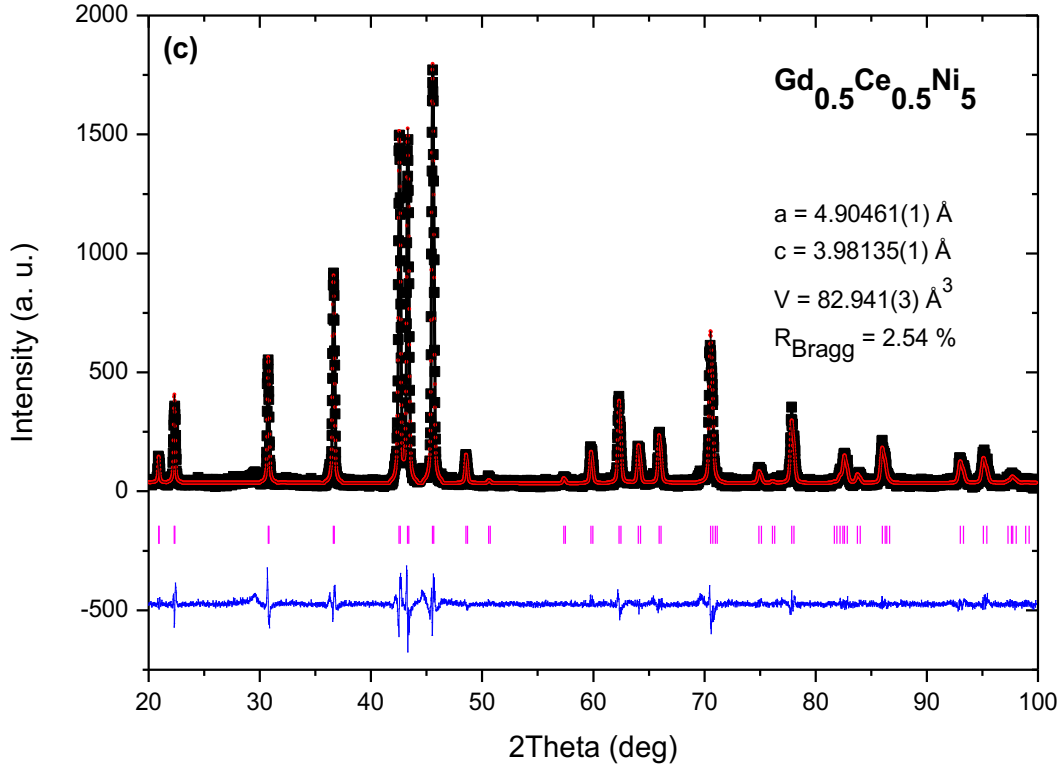
(c)
Gd0.5Ce0.5Ni5
a = 4.90461(1) Å
c = 3.98135(1) Å
V = 82.941(3) Å3
RBragg = 2.54 %
Intensity (a. u.)
2Theta (deg)

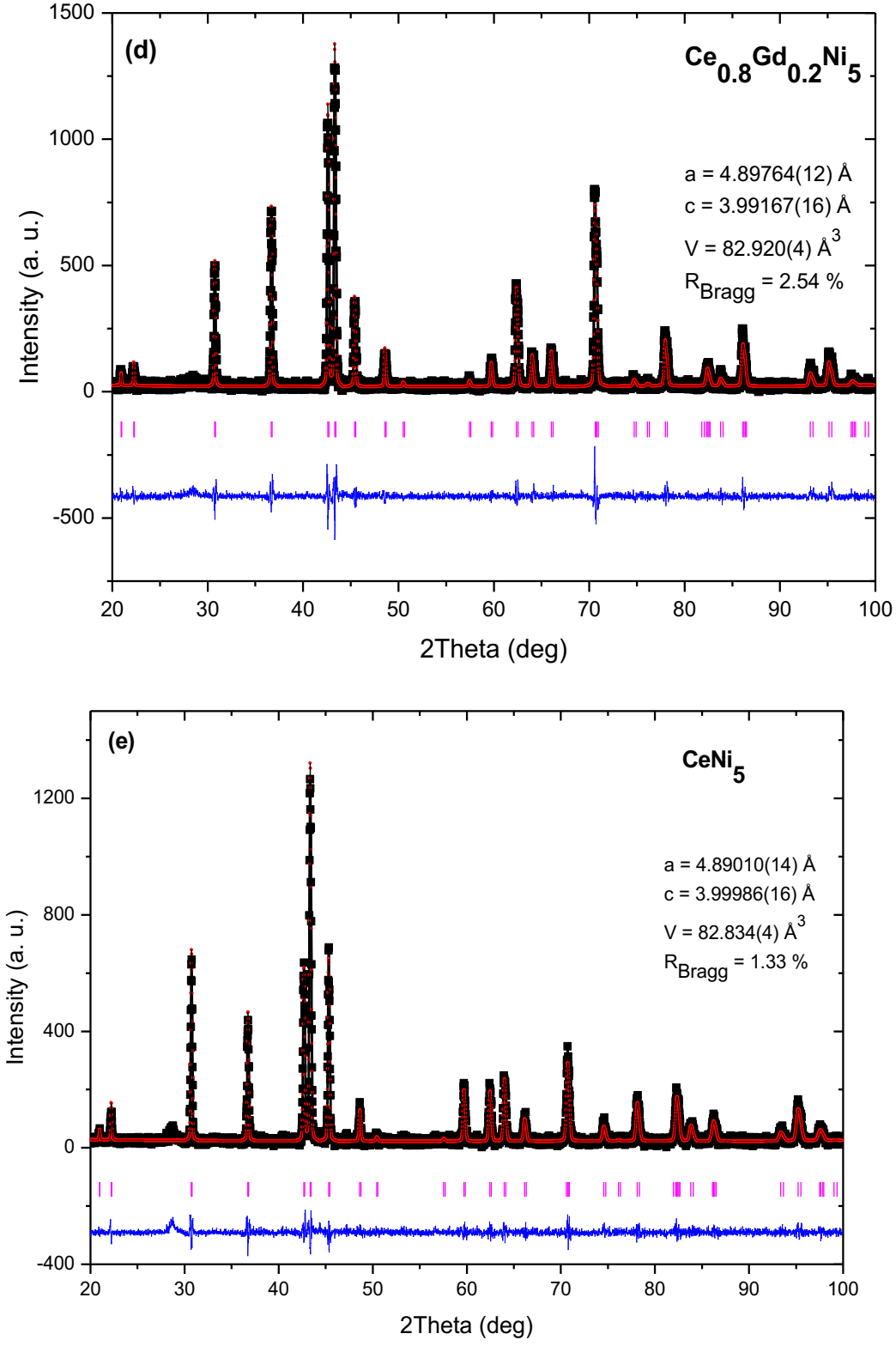

Figure 5.21 Rietveld refinement for ribbon samples of $Gd_{1-x}Ce_xNi_5$ system. (a) $GdNi_5$ and obtained cell parameters; (b) $Gd_{0.8}Ce_{0.2}Ni_5$ and obtained cell parameters; (c)

$Gd_{0.5}Ce_{0.5}Ni_5$ and obtained cell parameters; (d) $Gd_{0.2}Ce_{0.8}Ni_5$ and obtained parameters; (e) $CeNi_5$ and obtained cell parameters.

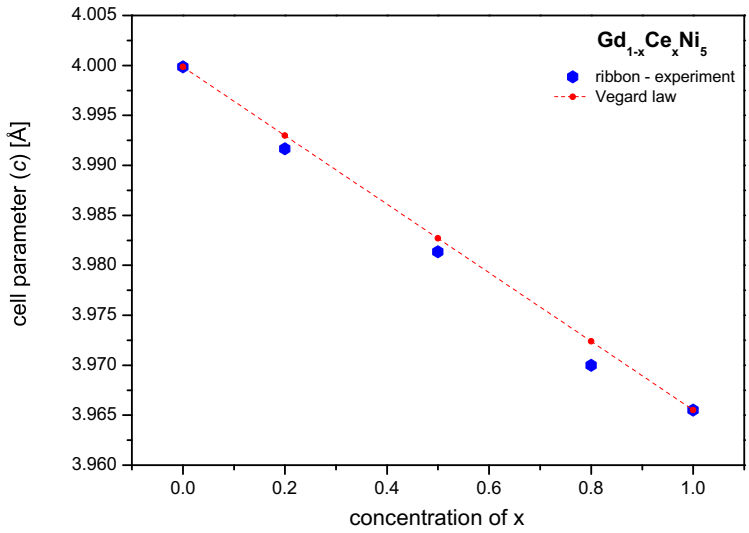

Figure 5.22 The comparison of Vegard's law (red symbol) and obtained experimental data (blue symbol) for ribbon samples of $Gd_{1-x}Ce_xNi_5$ system.

Table 5 Summary of experimental values for cell parameters of ribbon samples of $Gd_{1-x}Ce_xNi_5$ system.

$Gd_{1-x}Ce_xNi_5$ ribbon	x = 0	x = 0.2	x = 0.5	x = 0.8	x = 1
a [Å]	4.9120	4.91429	4.90461	4.89764	4.8901
c [Å]	3.9552	3.970	3.98135	3.99167	3.99986
V [Å^3]	82.860	82.927	82.941	82.920	82.834

The comparison of results from bulk and ribbon samples yields to conclusion that obtained cell parameters are very similar. This gives us information that two different processes of sample preparation have similar results. In this case, from XRD analysis it is not possible to say, if a rapid quenching method influences a change of cell parameters.

5.2.2 Electron Microscopy

Microstructural analysis was provided by electron microscopy. The results are shown in the Figure 5.23, Figure 5.24, Figure 5.25. The surface of samples containing Ce is different from samples without Ce. In Figure 5.23 (left) one can see small grain having the same thickness, what was confirmed by EDX analysis. Samples with Ce show more likely shoulders and with increasing content of Ce these shoulders get straight.

From theoretical calculations for compositions there are not high deviations - only ± 2 %.

SEM is not possible to compare with another analysis for ribbons, because in published paper [144], where rare earth ribbons were studied, this kind of microstructural analysis does not exist. Moreover, when we compare bulk and ribbon samples with ribbon samples of the same composition, the surfaces show similar results. Only $GdNi_5$ is little different from them.

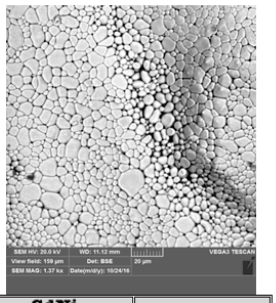

$GdNi_5$ ribbon	Atomic %
Gd	16.23
Ni	83.77
TOTAL	100.00

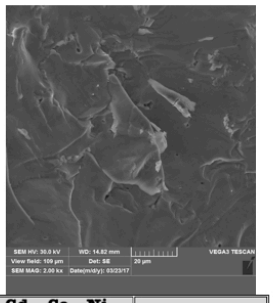

$Gd_{0.8}Ce_{0.2}Ni_5$ ribbon	Atomic %
Gd	12.63
Ce	3.8
Ni	83.57
TOTAL	100.00

Figure 5.23 SEM photos and obtained compositions for ribbon samples of $GdNi_5$ (on the left) and $Gd_{0.8}Ce_{0.2}Ni_5$ (on the right).

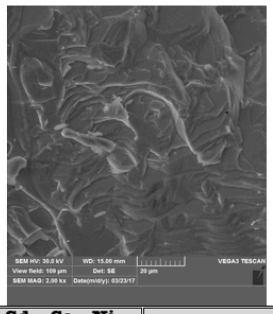

$Gd_{0.5}Ce_{0.5}Ni_5$ ribbon	Atomic %
Gd	9.00
Ce	9.47
Ni	81.53
TOTAL	100.00

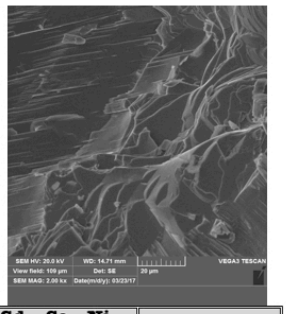

$Gd_{0.2}Ce_{0.8}Ni_5$ ribbon	Atomic %
Gd	3.37
Ce	14.12
Ni	82.14
TOTAL	100.00

Figure 5.24 SEM photos and obtained compositions for ribbon samples of $Gd_{0.5}Ce_{0.5}Ni_5$ (on the left) and $Gd_{0.2}Ce_{0.8}Ni_5$ (on the right).

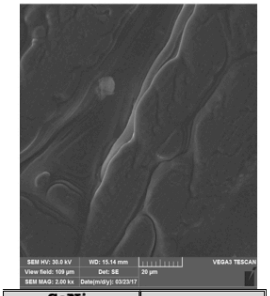

$CeNi_5$ ribbon	Atomic %
Ce	16.7
Ni	83.3
TOTAL	100.00

Figure 5.25 SEM photo and obtained composition for ribbon sample of $CeNi_5$.

5.2.3 Magnetic Measurements

The following methods of investigations and magnetic measurements have been performed at the same equipment – DynaCool located at the University of Prešov. The Figure 5.26 presents the temperature dependence of magnetization in ZFC-FC regime for $GdNi_5$.

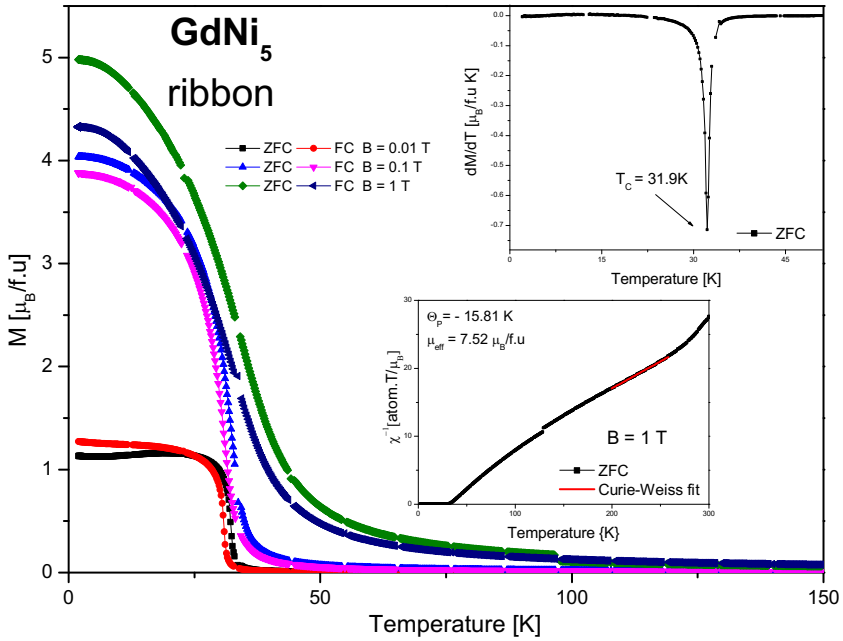

Figure 5.26 Temperature dependence of ZFC-FC magnetization at three different applied magnetic fields for $GdNi_5$ ribbon sample. The inset (up) shows the dM/dT with calculation of T_c. The inset (down) shows, the inverse of the magnetic susceptibility fitted to a CW law.

The results show, that transition temperature is an agreement with bulk sample of $GdNi_5$ and with data reported in the literature [79, 135, 136]. Behaviour of temperature dependencies has a character typical for antiferromagnetic materials. This prediction is partially supported by a negative value of paramagnetic Curie temperature. The question of antiferromagnetic interaction exists in [145]. During the systematic investigations performed in last decades, temperature dependencies of magnetization were done only at high applied magnetic fields ($B \geq 1$ T), but antiferromagnetic character is manifested at lower magnetic fields. However, the study of other physical properties does not confirm antiferromagnetic ordering. In the paramagnetic region, a Curie-Weiss fit was provided. The obtained effective paramagnetic moment is of 7.52 μ_B/f.u., which is lower than value for bulk sample. This deviation can be explained in a way that the piece of sample was not homogenous and, on its surface, there could be more Ce than Gd, what yields from microstructural analysis.

Another studied sample is $Gd_{0.8}Ce_{0.2}Ni_5$ (Figure 5.27). Here, the transition temperature (T_c = 30.1 K) is higher than T_c for bulk sample (T_c = 24.1 K) with the same

composition. Characteristics of *M(T)* can be separated into two parts. The first one, arises at small applied magnetic fields, where around T = 100 K a magnetization starts to increase until reaching the transition temperature. On the other hand, when a high magnetic field is applied the sharp maximum is diminished. This behaviour can be caused by different way of sample preparation. The fitting by Curie-Weiss law in a high temperature range yields to the effective paramagnetic moment of 7.02 μ_B/f.u and positive paramagnetic Curie temperature.

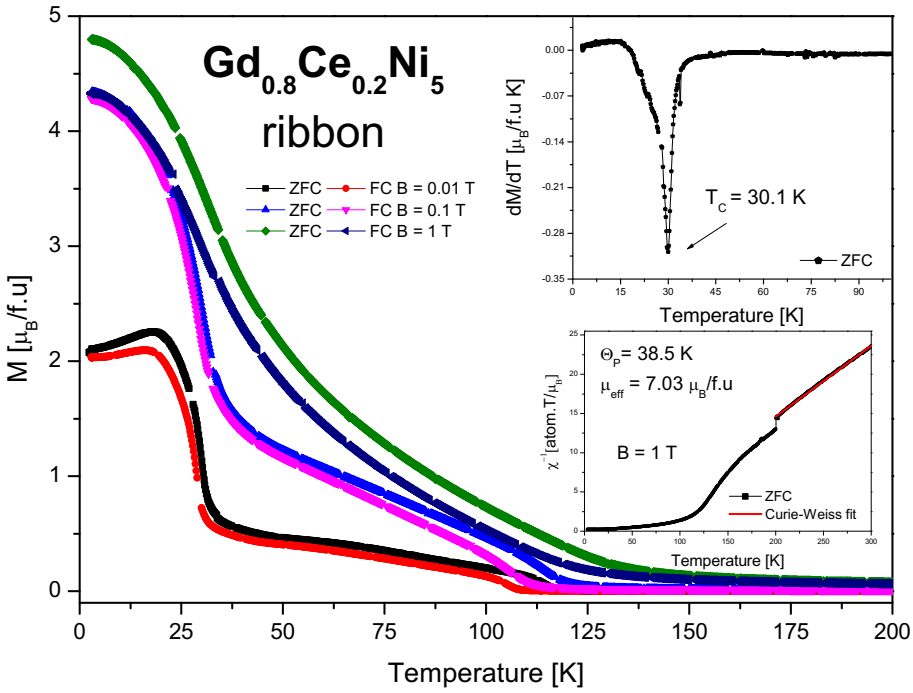

Figure 5.27 Temperature dependence of ZFC-FC magnetization at three different applied magnetic fields for $Gd_{0.8}Ce_{0.2}Ni_5$ ribbon sample. The inset (up) shows the dM/dT with calculation of T_c. The inset (down) shows, the inverse of the magnetic susceptibility fitted to a CW law.

Magnetization as a function of temperature for equal percentage amount of Ce and Gd content is plotted in Figure 5.28. When we compare results from a bulk and a ribbon measurement we can see the same differences as in the previous samples. In addition, Curie temperature has a tendency to decrease. Obtained transition temperature is of the value of 16.9 K, while for bulk sample T_c is higher (T_c = 20.9 K). Similar situation is observed for an effective paramagnetic moment, which is lower. Paramagnetic Curie temperature is negative, which could indicate an antiferromagnetic interaction.

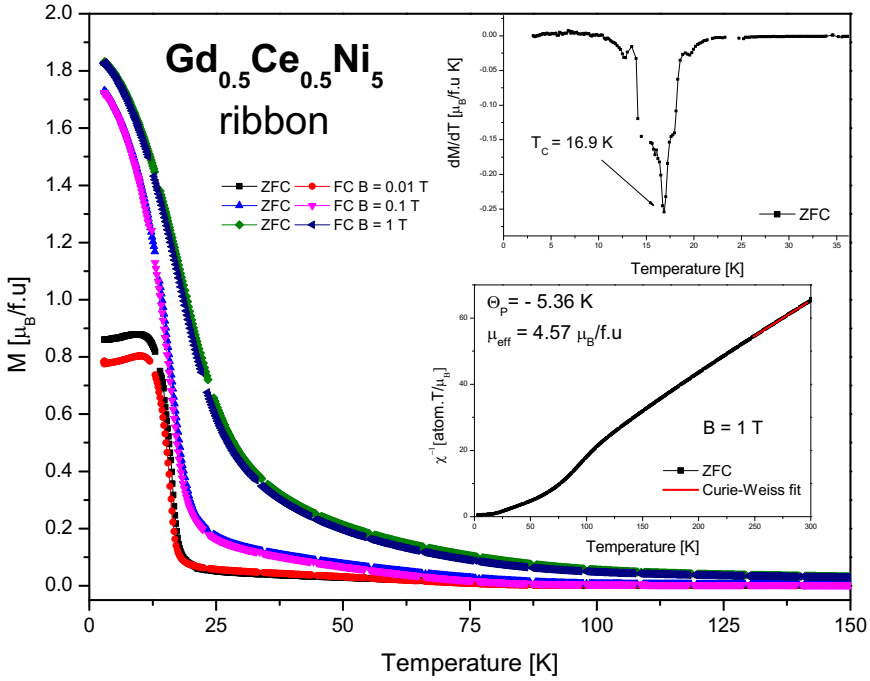

Figure 5.28 Temperature dependence of ZFC-FC magnetization at three different applied magnetic fields for $Gd_{0.5}Ce_{0.5}Ni_5$ ribbon sample. The inset (up) shows the dM/dT with calculation of T_c. The inset (down) shows, the inverse of the magnetic susceptibility fitted to a CW law.

The last studied sample with Gd is $Gd_{0.2}Ce_{0.8}Ni_5$. Temperature dependence of ZFC-FC regime at different applied magnetics fields is displayed in Figure 5.29. From the minimum of the first derivative of the $M(T)$ plot (displayed in the inset up) in the phase transition region we obtained a Curie temperature T_c of 4.7 K. Again, the temperature is lower than the T_c for a bulk sample with the same concentration obtained in the same way. On the other hand, from Curie-Weiss fit, paramagnetic Curie temperature has a negative value as a previous sample with 50 % of Gd and Ce. An effective paramagnetic moment estimated from the same fit is of 4.38 μ_B/f.u, which is practically the same value as for $Gd_{0.2}Ce_{0.8}Ni_5$ bulk sample.

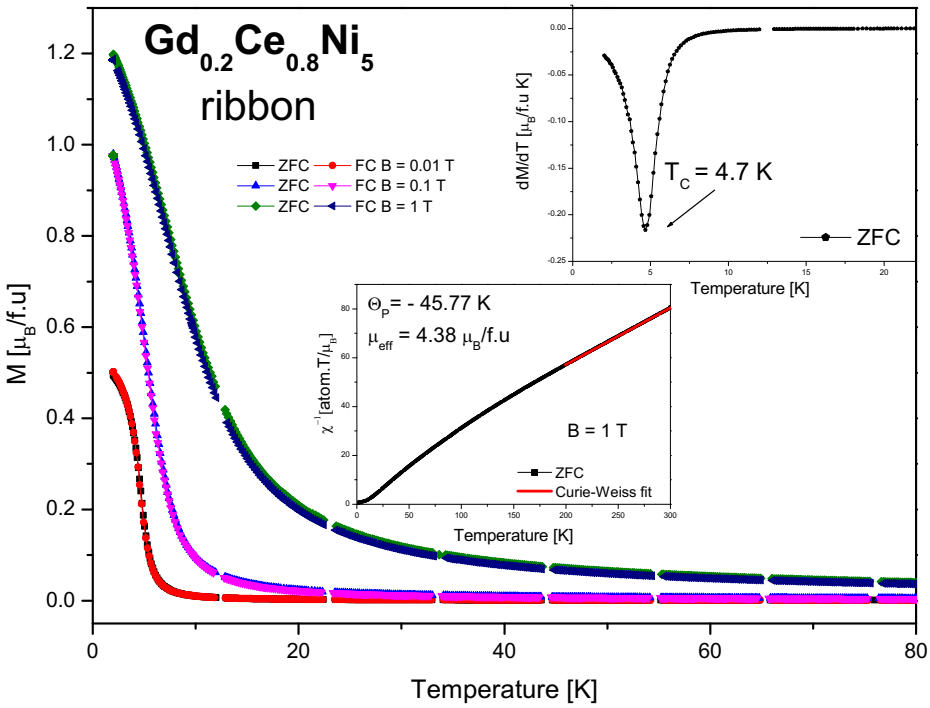

Figure 5.29 Temperature dependence of ZFC-FC magnetization at three different applied magnetic fields for $Gd_{0.2}Ce_{0.8}Ni_5$ ribbon sample. The inset (up) shows the dM/dT with calculation of T_c. The inset (down) shows, the inverse of the magnetic susceptibility fitted to a CW law.

In order to see the effect of spin fluctuations, observed and published in several publications e. g [66, 146], the $CeNi_5$ compound in a ribbon form was prepared. As it is plotted in Figure 5.30, between T = 100 K and T = 150 K a shoulder is visible, which corresponds with maximum observed in polycrystalline $CeNi_5$ compound [147]. It can be explained in several ways. The first one is based on [73, 148], where the authors think, that it is an intrinsic feature of material. It is known, that only a small percentage of magnetic impurities can change the characteristics of *M(T)*. Moreover, previous study did not show a low temperature change [71, 149, 150]. This maximum is created due to the spin fluctuation effect, where magnetic moments are pressed to be ordered and no magnetic field can diminish it. An effective paramagnetic moment for this sample is of 3.52 μ_B/f.u, which is a little higher than for Ce^{3+} ion. It can be due to the fact of CEF splitting of Ce^{3+} ion.

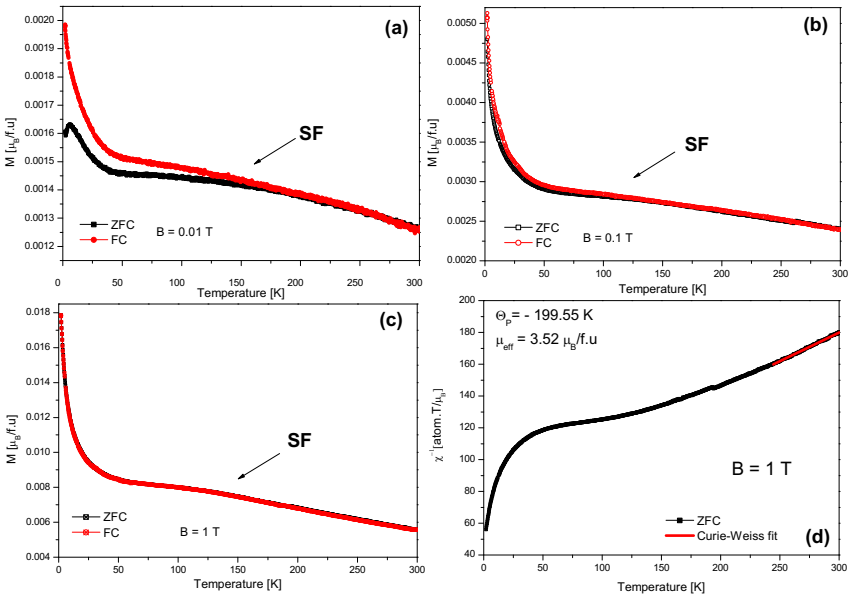

Figure 5.30 Temperature dependence of ZFC-FC magnetization at three different applied magnetic fields (a) B = 0.01 T; (b) B = 0.1 T and (c) B = 1 T for $CeNi_5$ ribbon sample. The (d) shows the estimated contributions.

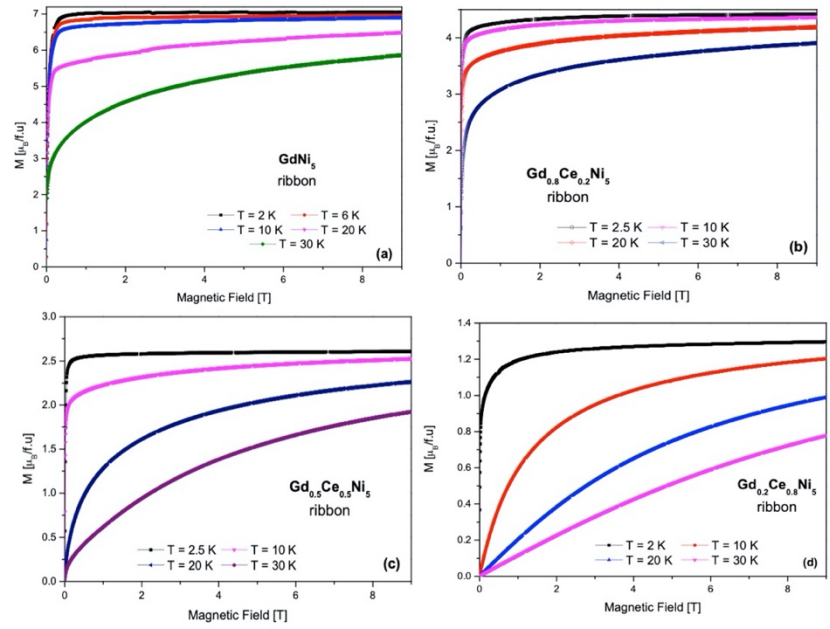

Figure 5.31 Isothermal magnetization as a function of magnetic fields of ribbon samples: (a) $GdNi_5$; (b) $Gd_{0.8}Ce_{0.2}Ni_5$; (c) $Gd_{0.5}Ce_{0.5}Ni_5$; (d) $Gd_{0.2}Ce_{0.8}Ni_5$.

In general, saturation decreases with increasing Ce content. It is plotted in Figure 5.31 and this behaviour can be explained as a result of substitution Gd/Ce. Isothermal magnetization as a function of the applied magnetic fields at different temperatures is

plotted in Figure 5.32 on the left. Ce has lower contribution to total magnetization than Gd. On the other hand, B_{SAT} is lower for ribbons in comparison with bulk samples of the same composition. Due to the process of sample preparing the anisotropy is lower in general for ribbons. Obtained results are in an agreement with previous published paper about polycrystalline $RENi_5$ compounds [79, 133].

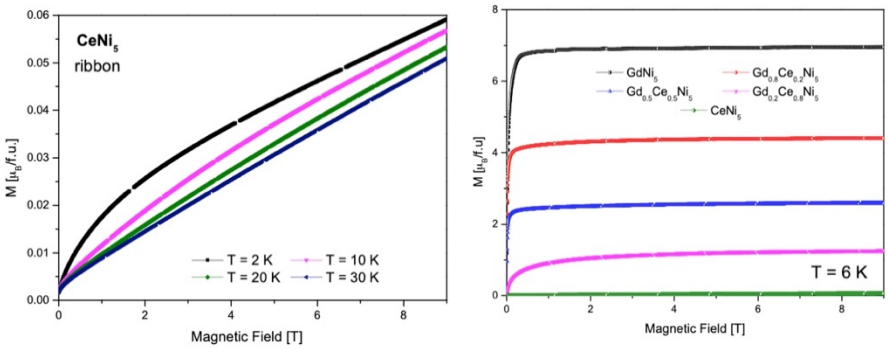

Figure 5.32 On the left - Isothermal magnetization as a function of the magnetic fields of $CeNi_5$ ribbon. On the right - Characteristic behaviour of the magnetic field dependence at very low temperatures of the magnetization for ribbon samples.

5.2.4 Heat Capacity Measurements

Heat capacity measurements were done by 2τ techniques by the same DynaCool equipment. The temperature dependence of heat capacity is presented in Figure 5.33 (on the left). The presence of peak at zero applied magnetic field is associated with transition temperature determined from *dM/dT* for $GdNi_5$. When the applied magnetic fields increase, the maximum is shifted to higher temperatures and then is diminished. On the right side, the results of calculation of a phonon contribution and 4*f* contribution to the heat capacity are presented. At zero applied magnetic field, C_{4f} is dominated by λ-like anomaly at T_c = 31.0 K. In a high temperature range, it follows Dulong-Petit law. The comparison of heat capacity measurements in a bulk and ribbon sample shows, that both T_c temperatures are located at the same position and dependences have the same shape.

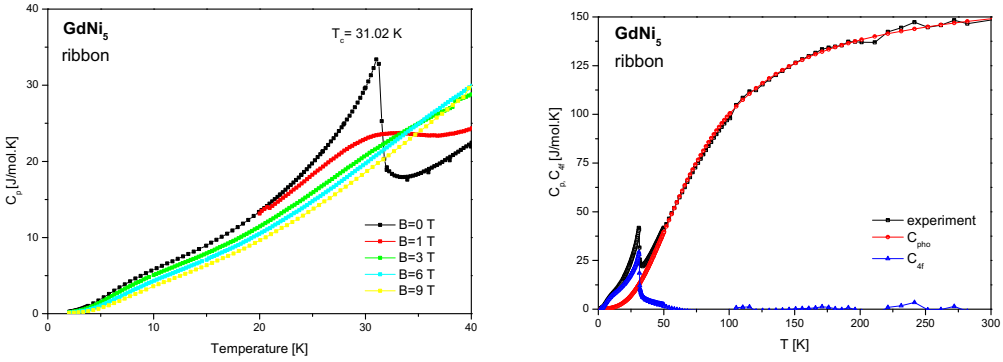

Figure 5.33 Low temperature detail of $C_p(T)$ measured at different applied magnetic fields for ribbon sample of $GdNi_5$ with T_c (on the left) and calculated contributions to the total heat capacity (on the right).

Another ribbon sample is $Gd_{0.8}Ce_{0.2}Ni_5$. The heat capacity collected data are plotted in Figure 5.34, where a low temperature detail is shown (on the left). At zero applied magnetic field, transition temperature is clearly reached at T_c = 29.0 K. Its position is one K lower than the T_c calculated from magnetization measurements. On the other hand, this temperature is higher than observed maximum corresponding with T_c for bulk with the same concentration. It seems to be due to the local problem with quality of the sample. On the right Figure 5.34, the contribution to the total heat capacity are shown. The high temperature value corresponds with $3nR$ – Dulong-Petit law at B = 0 T.

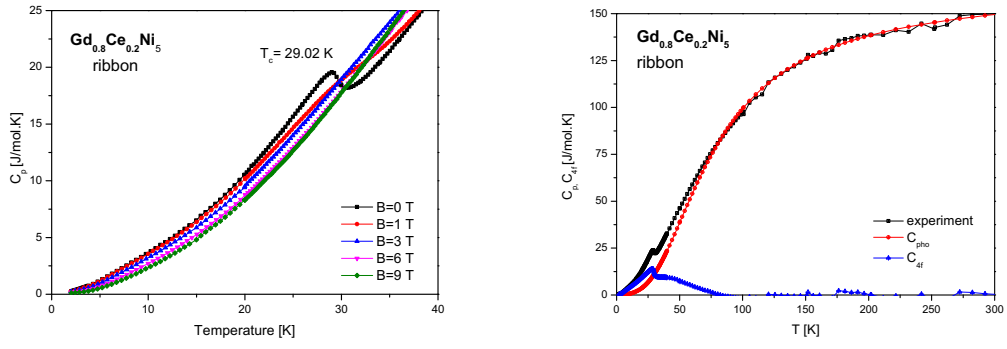

Figure 5.34 Low temperature detail of $C_p(T)$ measured at different applied magnetic fields for ribbon sample of $Gd_{0.8}Ce_{0.2}Ni_5$ with T_c (on the left) and calculated contributions to the total heat capacity (on the right).

The heat capacity measurements of $Gd_{0.5}Ce_{0.5}Ni_5$ ribbon sample are plotted in Figure 5.35 (on the left). At zero applied magnetic field a maximum at T_c = 15.5 K is observed. Magnetic measurements show the transition temperature of 16.9 K. When magnetic fields are applied (B > 0 T), maximum is depressed. The right side of this figure represents contributions to the total heat capacity.

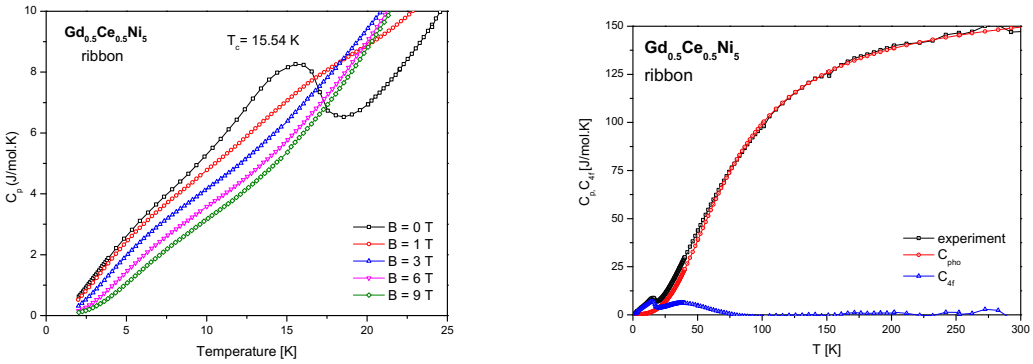

Figure 5.35 Low temperature detail of $C_p(T)$ measured at different applied magnetic fields for ribbon sample of $Gd_{0.5}Ce_{0.5}Ni_5$ with T_c (on the left) and calculated contributions to the total heat capacity (on the right).

The last studied compound contains Gd and Ce was $Gd_{0.8}Ce_{0.2}Ni_5$. It is displayed in Figure 5.36. Transition temperature is observed as a sharp peak at zero applied magnetic field at T_c = 4.4 K. Maximum is shifted, when magnetic field of B = 1 T is applied. A higher magnetic field erased it ($B \geq 2$ T). The calculated contributions are also shown on the right part of this figure. At high temperatures, C_p follows Dulong-Petit law. Here, the electron contribution is very small.

For pure $CeNi_5$ the low temperature anomaly was not observed. It is possible to see it in Figure 5.37 (on the left). Results from heat capacity analysis are presented on the right in Figure 5.37.

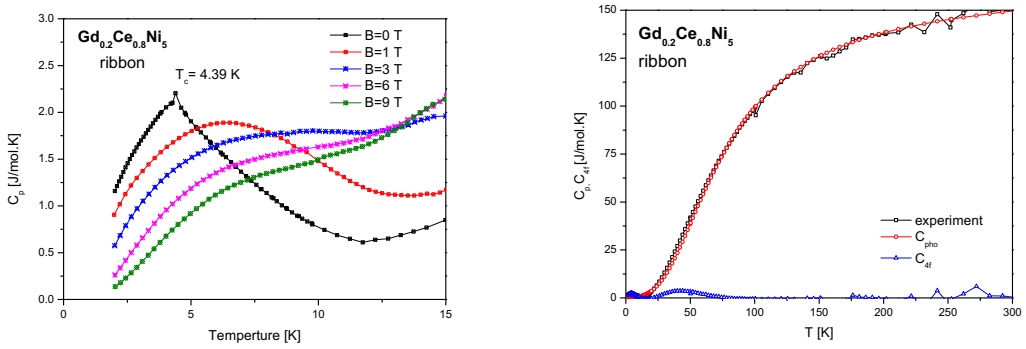

Figure 5.36 Low temperature detail of $C_p(T)$ measured at different applied magnetic fields for ribbon sample of $Gd_{0.2}Ce_{0.8}Ni_5$ with T_c (on the left) and calculated contributions to the total heat capacity (on the right).

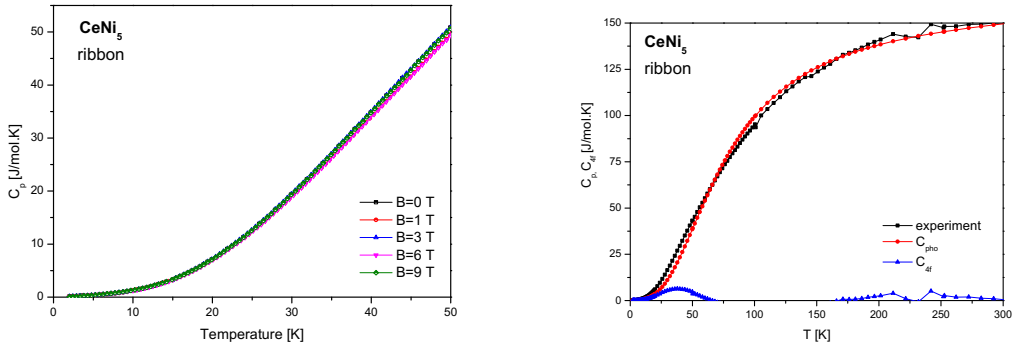

Figure 5.37 Low temperature detail of $C_p(T)$ measured at different applied magnetic fields for ribbon sample of $CeNi_5$ with T_c (on the left) and calculated contributions to the total heat capacity (on the right).

In order to compare the temperature behaviour of all studied ribbon samples, Figure 5.38 was created. It is evident, that increasing Ce content decreases a position of low temperature anomaly. As we have expected $CeNi_5$ has no magnetic ordering down to very low temperatures. The conclusion is that substitution of Gd with Ce tends to supress magnetic ordering similar as in the bulk samples.

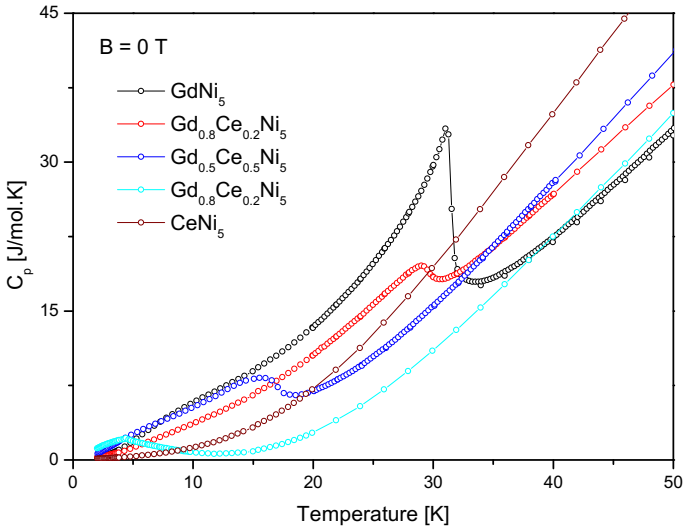

Figure 5.38 Temperature dependence of the heat capacity for different compositions at B = 0 T. Inset shows a low temperature detail and transition temperatures are more visible.

The Sommerfeld coefficient was calculated from *Cp(T) vs* T^2 by the same way than for bulk samples. We have used the data obtained at the applied magnetic field of 9 T, because in zero applied magnetic field the magnetic contribution is significant. Moreover, there is not a heavy fermion behaviour in this system. Therefore, magnetic field depresses these contributions. Observations are reported in Table 6. When the results are compared with bulk samples, Sommerfeld coefficients have lower values for ribbon samples for every sample from the studied $Gd_{1-x}Ce_xNi_5$ system

Table 6 The electronic Sommerfeld coefficients for ribbon samples of $Gd_{1-x}Ce_xNi_5$ *system.*

$Gd_{1-x}Ce_xNi_5$ ribbon	x = 0	x = 0.2	x = 0.5	x = 0.8
γ_{9T} [mJ/mol.K^2]	32	30	16	9

5.2.5 Conclusion

Ribbon samples of $Gd_{1-x}Ce_xNi_5$ (x = 0; 0.2; 0.5 and 0.8) system were prepared by melt spinning techniques. Ground state physical properties were studied. Despite of the single crystallization obtained from XRD analysis and rather good agreement of microstructural analysis, which show only a small deviation from theoretical prediction, the quality of sample is lower than of polycrystalline material. This fact is presented in Figure 5.39. One can see, that better peaks for $K\alpha_1$ and $K\alpha_2$ radiation are presented in bulk sample than in the ribbon one. Similar behaviour is observed for the whole family. From the magnetic point of view, transition temperature is observed for every compound, except of the $CeNi_5$, where spin fluctuations play the important role. When we compare ribbons vs. bulk samples, the differences exist in transition temperatures. But the character and shapes of collected data are very similar. This seems to indicate that the effect of Gd/Ce doping suppress the spin fluctuations effect. Heat capacity measurements and analyses support these observations. An interesting fact is, that for $GdNi_5$ the transition temperature is the same for bulk and for ribbon. When Gd is being doped by Ce, the differences between T_c for bulk and ribbon samples arise. It could be due to different type of sample preparation method. But it is not possible to come to conclusion, that bulk or ribbon samples have better physical properties.

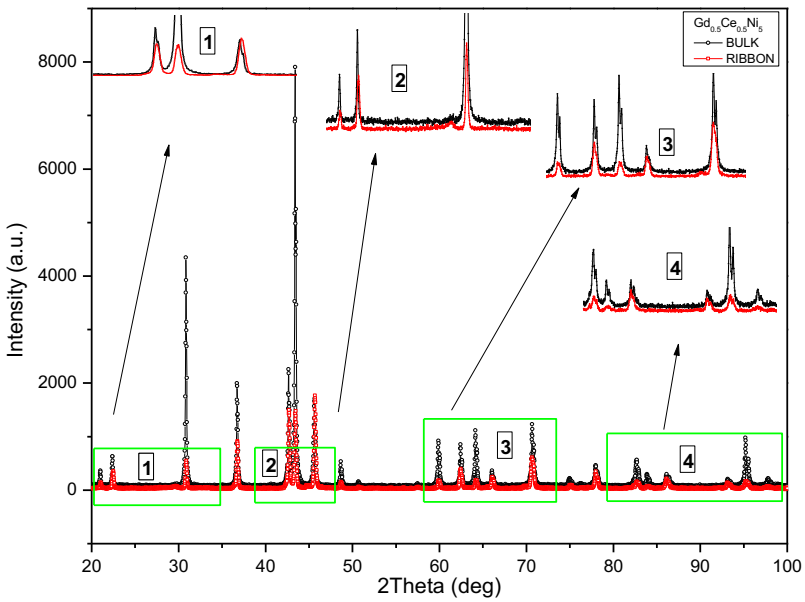

Figure 5.39 Comparison of XRD data from bulk and ribbon $Gd_{0.5}Ce_{0.5}Ni_5$ samples.

The idea was to perform both, resistivity and magnetoresistivity measurements. The problem is the size of samples and their mechanical properties. They are very fragile. So, we were not successful with electron transport measurements.

With the aim to study the influence of microstructure on physical properties, our next step was to plan the preparation of microwires. We tried to use Taylor Ulitovsky method, described in e. g. [151]. However, we had a technical problem. An idea of this method is to cover a metal core by glass. Due to the high temperature melting point of $Gd_{1-x}Ce_xNi_5$ (x = 0; 0.2; 0.5; 0.8 and 1) materials, which are the metal core in this case, it was not possible to prepare microwires.

5.3 (Ce, Gd)Ni_5 - in the Vicinity of the Magnetic Phase Transition

Disappearance of magnetic transition in $Ce_xGd_{1-x}Ni_5$ (x = 0.85; 0.9; 0.95 and 0.97) has been studied. The samples were prepared in order to find a borderline between magnetically ordered state and not ordered state. Next aim is to find where the spin fluctuations effect arises. Results, which have been achieved, are described in a detail in this subchapter.

5.3.1 X-Ray Diffraction

The results of Rietveld refinement are summarized in Figure 5.40. and cell parameters are presented in Table 7. Analysis of $Ce_{0.85}Gd_{0.15}Ni_5$ does not show a preferred orientation. The atomic positions of $CeNi_5$ or $GdNi_5$ were taken as starting values and the structures were successfully refined by using FullProf program [117].

Table 7 Summary of experimental values of cell parameters.

$Ce_xGd_{1-x}Ni_5$ bulk	x = 0.85	x = 0.9	x = 0.95	x = 0.97
a [Å]	4.8902	4.8922	4.8797	4.8796
c [Å]	3.9997	3.9979	4.0073	4.0099
V [Å^3]	82.835	82.904	82.602	82.686

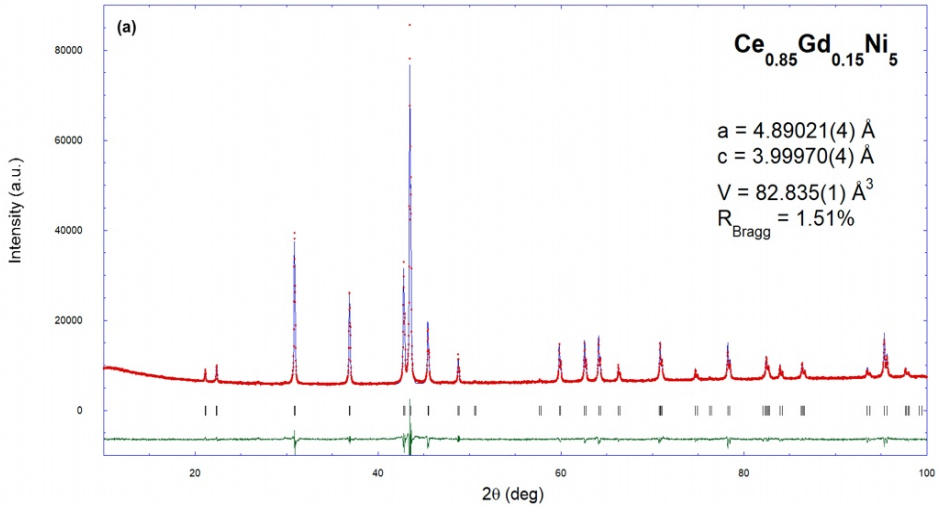
(a)
Ce0.85Gd0.15Ni5
a = 4.89021(4) Å
c = 3.99970(4) Å
V = 82.835(1) Å3
RBragg = 1.51%
Intensity (a.u.)
2θ (deg)

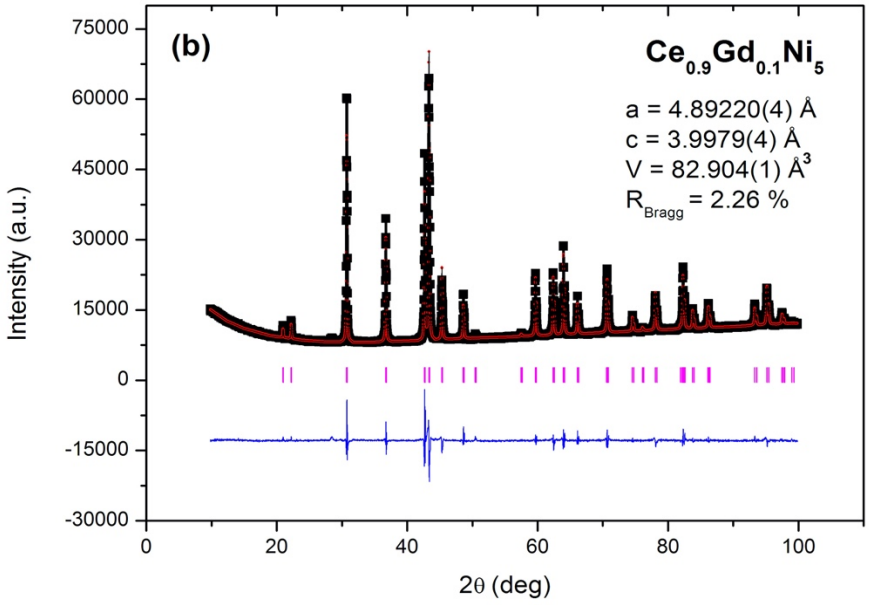
(b)
Ce0.9Gd0.1Ni5
a = 4.89220(4) Å
c = 3.9979(4) Å
V = 82.904(1) Å3
RBragg = 2.26 %
Intensity (a.u.)
2θ (deg)

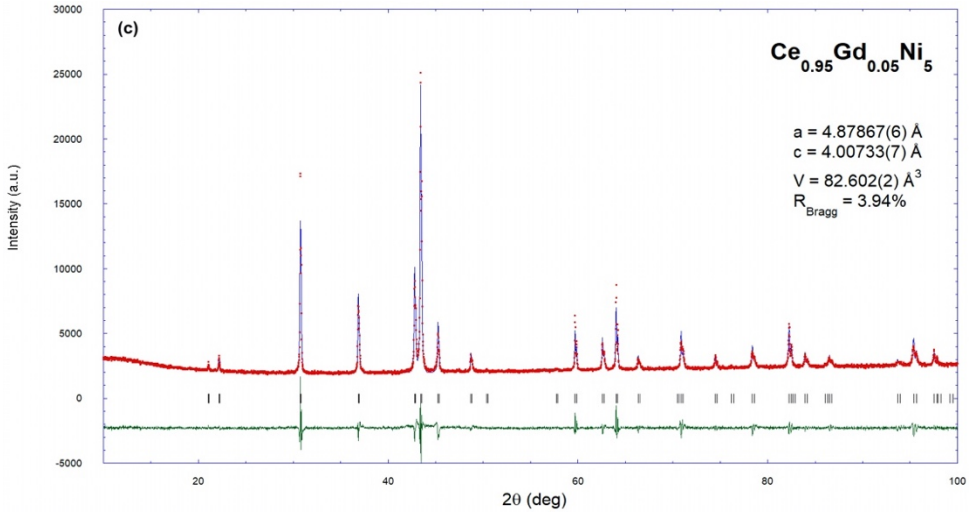
(c)
Ce0.95Gd0.05Ni5
a = 4.87867(6) Å
c = 4.00733(7) Å
V = 82.602(2) Å3
RBragg = 3.94%
Intensity (a.u.)
2θ (deg)

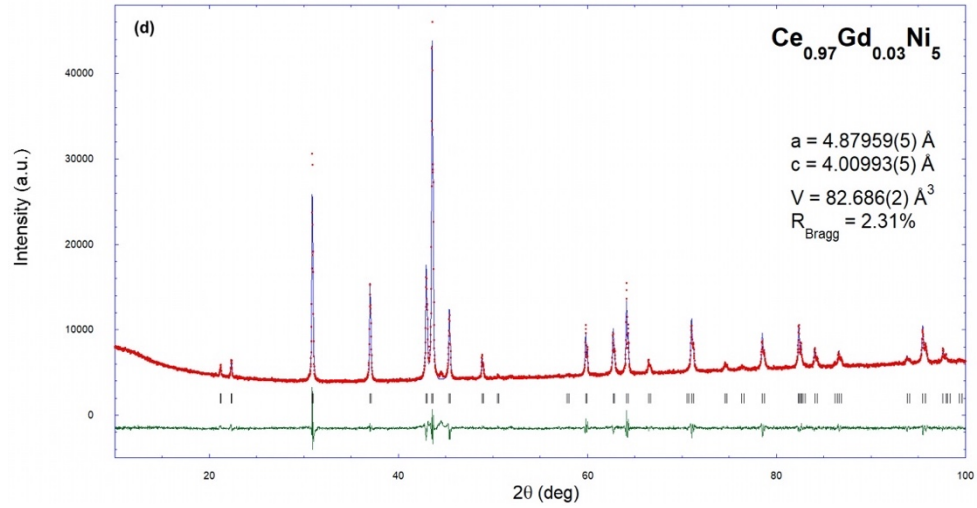

Figure 5.40 Rietveld refinement for samples with higher concentration of Ce. (a) $Ce_{0.85}Gd_{0.15}Ni_5$ and obtained cell parameters; (b) $Ce_{0.9}Gd_{0.1}Ni_5$ and obtained cell parameters; (c) $Ce_{0.95}Gd_{0.05}Ni_5$ and obtained cell parameters; (d) $Ce_{0.97}Gd_{0.03}Ni_5$ and obtained parameters.

These results confirm the hypothesis prediction, that samples crystalize in the hexagonal $CaCu_5$ type crystal structure with *P6/mmm* space group. Rietveld refinement shows, that obtained parameters are very similar, due to very small differences between prepared concentrations.

5.3.2 Electron Microscopy

Microanalysis of $Ce_xGd_{1-x}Ni_5$ (x = 0.85; 0.9; 0.95 and 0.97) samples was performed by JEOL JSM-6610LV-Scanning electron microscopy situated in Slovak Academy of Science in Košice. Analysis shows a good agreement with calculations of composition. Results are plotted in Figure 5.41. Here we present images, tables with the real representation of each element and the observed spectra.

The surfaces of samples have the same characteristics as previous bulks, where with increasing of Ce content the superficial area gets smoother. Also, a single phase was confirmed for all compounds.

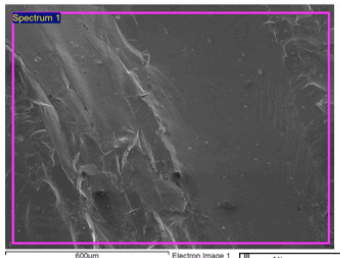

$Ce_{0.85}Gd_{0.015}Ni_5$	Atomic %
Gd	1.58
Ce	11.11
Ni	87.31
TOTAL	100.00

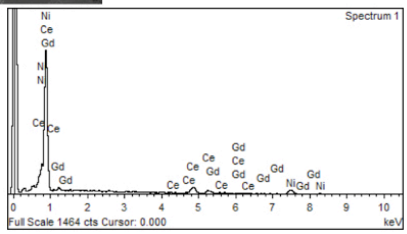

(a)

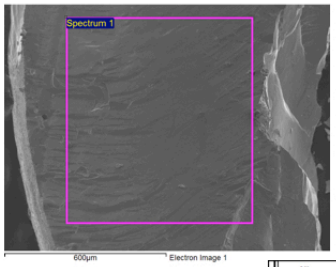

$Ce_{0.9}Gd_{0.1}Ni_5$	Atomic %
Gd	1.83
Ce	16.02
Ni	82.15
TOTAL	100.00

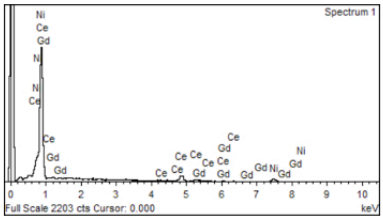

(b)

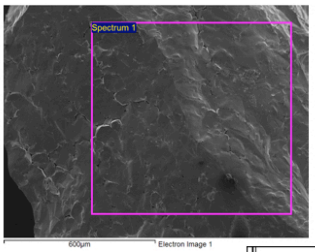

$Ce_{0.95}Gd_{0.05}Ni_5$	Atomic %
Gd	0.48
Ce	17.05
Ni	82.46
TOTAL	100.00

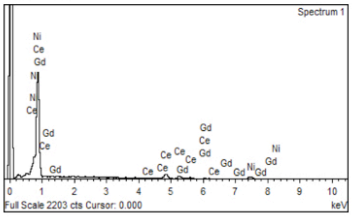

(c)

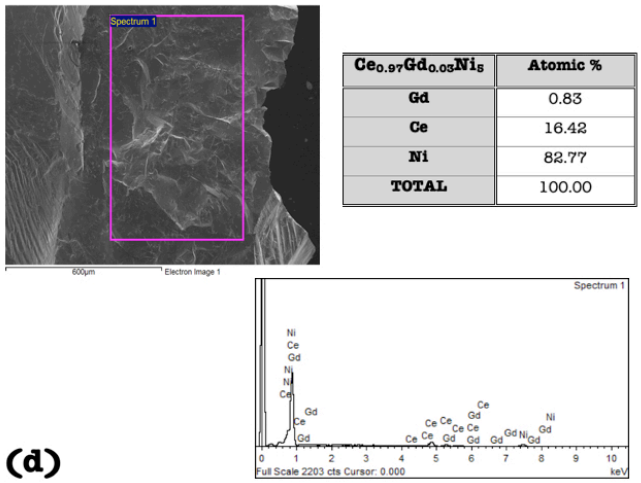

$Ce_{0.97}Gd_{0.03}Ni_5$	Atomic %
Gd	0.83
Ce	16.42
Ni	82.77
TOTAL	100.00

Figure 5.41 SEM images for samples with high content of Ce.

5.3.3 Magnetic Measurements

With a focus on materials containing more Ce atoms, magnetic properties have been studied. Temperature dependences of zero field (ZFC) – field cooling (FC) were carried out.

Figure 5.42 shows a temperature dependence of the ZFC-FC regime measured at three different applied magnetic fields. At the lowest magnetic fields, an anomaly is observed, which was verified by the derivative *dM/dT* (plotted inset of Figure 5.42). A transition temperature reaches the value of 4.9 K, which agrees with the idea of decreasing T_c, when Ce content increases. An applied magnetic field wipes out this transition. A Curie-Weiss law was applied to the inverse of the magnetic susceptibility and obtained values are: an effective paramagnetic moment is $\mu_{eff} = 4.56\ \mu_B$/f.u, which is value between Gd^{3+}ion and Ce^{3+} ion and θ_p is of - 74.33 K.

The same kind of analysis has been performed for all concentrations from this family of compounds.

When the $Ce_{0.9}Gd_{0.1}Ni_5$ sample (see in Figure 5.43) was studied, no magnetic ordering was observed from $T = 2$ K up to $T = 300$ K. A large maximum which is typical for systems, in which spin fluctuation effect has an important role, [152, 153] is not observed in this temperature range. A value obtained from a high temperature Curie-Weiss fit corresponds with expectations.

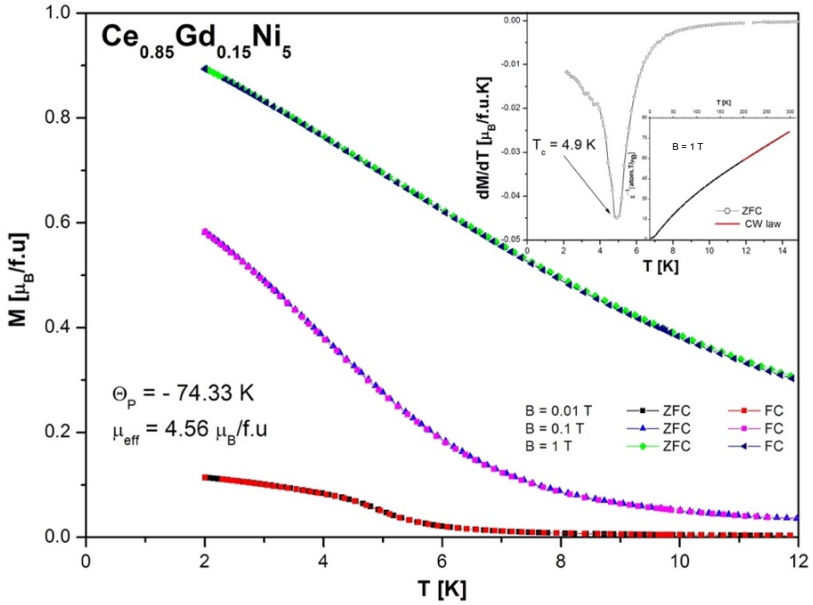

Figure 5.42 Temperature dependence of the ZFC-FC magnetization of $Ce_{0.85}Gd_{0.15}Ni_5$ under three different applied magnetic fields. The inset shows the dM/dT derivative, fixing the T_c and the CW fit [154].

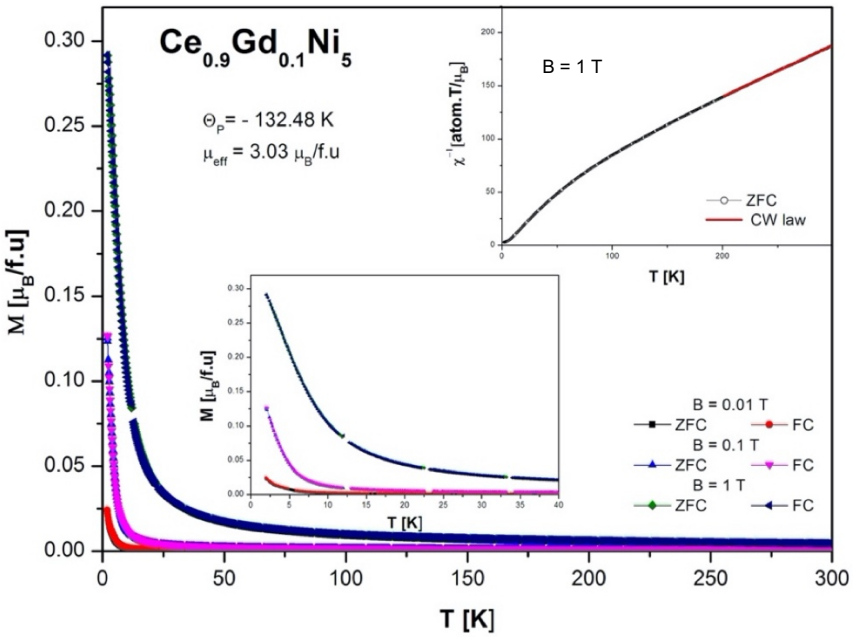

Figure 5.43 M(T) of $Gd_{0.9}Ni_{0.1}Ni_5$ in three different applied magnetic fields. Inset (down) shows low temperature zoom of M(T). Inset (up) represents inverse magnetic susceptibility with CW fit in high temperatures paramagnetic region.

From the point of view of the influence of spin fluctuations, $Ce_{0.95}Gd_{0.05}Ni_5$ is an interesting compound (see Figure 5.44). In Figure 5.44, a minimum is observed around T = 20 K. Irreversibility curves irreversibility indicate, that in this sample a short-range order is present at low applied magnetic fields. Moreover, higher magnetic fields diminish it (see in Figure 5.45). These correlations correspond with spin fluctuation effect and another one of paramagnetic origin [154]. Their contribution is calculated and plotted in Figure 5.44. For pure $CeNi_5$ [66,150] a minimum at low temperature region has not been observed in the magnetic measurements. A small shoulder around T = 130 K at B = 0.1 T at 1 T with relation to spin fluctuations could be observed. This effect is typical for $CeNi_5$ published e.g. [147]. In this case, substitution of Ce with Gd entail that spin fluctuations maximum is shifted to lower temperatures. The inset of Figure 5.45 represents inverse magnetic susceptibility with Curie–Weiss fit at high temperatures. The obtained values for paramagnetic Curie temperature and an effective magnetic moments support presented results.

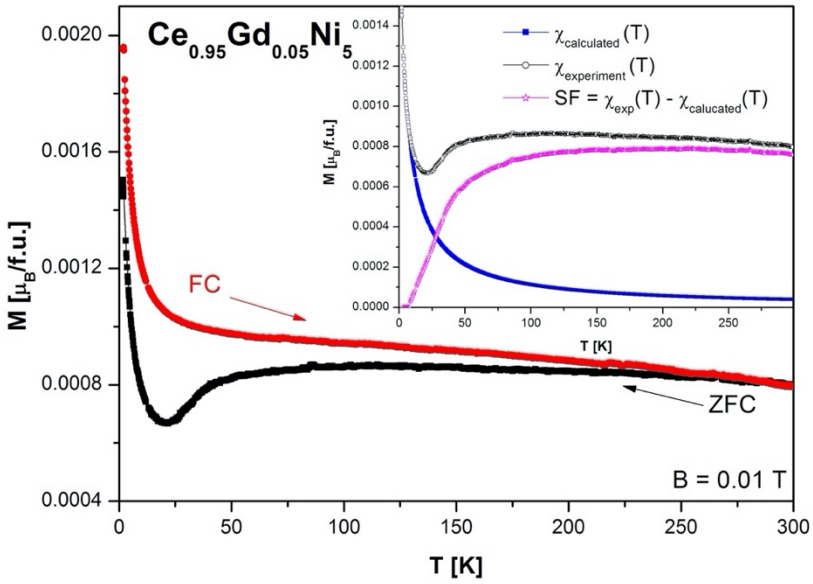

Figure 5.44 M(T) of the ZFC-FC magnetization at B = 0.01 T for $Ce_{0.95}Gd_{0.05}Ni_5$ compound. The inset displays a comparison with the calculated data and the difference between experimental and calculated data [154].

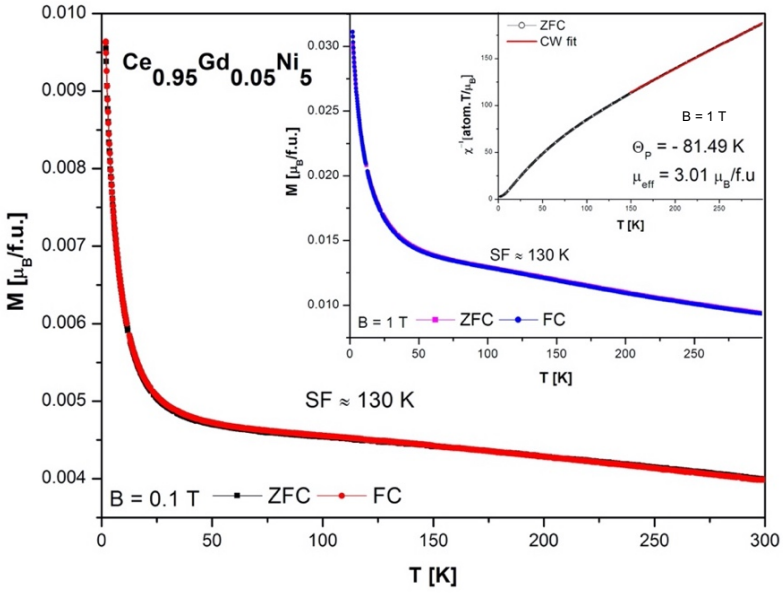

Figure 5.45 M(T) of the ZFC-FC magnetization at B = 0.1 T and 1 T for $Ce_{0.95}Gd_{0.05}Ni_5$ compound. The inset shows inverse magnetic susceptibility with applied Currie – Weiss fit at high temperatures [154].

The last polycrystalline sample from this group is $Ce_{0.97}Gd_{0.03}Ni_5$ compound. Magnetic measurements data are shown in Figure 5.46. One could see, that maximum of magnetization is clearer than for samples containing more Gd. Its position is in agreement with pure $CeNi_5$. The obtained value for effective paramagnetic moment (μ_{eff} = 2.49 μ_B) is, despite the Gd, lower than value for Ce^{3+} ion (2.54 μ_B). It can be caused by splitting of CEF or by noninteger valency state of Ce.

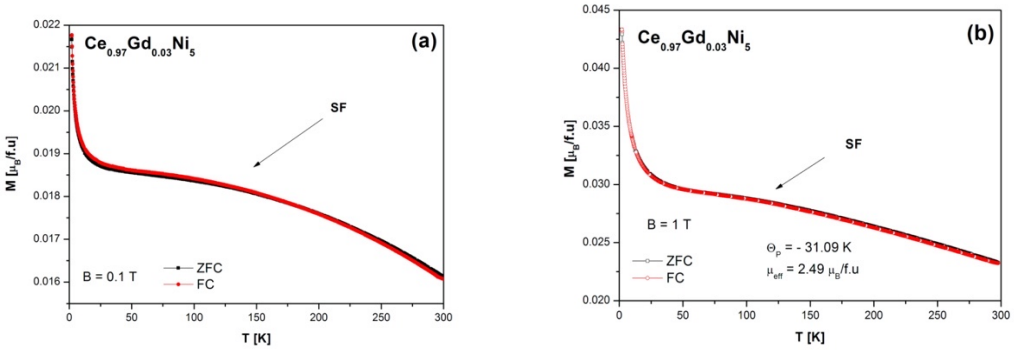

Figure 5.46 (a) Temperature dependence of magnetization at B = 0.1 T with shoulder corresponding to spin fluctuation effect for $Ce_{0.97}Gd_{0.03}Ni_5$. (b) Temperature dependence of magnetization at B = 1 T with shoulder corresponding to spin fluctuation effect and obtained data from CW fit for $Ce_{0.97}Gd_{0.03}Ni_5$.

In order to determine a saturation magnetization, the Figure 5.47 was plotted. When the Gd decreases, saturation magnetization has tendency to decrease, which is in agreement with compounds studied in [133].

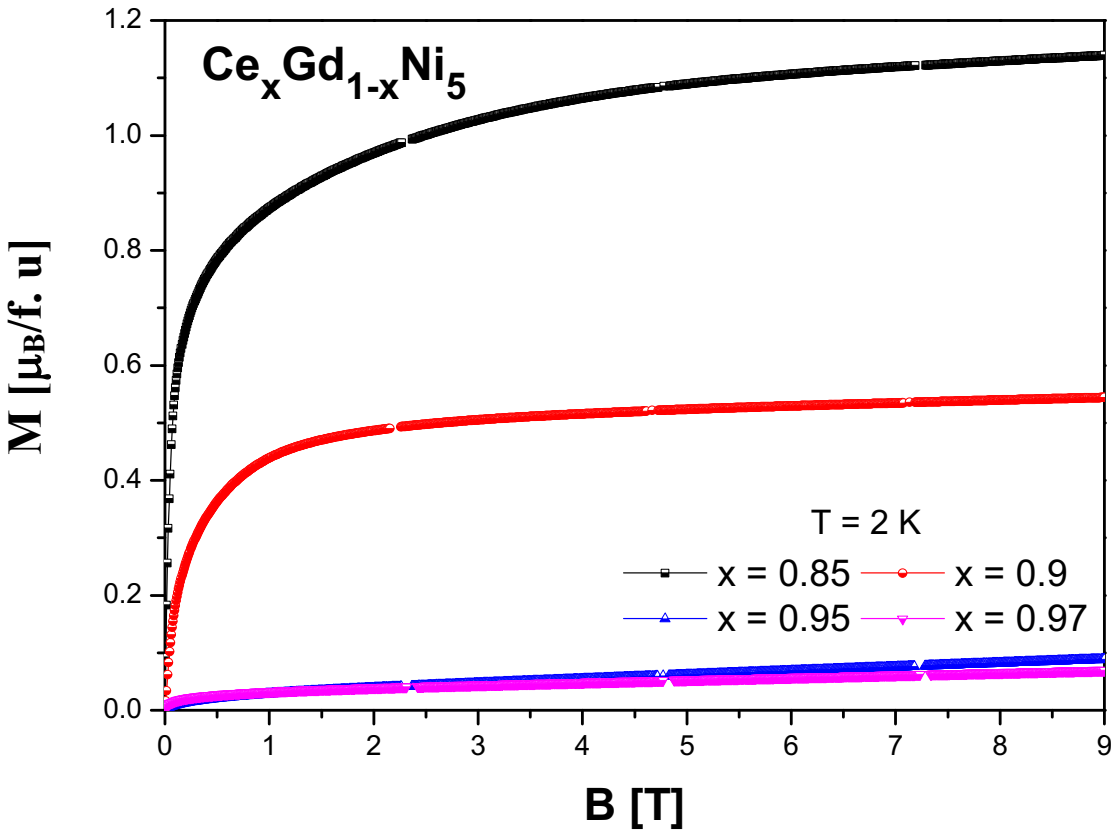

Figure 5.47 M(B) for $Ce_xGd_{1-x}Ni_5$ compounds at T = 2 K [154].

5.3.4 Heat Capacity Measurements

Heat capacity measurements were performed basically in a temperature range from $T = 2$ K up to $T = 300$ K. Due to the indication, that interesting physical properties could exist at very low temperature range, the concentrations $Ce_{0.85}Gd_{0.15}Ni_5$ and $Ce_{0.9}Gd_{0.1}Ni_5$ were also measured at very low temperatures with the use of ^{3}He refrigerator.

For $Ce_{0.85}Gd_{0.15}Ni_5$ compound, the temperature dependence of heat capacity is plotted in Figure 5.48. One could see, that λ-like anomaly is observed around $T < 5$ K, which is in good agreement with transition temperature obtained from *dM/dT*. If higher magnetic field is applied, a maximum is shifted to higher temperatures and finally

diminished. At high temperatures heat capacity follows Dulong – Petit law and achieve $3nR \sim 150$ J/mol.K.

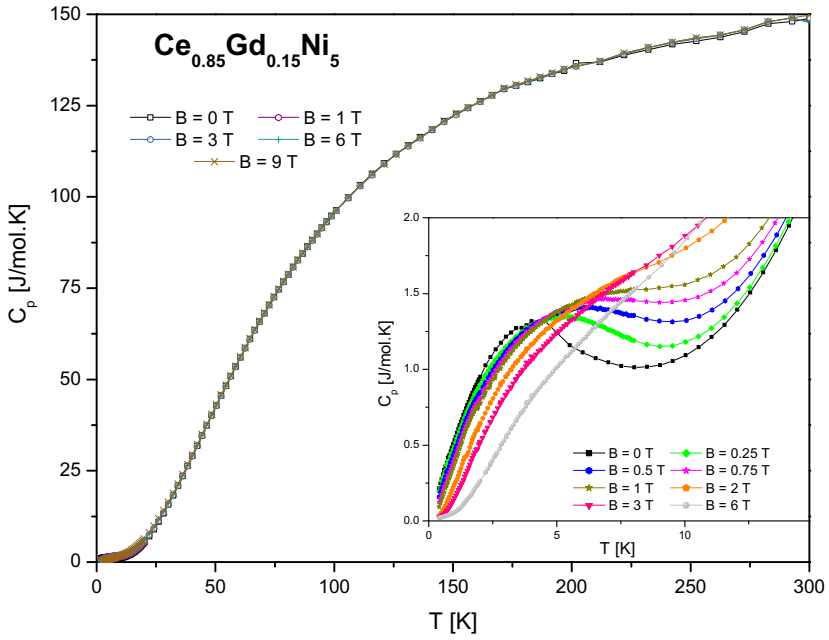

Figure 5.48 Temperature dependence of heat capacity measured at different magnetic fields for $Ce_{0.85}Gd_{0.15}Ni_5$. The inset shows low temperature measurements at different applied magnetic fields with transition temperature [154].

Another studied concentration is $Ce_{0.9}Gd_{0.1}Ni_5$ and $C_p(T)$ is shown in Figure 5.49. No magnetic ordering is observed from $T = 0.5$ K up to high temperatures. Dulong – Petit law is confirmed again at high temperatures.

Temperature dependences of heat capacities for $Ce_{0.95}Gd_{0.05}Ni_5$ and $Ce_{0.97}Gd_{0.03}Ni_5$ samples are plotted in Figure 5.50. λ-like anomaly is not present. It is characteristic feature of magnetic measurements, in which no transition temperatures were determined. High temperature values follow Dulong – Petit law for both samples.

The Sommerfeld coefficients were estimated as in previous samples cases from heat capacity measurements. A value obtained for each sample is close to $\gamma_{9T} = 42$ mJ/(mol.K^2) as it is reported in [154].

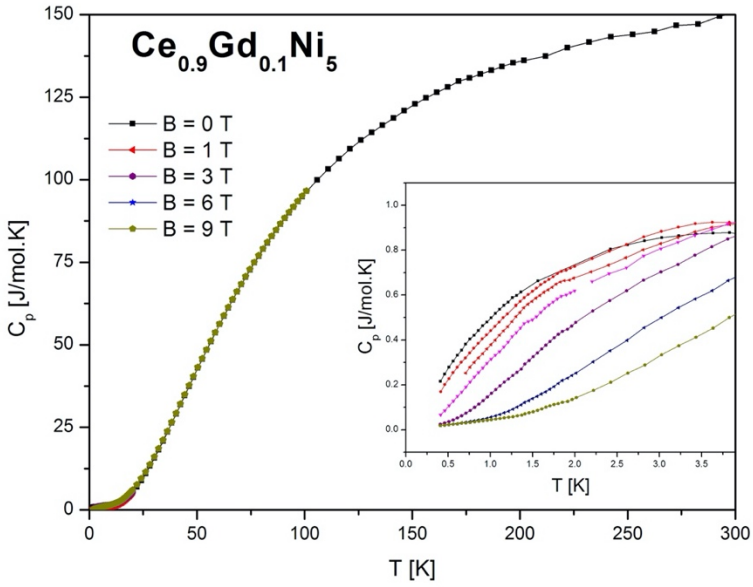

Figure 5.49 Temperature dependence of heat capacity measured at different magnetic fields for $Ce_{0.9}Gd_{0.1}Ni_5$. The inset shows a low temperature detail.

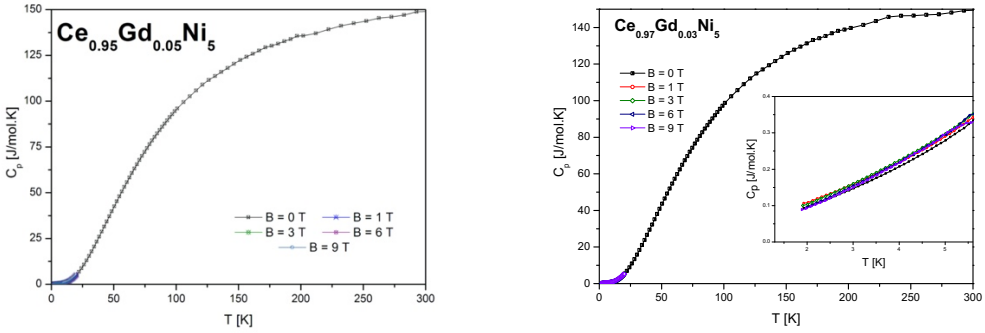

Figure 5.50 The left side represents $C_p(T)$ measured at different magnetic fields for $Ce_{0.95}Gd_{0.05}Ni_5$. The right side represents $C_p(T)$ measured at different magnetic fields for $Ce_{0.97}Gd_{0.03}Ni_5$. The inset show a low temperature detail for $Ce_{0.97}Gd_{0.03}Ni_5$ sample.

Disappearance of the magnetic transition in $Ce_xGd_{1-x}Ni_5$ system, where x = 0.85; 0.9; 0.95 and 0.97 can be better illustrated in Figure 5.51. For $Ce_{0.85}Gd_{0.15}Ni_5$, we determined magnetically ordered state below $T = 4.9$ K from magnetic measurements and from anomaly observed in heat capacity characteristics. Moreover, for samples with x = 0.95 and x = 0.97 no magnetic ordering is present. This trend is related to normal Fermi liquid behaviour. An interesting fact is, that compound $Ce_{0.9}Gd_{0.1}Ni_5$ follows a *-ln(T)* dependence in the temperature region ($T \sim 0.5$ K to 3.5 K) and for zero applied magnetic

field. It could basically indicate, that investigated system is located very close to a possible quantum critical point [4].

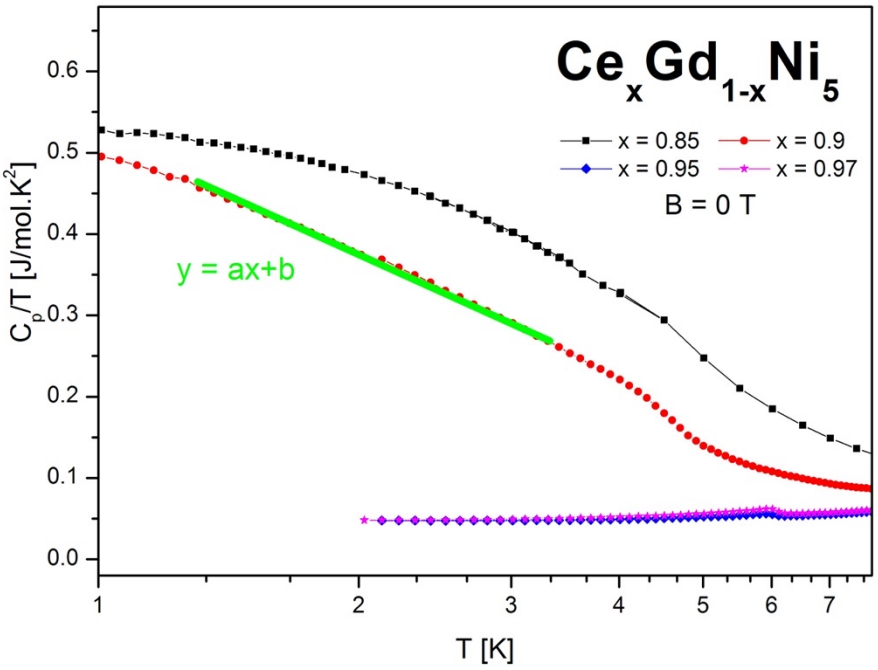

Figure 5.51 C_p/T vs log(T) plotted for all studied samples from the group $Ce_xGd_{1-x}Ni_5$ [154].

5.3.5 Electrical Resistivity and Magnetoresistivity Measurements

Electrical resistivity and magnetoresistivity of this group of compounds was studied in DynaCool devices. The interesting results were obtained for $Ce_{0.85}Gd_{0.15}Ni_5$ (see Figure 5.52) and for $Ce_{0.9}Gd_{0.1}Ni_5$ (see Figure 5.53). Samples containing more Ce content were measured also, but no substantial influence of applied magnetic field was observed (see Figure 5.54). Residual resistivity ratios were ~ 3 for all samples. The typical metal character is also observed. $Ce_{0.85}Gd_{0.15}Ni_5$ compound has a maximal negative magnetoresistivity at 2 K. When temperature increases, MR decreases and for $T = 30$ K is positive. One can see that in the inset of Figure 5.52 (a) a Kondo effect appears. For $Ce_{0.9}Gd_{0.1}Ni_5$ compound *-ln(T)* character on *R(T)* is observed. This fact supports our previous physical properties study – magnetic and heat capacity measurements. Higher applied magnetic fields ($B < 0.3$ T) depress this behaviour. Magnetoresistivity is negative

and at T = 2 K. For higher temperatures, the dependences behave as results of Lorentz force.

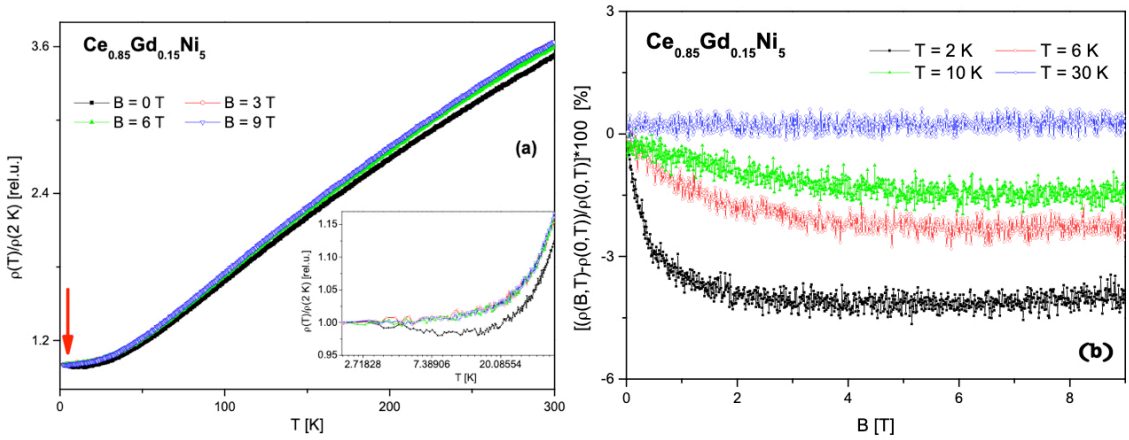

Figure 5.52 (a) Temperature dependence of ρ(T)/ρ(2K) of $Ce_{0.85}Gd_{0.15}Ni_5$ compound at different magnetic fields. The arrow shows the position of transition temperature. The inset shows a low temperature detail in ln scale for temperature. (b) Electrical magnetoresistivity of the same compound as a function of different temperatures.

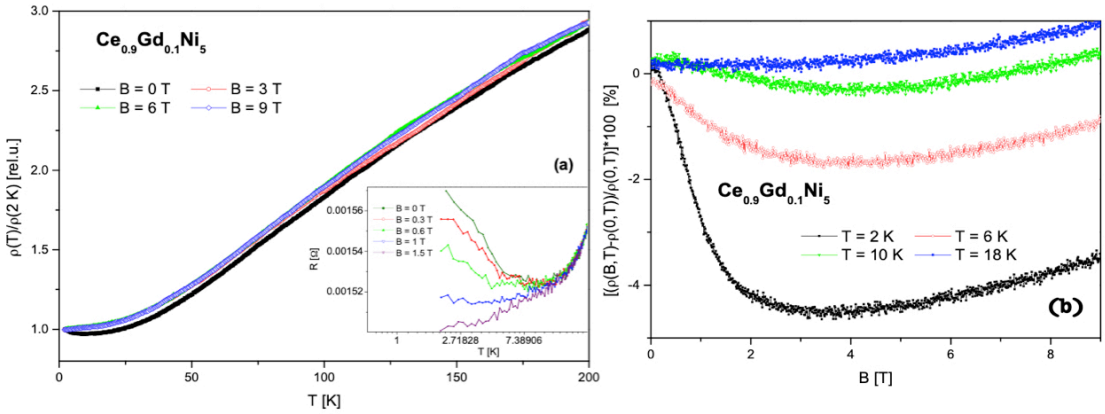

Figure 5.53 (a) Temperature dependence of ρ(T)/ρ(2K) of $Ce_{0.9}Gd_{0.1}Ni_5$ compound at different applied magnetic fields. The inset shows R(T) in ln scale. The results for small applied magnetic fields (B < 0.3 T) suppose a state close to the QCP. (b) Electrical magnetoresistivity of the same compound as a function of different temperatures.

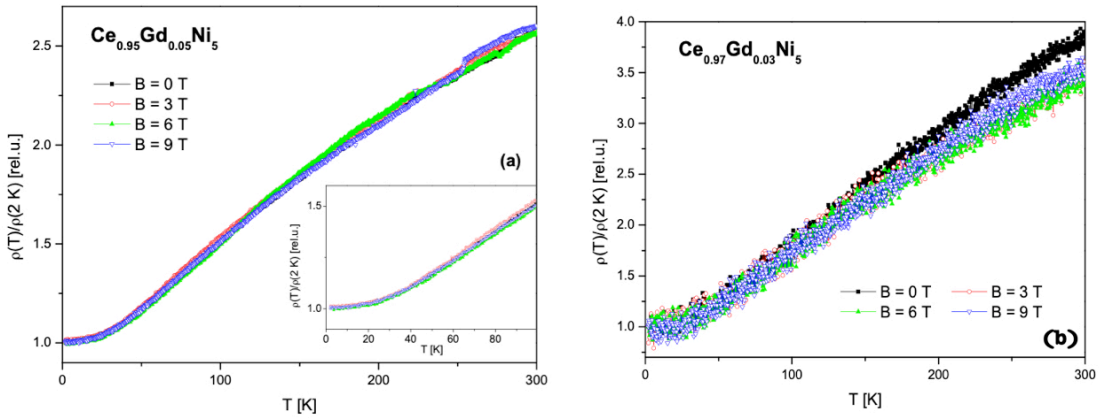

Figure 5.54 (a) Temperature dependence of ρ(T)/ρ(2K) of $Ce_{0.95}Gd_{0.05}Ni_5$ compound at different magnetic fields. The inset shows low temperature detail. (b) Temperature dependence of ρ(T)/ρ(2K) of $Ce_{0.97}Gd_{0.03}Ni_5$ compound at different magnetic fields.

5.3.6 Conclusion

The polycrystalline samples of $Ce_xGd_{1-x}Ni_5$, where x = 0.85; 0.9; 0.95 and 0.97 were prepared. From the XRD analysis, hexagonal crystal structure was observed with lattice parameter in accordance with the assumption. With increasing of Ce content, the lattice parameters increase as well. From the investigation of physical properties, we found out that, magnetic transition was observed at low temperature (T = 4.9 K) for concentration x = 0.85. For concentration x = 0.9, the observed *-ln(T)* dependence may indicate that the system is close to the QCP. However, further study is necessary. For the rest concentrations x = 0.95 and x = 0.97 effect of spin fluctuations dominates. In the future, it could be interesting to make a neutron diffraction, which can confirm our indications for presence of QCP in this system.

5.4 Samples Based on Yb

In this part of the work, the physical properties of samples based on Yb will be described. This class of materials is interesting due to different ways of their possible applications mostly, in the low temperature range. Yb-based sample is hard to prepare, because of the problem with evaporation - high vapour pressure [155]. Despite that, the

several samples have been prepared by inductive furnace melting process. After production samples were annealed - 10 days at 700 °C ($YbNi_5$, $Yb_{0.5}Ce_{0.5}Ni_5$ and $Yb_{0.5}Gd_{0.5}Ni_5$) and the second series in two different periods - 10 days at 700 °C and 11 days at 600°C ($Yb_{0.8}Lu_{0.2}Cu_4Ni$, $Yb_{0.8}Sc_{0.2}Cu_4Ni$, $YbCu_{4.7}Ni_{0.3}$ and $YbCu_{4.2}Ni_{0.8}$).

5.4.1 (Yb,Ce,Gd)Ni_5

Taking into consideration, that one of the main ideas of this thesis is focused on Yb-based materials, we investigated the influence of chemical pressure on physical properties. We wanted to study similar samples as a in the previous part. These samples were prepared by inductive melting technique. They are polycrystalline compounds based on – $YbNi_5$; $Ce_{0.5}Yb_{0.5}Ni_5$ and $Yb_{0.5}Gd_{0.5}Ni_5$. Due to the problem of Yb – high vapor pressure, it is very important to perform structural and microstructural analysis to be sure, if it is prepared in required stoichiometric compositions. XRD collected data were treated by PowderCell program.

The first studied sample was $YbNi_5$. Its crystallographic data are plotted in Figure 5.55. Indexed peaks belong mostly to theoretical pattern of $YbNi_5$. This means that crystallographic structure is hexagonal of $CaCu_5$ type with *P6/mmm* space group. The lattice parameters are calculated also. Some extra peaks come from the secondary phase, but we do not have any information about it. The existence of secondary phase could be due to small presence of Ta. The result of SEM analysis is shown in the inset of picture (Figure 5.55). $YbNi_5$ surface looks porous. Despite no single phase of this material, magnetic measurement indicates magnetically ordered state below $T = 2\ K$, as it was reported in [75].

When we get back to the chapter three of this thesis, where the main ideas are described in detail and drawn in a triangle, in the median there are 3 samples, having the composition 50 to 50. The first of them ($Gd_{0.5}Ce_{0.5}Ni_5$) is presented in previous subchapter, the second ($Ce_{0.5}Yb_{0.5}Ni_5$) and third ones ($Yb_{0.5}Gd_{0.5}Ni_5$) will be studied in this part.

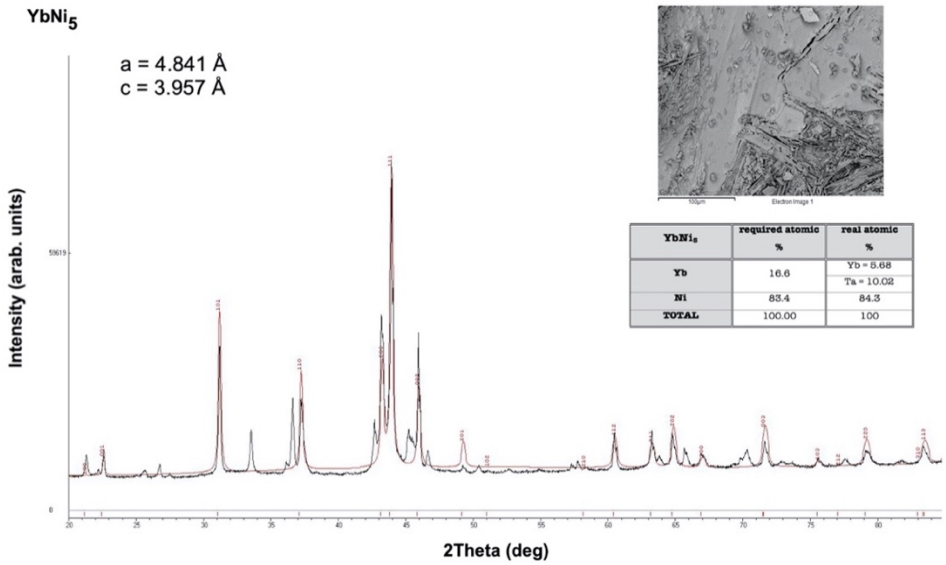

Figure 5.55 Experimental crystallographic pattern of $YbNi_5$ indexed with the theoretical patterns of $YbNi_5$. Inset shows microstructural analysis.

XRD analysis of $Ce_{0.5}Yb_{0.5}Ni_5$ is presented in Figure 5.56. The fitting is nice and corresponds with obtained peaks. Calculated lattice parameters are larger than for pure $YbNi_5$. Crystallographic structure is hexagonal as it is for the whole $RENi_5$ family. SEM analysis shows, that sample is well melted and required stoichiometric was successfully prepared. SEM picture seems to have surface contour.

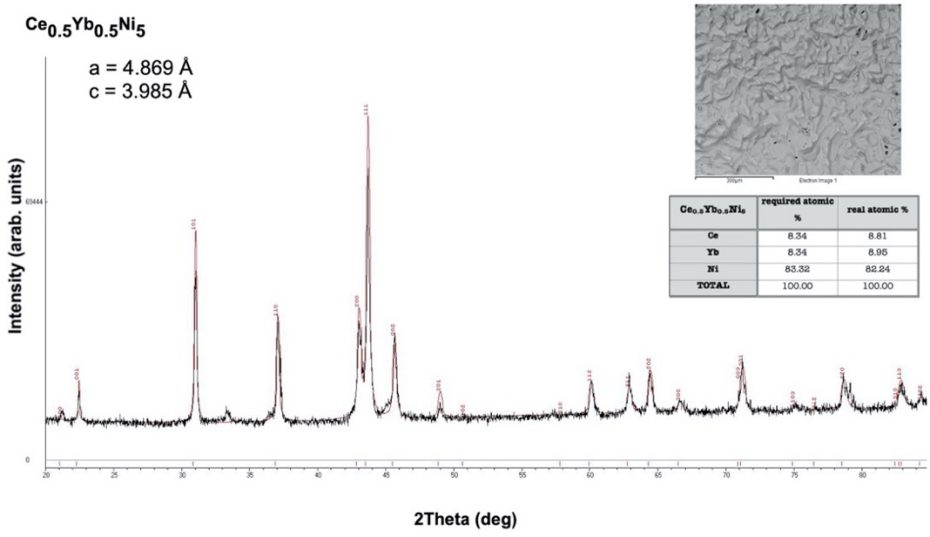

Figure 5.56 Experimental crystallographic pattern of $Ce_{0.5}Yb_{0.5}Ni_5$ sample with indexed peaks. Inset shows microstructural analysis.

$Yb_{0.5}Gd_{0.5}Ni_5$ sample and its XRD data are shown in Figure 5.57. Main phase lattice parameters are calculated and presented in this figure. A few more peaks belong to the secondary phase. But it was not successfully indexed. SEM analysis with EDX is given in the inset. The sample surface is porous and contains grains of non-regular shapes. The existence of the secondary phase could by caused by oxides. It was confirmed in this material. However, at this moment, we were not able to find it.

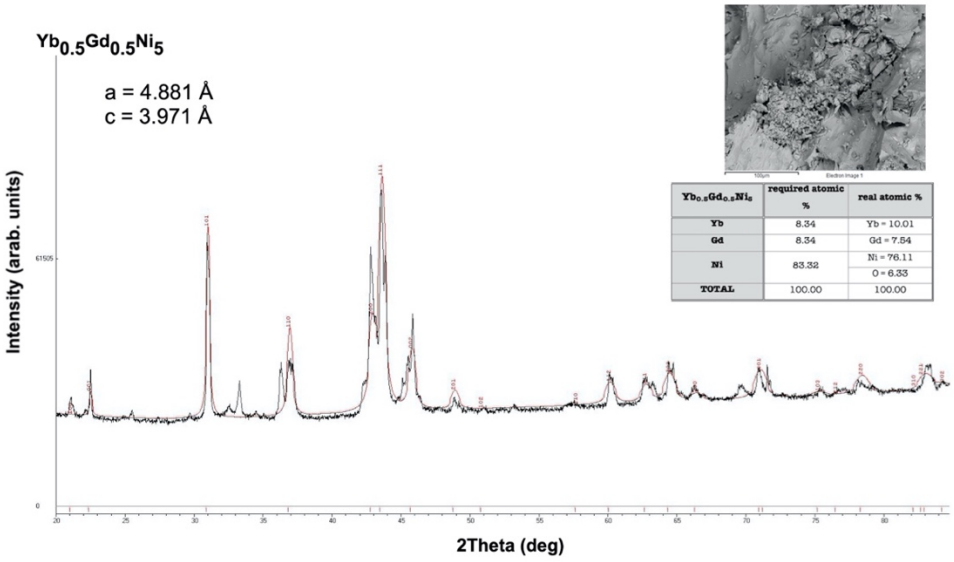

Figure 5.57 Experimental crystallographic pattern of $Yb_{0.5}Gd_{0.5}Ni_5$ sample with indexed peaks. Inset shows microstructural analysis.

Magnetic measurements have been performed on SQUID located at the University of Cantabria, Santander. With regard to structural problem of $YbNi_5$ other analysis of this material are not presented in literature. For $Ce_{0.5}Yb_{0.5}Ni_5$ compound, Figure 5.58 is plotted. (a) *M(T)* at very low field B = 0.1 T, where a clear maximum (T ~ 25 K) is observed. This anomaly can be caused by spin fluctuation effect, which is typical for $CeNi_5$ [147] and in this work it was also confirmed in other compositions. Its position is lower, which could be related to magnetic ordering of $YbNi_5$ [75]. Mentioned maximum is visible at B = 0.1 T, but with lower magnitude (b), and for B = 1 T (c) only small shoulder exists. Similar behavior of spin fluctuations was observed in CeNiGe [147]. From the inverse magnetic susceptibility, effective paramagnetic moment was calculated.

It yields to the value of μ_{eff} = 4.07 μ_B/f.u, which is between Ce^{3+} ion (2.54 μ_B) and Yb^{3+} ion (4.54 μ_B). Magnetization as a function of magnetic field is plotted in (d). In this temperature range $Yb_{0.5}Ce_{0.5}Ni_5$ does not reach saturation.

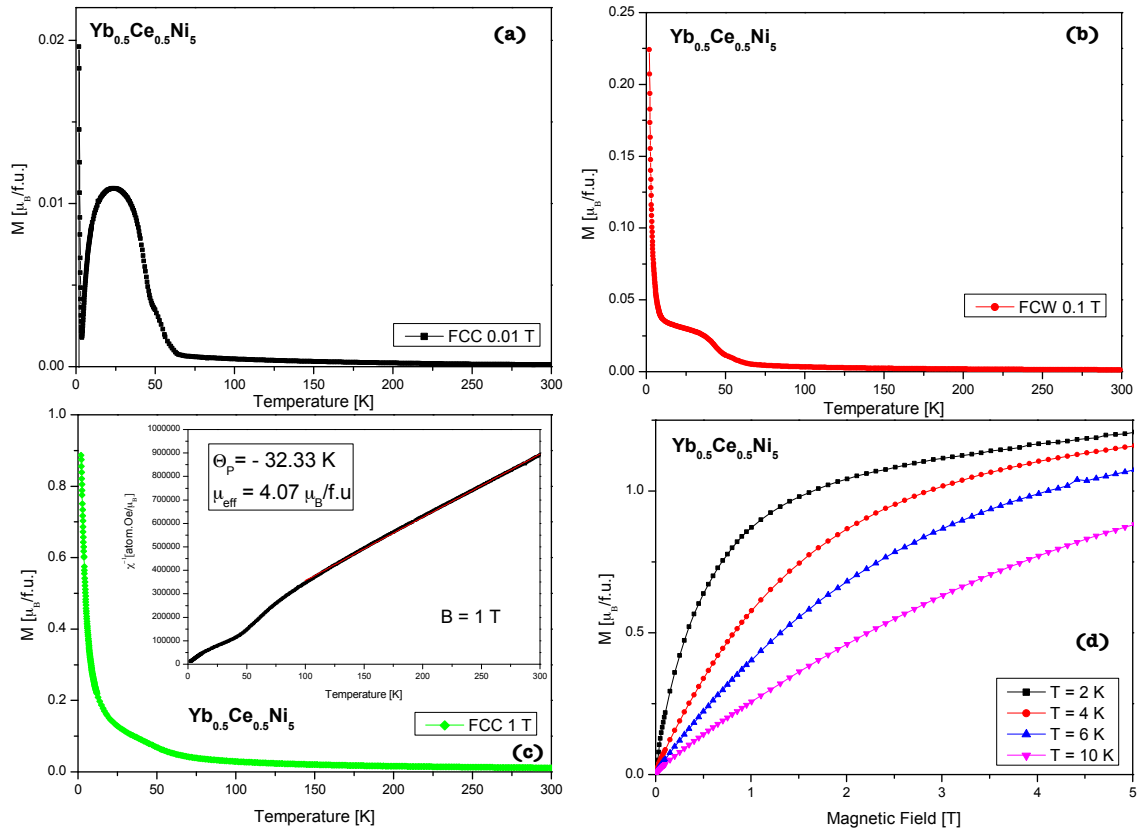

Figure 5.58 Magnetic measurements of $Ce_{0.5}Yb_{0.5}Ni_5$ compound at three different applied magnetic fields. Inset of (c) shows CW fit with obtained values. (d) M(B) at different temperatures.

Considering the existence of two phases for $Yb_{0.5}Gd_{0.5}Ni_5$ we have to write about alloy itself. Therefore, the idea about the possibility of better magnetocaloric properties, which comes from [147] yields us to calculation of magnetocaloric effect (MCE). From the isothermal magnetization data, a magnetic entropy changes $-\Delta S_M$ was determined by formula using a Maxwell relation:

$$\Delta S_M(T) = \int_0^B \left(\frac{M}{\partial T}\right)_B dB. \tag{37}$$

The MCE determined $-\Delta S_M$ for different magnetic fields is plotted in Figure 5.59. A broad maximum is visible at temperatures close to 24 K. Position of this maximum could be due to the observed T_c at 13.3 K in previous study [136]. And is behavior this in agreement with [83]. Moreover, the asymmetric shape of maximum with a tail at higher temperatures is probably due to the spin fluctuation effect [156]. It means, that alloy and compounds with multiple magnetic transition might create new materials to attain magnetic refrigeration technology in broad temperature range with comparison of classical materials.

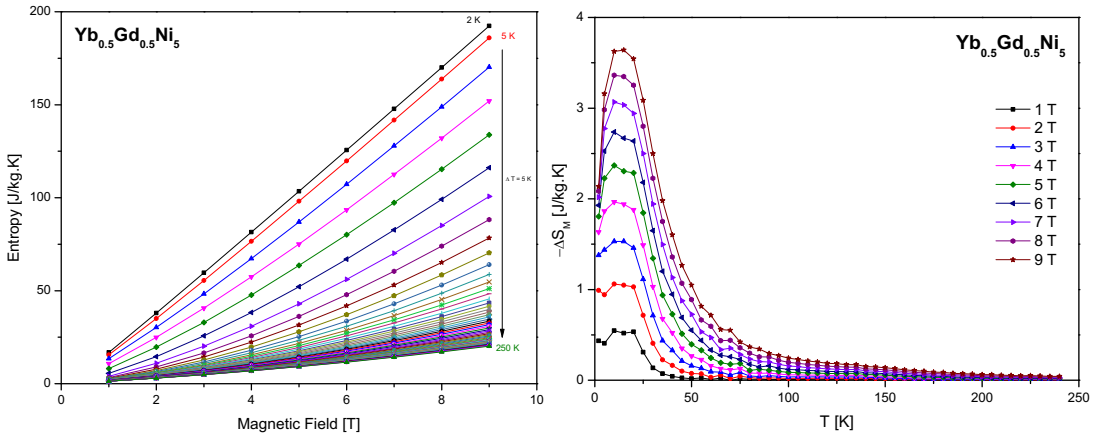

Figure 5.59 Field dependences MCE data at different temperatures of $Yb_{0.5}Gd_{0.5}Ni_5$ (on the left). $-\Delta S_M(T)$ for the $Yb_{0.5}Gd_{0.5}Ni_5$ alloy for various magnetic field changes (on the right).

On the basis of obtained information from structural analysis and magnetic measurements, heat capacity of $Ce_{0.5}Yb_{0.5}Ni_5$ sample was studied and measured. It is plotted in Figure 5.60. Magnetically ordered state is observed at T_c = 0.8 K. This temperature is about 0.3 K higher than the one of $YbNi_5$. As one can see in the inset, C_p upturn is shifted to higher temperatures, when higher magnetic fields are applied. Another anomaly has not been observed and maximum, which is visible at magnetic measurements is related to spin fluctuations comings from Ce. A high temperature region follows Dulong Petit law $3nR$ ~ 150 J/mol.K. Sommerfeld coefficient is γ_{9T} = 154 mJ/mol.K^2. Therefore, this material belongs to heavy fermion group. One can see a typical shape and value of C_p = 1.5 J/mol.K at low temperature maximum for Kondo compounds

at C_p (inset of Figure 5.60) [157]. However, it is necessary to confirms it by electrical resistivity measurements in very low temperatures.

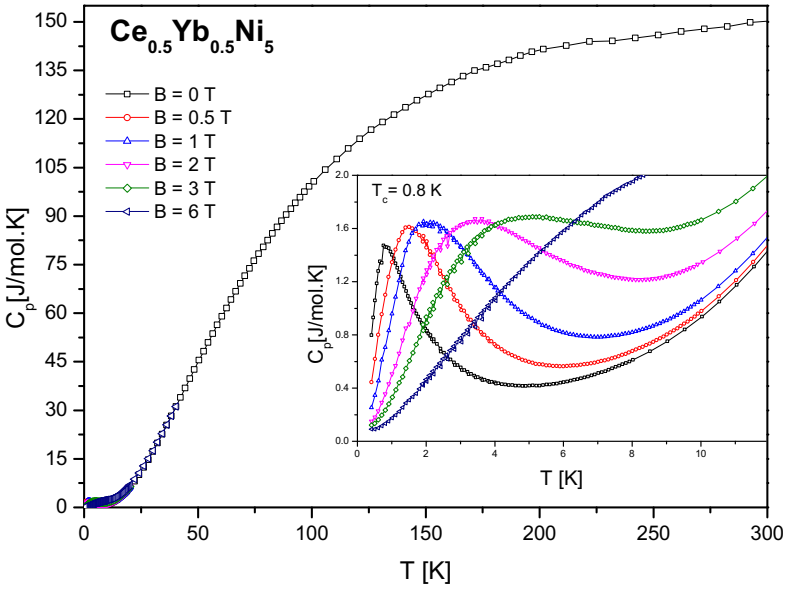

Figure 5.60 Heat capacity measurement of $Ce_{0.5}Yb_{0.5}Ni_5$ compound. Inset shows low temperature detail with transition temperature at 0.8 K.

Electrical transport properties between 2 K and 300 K are shown in Figure 5.61 for $Ce_{0.5}Yb_{0.5}Ni_5$ compound. Despite the maximum observed at heat capacity measurements (T_c = 0.8 K), electrical resistivity does not show the signs of transition temperature. The metal behaviour is detected here again. From the magnetoresistivity measurements we can conclude, that below 2 K magnetoresistivity is magnetic field independent and the obtained negative values are observed. On the other hand, when magnetic field is applied (B = 1 T), magnetoresistivity decreases about 1 %.

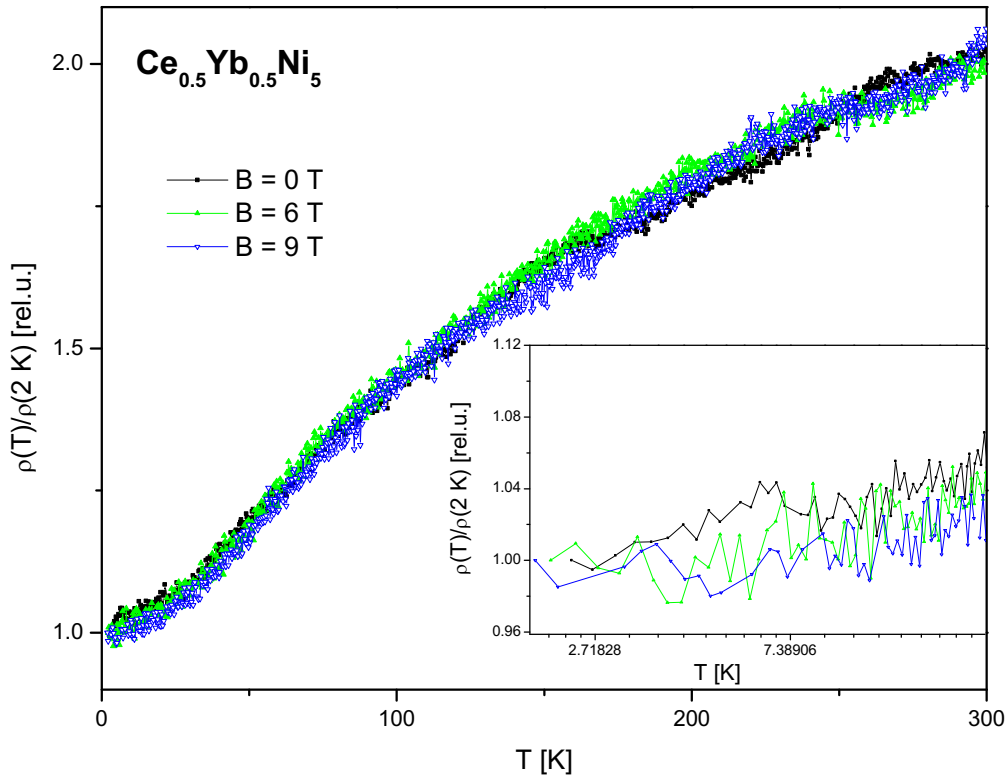

Figure 5.61 Electrical resistivity measurements of $Ce_{0.5}Yb_{0.5}Ni_5$ compound. Inset shows low temperature detail in logarithmic scale.

5.4.2 Yb-Cu-Ni

In order to continue with determination of precise position of QCP in the system based on $YbCu_4Ni$ [93 – 95], we prepared two samples with composition of $YbCu_{4.2}Ni_{0.8}$ and $YbCu_{4.7}Ni_{0.3}$.

Structural analysis is one of the principle analyses to start with when studying physical properties. The first sample from this group is $YbCu_{4.2}Ni_{0.8}$. Structural characterization is provided by XRD analysis and treated by PowderCell software. Results show a mixture of phases between cubic $MgCu_4Sn$ type and its monoclinic superstructure. Peaks of cubic phase are indexed. We are able to estimate an "average" lattice parameter for cubic structure. It is plotted in Figure 5.62. This lattice parameter (a = 0.659 nm) is the value very close to obtained one for $YbCu_4Ni$ published in [95]. Microstructural analysis shows very small deviation from required atomic percent composition for Yb and Ni (~ 2 %). The surface resembles to a long straw shape.

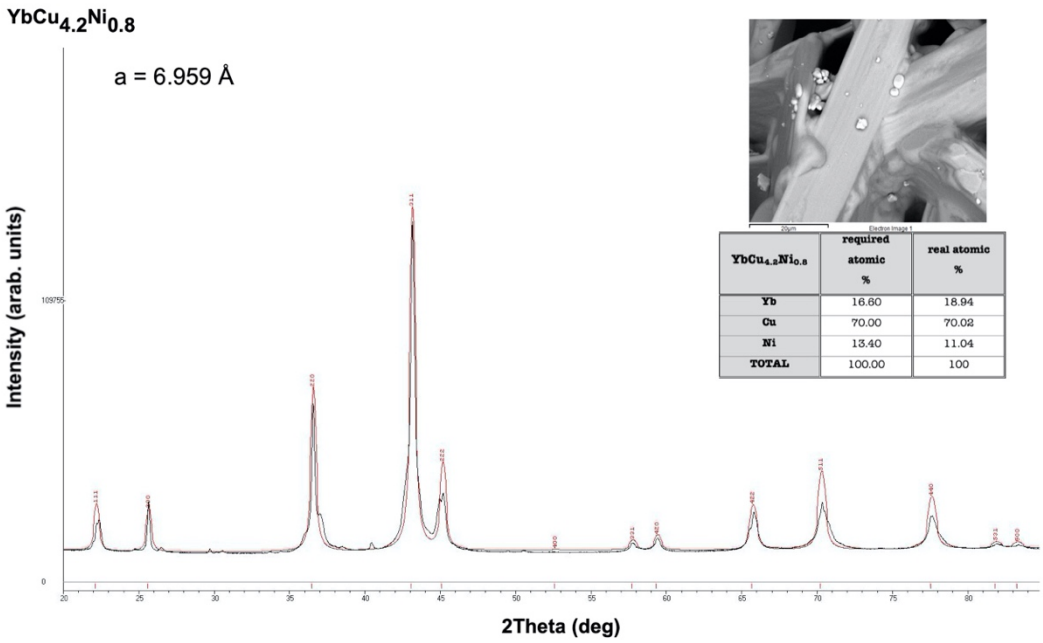

Figure 5.62 Experimental crystallographic pattern of $YbCu_{4.2}Ni_{0.8}$ sample with indexed peaks. Inset shows microstructural analysis.

The second sample belonging to this studied system is $YbCu_{4.7}Ni_{0.3}$. The results from XRD analysis are shown in Figure 5.63. Here, the black line represents experimental data, red indexed peaks originate from $YbCu_4Ni$ cubic structure and the green line is associated with difference between them. Whereas for other Yb-based samples we were able to obtain good results of fitting process, to find the proper positions and assign them to existing crystal structure, in this case we were not successful. The problem may have been caused by the fact that the sample was formed with Ta, which shows also EDX results in the inset of this figure show. However, the problem could also be associated with the evolution of monoclinic superstructure. Anyway, in regard to this structural problem no further measurements were made. In the future, it will be interesting to try to prepare a new sample having this composition.

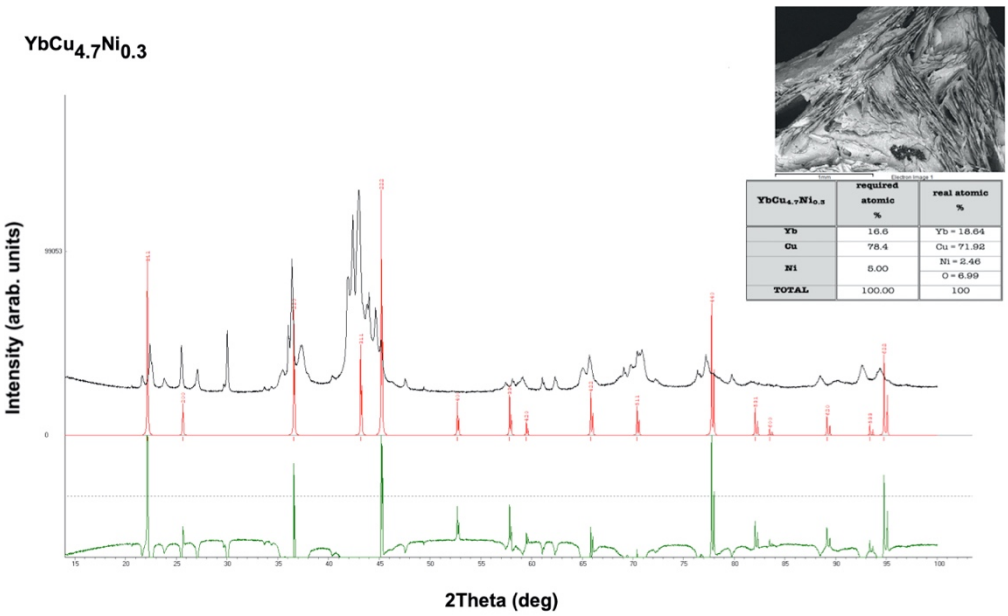

Figure 5.63 An illustration of crystallographic pattern of $YbCu_{4.7}Ni_{0.3}$ sample. Inset shows microstructural analysis.

Magnetic measurements of $YbCu_{4.2}Ni_{0.8}$ done by SQUID magnetometer are presented in *Figure 5.64*. One can see, that no anomaly is observed on a graphical representation of *M(T)* dependence. In inset, where an inverse magnetic susceptibility is plotted with Curie-Weiss fit, the obtained parameters indicate possible antiferromagnetic ordering at very low temperatures. An effective paramagnetic moment is lower than μ_{eff} of $YbCu_4Ni$ [95]. This fact can be caused by the evidence, that in this compound, there is more amount of Cu and lower amount of Ni in comparison to the reference material. Magnetization as a function of magnetic field (see Figure 5.64 (b)) indicates magnetic ordering below T = 2 K. It will be interesting to perform a measurement in ^{3}He refrigerator.

Figure 5.65 shows the temperature dependence of heat capacity for $YbCu_{4.2}Ni_{0.8}$. The observed dependence at room temperature follows Dulong-Petit law. No anomaly is observed in lower temperatures, so we did not mark any transition temperature. However, the inset of this figure is interesting. Dependence of C_p/T vs T is plotted there. At B = 0 T and 0.5 T a typical Fermi liquid behaviour is present. Moreover, higher magnetic field B = 3 T induces NFL behaviour. This behaviour vanishes again at very high magnetic fields B = 6 T and 9 T. Sommerfeld coefficient determined from the data, is taken at the applied magnetic field 9 T, because in zero magnetic field the magnetic contribution is significant.

It is of the value γ_{9T} = 383 mJ/mol.K^2, which corresponds with values typical for heavy fermion group of compounds. For more precise determination of this value it is necessary to measure heat capacity in very low temperature range.

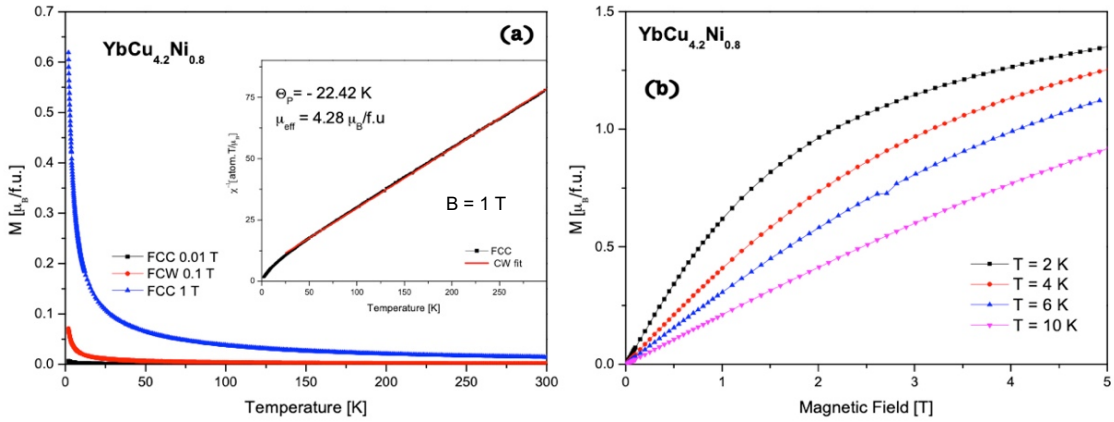

Figure 5.64 (a) M(T) at various applied magnetic fields for $YbCu_{4.2}Ni_{0.8}$. Inset represents inverse magnetic susceptibility with CW fit. Obtained parameters are also shown. (b) M(B) measured at different temperatures.

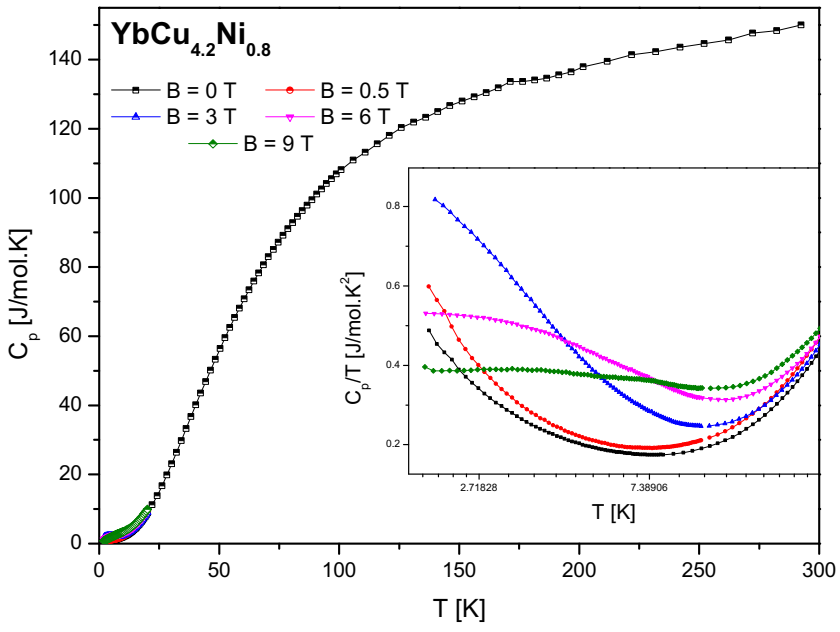

Figure 5.65 Temperature dependence of heat capacity at different applied magnetic fields. Inset represents C_p/T vs T dependence for $YbCu_{4.2}Ni_{0.8}$ sample.

5.4.3 Yb(Lu,Sc)Cu_4Ni

After the sample preparation and annealing process, XRD analysis was done for $Yb_{0.8}Lu_{0.2}Cu_4Ni$ and $Yb_{0.8}Sc_{0.2}Cu_4Ni$. The results, which are presented, show that $Yb_{0.8}Lu_{0.2}Cu_4Ni$ was prepared successfully with one phase and $Yb_{0.8}Sc_{0.2}Cu_4Ni$ includes another phase, which we were not able to confirm at that moment.

Figure 5.66 shows experimental data with fitting. A lattice parameter is $a = 0.6945$ nm and indexed peaks belong to cubic structure of $MgCu_4Sn$ type. SEM and EDX analysis confirmed a stoichiometric composition with deviation around 1 % from the theoretically calculated one. The obtained data are in a good agreement with fitting. The surface of this sample is unique.

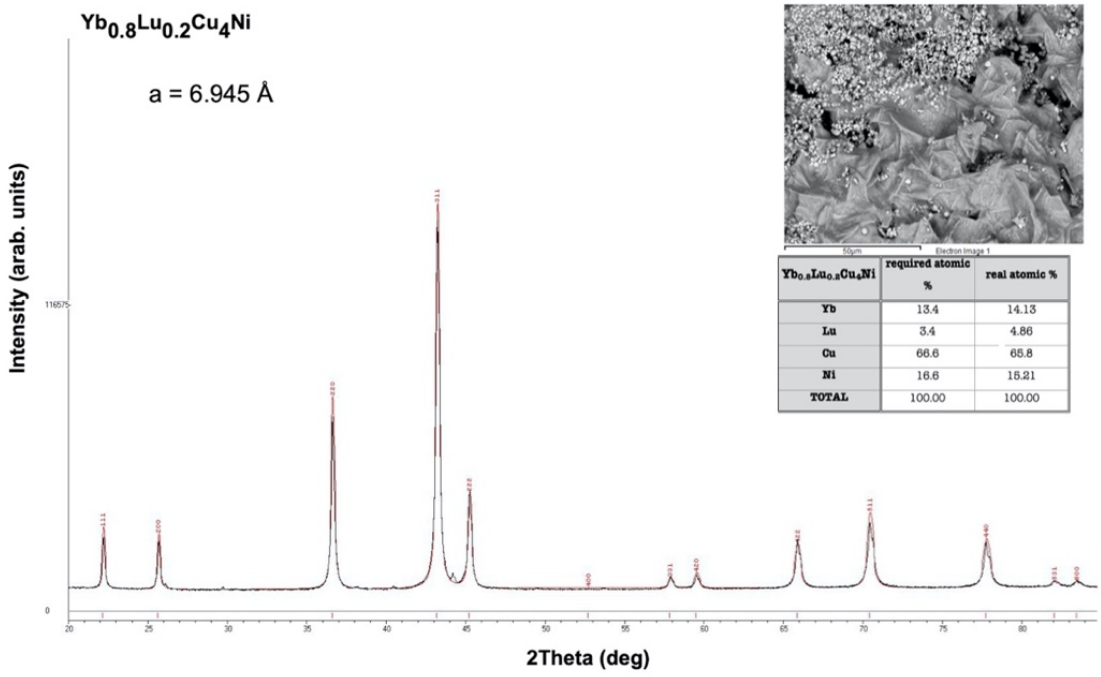

Figure 5.66 Experimental crystallographic pattern of $Yb_{0.8}Lu_{0.2}Cu_4Ni$ sample with indexed peaks. Inset shows microstructural analysis.

Another sample from this group is $Yb_{0.8}Sc_{0.2}Cu_4Ni$. The experimental data from XRD, SEM and EDX analyses are shown in Figure 5.67. The most of peaks are associated with an "average" cubic phase with a lattice parameter $a = 6.973$ Å. The second phase is probably a formation of the monoclinic superstructure, but it was never indexed. EDX

analysis shows that sample contains Ta from crucible, which was melted during the sample preparation, and also oxides. SEM photo shows a formation of grain on the surface. In the future it will be interesting to try to prepare this sample again without Ta and oxides. Due to the ambiguous structural characterization, the following of the physical properties were not provided.

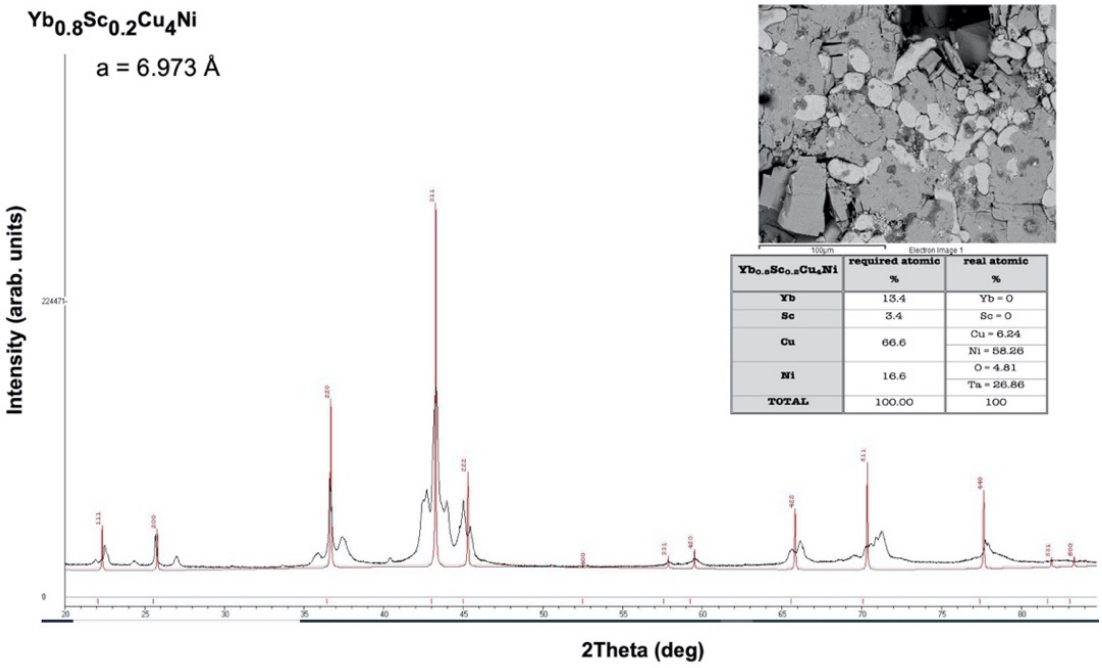

Figure 5.67 Experimental crystallographic pattern of $Yb_{0.8}Sc_{0.2}Cu_4Ni$ sample with indexed peaks. Inset shows microstructural analysis.

An investigation of physical properties continues with magnetic studies of $Yb_{0.8}Lu_{0.2}Cu_4Ni$ compound. Basically, magnetic properties of $YbCu_4Ni$ have been already studied and published [93]. $LuCu_4Ni$ compound was used as a phonon etalon [95]. Physical properties of this compound are plotted in Figure 5.68. In the temperature range from 2 K up to 300 K no magnetic ordering is present. Figure 5.68 (b) indicates, that critical temperature could be below T = 2 K. Inverse magnetic susceptibility in the inset of Figure 5.68 (a) with Curie-Weiss fit is shown. Here, the calculated negative value of paramagnetic Curie temperature indicates an antiferromagnetic interaction, which is in an agreement with initial $YbCu_4Ni$ compound [95]. The effective paramagnetic moment is of μ_{eff} = 3.97 μ_B/f.u, which is a lower value that the one for free Yb^{3+} ion. It can be caused by Lu substation of Yb content.

Figure 5.69 shows measurements of pressure response of rare earth ions, which exists in this compound. The final actual real pressure is calculated from the temperature of the Sn superconducting transition using an equation:

$$p_{real} = 5.041489 \cdot \left(T_c(0) - T_c(p)\right)^2 + 17.81287 \cdot \left(T_c(0) - T_c(p)\right). \qquad (38)$$

Regarding this picture, one can see, that applied hydrostatic pressure from p_1 = 2.48 kbar up to p_4 = 10.6 kbar does not show notable changes. On the contrary, small differences in magnetic measurements with pressure come from Curie-Weiss fit. Effective paramagnetic moment is below 4 μ_B/f.u, but when the pressure is applied, this value gets over 4 μ_B/f.u. Similar changes are observed for paramagnetic Curie temperatures. For measurements without applied hydrostatic pressure θ_P is negative with value of -19.79 K. Nevertheless, with pressure the value reaches $\theta_P \cong$ -25 K. On the *M(T)* dependence, no anomaly in this temperature range is observed.

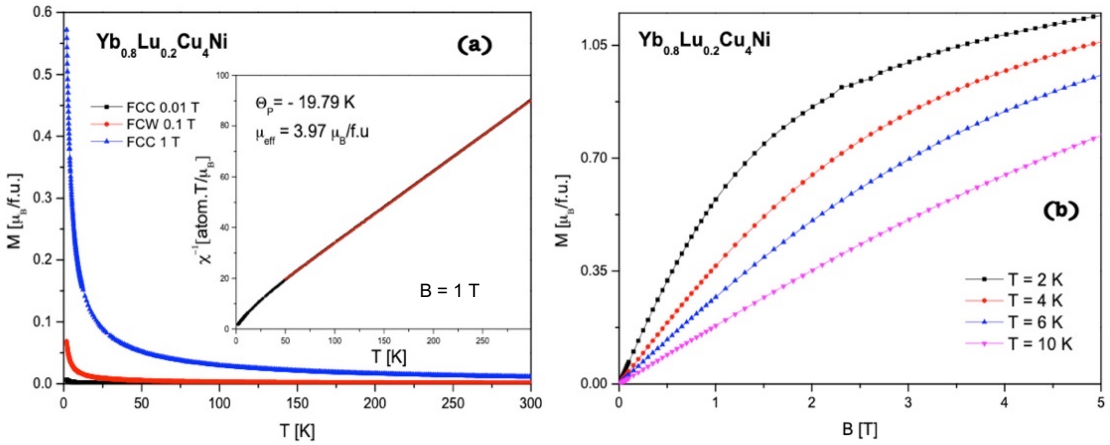

Figure 5.68 (a) M(T) at different applied magnetic fields. Inset shows inverse magnetic susceptibility, CW fit and obtained parameters from the fit. (b) Isothermal magnetization as a function of the magnetic fields of $Yb_{0.8}Lu_{0.2}Cu_4Ni$ at various temperatures.

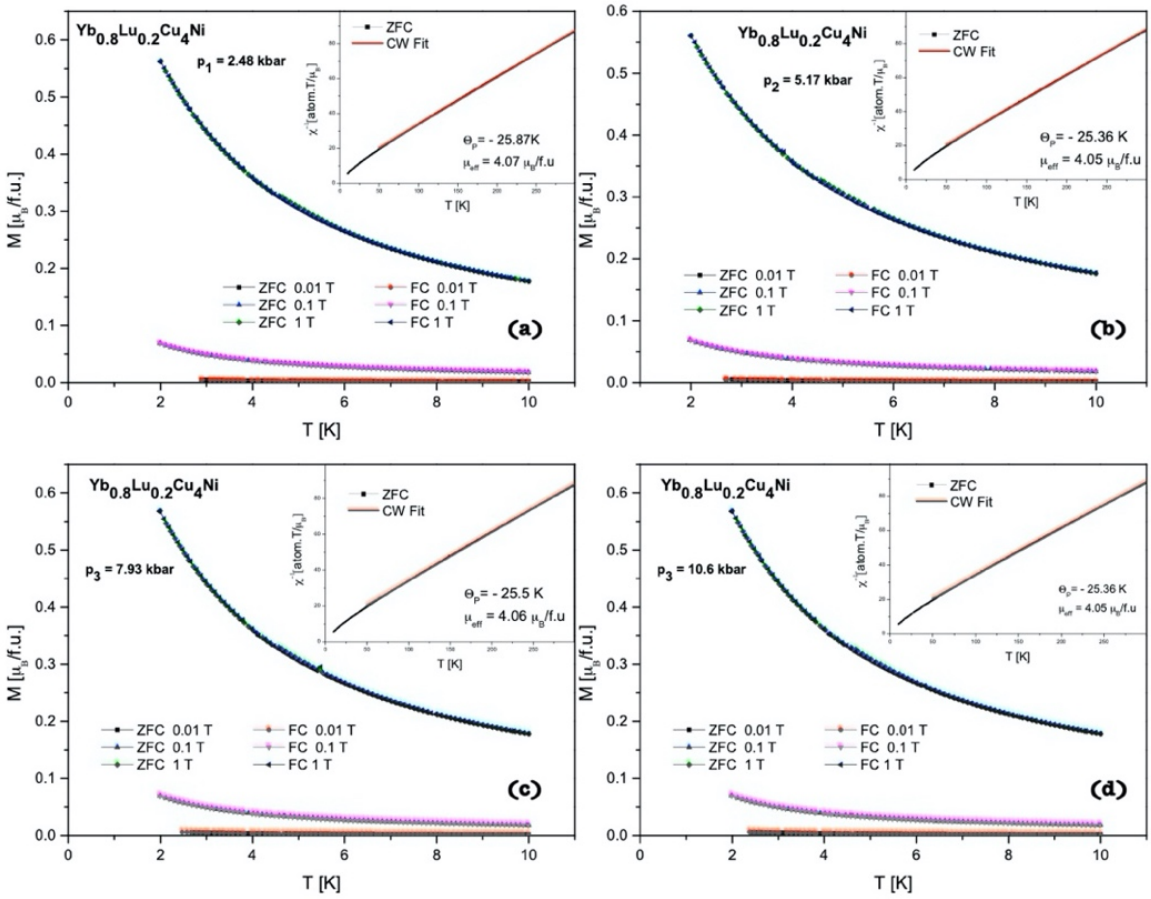

Figure 5.69 M(T) of $Yb_{0.8}Lu_{0.2}Cu_4Ni$ and application of various hydrostatic pressures. (a) $p_1 = 2.48$ kbar; (b) $p_2 = 5.17$ kbar; (c) $p_3 = 7.93$ kbar and (d) $p_4 = 10.6$ kbar. In the inset of every picture, there is a temperature dependence of inverse magnetic susceptibility with CW fit at $B = 1$ T.

Magnetic field dependences of magnetization measured at various temperatures with applications of mechanical pressure are plotted in Figure 5.70. Behaviour is practically similar to measurement performed without applied mechanical pressure. Even the pressure of 10.6 kbar does not show any difference. Our previous prediction that below $T = 2$ K magnetic order could exist, is confirmed.

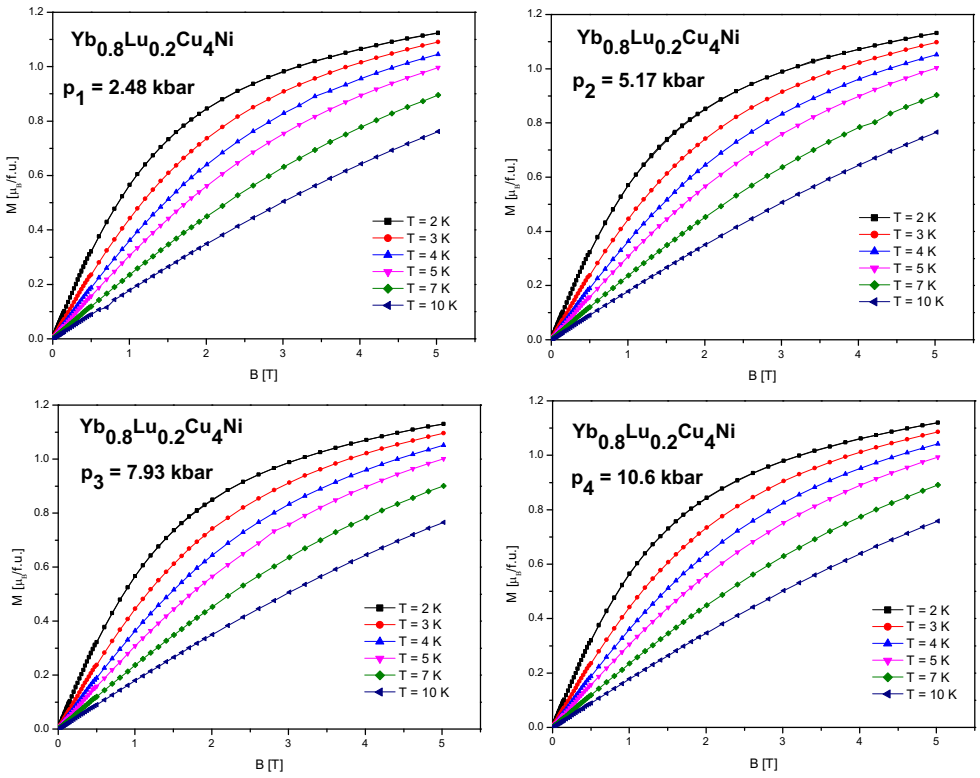

Figure 5.70 M(B) for $Yb_{0.8}Lu_{0.2}Cu_4Ni$ and application of various hydrostatic pressure. (a) p_1 = 2.48 kbar; (b) p_2 = 5.17 kbar; (c) p_3 = 7.93 kbar and (d) p_4 = 10.6 kbar.

Heat capacity measurement is plotted in Figure 5.71 for $Yb_{0.8}Lu_{0.2}Cu_4Ni$ compound. Transition temperature was not observed at $B = 0$ T in the whole temperature range even down to millikelvin temperatures. However, when magnetic field $B > 0.5$ T is applied, an anomaly related to magnetic transition is visible. It means, that transition temperature could be present, but at the temperature lower than 0.4 K. The analogic situation is in $YbCu_4Ni$ compound [95]. Here the C_p anomaly is observed at $B = 0$ T, while in studied compound it is visible only when higher magnetic fields are applied.

Electrical resistivity and magnetoresistivity are shown in Figure 5.72. Here (a) represents measurement at zero applied magnetic field. When temperature dependence is plotted in logarithmic scale, Kondo like behaviour is visible in low temperature range. Magnetoresistivity shows negative values and its maximum is at 2 K.

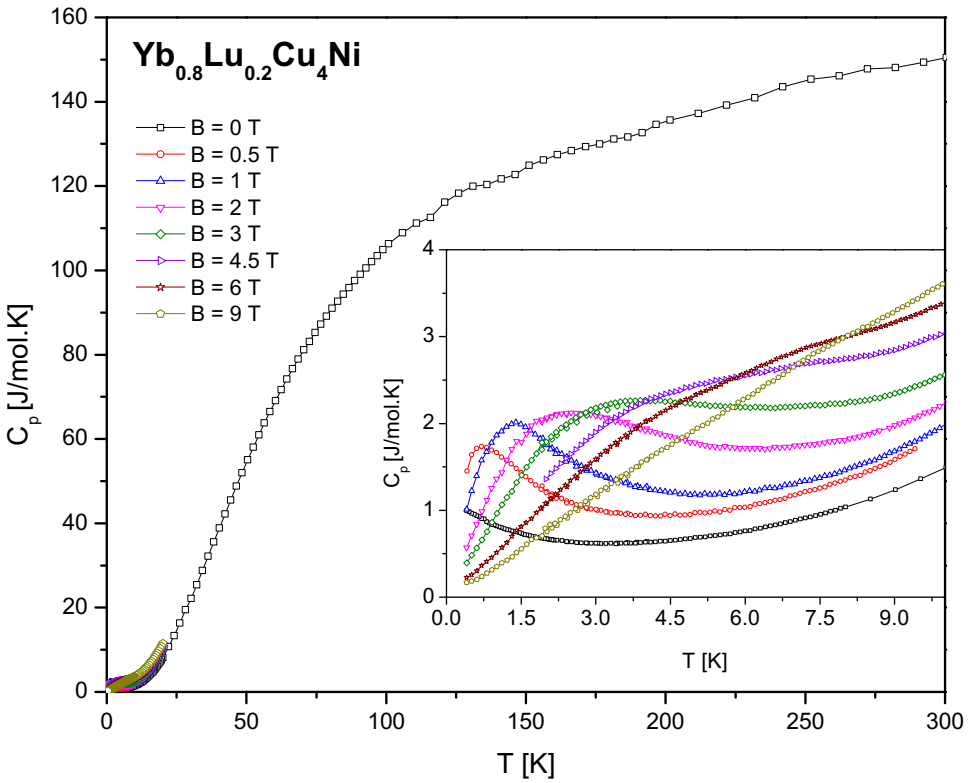

Figure 5.71 $C_p(T)$ of $Yb_{0.8}Lu_{0.2}Cu_4Ni$ at various applied magnetic fields. Inset shows $C_p(T)$ in very low temperature range.

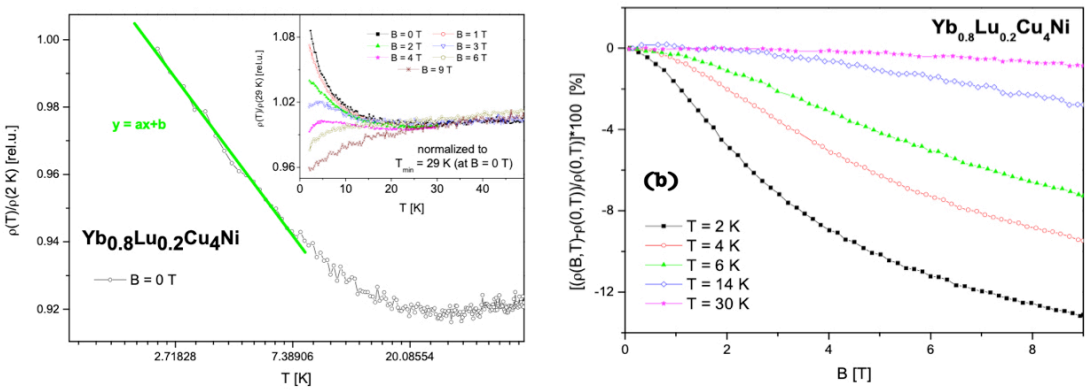

Figure 5.72 (a) Normalized electrical resistivity at B = 0 T in ln scale of temperature. Inset represents low temperature detail of normalized resistivity at various applied magnetic fields for $Yb_{0.8}Lu_{0.2}Cu_4Ni$ compound. (b) Magnetoresistivity as a function of magnetic field at different temperatures for $Yb_{0.8}Lu_{0.2}Cu_4Ni$ compound.

The study of physical properties of $Yb_{0.8}Lu_{0.2}Cu_4$ compound yields to several interesting and attractive facts. According to the one of mains aim of this work, we can conclude, that application of chemical pressure in the form of substitution Yb with Lu causes more visible influence on physical properties. Chemical pressure causes expansion of the lattice, while application of hydrostatic mechanical pressure causes opposite effect; therefore, the lattice is reduced. Mechanical pressure enhances density of localized 4*f* electrons, instant substitution Yb/Lu decrease density of localized 4*f* electron states.

5.4.4 $YbPd_2In$

A polycrystalline sample of $YbPd_2In$ has been prepared with inductive furnace and after the preparation process, it was annealed at 750 °C for 14 days. Structural analysis is shown in Figure 5.73. Results show, that $YbPd_2In$ crystallizes in cubic Heusler lattice, Cu_2MnAl-type structure in $Fm\bar{3}m$ space group. SEM confirms 1:2:1 stoichiometry. No spurious phases were found. In this figure, 111-plane represents the positions of atoms in this compound.

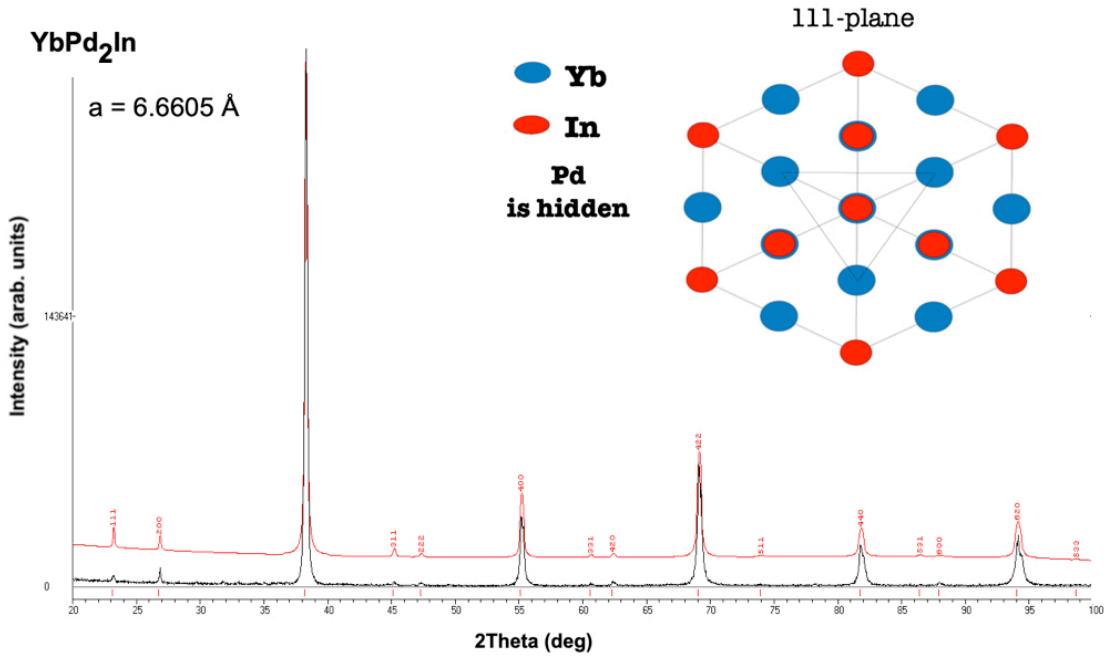

Figure 5.73 XRD pattern for $YbPd_2In$. In the right corner, there is 111-plane of observed crystal structure.

Magnetic measurements were performed in the temperature range from 2 K up to 300 K. Inverse magnetic susceptibility is presented in Figure 5.74 (a) together with a modified Curie-Weiss law, which is given by formula:

$$\chi(T) = \chi_0 + \frac{c}{T - \theta_P}. \tag{39}$$

Results from fitting are the following obtained values: for paramagnetic Curie temperature it is $\theta_P = -9\ K$, which indicates antiferromagnetic interaction and the effective paramagnetic moment of $\mu_{eff} = 4.49\ \mu_B$/f.u, which is very close to the free ion of Yb^{3+}. Magnetization as a function of applied magnetic fields confirms the obtained susceptibility results and it is shown in Figure 5.74 (b). The ordering temperature could be expected be below 2 K.

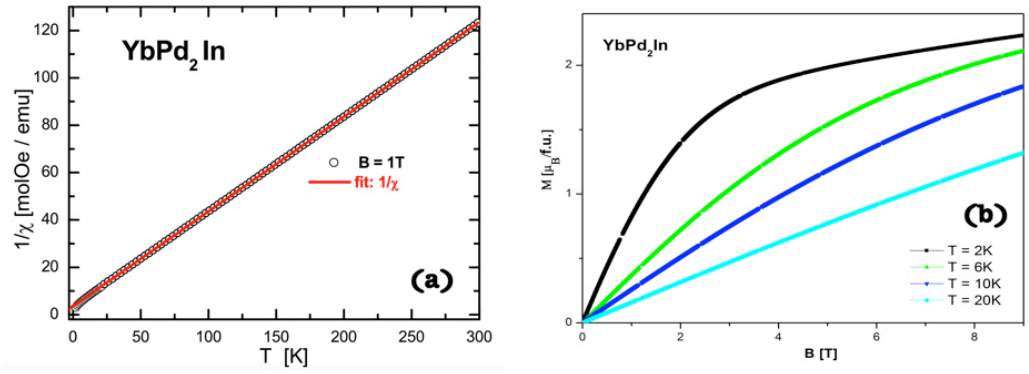

Figure 5.74 (a) Inverse magnetic susceptibility with modified CW fit of $YbPd_2In$ [158]. (b) Magnetization as a function of applied magnetic fields for $YbPd_2In$ compound.

The AC susceptibility measurements show interesting results. The inverse of the inductive signal (*1/m'*) looks quite linear down to $T = 6$ K and progressively turns down at lower temperatures, see Figure 5.75. Since no CEF effect is expected there, one may point to some variations in magnetic interactions. In fact, the dissipative signal (*m''*) also starts to change around that temperature. One possibility is, when m''(T) reveals the presence of a dissipative mechanism, that we could expect the mean field behaviour (represented by red line in figure) to be described by weak antiferromagnetic interaction ($T_{CW} \sim 3$ K). It is then affected by some more random interactions of similar intensity,

which become competitive below T = 6 K. Thus, the system is no more a standard paramagnet with classical excitation spectrum below this temperature. It starts to accumulate random correlations. Their density grows by lowering the temperature.

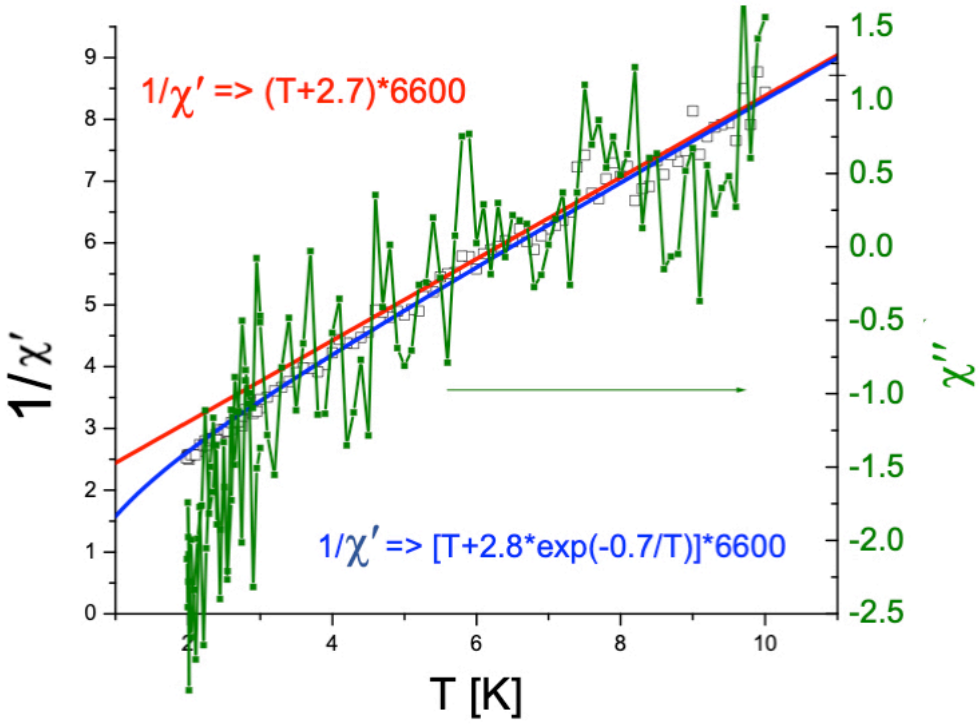

Figure 5.75 The inverse of the inductive signal of AC susceptibility measurement of $YbPd_2In$. Effective $T_{CW} \Rightarrow 0$ as $T \Rightarrow 0$ due to competition as it is presented by a blue line. Mean field behaviour is represented by a red line.

Thermal transport properties of $YbPd_2In$ compound have been studied from very low temperature range up to room temperature, where they follow Dulong-Petit law. More interesting results were obtained at very low temperatures (see Figure 5.76). Heat capacity upturns for $B \leq 0.75$ T reveal an arising anomaly. It reaches a maximum at T = 1.2 K for B = 1.5 T and continues to increase proportionally. Observed anomalies can be explained as Schottky-type anomalies above B = 4 T. $C_p(T)$ dependence reaches an expected value of 3.6 J/mol.K, which corresponds with a two-level system split by applied magnetic field behaviour. Figure 5.76 (b) represents heat capacity measurements only up to 1 K [158].

The transition temperature at $T_{cr} \sim 250$ mK decreases with applied magnetic field, then the magnetic degrees of freedom are transferred to higher temperatures with the consequent shift (see Figure 5.76 (b)).

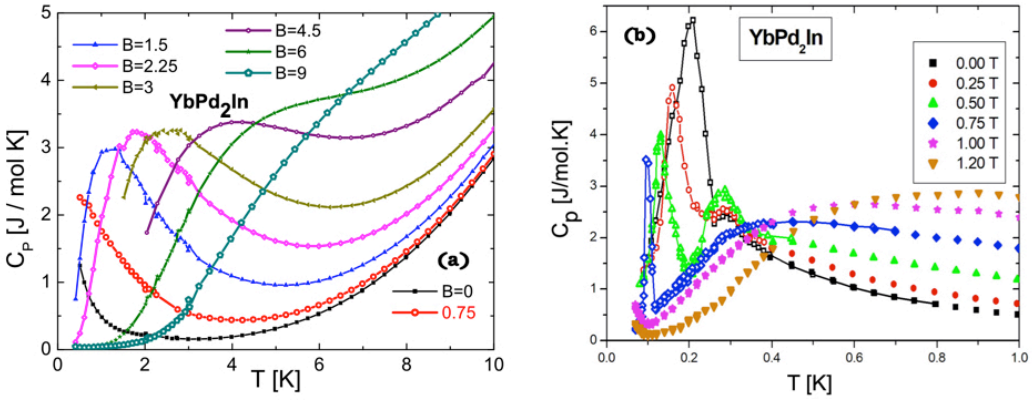

Figure 5.76 (a) $C_p(T)$ in various applied magnetic fields [158]. (b) $C_p(T)$ in various magnetic fields at very low temperatures. Both are plotted for $YbPd_2In$.

Next figure (Figure 5.77) shows a heat capacity at very low temperatures and at $B = 0$ T in a double logarithmic scale. From $T < 3$ K, the phonon contribution is equivalent. The nuclear contribution can be irrelevant at $T \sim 0.1$ K and $B = 0$ T. The trends of curve can be characterized by 3 different ways [158]:

1) C_m/T *jump* picking at T ~ 210 mK, a power- law dependence that properly describes the thermal decrease between 260 mK < T < 3 K, and a small jump at $T = 2.2$ K.
2) C_m/T jump observed at 210 mK < T < 260 mK indicates a magnetic transition that involves the Yb 4-*f* electrons.
3) At 0.3 K ≤ T ≤ 3 K, C_m/T can be properly fitted by a modified power law (in Figure 5.77 red).

This power-law coincides with $YbPt_2X$ compounds (X = In and Sn) [159].

Thermal dependence of C_p/T at 0.065 K < T < 0.7 K up to applied magnetic field of $B = 1.2$ T is shown in the inset of Figure 5.77. The critical temperature $T_{cr}(B)$ of the magnetic transition decreases linearly with the applied field and extrapolates to $T_{cr} = 0$ K for $B \sim 1$ T. The upturn at low temperatures for $B \sim 1.2$ T can be described by $1/T^2$. It can be properly accounted for as being due to nuclear contribution. Moreover, the low-

temperature upturn at $B \sim 1$ T still contains the tail of the magnetic transition occurring below the measurement limit. C_m/T_{cr} anomaly narrows keeping its maximum value up to $B = 0.5$ T. A strong increase is observed at $B = 0.75$ T. Higher applied magnetic fields shift T_{cr} below the lower temperature experimental limit, but this is still visible at $T = 65$ mK for $B = 1$ T. A constant value of C_m/T_{cr} is presented up to $B = 0.5$ T, which is a typical behaviour for heavy fermion compounds [160].

The unexpected dome arising at $T_D \sim 270$ mK, just above the transition at $B = 0$ T, increases its intensity up to $B = 0.5$ T without changing the temperature of its maximum. This satellite anomaly vanishes at $B = 1$ T. Simultaneously, a C_m/T maximum at $T_{max}(B)$ develops and becomes field dependent [158]. Description of the origin of domelike anomaly is unknown. The similar field dependences were observed in [161]. Here, it was related to magnetoelastics effect and explained as precursors of an antiferromagnetic interaction in $Ce(Co_{1-x}Fe_x)Si$ alloys.

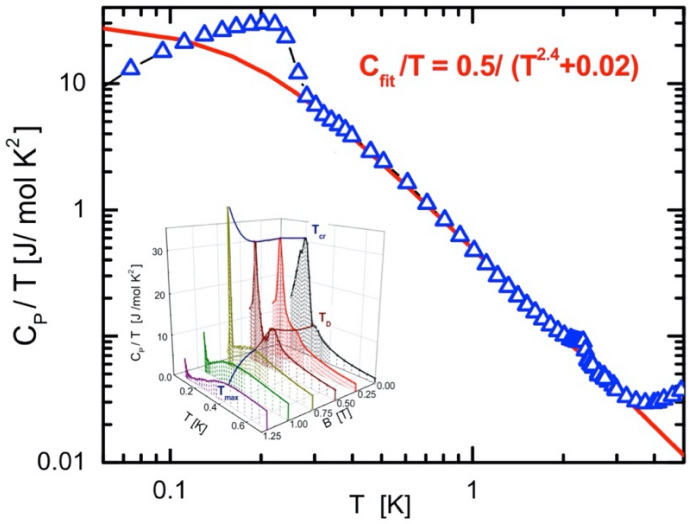

Figure 5.77 $C_p(T)/T$ at $B = 0$ T in double logarithmic representations. The red curve represents a modified power-law thermal dependence obtained within the 0.28 K < T < 3 K of $YbPd_2In$. Inset represents heat capacity over temperature of $YbPd_2In$ at various applied magnetic fields up to $B = 1.2$ T in a 3D representation. The upper continuous curve indicates the maximum value of $C_p/T(B)$ defining the critical temperature $T_{cr}(B)$. Lower continuous curve: at 0 T < B < 0.75 T it indicates the maximum of the small dome at $T_D \sim 270$ mK. For B > 0.75 T it traces the field dependent maximum. Vertical lines at T = 0.7 K are a guide to the eyes for respective field intensities [158].

Temperature dependence of $S_m/ln2$ is shown for various magnetic fields up to B = 1.5 T in Figure 5.78. The extrapolation of C_m/T to T = 0 K from the lowest measured temperature becomes relevant due to the significant entropy increase at a very low temperature range. The approach chosen to correct this uncertainty was to use a linear extrapolation according to the Nernst postulate ($S_m \rightarrow 0$ for T = 0 K). Here, the temperature reached at T = 1 K for the B = 0 T slightly overcomes the expected $S = Rln2$ value. Observed excess of entropy can be related to the entropy contained in the anomaly at $T_D \sim$ 270 mK. Dashed lines visualize this low temperature magnetic contribution at maximum intensity at B = 0.5 T after subtracting the T_D anomaly. An unusual nuclear – ground – state coupling mechanism should be taken into consideration. However, it is not easy to distinguish in this case. An adiabatic demagnetization path is also shown. A large $S_m(B)$ variation allows an adequate adiabatic demagnetization refrigeration by applying magnetic field up to 1.5 T at T = 0.9 K. The cooling down processes (to T = 0.16 K) remove the magnetic field [158]. The comparison of this mechanism with other rare-earth compounds is reported [162].

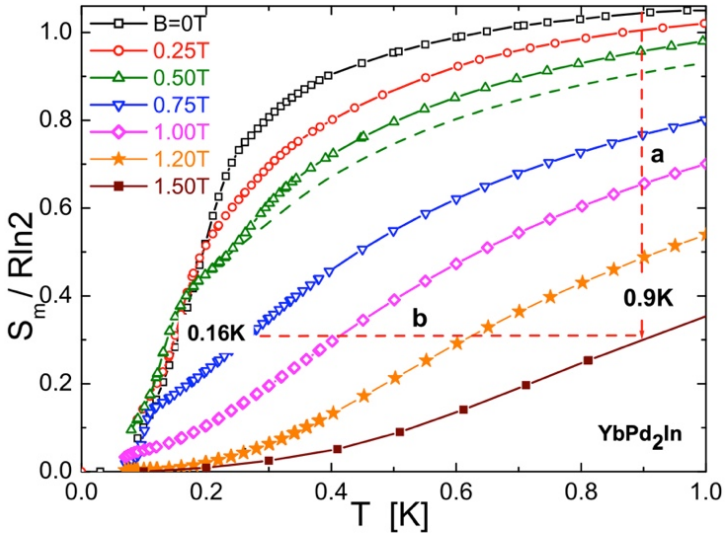

Figure 5.78 Thermal variation of the magnetic entropy normalized by the total entropy expected for doublet ground state Rln2. The dashed line shows entropy for B = 0.5 T after subtracting the T =270 mK anomaly contribution. Red dashed lines indicate that a refrigeration path is firstly isothermally (T = 0.9 K) magnetized at B =1.5 T (a) adiabatically demagnetized (b) reaching the final temperature of T = 0.16 K [158].

Thermal conductivity measurements are shown in Figure 5.79. They were provided in order to elucidate the small jump at T = 2.2 K, which could be related to the Yb oxides or it is an extrinsic or intrinsic feature effect of the sample. This idea comes from [160], where the same transition was reported in the isotypic $YbPd_2Sn$ compound. One can see a clear transition at that temperature indicating that some conduction electrons are actually condensed into the superconducting phase. Nevertheless, since that transition involves less than 1 % of *Rln2*, this observation confirms that localized Yb- 4*f* degrees of freedom are not involved in such a transition.

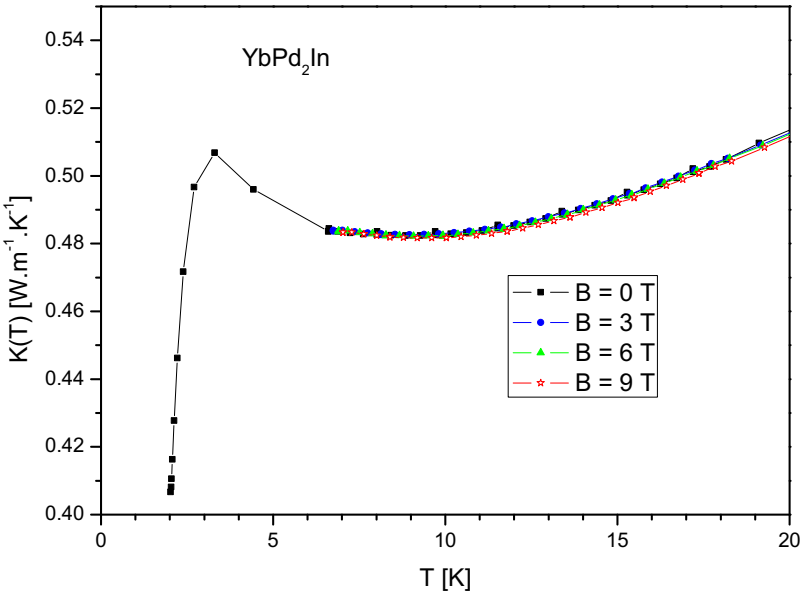

Figure 5.79 Thermal conductivity around T = 2 K revealing the superconductive character of that transition.

Temperature dependence of normalized electrical resistivity at two applied magnetic fields is plotted in Figure 5.80. Residual resistivity ratio is of a value 5.5, which indicates rather good quality of polycrystalline sample. One can see a positive trend of $\rho(T)$ dependence at low temperatures. Around T = 25 K a coherent regime is observed. The linear thermal variation of $\delta\rho/\delta T$ confirms this attribute. This function correlates with relation:

$$\rho(T) = \rho_0 + AT^2, \tag{40}$$

for a Fermi liquid (in Figure 5.80 it is a straight line). However, the negative curvature is around T = 70 K [158]. This fact could be related to the strongly hybridized crystal electric-field excited levels [163]. Magnetoresistance effect was not observed, practically.

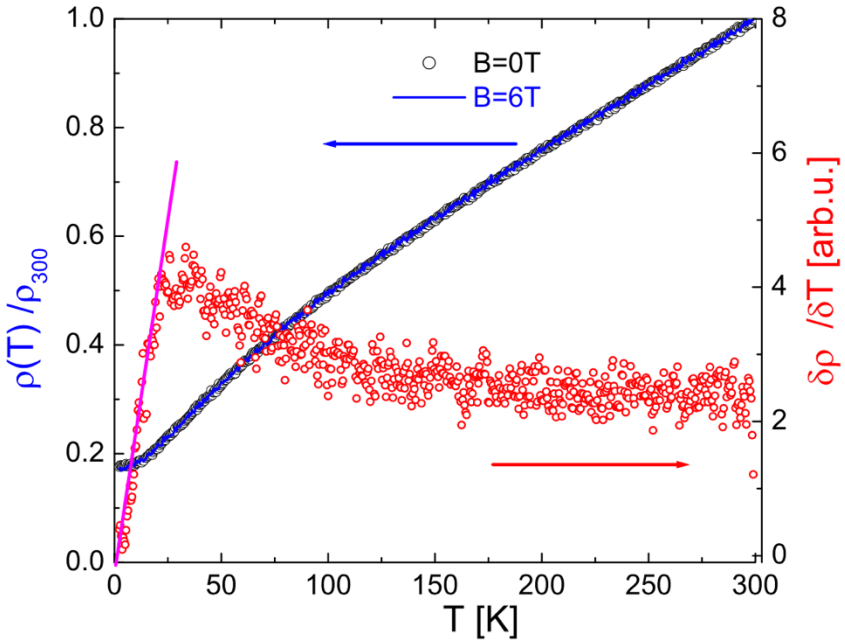

Figure 5.80 Left axis represents $\rho(T)/\rho_{300}$ of $YbPd_2In$ compound. Right axis represents $\delta\rho/\delta T$, which shows nearly linear increase between temperatures from 2 K to 25 K [158].

The results, obtained from the whole series of physical measurements can be presented in a magnetic phase diagram (see Figure 5.81). It contains the field dependence of the phase boundary T_{cr} and 0 K $\leq T \leq T_{cr}(B)$, that accounts for the degrees of freedom condensed into the ordered phase S_{MO}, which is also included. The circle at T_{cr} for B = 1 T represents an extrapolation of the T_{cr} for magnetic fields higher than 1 T. It is placed below the lowest accessible temperature of T = 65 mK, a turn up to the C_m/T (B = 1 T) curve (see in the inset of Figure 5.77) and it reveals the reminiscence of that transition below this temperature [158].

This type of behaviour was observed in a systematic investigation of low temperature magnetic phase diagrams of Ce compounds. The aim of this study was to distinguish between different $S_{MO}(T \rightarrow 0)$ trajectories observed in magnetically ordered phases [164].

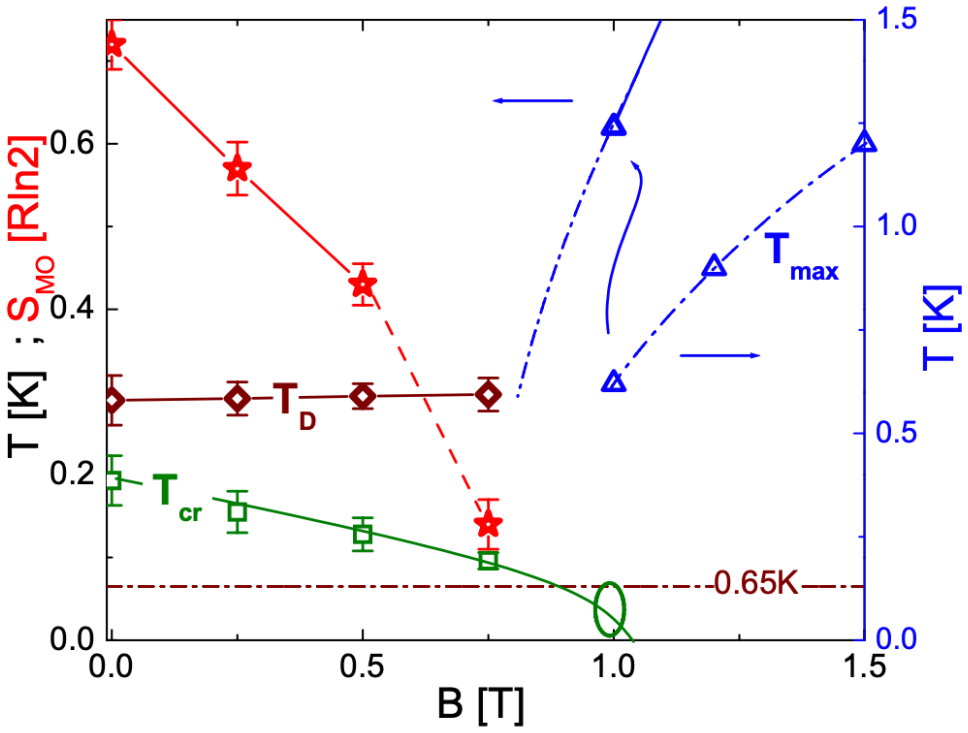

Figure 5.81 Magnetic phase diagram as a function of applied magnetic field. On the left axis there are the following quantities: the ordering temperature T_{CR}, the entropy gains within the ordered phase S_{MO} and the temperature of the dome T_D. Continuous green curve is a guide to the eyes for the $T_{cr}(B) = 0$ T and the ellipse represents an extrapolated point at $B = 1$ T. The dash-dot line at $T = 65$ mK indicates the thermal experimental limit. Continuous red line in $S_{MO}(B)$ covers the second-order-type transitions while the dashed segment extrapolates to the first-order one. On the right axis, the temperature of the maximum of $C_M/T(T_{max})$ is shown. The extrapolation of $T_{max}(B)$ to $B < 1$ T (dashed-dot blue line) is compared with the $T_D(B)$ using the left axis scale as indicated by the left pointing blue arrow [158].

In the presented magnetic phase diagram, one might appreciate that, although both $T_{cr}(B)$ and $S_{MO}(B)$ extrapolate to zero, the latter drops faster than expected at $B = 0.75$ T in coincidence with the first-order character of that transition [158].

The similar situations have been observed and published for the following systems: URu_2Si_2 [165], $PrFe_4P_{12}$ [166] and $Ce_2(Ni_{1-x}Pd_x)_2Sn$ [167]. In all of them, second-order magnetic transitions get transformed into the first-order ones and entropy is

quickly reduced. In URu_2Si_2 and in $Ce_2(Ni_{1-x}Pd_x)_2Sn$ compounds a formation of an exotic phase around $T \rightarrow 0$ K was found out. This fact cannot be ignored for YbP_2In system.

5.4.5 Conclusion

The obtained results for Yb-based material can be separated into several groups. In the first group, there are samples as $YbNi_5$, $YbCu_{4.7}Ni_{0.3}$ and $Yb_{0.8}Sc_{0.2}Cu_4Ni$ where the problem has already started with ambiguous foundation of crystal structure. From SEM and EDX analyses, we known that they include not only a required content, but also a Ta from Ta crucible and some oxides. An interesting material belonging to this group is $Yb_{0.5}Gd_{0.5}Ni_5$, where existence of more phases is not so bad, because of the knowledge of magnetocaloric effect. It was calculated for this compound. Here, results from EDX analysis show only the presence of oxides, which could arise during sample preparation.

The second group includes material, where the effect of spin fluctuations was observed. It is $Ce_{0.5}Yb_{0.5}Ni_5$ compound.

Next one is the group, where investigation of ground state properties showed, that $YbCu_{4.2}Ni_{0.8}$ and $Yb_{0.8}Lu_{0.2}Cu_4Ni$ systems are close to the possible quantum critical point. To confirm this interesting fact, other analyses are necessary.

The last sample from this material is $YbPd_2In$, where detailed studies and analyses showed, that it is a promising candidate for adiabatic demagnetization cooling processes.

Conclusions

This work deals with an experimental study of emergent ground state behaviour mostly in $RENi_5$ (RE = Ce, Yb, Gd) system, where common factor is a rare earth. Thesis consists of five chapters. The first, describes a theory, interactions and effects, which are important for understanding the theoretical background. The second part defines a motivation of our studies. The third chapter explains in detail the main aims of the thesis. The experimental techniques, which were used, are described in chapter four. The largest part is the chapter five, where experimental results and discussions are reported. Experimental results can be separated into 4 groups, where 21 intermetallic samples have been prepared. They are the subject for the study.

Bulk samples of $Gd_{1-x}Ce_xNi_5$ (x = 0; 0.2; 0.5 and 0.8) system

The bulk samples were prepared by arc melting technique, which is a typical method for preparation of polycrystalline materials. XRD analysis shows a hexagonal $CaCu_5$ crystal structure with *P6/mmm* space group and confirms a single phase of all samples. SEM and EDX analyses confirm required stoichiometric composition for all of them. Physical properties studies, show several interesting facts. From the *dM/dT* dependence, critical temperatures were determined. They were confirmed by heat capacity and electrical resistivity measurements. Determined Sommerfeld coefficients give us an information that materials do not belong to the heavy fermion systems. Residual resistivity ratio varies from 2.43 for $GdNi_5$ up to 6 for $Gd_{0.2}Ce_{0.8}Ni_5$ compound. Consequently, the transition temperatures to the magnetically ordered state were observed in all compounds from this system. These temperatures continuously decrease with increasing Ce content. Influence of spin fluctuation effect has not been observed. Only 20 % of Gd dominates and inhibits possible short-range order correlations.

Ribbon samples of $Gd_{1-x}Ce_xNi_5$ (x = 0; 0.2; 0.5 and 0.8) system

Samples prepared by a rapid quenching method show that we were successful and we prepared crystalline materials. This was confirmed by XRD and SEM analyses. Crystal structure is hexagonal $CaCu_5$ type and *P6/mmm* space group for all studied $RENi_5$ compounds. Small deviation from required stoichiometric composition is reported.

Studied physical properties show similar behaviour as the samples with same composition prepared by arc melting. On the other hand, the quality of samples is lower, what is presented in the part devoted to ribbon samples. Transition temperatures were observed for compounds with certain Gd content. Pure ribbon of $CeNi_5$ features the influence of spin fluctuation effect, which is visible in magnetic measurements. Due to the mechanical problem of these samples, electrical transport properties were not studied. From performed measurements and their analyses, it is possible to conclude, that an influence of microstructure on the physical properties in this $Gd_{1-x}Ce_xNi_5$ system is not so pronounced.

(Ce,Gd)Ni_5 – in the vicinity of the magnetic phase transitions

The bulk samples were prepared by arc melting method. Structural analysis confirmed a hexagonal lattice $CaCu_5$ type with *P6/mmm* space group again. With increasing Ce content, lattice parameter *c* expands, while *a* decrease. SEM and EDX analyses show good results for microstructure. From the investigations of other physical properties, it was determined that magnetic properties, for $Ce_{0.95}Gd_{0.05}Ni_5$ and $Ce_{0.97}Gd_{0.03}Ni_5$ are influenced by spin fluctuations effect. No magnetic ordering was confirmed down to 2 K. Moreover, the interesting physical properties were observed in sample $Ce_{0.9}Gd_{0.1}Ni_5$ sample. Its behaviour in low temperature range shows, that the system could be close to the quantum critical points. For its exact assessment, it would be interesting to perform a neutron scattering experiment in order to determine the magnetic structure. For the last sample of this group, $Ce_{0.85}Gd_{0.15}Ni_5$ transition temperature was observed in a decreasing trend, when Ce content was increasing.

Samples based on Yb

In this group 8 samples were prepared. All of them were prepared by the same method – inductive melting process. On the basis of obtained results, a conclusion can be separated into the following categories. In the first one we have samples, where structural analysis shows many other peaks, which cannot be indexed ($YbNi_5$, $YbCu_{4.7}Ni_{0.3}$ and $Yb_{0.8}Sc_{0.2}Cu_4Ni$). On the other hand, XRD results, which show an unspecified secondary phase of $Yb_{0.5}Gd_{0.5}Ni_5$ sample, are suitable for possible magnetocaloric applications. Here, the magnetocaloric properties were studied and they could lead to potential

technical application in the future. On the other hand, $Yb_{0.5}Ce_{0.5}Ni_5$ shows a shoulder at magnetization measurements, which is connected with spin fluctuation effect. Next category includes two materials: $YbCu_{4.2}Ni_{0.8}$ and $Yb_{0.8}Lu_{0.2}Cu_4Ni$, where our main aim was to find more precise position of quantum critical points. The last compound belonging to this group is $YbPd_2In$. Results from its physical properties studies show, that $YbPd_2In$ is a candidate for adiabatic demagnetization cooling process.

From our point of view, we can conclude, that the main objectives of this dissertation thesis were achieved taking into account the obtained results.

Conclusions Related to Further Development and Potential Applications

In this work, we prepared and studied the intermetallic materials on the basis of rare earths. Further development can be divided into three different aims.

Basically, the samples were prepared in a polycrystalline form. Due to the possible influence of the structure on physical properties, one part of this thesis deals with ribbon samples. The results from this point of view do not show any differences between bulk and ribbon samples. Here it is still an open question, whether one could expect better properties like crystallinity for the samples prepared by microwire technology. In the future it will be interesting to solve a technical problem with glass, which concerns the transformation of a metal form into a glass-coated material.

On the other hand, $Ce_{0.9}Gd_{0.1}Ni_5$ and two samples from Yb-based family ($YbCu_{4.2}Ni_{0.8}$ and $Yb_{0.8}Lu_{0.2}Cu_4Ni$) show a possible existence of quantum critical point. In the future, it will be interesting to find and confirm it by other scientific methods, for example, neutron diffraction. This type of research can give information about ground state properties of rare-earth intermetallic compounds for theory and practice.

The most interesting results were obtained for the $YbPd_2In$ compound. The detailed investigations show, that the withdrawal of ground state degeneracy by magnetic fields produces a significant shift of the entropy. This process documents that $YbPd_2In$ can be a suitable material for adiabatic demagnetization in cooling processes.

Other conclusion is, that in this type of research an international collaboration among scientists is very important. Other experimental studies can bring interesting and attractive knowledge of ground state properties in the condensed matter fields, where investigation of materials based on rare earth has an irretraceable place.

Resumé v slovenčine

Predkladaná dizertačná práca sa zaoberá experimentálnym štúdiom správania sa základného stavu v systéme $RENi_5$ (RE = Ce, Yb, Gd). Základným vodítkom je vzácna zemina, kde sa postupne v celej práci dostávame až ku zamieňaniu atómov Ni inými atómami (Cu, Pd a In). V tomto type vzácnozeminových zlúčenín, je podmriežka tvorená niklovými iónmi, nevykazujúcimi žiadne magnetické usporiadanie. Vzhľadom ku skutočnosti, že 3*d* pásmo niklu je celé obsadené vonkajšími elektrónmi, nemôže prispievať k spontánnemu magnetickému momentu. Častokrát sa v tejto triede materiálov objavujú ťažkofermiónové systémy s vysokou hodnotou Sommerfeldovho γ koeficientu. Tieto systémy sú zaujímavé vďaka svojim výnimočným fyzikálnym vlastnostiam a to napr. kvôli neceločíselnej valenčnosti, Kondovským interakciám, koherentným efektom či štiepeniu kryštálového elektrického poľa.

Hlavným cieľom tejto práce je experimentálne štúdium základného stavu v systéme $RENi_5$ (RE = Ce, Yb, Gd). Za účelom jeho naplnenia, sme stanovili nasledovné čiastkové úlohy:

1) Príprava a štruktúrna charakterizácia polykryštalických materiálov $(RE1_{1-x}RE2_x)Ni_5$ (RE1, RE2 = Ce, Yb, Gd); $YbPd_2In$, $Yb_{0.8}Lu_{0.2}Cu_4Ni$, $Yb_{0.8}Sc_{0.2}Cu_4Ni$, $YbCu_{4.7}Ni_{0.3}$ a $YbCu_{4.2}Ni_{0.8}$.
2) Štúdium fyzikálnych vlastností s dôrazom na štúdium konkurencie medzi efektom spinových fluktuácií a možnou existenciou kvantového kritického bodu.
3) Vplyv rozmeru na fyzikálne vlastnosti v zlúčeninách $(RE1_{1-x}RE2_x)Ni_5$ (RE = Ce, Gd).
4) Vplyv chemického tlaku na fyzikálne vlastnosti na $Yb_{0.8}Lu_{0.2}Cu_4Ni$, $Yb_{0.8}Sc_{0.2}Cu_4Ni$, $YbCu_{4.7}Ni_{0.3}$ a $YbCu_{4.2}Ni_{0.8}$.
5) Základný stav a nízkoteplotné vlastnosti zlúčeniny $YbPd_2In$.

Samotná práca pozostáva z piatich kapitol. Prvá kapitola je teoretická, kde sa venujeme rôznym interakciám, mechanizmom a efektom, ktoré zohrávajú dôležitú úlohu pri štúdiu vybraných systémov. Druhá kapitola popisuje motiváciu, prečo sú študované práve zvolené systémy. Ďalšia a teda tretia časť práce je venovaná detailnému popisu stanovených cieľov. Štvrtá časť je venovaná požitým experimentálnym metodikám. Najrozsiahlejšou je práve piata kapitola, v ktorej sa venujeme dosiahnutým výsledkom.

Prvky vzácnych zemín a ich chemické vlastnosti sú vo svojej podstate veľmi podobné a to vďaka trivalentnej konfigurácii. Avšak ak zameníme prvok vzácnej zeminy v zlúčenine dokážeme aj výrazne zmeniť fyzikálne vlastnosti materiálu. So zapĺňaním 4*f* vrstvy úzko súvisí spinovo-orbitálny moment a zmena prvku vzácnej zeminy ho výrazne ovplyvňuje.

V intermetalických zlúčeninách sa skúma najmä pôvod magnetizmu, ktorý pochádza od 4*f* lokalizovaných elektrónov. Lantanoidy môžeme rozdeliť podľa niekoľkých kritérií do viacerých skupín. Jedna z podskupín lantanoidov je práve taká, kde vzácne zeminy nevykazujú magnetické správanie. Radíme sem: tetravalentný cér (Ce); trivalentné ytrium (Y), lantán (La), európium (Eu), lutécium (Lu) a divalentné yterbium (Yb). Zaujímavým faktom pre ďalšie skúmanie materiálov na báze vzácnych zemín je možnosť prechodu Ce iónu do nemagnetického stavu a Yb iónu do magnetického stavu vplyvom aplikovania mechanického tlaku. Práca sa zaoberá zlúčeninami, kde za vzájomne zamieňajú tieto vzácnozeminové prvky: Ce/Gd, Ce/Yb, Gd/Yb, Yb/Lu resp. Yb/Sc. Tento koncept je vybraný kvôli ukazujúcim sa zaujímavým fyzikálnym vlastnostiam. Na jednej strane je to potlačenie magnetizmu v oblasti nízkych teplôt efektom spinových fluktuácií. Na druhej strane je to nízkoteplotné správanie sa nie podľa modelu Fermiho kvapaliny (z anglického *non-Fermi liquid behaviour* tzv. *NFL behaviour*). Predpoklad pre existenciu tohto NFL stavu je magnetická nestabilita pri T = 0 K, čo môže viesť aj k možnej prítomnosti kvantového kritického bodu v pripravovaných vzácnozeminových materiáloch. Detailné štúdium základných fyzikálnych a chemických vlastností ponúka nové poznatky pre tak rýchlo sa rozvíjajúce odvetvie vedy akým je technika. Vzhľadom k uvedeným skutočnostiam môžeme konštatovať, že aj tento základný výskum je pre oblasť vedy veľmi dôležitý.

Na základe vyššie uvedených cieľov, študované druhy zlúčenín môžeme rozdeliť do nasledujúcich skupín, ktorým sa v tejto práci venujeme:

- masívne polykryštalické materiály systému $Gd_{1-x}Ce_xNi_5$ (kde x = 0; 0.2; 0.5 a 0.8).
- vzorky vo forme rýchlo chladených pások systému $Gd_{1-x}Ce_xNi_5$ (kde x = 0; 0.2; 0.5; 0.8 a 1).
- masívne polykryštalické vzorky systému $(Ce,Gd)Ni_5$.
- masívne polykryštalické materiály na báze Yb.

Masívne polykryštalické materiály systému $Gd_{1-x}Ce_xNi_5$ (kde x = 0; 0.2; 0.5 a 0.8)

Prvými pripravenými polykryštalickými materiálmi boli vzorky, kedy sme zamieňali atómy Ce a Gd v systéme $Gd_{1-x}Ce_xNi_5$ a to v týchto koncentráciách x = 0; 0.2; 0.5 a 0.8. Polykryštály boli pripravené oblúkovým tavením s celkovou hmotnosťou pre každú jednu vzorku m = 2 g. Vzorky boli pripravené na Univerzite v Kantábrii, Santander, Španielsko.

Röntgenová analýza bola robená pri izbovej teplote. Výsledky ukazujú, že všetky 4 vzorky kryštalizujú v hexagonálnej mriežke typu $CaCu_5$ s priestorovou grupou *P6mmm*. Veľkosť mriežkových parametrov a a c sa mierne mení v závislosti od koncentrácie, pričom bol naplnený Vegardov zákon. Mikroštruktúrna analýza potvrdila požadované zloženie pre každú jednu zo vzoriek. Príprava vzoriek a tiež štruktúrna analýza boli robené na Univerzite v Kantábrii, Santander, Španielsko.

Ďalším krokom v našom štúdiu bolo meranie magnetických a transportných vlastností. Tieto merania boli uskutočnené na experimentálnom zariadení DynaCool na Prešovskej univerzite v Prešove, Slovensko. Teplotné závislosti magnetizácie ukázali, že v tejto sade vzoriek sa nachádza fázový prechod do magneticky usporiadaného stavu. Prechodová teplota postupne klesá a to nasledovne: T_c = 31.8 K pre $GdNi_5$, T_c = 24.1 K pre $Gd_{0.8}Ce_{0.2}Ni_5$, T_c = 20.9 K pre $Gd_{0.5}Ce_{0.5}Ni_5$ a T_c = 5.3 K pre $Gd_{0.2}Ce_{0.8}Ni_5$. Z inverznej magnetickej susceptibility a následnej aplikácie Curie-Weissovho zákona boli určené parametre pre efektívny paramagnetický moment a pre Curieho teplotu. Hodnota saturačného momentu pre jednotlivé zlúčeniny klesá so zvyšujúcim sa percentom Ce.

Merania tepelnej kapacity boli tiež uskutočnené. Aj pri tomto meraní sme pozorovali anomáliu, ktorá je spojená s prechodom do magneticky usporiadaného stavu. S narastajúcim naloženým magnetickým poľom sa toto maximum posúva do oblasti vyšších teplôt až ho pole o veľkosti 9 T úplne vyhladí. Vysokoteplotná tepelná kapacita sa správa podľa Dulong-Petitovho zákona. Okrem toho sme stanovili magnetický a fonónový príspevok, ktoré prispievajú do celkovej tepelnej kapacity. Hodnota $S_{mag}(T)$ bola tiež stanovená na základe vzorca: $S_{mag} = \int_0^T \frac{C_{mag}(T)}{T} dT$. Pre $GdNi_5$ je táto hodnota ~ 17.28 J/mol.K. Sommerfeldov koeficient je nízky a pri týchto zlúčeninách nemôžeme hovoriť, že patria k ťažkofermiónovým.

Elektrická rezistivita a magnetorezistivita, ktorá bola experimentálne meraná pomocou 4-bodovej metódy, ukazuje kovový priebeh. Fázové prechody sa prejavili v podobe malého maxima na elektrickej rezistivite. Tak ako pri meraní tepelnej kapacity aj tu sme stanovili magnetický príspevok. Magnetorezistivita nadobúdala najväčšiu hodnotu v oblasti prechodu.

Pri tak vysokých koncentráciách pre Gd nebol pozorovaný vplyv spinových fluktuácií, ktorý je typický pre $CeNi_5$, ale prevažuje tu magneticky usporiadaný stav pod prechodovou teplotou.

Vzorky vo forme rýchlo chladených pások systému $Gd_{1-x}Ce_xNi_5$ (kde x = 0; 0.2; 0.5, 0.8 a 1)

Za účelom štúdia vplyvu mikroštruktúry na fyzikálne vlastnosti, boli pripravené pásky pomocou metódy rýchleho liatia taveniny na rýchlo rotujúci medený valec. Zvolené koncentrácie pások boli rovnaké ako pri masívnych vzorkách. Pásky boli pripravované na Univerzite Pavla Jozefa Šafárika v Košiciach, Slovensko.

Štruktúrna analýza aj tu ukázala, že všetky pásky kryštalizujú v hexagonálnej mriežke typu $CaCu_5$ s priestorovou grupou *P6/mmm*. Mriežkové parametre sa jemne odlišujú od tých, ktoré boli stanovené pre masívne vzorky. Pomocou skenovacej elektrónovej mikroskopie s funkciou spätne odrazených elektrónov bol skúmaný pomer jednotlivých prvkov v danej zlúčenine. Získané výsledky hovoria o tom, že týmto spôsobom pripravené vzorky nemajú úplne požadované stechiometrické zloženie a pozorujeme tu malé zmeny na úrovni ± 2 %.

Magnetické merania, ktoré boli robené v 2 módoch tzv. chladenie v poli (FC) a chladenie bez poľa (ZFC) rovnako ako pri masívnych vzorkách ukázali prechod z paramagnetického do magneticky usporiadaného stavu: T_c = 31.9 K pre $GdNi_5$, T_c= 30.1 K pre $Gd_{0.8}Ce_{0.2}Ni_5$, T_c = 16.9 K pre $Gd_{0.5}Ce_{0.5}Ni_5$ a T_c= 4.7 K pre $Gd_{0.2}Ce_{0.8}Ni_5$. Pre čistý $CeNi_5$ magneticky usporiadaný stav v teplotnom rozsahu od 2 K do 300 K nebol pozorovaný. Avšak na magnetizácii sa prejavil efekt spinových fluktuácií a to maximom pri T = 100 K do 150 K a ani magnetické pole s veľkosťou 1 T ich nepotlačilo. Saturačná hodnota magnetizácie opäť klesá s narastajúcim percentom Ce v skúmanej vzorke.

Tepelná kapacita, ktorá bola meraná v teplotnom rozsahu od 2 K do 300 K potvrdila prechody u všetkých vzoriek, ktoré obsahovali Gd. Na čistom $CeNi_5$ sa

neprejavila žiadna anomália. Podobne ako pri masívnych vzorkách sme aj tu stanovili jednotlivé príspevky do tepelnej kapacity. Hodnoty pre Sommerfeldov koeficient sú trocha vyššie ako pri masívnych vzorkách, ale stále sa nejedná o ťažkofermiónové materiály. S narastajúcim obsahom Ce tento γ koeficient klesá.

Merania elektrickej rezistivity a magnetorezistivity neboli robené. Dôvodom je fakt, že takto pripravené pásky boli veľmi krehké, lámali sa a manipulácia bola veľmi náročná.

Zo získaných výsledkov štúdia pások nie je možné úplne jednoznačne povedať, ktorý spôsob prípravy vzoriek je lepší, resp. pri ktorom type prípravy má daný materiál lepšie fyzikálne vlastnosti.

Vzhľadom k tomu, že jedným z našich cieľov je študovať vplyv mikroštruktúry na fyzikálne vlastnosti, ďalšou metódou prípravy vzoriek boli mikrodrôty s využitím Taylorovej-Ulitovského metódy, kde je kovové jadro pokryté sklom. Pri tejto metóde sme mali technické problémy, pretože teplota tavenia materiálu bola vyššia ako pracovná teplota skla a z toho dôvodu sme neboli úspešní a mikrodrôty sme doposiaľ nepripravili.

Masívne polykryštalické vzorky systému (Ce,Gd)Ni_5

Polykryštalické vzorky, ktoré boli pripravené rovnakým spôsobom ako predošlé masívne vzorky, kedy prevažoval Ce nad Gd, boli predmetom skúmania vymiznutia magnetického fázového prechodu v systéme (Ce,Gd)Ni_5.

Pomocou röntgenovej analýzy sme zistili, že aj táto skupina materiálov kryštalizuje v hexagonálnej mriežke typu $CaCu_5$ s priestorovou grupou *P6/mmm*. Mikroštruktúrna analýza ukázala, že pripravené vzorky majú požadovanú stechiometrickú kompozíciu.

Magnetické merania priniesli informácie o tom, že fázový prechod je pozorovaný pri koncentrácii $Ce_{0.85}Gd_{0.15}Ni_5$ pri teplote $T_c = 4.9$ K. Ostatné koncentrácie $Ce_{0.9}Gd_{0.1}Ni_5$, $Ce_{0.95}Gd_{0.05}Ni_5$ a $Ce_{0.97}Gd_{0.03}Ni_5$ nevykazovali magneticky usporiadaný stav. Z pohľadu spinových fluktuácií sú zaujímavými koncentrácie $Ce_{0.95}Gd_{0.05}Ni_5$ a $Ce_{0.97}Gd_{0.03}Ni_5$, kde sa na teplotnej závislosti magnetizácie objavuje maximum, typické práve pre tento efekt.

Tepelná kapacita pre koncentrácie $Ce_{0.85}Gd_{0.15}Ni_5$ a $Ce_{0.9}Gd_{0.1}Ni_5$ bola meraná až do mK oblastí na ^{3}He refrigerátore. Pre prvú spomínanú koncentráciu bol potvrdený fázový prechod, ktorý sa na tepelnej kapacite prejavil anomáliou. Tá sa s rastúcim poľom

posúvala do oblasti vyšších teplôt. Najvyššie naložené pole potlačilo tento prejav. Na vzorkách $Ce_{0.95}Gd_{0.05}Ni_5$ a $Ce_{0.97}Gd_{0.03}Ni_5$ sa nepotvrdilo magnetické usporiadanie. Najzaujímavejším materiálom v tejto skupine je práve koncentrácia $Ce_{0.9}Gd_{0.1}Ni_5$, kde sa v závislosti *C/T* vs *T* v logaritmickej škále vyskytuje lineárna závislosť *-ln(T*), čo naznačuje možnú blízkosť kvantového kritického bodu v tejto zlúčenine.

Merania elektrickej rezistivity a aj magnetoresistivity podporujú naše úvahy, ku ktorým sme sa dopracovali pri analyzovaní magnetických vlastností a tiež pri popise tepelnej kapacity. Opäť sme aj pri tomto type skúmania fyzikálnych vlastností pozorovali správanie podľa závislosti *-ln(T)* a to pre $Ce_{0.9}Gd_{0.1}Ni_5$ zlúčeninu.

Masívne polykryštalické materiály na báze Yb

Príprava vzoriek, ktoré obsahujú Yb, je na rozdiel od iných vzácnozeminových zlúčenín o niečo náročnejšia. Táto komplikácia je spôsobená vysokým tlakom nasýtených pár samotného Yb pri teplote tavenia zlúčeniny a preto je výhodnejšie Yb materiály pripravovať indukčným tavením. Princíp tejto metódy spočíva v tom, že jednotlivé prvky sú zatavené do Ta misky, aby sa predišlo stratám Yb. Tá je potom vložená do skúmavky, ktorá je súčasťou indukčnej pece. Tento spôsob prípravy prebiehal na Univerzite v Janove, Janov, Taliansko. Vzorky boli žíhané.

- $(Yb,Ce,Gd)Ni_5$

Aby sme sa držali prvotnej idey tejto práce, pripravili sme 3 vzorky systému $(Yb,Ce,Gd)Ni_5$, kde sme zamieňali medzi sebou prvok vzácnej zeminy. Štruktúrna analýza opätovne preukázala v majoritnej miere hexagonálnu mriežku typu $CaCu_5$. Niekoľko extra difrakčných maxím bolo pozorovaných pre $YbNi_5$, kde aj skenovacia elektrónová mikroskopia ukázala, že sa vo vzorke nachádza aj Ta. Viac fázovosť sa potvrdila aj pri $Gd_{0.5}Yb_{0.5}Ni_5$, kde sme extra difrakčné maximá nevedeli identifikovať pomocou žiadnych Millerových indexov. Najlepšiu zhodu s fitom sme získali pre $Ce_{0.5}Yb_{0.5}Ni_5$. Skenovacia elektrónová mikroskopia ukázala, že sa nám podarilo pripraviť požadovanú stechiometrickú koncentráciu. Keďže viac fázovosť je vhodná pre magnetokalorické materiály, pre $Yb_{0.5}Gd_{0.5}Ni_5$ sme spočítali magnetokalorický efekt. Pri $Ce_{0.5}Yb_{0.5}Ni_5$ sa ukázalo, že je tu prítomný efekt spinových fluktuácií. Pri veľmi nízkych teplotách sa objavila anomália. Elektrická rezistivita neukázala anomáliu spojenú s prechodom do magneticky usporiadaného stavu a to ani v mK oblasti.

- Yb-Cu-Ni

Jedným z našich cieľov, bolo študovanie vplyvu chemického tlaku na fyzikálne vlastnosti. Pre tento účel boli pripravené vzorky $YbCu_{4.2}Ni_{0.8}$ a $YbCu_{4.7}Ni_{0.3}$. Pri prvej z nich sa pri štúdiu štruktúrnej analýzy ukázalo, že mriežkový parameter *a* je veľmi blízko mriežkového parametra pre $YbCu_4Ni$. Pre druhú vzorku z tejto skupiny bolo nemožné určiť polohu píkov. Dôvodom toho môže byť aj fakt, že sa vo vzorke okrem požadovaných prvkov nachádza aj takmer 7 % oxidu. Vzhľadom k týmto skutočnostiam, sme ďalej podrobili skúmaniu už len materiál $YbCu_{4.2}Ni_{0.8}$. Magnetické merania v teplotnej oblasti od 2 K do 300 K neukázali žiadny prechod do magneticky usporiadaného stavu. Tepelná kapacita meraná v rovnakej teplotnej oblasti tento scenár potvrdzuje. Zaujímavým faktom je to, že závislosť *C/T vs T* v logaritmickej škále ukazuje magnetickým poľom indukované NFL správanie. Sommerfeldov koeficient je vysoký a môžeme teda hovoriť o ťažkofermiónovej zlúčenine. V budúcnosti bude zaujímavé sa tomuto faktu viac venovať a určiť polohu možného kvantového kritického bodu.

- $Yb(Lu,Sc)Cu_4Ni$

Idea prípravy tejto skupiny vzoriek je podobná ako predchádzajúca. Jedným z dôležitých faktov je skutočnosť, že sa Yb zamieňa s Lu, resp. so Sc. Výsledky štruktúrnej analýzy ukázali, že $Yb_{0.8}Sc_{0.2}Cu_4Ni$ je dvojfázová vzorka kubickej a pravdepodobne monoklinickej superštruktúry. Skenovacím elektrónovým mikroskopom sme zistili, že tento materiál obsahuje okrem požadovaných prvkov aj niekoľko percent Ta a oxidov. Z tohto dôvodu sme sa ďalej venovali len vzorke s obsahom Lu. Tu štruktúrna analýza potvrdila kubickú štruktúru a jednofázovosť materiálu. Magnetické merania boli uskutočnené aj pomocou tlakovej komôrky, kde môžeme konštatovať, že chemický tlak súvisí s expanziou mriežky, kým mechanický tlak má súvis so zmenšením mriežky. Merania tepelnej kapacity tejto zlúčeniny ukazujú, že určitá anomália, ktorá by mohla byť spôsobená fázovým prechodom je v oblasti pod 0.4 K. Sommerfeldov koeficient je vysoký a teda $Yb_{0.8}Lu_{0.2}Cu_4$ patrí do skupiny ťažkofermiónových zlúčenín. Elektrická rezistivita a magnetorezistivita ukazuje, že pri nulovom magnetickom poli je viditeľný Kondov efekt.

- $YbPd_2In$

Jedným z najzaujímavejších materiálov, ktorým sme sa v tejto dizertačnej práci venovali je $YbPd_2In$. Štruktúrna analýza priniesla informácie o tom, že táto zlúčenina kryštalizuje v kubickej Heuslerovej mriežke. Magnetické merania v teplotnej oblasti od

2 K do 300 K naznačujú, že by sa pod 2 K mohol nachádzať fázový prechod. Tento fakt bol potvrdený a to meraním na zmiešavacom ^{3}He -^{4}He refrigerátore. Bolo robené aj meranie tepelnej vodivosti, elektrickej rezistivity a magnetorezistivity. Získané výsledky hovoria o tom, že práve $YbPd_2In$ je vhodným kandidátom pre adiabatické demagnetizačné chladenie.

Môj podiel na tejto práci je nasledovný: Pripravila som všetky vzorky s výnimkou $YbPd_2In$. Podieľala som sa na všetkých meraniach okrem meraní na zmiešavacom refrigerátore. Spracovávala som merania a participovala som na vedeckých diskusiách, ktoré boli robené pri interpretácií získaných dát. Taktiež som sa podieľala na príprave už publikovaných článkov a tiež sa podieľam na príprave ďalších článkov, ktoré sú v procese prípravy.

V budúcnosti bude zaujímavé sa sústrediť na odstránenie technických problémov pri príprave kryštalických mikrodrôtov. Jedným z dôležitých faktov bude stanovenie možného kvantového kritického bodu, na ktorého možnú existenciu poukazujú viaceré získané výsledky. Ďalšie experimentálne skúmanie môže priniesť nové poznatky už aj teraz v tak zaujímavom prostredí fyziky kondenzovaných látok, kde skúmanie materiálov na báze vzácnych zemín má svoje neodmysliteľné miesto. Dôležitá je však medzinárodná spolupráca, čoho príkladom je aj táto dizertačná práca.

Resumen en Español

La presente tesis aborda un estudio experimental sobre el comportamiento del estado fundamental en el sistema $RENi_5$ (RE = Ce, Yb, Gd). En este tipo de compuestos de tierras raras, la subred formada por iones de Ni no muestra orden magnético. Esto es debido al hecho de que la banda 3*d* del níquel se encuentra completamente ocupada por electrones, no pudiendo contribuir a un momento magnético espontáneo. A menudo, es en esta clase de materiales en donde aparecen conductas de fermión pesado, en los cuales el factor de Sommerfeld γ tiene un alto valor. Estos sistemas son interesantes debido a sus propiedades excepcionales, como por ejemplo su valencia intermedia, las interacciones de tipo Kondo, los efectos de coherencia o los debidos al desdoblamiento del campo eléctrico cristalino.

El objetivo principal de este trabajo es el estudio experimental del estado fundamental en el sistema $RENi_5$ (RE = Ce, Yb, Gd). Con objeto de cumplir este propósito, hemos dividido el trabajo en las siguientes apartados:

1) Preparación y caracterización estructural de los materiales policristalinos $(RE1_{1-x}RE2_x)Ni_5$ (RE1, RE2 = Ce, Yb, Gd); $YbPd_2In$, $Yb_{0.}Lu_{0.2}Cu_4Ni$, $Yb_{0.8}Sc_{0.2}Cu_4Ni$, $YbCu_{4.7}Ni_{0.3}$ y $YbCu_{4.2}Ni_{0.8.}$
2) Estudio de las propiedades físicas con énfasis en el estudio de la competición entre el efecto de las fluctuaciones de espín y la posible existencia de un punto crítico cuántico.
3) Influencia del tamaño en las propiedades físicas de los compuestos $(RE_{1-x}RE_x)Ni_5$ (RE = Ce, Gd).
4) Influencia de la presión química sobre las propiedades físicas en $Yb_{0.8}Lu_{0.2}Cu_4Ni$, $Yb_{0.8}Sc_{0.2}Cu_4Ni$, $YbCu_{4.7}Ni_{0.3}$ y $YbCu_{4.2}Ni_{0.8}$.
5) Estado fundamental y propiedades de los compuestos de baja temperatura $YbPd_2In$.

El trabajo en sí consta de cinco capítulos. El capítulo primero es teórico, y se dedica a las diversas interacciones, mecanismos y efectos, que juegan un papel importante en el estudio de los sistemas seleccionados. El segundo capítulo describe la motivación por la cual se han estudiado los sistemas elegidos. La siguiente y, por tanto, tercera parte del trabajo se dedica a la descripción detallada de los objetivos establecidos. La cuarta

parte se dedica a los distintos métodos experimentales utilizados. El más extenso es el quinto capítulo, en el que se exploran los resultados obtenidos.

Los elementos de tierras rara, así como sus propiedades químicas son muy similares en su naturaleza debido a su configuración trivalente. No obstante, si reemplazamos el elemento de tierras raras en el compuesto, también es posible cambiar significativamente las propiedades físicas del material. El momento angular orbital se encuentra estrechamente relacionado con el llenado de la capa 4*f* y, el cambio del elemento de tierras raras, influye en él significativamente.

En compuestos intermetálicos, se investiga en particular el origen del magnetismo, que proviene de los electrones localizados en 4*f*. Los lantánidos pueden ser divididos en varios grupos según diversos criterios. Uno de los subgrupos de lantánidos es precisamente el formado por las tierras raras que no exhiben ningún comportamiento magnético. Aquí es posible enumerar: cerio tetravalente (Ce); itrio trivalente (Y), lantano (La), europio (Eu), lutecio (Lu) e Yterbio divalente (Yb). Un hecho interesante, y que puede seguir dando juego en futuras investigaciones de materiales basados en tierras raras, es la posibilidad de intercambio del ion Ce al estado no magnético y del ion Yb al estado magnético, debido a la presión mecánica. En este trabajo, hacemos referencia a compuestos en donde se intercambian los siguientes elementos de tierras raras: Ce/Gd, Ce/Yb, Gd/Yb, Yb/Lu e Yb/Sc. Estos intercambios han sido elegidos debido a las interesantes propiedades físicas esperadas. Por un lado está la supresión del magnetismo en la zona de bajas temperatura por efecto de las fluctuaciones de espín. Por otro, el comportamiento a bajas temperaturas tiene lugar según el modelo del líquido de no Fermi (del inglés *non-Fermi liquid behaviour*, también llamado *NFL behaviour*). La condición previa para la existencia de este estado de NFL es la inestabilidad magnética en T = 0 K, que también puede conducir a la posible existencia de un punto crítico cuántico en los materiales preparados de tierras raras. Un estudio detallado de las propiedades físicas y químicas básicas, ofrece nuevas perspectivas sobre el rápido desarrollo de esta emergente rama de la ciencia. En este sentido, podemos decir que la investigación básica es muy importante en este campo científico.

En base a los objetivos mencionados, los tipos de compuestos estudiados se pueden dividir en los siguientes grupos, los cuales abordamos en este trabajo:

- materiales policristalinos masivos del sistema $Gd_{1-x}Ce_xNi_5$ (donde x = 0; 0.2; 0.5 y 0.8).

- muestras en forma de cintas obtenidas por enfriamiento rápido del sistema $Gd_{1-x}Ce_xNi_5$ (donde x = 0; 0.2; 0.5; 0.8 y 1)
- muestras policristalinas masivas del sistema (Ce, Gd) Ni_5 con muy alto contenido de Ce
- materiales policristalinos masivos basados en Yb.

Materiales policristalinos masivos del sistema $Gd_{1-x}Ce_xNi_5$ (donde x = 0; 0.2; 0.5 y 0.8)

En la primera familia de materiales hemos preparado muestras policristalinas en las que hemos mezclado átomos de Ce y Gd en el sistema de $Gd_{1-x}Ce_xNi_5$ y con las siguientes concentraciones: x = 0, 0.2, 0.5 y 0.8. Los policristales se prepararon mediante soldadura por arco con un peso total para cada muestra de m = 2 g. Las muestras se prepararon en la Universidad de Cantabria, Santander, España.

El análisis mediante rayos X se realizó a temperatura ambiente. Los resultados arrojados indicaron que las 4 muestras cristalizaron en la red hexagonal de tipo $CaCu_5$, en el grupo de espacio *P6/mmm*. El valor de los parámetros *a* y *c* varía ligeramente dependiendo de la concentración, cumpliendo la ley de Vegard. El análisis microestructural confirmó la composición requerida para cada una de las muestras. La preparación de las muestras, así como el análisis estructural, se realizaron en la Universidad de Cantabria, Santander, España.

El siguiente paso en nuestro estudio fue la medición de las propiedades magnéticas y de transporte. Estas mediciones se realizaron con el dispositivo experimental DynaCool en la Universidad de Prešov, en Prešov, Eslovaquia. La dependencia de la imanación con la temperatura mostró que en este conjunto de muestras existe un cambio de fase a un estado magnéticamente ordenado. La temperatura de la transición disminuye gradualmente de la siguiente manera: T_c = 31.8 K para $GdNi_5$, T_c = 24.1 K para $Gd_{0.8}Ce_{0.2}Ni_5$, T_c = 20.9 K para $Gd_{0.5}Ce_{0.5}Ni_5$ y T_c = 5.3 K para $Gd_{0.2}Ce_{0.8}$ Ni_5.

A partir de la inversa de la susceptibilidad magnética y la posterior aplicación de la ley de Curie-Weiss, se determinaron los valores del momento paramagnético efectivo (μ_{eff}) y de la temperatura de Curie (θp). El valor del momento de saturación para cada uno de los compuestos disminuye con el aumento del porcentaje de Ce.

Las medidas del calor especifico muestran el comportamiento clásico propio de la dependencia térmica de un metal. Además, en estas medidas se ha observado un máximo (anomalía lambda) asociado con el establecimiento de un orden magnético. Con el aumento del campo magnético aplicado, este máximo se traslada a un rango de temperatura más alto hasta que un campo de 9 T lo elimina por completo. La capacidad calorífica a alta temperatura se comporta según la ley de Dulong-Petit.

Además de esto, han sido determinadas las contribuciones magnéticas y fonónicas que contribuyen a la capacidad calorífica total. El valor de $S_{mag}(T)$ también se determinó mediante la fórmula: $S_{mag} = \int_0^T \frac{C_{mag}(T)}{T} dT$. Para el $GdNi_5$ este valor es de ~ 17.28 J/mol.K. El coeficiente de Sommerfeld es bajo y por tanto no podemos decir que estos compuestos pertenezcan al grupo de los fermiones pesados.

La resistividad eléctrica y la magnetorresistividad, que se midieron experimentalmente con ayuda del método de las 4 puntas, muestran un comportamiento metálico. Los ordenamientos magnéticos se manifestaron en forma de un pequeño máximo en la resistividad eléctrica. Al igual que con las medidas de el calor especifico, determinamos también la contribución magnética. La magnetorresistividad alcanzó el mayor valor en la temperatura de orden.

En esta familia de compuestos, las concentraciones de Gd son suficientemente altas como para no observar el efecto de las fluctuaciones de espín, que es típico para $CeNi_5$, y hacer que prevalezca el estado magnéticamente ordenado por debajo de una temperatura critica.

Muestras en forma de cintas obtenidas por enfriamiento rápido del sistema $Gd_{1-x}Ce_xNi_5$ (donde x = 0; 0.2; 0.5, 0.8 y 1)

Con el fin de estudiar el efecto de la microestructura sobre las propiedades físicas, fueron preparadas las cintas por el método de fusión rápida sobre un cilindro de cobre de rotación rápida. Las concentraciones en las cintas seleccionadas fueron las mismas que para las muestras masivas. Las cintas fueron preparadas en la Universidad Pavel Jozef Šafárik en Košice, Eslovaquia.

El análisis estructural también mostró que todas las cintas cristalizan en una red hexagonal de tipo $CaCu_5$, en el espacio del grupo *P6/mmm*. Los parámetros de la red

difieren ligeramente de aquellos determinados para muestras masivas. Con ayuda de un microscopio electrónico de barrido con un sistema de electrones retrodispersada, se ha estudiado la concentración relativa de elementos en cada compuesto. Los resultados muestran que, mediante esta forma de preparar la muestra, no tienen una composición estequiométrica completa, observado pequeñas variaciones de ± 2 %.

Las medidas magnéticas, se realizaron siguiendo 2 procedimientos, el enfriamiento con campo (FC) y enfriamiento sin campo (ZFC) tal y como se hizo en muestras masivas. Estas medidas mostraron la evolución de un estado paramagnético a un estado magnéticamente ordenado: T_c = 31.9 K para $GdNi_5$, T_c = 30.1 K para $Gd_{0.8}Ce_{0.2}Ni_5$, T_c = 16.9 K para $Gd_{0.5}Ce_{0.5}Ni_5$ y T_c = 4.7 K para $Gd_{0.2}Ce_{0.8}Ni_5$. Para el $CeNi_5$, no se observa ningún estado magnéticamente ordenado en el intervalo de temperatura de 2 K a 300 K. No obstante, el efecto de las fluctuaciones de espín se manifestó en la imanación, con un máximo en T = 100 K hasta 150 K, e incluso un campo magnético de 1 T no las suprimió. El valor de saturación de la imanación disminuye de nuevo al aumentar el porcentaje de Ce en las muestras examinadas.

El calor especifico, que se midió en el rango de temperatura de 2 K a 300 K, confirmó las transiciones magnéticas en todas las muestras que contenían Gd. No hubo anomalías para la muestra de $CeNi_5$ pura. De igual modo que en las muestras masivas, hemos analizado las diferentes contribuciones del calor especifico. Los valores del coeficiente de Sommerfeld son ligeramente más altos que en las muestras en "bulk", pero aún no manifiestan un comportamiento de fermión pesado. Al aumentar el contenido de Ce, el valor de γ disminuye.

No se realizaron medidas de resistividad eléctrica ni de magnetorresistividad. La razón se debe a que las cintas preparadas de esta manera eran muy frágiles y se rompieron, ya que su manejo era muy difícil.

A partir de los resultados obtenidos del estudio de las cintas, no es posible decir con exactitud qué método de preparación de la muestra es mejor, en concreto qué tipo de preparación del material dado es el que da lugar a mejores propiedades físicas.

Puesto que uno de nuestros objetivos es estudiar la influencia de la microestructura en las propiedades físicas, otro método de preparación de muestras fueron los microhilos, empleando el método Taylor-Ulitovský, donde el núcleo de metal está cubierto con vidrio. A la hora de emplear este método, ha habido problemas técnicos, ya

que el punto de fusión del material es mayor que la temperatura de trabajo del alambre y por esta razón no tuvimos éxito puesto que no fuimos capaces de preparar los microhilos.

Muestras policristalinas masivas del sistema (Ce,Gd)Ni_5 en las proximidades de la desaparición de la transición magnética

El análisis de estas muestras policristalinas, que se prepararon de la misma manera que las muestras masivas mencionadas anteriormente, tubo por objeto el estudiar la desaparición de la fase magnética en el sistema (Ce,Gd)Ni_5.

Mediante el análisis con rayos X, encontramos que incluso este grupo de materiales cristaliza en una red hexagonal tipo $CaCu_5$, con grupo espacial *P6/mmm*. El análisis microestructural mostró que las muestras preparadas tenían la composición estequiométrica deseada.

Las medidas magnéticas mostraron que para el compuesto $Ce_{0.85}Gd_{0.15}Ni_5$ la transición magnética se produce a una temperatura T_c = 4.9 K. Para concentraciones mas altas de Ce: $Ce_{0.9}Gd_{0.1}Ni_5$, $Ce_{0.95}Gd_{0.05}Ni_5$ y $Ce_{0.97}Gd_{0.03}Ni_5$, no se observo un un estado magnéticamente ordenado. Desde el punto de vista de las fluctuaciones de espín, las muestras de $Ce_{0.95}Gd_{0.05}Ni_5$ y $Ce_{0.97}Gd_{0.03}Ni_5$ son las más interesantes, puesto que es donde aparece un máximo en la dependencia de la temperatura de magnetización, típica para este efecto.

El calor específico para concentraciones de $Ce_{0.85}Gd_{0.15}Ni_5$ y $Ce_{0.9}Gd_{0.1}Ni_5$ se midió hasta el rango de mK, en un refrigerador de ^3He. Para la primera concentración mencionada, se confirmó la transición de fase magnética, que se manifestó por la aparición de una anomalía en el calor específico. Con el incremento del campo magnético aplicado, el máximo se traslada a temperaturas más elevadas y va disminuyendo en intensidad. Al aplicar el campo máximo, la anomalía desaparece. En las muestras de $Ce_{0.95}Gd_{0.05}Ni_5$ y $Ce_{0.97}Gd_{0.03}Ni_5$ se observó que no había ninguna transición magnética. El material más interesante en este grupo lo representa la concentración de $Ce_{0.9}Gd_{0.1}Ni_5$, donde la dependencia de *C/T vs T* en la escala logarítmica muestra una dependencia lineal -*ln(T)*, que indica la posible proximidad de un punto crítico cuántico en este compuesto.

Las medidas de la resistividad eléctrica, así como la magnetoresistividad apoyan los resultados anteriores, obtenidos mediante el análisis de propiedades magnéticas y del

calor especifico. En particular, estas mediadas muestran de nuevo un comportamiento logarítmico en la resistividad del tipo -*ln(T)* en el compuesto $Ce_{0.9}Gd_{0.1}Ni_5$.

Materiales policristalinos masivos de base Yb

La preparación de muestras que contengan Yb es, a diferencia de otros compuestos de tierras raras, ligeramente más difícil. Esta dificultad se debe a la alta presión de vapor del Yb en el punto de fusión del elemento. por ello, es más sencillo preparar materiales de Yb por técnicas de fusión por inducción. El principio de este método parte de que los elementos individuales se sellan en un tubo de Ta para evitar pérdidas de Yb. Después, este tubo se inserta en otro tubo de ensayo, que a su vez forma parte del horno de inducción. Este método de preparación tuvo lugar en la Universidad de Génova, Génova, Italia. Posteriormente, las muestras fueron recocidas en un horno.

- $(Yb,Ce,Gd)Ni_5$

En orden a mantenernos fieles a la idea original de este trabajo, hemos preparado 3 muestras del sistema $(Yb,Ce,Gd)Ni_5$, en el que intercambiamos el elemento de tierras raras. El análisis estructural mostró nuevamente una red predominantemente hexagonal del tipo $CaCu_5$. Se observaron varios picos adicionales en el $YbNi_5$, y el microscopio electrónico de barrido mostró que también había Ta presente en la muestras. En el $Gd_{0.5}Yb_{0.5}Ni_5$ se observaron fases adicionales que no pudimos identificar mediante los índices de Miller. El mejor ajuste lo conseguimos para $Ce_{0.5}Yb_{0.5}Ni_5$. El escaneado por microscopia electrónica mostró que logramos preparar la muestra con la estequiométrica requerida. Dado que los materiales multifásicos pueden ser adecuados como materiales magnetocalóricos, en el $Yb_{0.5}Gd_{0.5}Ni_5$ calculamos el efecto magnetocalórico. Se ha observado que en el $Ce_{0.5}Yb_{0.5}Ni_5$ existen fluctuaciones de espín. En el calor especifico se observo un máximo a temperaturas muy bajas, sin embargo, la resistividad eléctrica no mostró ninguna anomalía asociada con la transición a un estado magnéticamente ordenado, ni siquiera en la región mK.

- Yb-Cu-Ni

Uno de nuestros objetivos fue estudiar el efecto de la presión química en las propiedades físicas. Con este propósito, se prepararon muestras de $YbCu_{4.2}Ni_{0.8}$ y $YbCu_{4.7}Ni_{0.3}$. En la primera de ellas, el estudio del análisis estructural mostró que el parámetro de red *a* es muy cercano al parámetro de red para $YbCu_4Ni$. Para la segunda muestra de este grupo, fue imposible determinar la posición de los picos. La razón puede

deberse al hecho de que, además de los elementos esperados, la muestra también contiene casi el 7 % de óxido. Debido a esto, examinamos más a fondo solo el material $YbCu_{4.2}Ni_{0.8}$. Las medidas magnéticas en el rango de temperatura de 2 K a 300 K no mostraron ninguna transición a un estado magnéticamente ordenado. La capacidad calorífica, medida en el mismo rango de temperatura, confirma este escenario. Un hecho interesante es que la dependencia de *C/T vs T* en la escala logarítmica muestra el comportamiento de NFL inducido por el campo magnético. El coeficiente de Sommerfeld es alto y, por tanto, podemos hablar de un compuesto tipo fermión pesado. En el futuro, será interesante prestar más atención a este hecho y tratar de encontrar un posible punto crítico cuántico.

- $Yb(Lu,Sc)Cu_4Ni$

La idea de preparar este grupo de muestras es similar a la anterior. En este caso, lo importante es la sustitución del Yb por Lu y Sc. Los resultados del análisis estructural mostraron que $Yb_{0.8}Sc_{0.2}Cu_4Ni$ es una muestra bifásica formada por una red cúbica y otra probablemente monoclínica. Por medio de microscopía electrónica de barrido, encontramos que este material contenía, además de los elementos requeridos, también un pequeño porcentaje de Ta y de óxidos. Por esta razón, hemos continuado enfocándonos solo en la muestra que contiene Lu. En la misma, el análisis estructural confirmó que el material es monofásico con una estructura cúbica. Las medidas magnéticas se realizaron con la ayuda de una celda de presión. Esta produce una presión mecánica que origina una contracción de la red, al contrario de la presión química que puede producir una expansión. Las medidas de la capacidad térmica de este compuesto muestran que una cierta anomalía, que podría ser causada por una posible transición que tendría lugar en la región por debajo de 0.4 K. El coeficiente de Sommerfeld es grande y, por lo tanto, el $Yb_{0.8}Sc_{0.2}Cu_4$ pertenece al grupo de compuestos de los fermiones pesados. La resistividad eléctrica y la magnetoresistividad muestran que el efecto Kondo es visible en ausencia de campo magnético.

- $YbPd_2In$

Uno de los materiales más interesantes que hemos tratado en esta tesis es el $YbPd_2In$. El análisis estructural mostró que este compuesto cristaliza en una red cúbica tipo Heusler. Las medidas magnéticas en el rango de temperatura de 2 K a 300 K muestran que la transición magnética podría estar por debajo de 2 K. Este hecho fue confirmado por medidas en un refrigerador ^3He-^4He. También se realizaron medidas de

conductividad térmica, de resistividad eléctrica y de magnetoresistividad. Los resultados obtenidos muestran que $YbPd_2In$ es un candidato adecuado para el enfriamiento por desmagnetización adiabática.

Mi contribución en este trabajo es la siguiente: he preparado todas las muestras a excepción de $YbPd_2In$. He participado en todas las medidas excepto en las realizadas con el criostáto de dilución. He procesado las medidas y he participado en las discusiones científicas que se realizaron para la interpretación de los datos obtenidos. También he participado en la preparación de artículos ya publicados, así como también en la preparación de otros artículos que se encuentran en proceso de elaboración.

En el futuro, será interesante concentrarse en la eliminación de los problemas técnicos surgidos en la preparación de los microhilos cristalinos. Uno de los hechos más importantes será la determinación de un posible punto crítico cuántico, cuya existencia ha sido indicada por varios de los resultados obtenidos. Futuro trabajo experimental podrá aportar nuevos conocimientos en un campo tan interesante como la física de materia condensada, en donde el estudio de materiales basados en tierras raras ocupa un lugar destacado. Además, es necesario reseñar que la cooperación internacional es importante, como lo demuestra la presente memoria.

REFERENCES

[1] G. R. Stewart, *Rev. Mod. Phys*. 56, 711 (1997)

[2] M. B. Maple, *Journal of Magnetism and Magnetic Materials* **177-181**, 18 (1998)

[3] Q. Si, F. Steglich, *Science* **329**, 1161 (2010)

[4] G. R. Stewart, *Rev. Mod. Phys.* **73**, 797 (2001)

[5] N. Ashcroft and N. Mermin, Solid State Physics, HRW, international editions (Holr, Rinehart and Winston, NY, 1976). ISBN: 978-0-03-083993-1

[6] G. Grimwall: *The Electron-Phonon Interaction in Metals* (Elsevier North-Holland; 1st edition, 1981). ISBN: 978-0-44-486105-4

[7] D. Pines and P. Nozieres: *The Theory of Quantum Liquids* (Vol. 1, Normal Fermi-liquid, Addison-Wesley, MA 1987). ISBN: 978-0-20-140774-7

[8] J. Spalek: *Liquids, Theory of: Fermi Liquids*. In: Saleem Hashmi (editor-in-chief), Reference Module in Materials Science and Materials Engineering. Oxford: Elsevier; 2016. pp. 1-20. ISBN: 978-0-12-803581-8

[9] H. von Löhneysen, *J. Phys, Condens Matter* **8**, 9689 (1996)

[10] H. von Löhneysen, A. Rosch, M. Vojta and P. Wolfe, *Rev. Mod. Phys* **79**, 1015 (2007)

[11] K. Kadowaki et al., *Solid State Communication* **58**, 507 (1986)

[12] P. Fulde: *Crystal fields*. In: Handbook on the Physics and Chemistry of Rare Earths ". Chapter 17. Volume 2. Eds. K.A. Gschneidner, L. Eyring (North Holland – Amsterdam 1978) ISBN: 444-85021-X

[13] H. A. Bethe *Ann. Phys.* **3**, 133 (1929)

[14] K. W. H. Stevens, *Proc. Phys. Soc.* **A65**, 209 (1952)

[15] B. R. Judd, *Proc. R. Soc. A* **232**, 458 (1955)

[16] G. M. Dieke: *Spectra and Energy Levels of Rare Earth Ions in Crystal* (Interscience Publishers Inc. New York, 1968)

[17] B. Barbara, D. Gignoux, C. Vettier, *Lectures on Modern Magnetism* (Science Press Beijing and Springer-Verlag Berlin Heidelberg 1988)

[18] K. Taylor, M. Darby, *Fizika redkozemel'nych sojedinenij* (Nauka - Moskva 1974)

[19] M. T. Hutchings, *Solid State Phys.* **16**, 227 (1964)

[20] W. U. S. Rao, W. E. Wallace, *Phys. Rev.* **B2**, 4613 (1970)

[21] I. Frankowski, P. Wachter, *Solid State Commun.* **41**, 577 (1982)

[22] K. H. T. Barron, K. G. White, *Heat Capacity and Thermal Expansion at Low Temperatures* (New York: Kluwer Academy - Plenum Publisher – 1999)

[23] K. Taylor, M. Darby, *Physics of Rare Earth Solids* (London 1972)

[24] M. A. Ruderman, Ch. Kittel, *Phys. Rev.* **96**, 99 (1954)

[25] T. Kasuya, *Prog. Theor. Phys.* **16**, 45 (1956)

[26] K. Yosida, *Phys. Rev.* **106**, 893 (1957)

[27] Ch. Kittel, *Indirect exchange interactions in metals* (New York 1968)

[28] S. Süllow, M. C. Aronsom, B. D. Rainford, P. Haen, *Phys. Rev. Lett.* **82**, 2963 (1999)

[29] B. Andraka, R. G. Stewart, *Phys. Rev. B* **6**, 3208 (1993)

[30] E. C. Stoner, *Proc. Roy. Soc.* **A154**, 656 (1936)

[31] E. P. Wohlfarth, *Phil. Mag.* **42**, 374 (1951)

[32] M. Shimizu, *Proc. Phys. Soc.* **86**, 147 (1965)

[33] E. P. Wohlfarth, P. Rhodes *Phil. Mag.* **7**, 1817 (1962)

[34] B. Coqblin, J. R. Iglesias-Sicardi, R. Julien, *Contemp. Phys.* **19**, 327 (1978)

[35] T. Izuyama, D. J. Kim, K. Kubo, *J. Phys. Soc. Japan* **18**, 1025 (1963)

[36] K. Sköld, C. A. Pelizari, P. Kleb, G. E. Ostrowski, *Phys. Rev. Lett.* **37**, 842**,** 84 (1976)

[37] A. B. Kaiser, S. Doniach, *Internat. J. Magn.* **1**, 11 (1970)

[38] D. Gignoux, F. Givord, R. Lemaire, H. Launois, F. Sayetat, *J. de Phys.* **43**, 173 (1982)

[39] W. F. Brikman, S. Engelsberg, *Phys. Rev.* **169**, 417 (1968) 417

[40] M. T. Beál-Monod, S. K. Ma, D. R. Fredklin, *Phys. Rev. Lett.* **20**, 929 (1968)

[41] B. Andraka, G. R. Stewart, *Phys. Rev.* **B6**, 3208 (1993)

[42] V. H. Tran, *J. Alloys and Compounds* **383**, 281 (2004)

[43] Ch. Ye, W. Zongfa, M. Smidman, L. Xin, Y. Huiqiu, *Chinese Physics B* **25**, 7, 077401 (2016)

[44] D. Britz, *Dissertation thesis*, Johanesburg (2015)

[45] M. Vojta, *Rep. Prog. Phys* **66**, 2069 (2003)

[46] P. Gegenwart et al., *Nature Physics* 4, 186 (2008)

[47] Focus Issue: "Quantum Phase Transitions", *Nature Physics* **4**, 167 (2008)

[48] T. Senthil, M. Vojta, S. Sachdev, *Phys. Rev. B* 69, 035111 (2004)

[49] Q. Si et al., *Nature* **413**, 804 (2001)

[50] D. Giuliano et al., *Eur. Phys. Lett.* **58**, 401 (2002)

[51] S. Horiuchi et al., *Science* **299**, 229 (2003)

[52] S. Sachdev: *Quantum Phase Transitions*, Cambridge Univ. Press, Cambridge (1999)

[53] H. von Löhneysen, *J. Magn. Magn. Mat.* **200**, 532 (1999)

[54] A. J. Milis, *Phys. Rev. B* **48**, 7183 (1993)

[55] J. A. Hertz, *Phys. Rev. B* **14**, 1165 (1976)

[56] T. Moriya, T. Takimoto, *J. Phys. Soc. Jpn.* **64**, 960 (1995)

[57] C. Pfleiderer, G. J. McMullan, S. R. Julian, G. G. Lonzarich, *Phys. Rev. B* 55, 8330 (1997)

[58] P. Coleman et al., *J. Phys: Cond. Mat.* **13**, R723 (2001)

[59] Q. Si et al., *Nature* **413**, 804 (2002)

[60] G. Wiesinger et al., *Physica B **206 & 207***, 261-263 (1995)

[61] E. Bauer et al., *Phys. Rev. B* **56**, 711 (1997)

[62] J. J. Rhyne, T. R. McGuire, *IEEE Transactions on Magnetics* **8** (1972)

[63] R. J. Elliot, Ed., Magnetic Properties of Rare – Earth Metals (Plenum Press, New York 1972)

[64] Š. Jánoš, *Dissertation Thesis* (*in Slovak)*, PF UPJŠ Košice (1974)

[65] A. Džubinská, *Diploma thesis* (*in Slovak*), FHPV UNIPO, Prešov (2016)

[66] D. Gignoux, J. C. Goméz Sal, *J. Appl. Phys.* **57**, 3125 (1985)

[67] D. Gignoux et. al, *J. de Phys.* **173,** 43 (1983)

[68] K. H. J. Buschow, M. Brouha, H. J. van Daal, H. R. Miedema*, in "Valence instabilities and related narrow bands phenomena"* (Rochester 1977)

[69] K. R. Buchspisess et. al, *Valence Fluctuations in Solids* (North Holland, Amsterdam 1981)

[70] J. H. Wernick, S. Geller, *Acta cryst.* **12**, 662 (1959) 662

[71] D. Gignoux, F. Givord, R. Lemaire, F. Tasset, *J. de Phys.* **C7**, 252 (1982)

[72] L. Nordstrom, M. S. S. Brooks, B. Johansson, *Phys. Rev. B* **46**, 3458 (1992)

[73] S. Nasu, et. al, *J. Phys. Chem. Solids* **52** 2779 − 2783 (1971)

[74] Y. Naidyuk et. al., *Intern. J. of Mod. Phys.* **B7** 222 – 225 (1993) 222 − 225

[75] J. Hodges et. al., *European Physical Journal B* **57**, 4, 365 – 370 (2007)

[76] E. Burzo, I. Ursu, *Sol. State Commun.* **9**, 2289 − 2292 (1971)

[77] A. Szewczyk et. al., *J. of Magnetism and Magn. Mat.* **104-107,** 1319 − 1320 (1992)

[78] P. C. Riedi, *Solid State Commun.* **27,** 673 − 675 (1978)

[79] F. Kayzel, *Magnetic and Thermodynamic Properties of* RNi_5, Amsterdam (1997). ISBN 90-74795-69-2

[80] A. Amato et. al., *Solid State Commun.* **82**, 767 - 771 (1992)

[81] P. Svoboda et. al, *J. of Magnetism and Magn. Mat.* **272-276**, 595 − 596 (2004)

[82] R. A. Monef, *J. of Kirkuk University* **2**, 70 − 77 (2007)

[83] A. Bajorek, G. Chełkowska, A. Chrobak, *Intermetallics* **32**, 384 − 393 (2013)

[84] D. Gignoux, F. Givord, R. Lemaire, *J. Less Common Metals* **94**, 1 − 15 (1983)

[85] E. Burzo et. al, *J. of Physics Cond. Matter* **18**, 4861− 4877 (2006)

[86] A. Iandelli, A. Palenzona, *J. Less Common Metals* **25,** 133 (1971)

[87] J. He et al., *J. Alloys Compounds* **240**, 261 (1996)

[88] N. Tsujii et. al, *Phys. Rev. B* **56**, 8103 (1997)

[89] M. Reiffers et. al., *Physica B* **738**, 378-380 (2006)

[90] P. Carreta et al., *Phys. Rev. B* **79**, 020401 (2009)

[91] H. Yamaoka et al., *Phys. Rev. B* **80**, 035129 (2009)

[92] H. Yamaoka et al., *Scientific Reports* **7**, 5846 (2017)

[93] I. Curlik et al., *17th Conference of Czech and Slovak Physicists*, Proceedings 95 – 96 (2011). ISBN: 978-809706254-5

[94] I. Curlik et al., *Acta Physica Polonica A* **122**, 1, 3 – 5 (2012)

[95] J. Sereni et al., *Phys. Rev. B* **98**, 9 (2018)

[96] C. Rossel, K. N. Yang, and M. B. Maple *Phys. Rev. B* **35**, 4 (1987)

[97] M. Giovannini, R. Pasero, S. De Negri, A. Saccone, *Intermetallics* **16**, 399 (2008)

[98] A. Iandelli, A. Palenzona, *Rev. Chim. Miner.*, **101**, 303 (1973)

[99] H. Okamoto, *J. Phase Equilibria*, **14**, 770 – 771 (1993)

[100] K. Takao et al., *J. Alloys Compd.*, **193**, 131, 4 (1993)

[101] H. Okamoto, T.B Massalski, *Monogr. Ser. Alloy Phase Diagrams, ASM Int. Mater. Park. Ohio*, **142**, (1992)

[102] J. Knigh, D. Rhys, *J. Less-Common Met.*, **1**, 292 (1959)

[103] A. Palenzona, S. Cirafici, *J. Phase Equilibria*, **10**, 588 – 592 (1989)

[104] O. D. McMasters, *J. Less-Common Met.*, **23**, 253 – 262 (1971)

[105] P. Villars, K. Cenzual, *Materials Park*, O.P. crystal data R. 2016/17 A.I. (2016)

[106] M. Giovannini, E. Bauer, H. Michor, G. Hilscher, *Intermetallics*, ***9***, 481 – 485, (2001)

[107] K. Katoh et al., *J. Alloys Compd.*, **360**, 225 – 230 (2003)

[108] E. Bauer et al., *Acta Phys. Pol. B*, **34**, 367 – 370, (2003)

[109] V. I. Zaremba et al., *Solid State Sci.*, **4**, 1293–1298, (2002)

[110] Y. Galadzhun et al., *Eur. J. Inorg. Chem.*, 975 – 979, (1999)

[111] R. Hoffmann et al., *Naturforsch. B*, **55**, 834 – 840, (2000)

[112] A. Džubinská, *Diploma Thesis*, FHPV UNIPO, Prešov (2018)

[113] Compact Arc Melter MAM-1, [online] [cit. 17.03.2020] available from: https://www.edmund-buehler.de/en/materials-science/arc-melting/compact-arc-melter-mam-1/

[114] Melt Spinner SC, [online] [cit. 17.03.2020] available from: https://www.edmund-buehler.de/en/materials-science/melt-spinning/melt- spinner-sc/

[115] B. D. Cullity, The e*lements of X-Ray Diffraction* (Reading, Massachusetts: Addison Wesley, 1978)

[116] P. Sovák, M. Dománková, Ľ. Čaplovič, J. Janovec, *Vybrané moderné metódy štruktúrnej analýzy kovov (in Slovak)*. Košice: Univerzita Pavla Jozefa Šafárika v Košiciach, 2007. ISBN 978-8-07-097685-2

[117] J. Rodriguez-Carvajal, *Physica B* **55**, 192 (1993)

[118] A. Plecenik, M. Zahoran, *Rastrovacia elektrónová a sondova mikroskopia (in Slovak)*. [online] [cit. 23.03.2020] available from: www.mikroskopia.sk/materials/SKRIPTA_SEM_a_SPM.doc

[119] R. Kelsall, I. W. Hamley and M. Geoghegan, *Nanoscale science and technology*. (John Wiley & Sons, 2005)

[120] Physical Property Measurement System, DynaCool^{TM} User's Manual, Part Number 1307-110, A0 [online] [cit. 23.03.2020] available from: https://www.mrfn.org/sites/mrfn.org/files/instrument/DynaCool_Manual_A0.pdf

[121] Vibrating Sample Magnetometer (VSM) Option User's Manual, Part Number 1096-100, B0 [online] [cit. 24.03.2020] available from: https://web.njit.edu/~tyson/PPMS_Documents/PPMS_Manual/1096-100%20Rev.%20A3%20VSM.pdf

[122] I. Čurlik, *Dissertation Thesis* (*in Slovak*), PF UPJŠ Košice (2012)

[123] Physical Property Measurement System, Heat Capacity Option User's Manual Part Number 1085-150, Rev. L3 [online] [cit. 24.03.2020] available from: https://web.njit.edu/~tyson/PPMS_Documents/PPMS_Manual/1085-150%20Heat%20Capacity.pdf

[124] Physical Property Measurement System Resistivity Option User's Manual Part Number 1076-100A [online] [cit. 24.03.2020] available from: https://web.njit.edu/~tyson/PPMS_Documents/PPMS_Manual/1076-100%20Rev.%20A0%20Resistivity.pdf

[125] Physical Property Measurement System Thermal Transport Option User's Manual Part Number 1684-100B [online] [cit. 25.03.2020] available from: https://web.njit.edu/~tyson/PPMS_Documents/PPMS_Manual/1684-100%20Rev.%20B0%20TTO.pdf

[126] P. Marcon and K. Ostanina, PIERS Proceedings, Kuala Lumpur, MALAYSIA 420 – 424 (2012)

[127] C. Echevaria, *Dissertation Thesis,* CITIMAC Unican Santander (2014)

[128] EasyLab Mcell 10, [online] [cit. 27.03.2020] available from: https://www.almax- easylab.com/ProductDetails.aspx?PID=79

[129] Physical Property Measurement System, User's Manual (Quantum Design – USA) (2015)

[130] Š. Jánoš, *Fyzika nízkych teplôt* (*in Slovak*) (SPN, Bratislava, 1979)

[131] Cryo-free regriferator Oxford, [online] [cit. 29.3.2020] available from: https://wwwnew.saske.sk/uef-intranet-old/files/Infrastructure/ssp/triton.JPG

[132] L. Vegard; Zeitschrift für Physik **5**, 17 (1921)

[133] A. Dzubinska et. al., *Acta Physica Polonica A* **131**, no 4 part 2, 997 – 999 (2017)

[134] V. M. T. S. Barthem et. al, *Phys. Rev. B* **37**, 1733 (1988)

[135] D. Gignoux, D. Givord, A. Del Moral,Solid State Commun. **19**, 891 (1976)

[136] A. Bajorek, G. Chelkowska, B. Andrzejewski, *J. Alloys Comp.* **509**, 578 (2011)

[137] S. Raaen, R. D. Parks, *Solid State Commun.* **48**, 2 (1983)

[138] N. Marcano et al., *Phys. Rev.* B **71**, 134401 (2005)

[139] M. Reiffers et al., *Physica Status Solidi B* **13**, 13679993 (1982)

[140] H. Yamada, S. Takada, *Progress of Theoret. Phys.* **48**, 6A (1972)

[141] R. Varga, *Scripta Materialia* **65**, 8 (2011)

[142] P. Ibarra-Gaytán *J. Alloys and Compounds* **786**, 65 – 70 (2019)

[143] L. Frolova et al., *J. Alloys and Compounds* **747**, 21 – 25 (2018)

[144] J. García Soldevilla et al., *J. Magn. Magn. Mat.* **157/158,** 624 – 626 (1996)

[145] W. E. Wallace et al., *International Colloquium of the French National Center of Scientific Research*, **2**, 427, CNRS Paris (1970)

[146] M. Reiffers et al., *J. Magn. Magn. Mat.* **272-276**, 605 – 607 (2004)

[147] M. Zapotokova et al., *European Physical Journal B*, **86**, 4 (2013)

[148] J. Tang et al., *J. Alloys and Compounds* **207/208**, 241 (1994)

[149] O. Musil et al., *J. Phys.* **54,** D311 (2004)

[150] M. Coldea et al., *J. Magn. Magn. Mat.* **157**, 627 (1996)

[151] L. Galdun, *Dissertation Thesis* UPJŠ and Universidad de Oviedo (2018)

[152] K. Ikeda et al., *J. Magn. Magn. Mat.* **100**, 292 – 321 (1991)

[153] J. Lawrence, *Mod. Phys. Lett. B* **22,** 1273 – 1295 (2008)

[154] A. Dzubinska et al., *Acta Physica Polonica A,* **137** (2020) in press

[155] C. E. Haberman: *Vapor Pressure of the Rare Earth Metals* (Iowa State University, 1963) [online] [cit. 05.04.2020] available from: https://lib.dr.iastate.edu/cgi/viewcontent.cgi?article=3533&context=rtd

[156] T. P. Rashid et al., *J. Applied Phys.* **122**, 093903 (2017)

[157] E. Bauer – private communication (2019)

[158] F. Gastaldo, S. Gabani, A. Dzubinska et al., *Phys. Rev. B* **100**, 174422 (2019)

[159] T. Gruner et al., *J. Phys. Cond. Matt* **26**, 485002 (2014)

[160] J. G. Sereni, *J. Low. Temp. Phys.* **179**, 126 (2015)

[161] V. Correa et al., *J. Phys. Cond. Matt* **28**, 346003 (2016)

[162] J. G. Sereni, *Philos. Mag.* **100**, 1211 – 1225 (2020)

[163] M. Babaten et al., *Physica B* **213 – 214**, 300 (1995)

[164] J. G. Sereni, *Philos. Mag.* **93**, 409 (2013)

[165] M. Jaime et al., *Phys. Rev. Lett.* **89**, 287201 (2002)

[166] T. D. Matsuda et al., *Physica B* **281 – 282***,* 220 (2000)

[167] J. G. Sereni et al., *Phys. Rev. B* **85,** 134404 (2012)

List of Publications

List of published CC articles related to this thesis:

[1] A. Dzubinska, M. Reiffers, J. I. Espeso, J. R. Fernandez: Magnetic and Heat Capacity Study of the new $Gd_{1-x}Ce_xNi_5$ Series, *Acta Physica Polonica A* **131**, 994 – 999 (2017).

[2] F. Gastaldo, S. Gabáni, **A. Džubinská**, M. Reiffers, G. Pristáš, I. Curlík, P. Skyba, M. Clovecko, F. Vavrek, J. G. Sereni, M. Giovannini: $YbPd_2In$: A promising candidate for strong entropy accumulation at very low temperature, *Phys. Rev. B* **100**, 174422 (2019).

[3] A. Dzubinska, J. R. Fernandez, M. Reiffers, J. I. Espeso, J. C. Gomez Sal: Disappearance of Magnetic Transition in (Ce,Gd)Ni_5 System, *Acta Physica Polonica A* **137**, (2020) in press

In preparation preparation process:

- **A. Dzubinska**, J. R. Fernandez, M. Reiffers, J. I. Espeso[2], R. Varga, K. Arun, J. C. Goméz Sal: "Influence of microcrystalline structure on competition between 4*f* rare earth magnetism and spin fluctuations in (Gd,Ce)Ni_5 intermetallic system"

List of results presented at conferences workshops:

→ 05. 09. – 08. 09. 2016 22th conference of Slovak physicists (Košice, Slovakia) - Physical properties of polycrystalline $Ce_{1-x}Gd_xNi_5$ system; ORAL

→ 17. 07. – 21. 07. 2017 Join European Magnetic Symposia (Prague, Czech Republic) – Heat capacity and transport properties of the novel $Gd_{1-x}Ce_xNi_5$ system; POSTER

→ 17. 07. – 21. 07. 2017 Join European Magnetic Symposia (Prague, Czech Republic) – Low temperature anomaly of heat capacity in the novel $YbPd_2In$ indide; POSTER

→ 04. 09. – 07. 09. 2017 19th conference of Czech and Slovak physicist (Prešov, Slovakia) – Preparation and characterization of Gd-Ce-Ni system; ORAL

→ 17. 09. – 20. 09. 2017 Magnetic measurements (Prague, Czech Republic) – Study of magnetic properties in ternary system Ce-Gd-Ni; POSTER

→ 09. 10. – 21.10. 2017 European School on Magnetism (Cargèse, France) - Experimental study of high magnetic field influecne on ground state in Ce-Gd-Ni system; POSTER

→ 04. 07. – 07. 07. 2018 12th Colloquium on *f* – electron Systems (Prague, Czech Republic) – The physical properties study of system based on Ce and Gd; ORAL

→ 05. 09. – 08. 09. 2018 23th conference of Slovak physicists (Smolenice, Slovakia) – The physical properties study of intermetallic system based on rare earths Ce and Gd; ORAL

→ 05. 09. – 08. 09. 2018 23th conference of Slovak physicists (Smolenice, Slovakia) – Low temperature properties of novel material $YbPd_2In$; ORAL

→ 26. 08. – 30. 08. 2019 Join European Magnetic Symposia (Uppsala, Sweden) – Spin fluctuations in $(Ce_{0.5}Yb_{0.5})Ni_5$ intermetallic system; POSTER

→ 02. 09. – 05. 09. 2019 24th conference of Slovak physicists (Žilina, Slovakia) - Experimental study of the rare earth magnetism in $(Yb/Ce)Ni_5$ compounds; ORAL

→ 13. 10. – 18.10. 2019 FERMI – SCES (Les Houches, France) – The competition of magnetic ordering and effect of spin fluctuations in $RENi_5$ (RE – Gd, Ce, Yb); POSTER

Another CC publication with number of citations, which were published during PhD. study:

[1] T. P. Rashid, K. Arun, I. Curlik, S. Ilkovic, M. Reiffers, **A. Dzubinska**, R. Nagalakshmi: Effect of spin fluctuations in magnetocaloric and magnetoresistance properties of $Dy_{10}Co_{20}Si_{70}$ alloy, *Journal of Applied Physics* **122,** 093903 (2017).

citation: [1] H. Bouhani et al.: Magnetocaloric effect in ternary ErAgAl: Ab initio, mean field and Monte Carlo approaches, *Results in Physics* **10**, 849 – 845 (2018).

citation: [2] Y. Jia et al.: Magnetic anisotropy and large low field rotating magnetocaloric effect in NdGa single crystal, *Journal of Alloys and Compounds* **757**, 44 – 48 (2018).

[2] S. Nallamuthu, **A. Džubinská**, M. Reiffers, J. R. Fernandez, R. Nagalakshmi: Ferromagnetism in orthorhombic $RAgAl_3$ (R = Ce and Pr) compounds, *Physica B* **521**, 128 – 133 (2017).

citation: [1] S. Seidel et al.: SrPdGa3 type gallides $RERhGa_3$ with RE = La, Ce and Pr, *Zeitschrift fur Kristallographie-Crystalline Materials* **235**, 3 (2020).

[3] S. Nallamuthu, **A. Džubinská**, M. Reiffers, R. Nagalakshmi: Low Temperature Magnetic Ordering in $NdAgAl_3$, *Acta Physica Polonica A* **131**, 1015 – 1017 (2017).

[4] T. P. Rashid, K. Arun, I. Curlik, S. Ilkovic, M. Reiffers, **A. Dzubinska**, R. Nagalakshmi: Influence of spin fluctuations on the magnetocaloric behavior of $Gd_2Co_3Al_9$ compound, *Journal of Magnetism and Magnetic Materials* **466**, 283 – 288 (2018).

citation: [1] S. Pakhira et al.: Magnetic and magnetocaloric properties of $(Gd_{1-x}Y_x)_{(2)}NiSi_3$ compounds (x = 0.25, 0.5, 0.75) *Journal of Magnetism and Magnetic Materials* **484**, 456 – 461 (2019).

citation: [2] S. Pakhira et al.: Magnetocaloric properties of cluster glass compound $Pr_{(2)}Ni_{(0.95)}Si_{2.95}$, *Interletallics* **111**, 106490 (2019).

citation: [3] L. Li et al.: Recent progresses in exploring the rare earth based intermetallic compounds for cryogenic magnetic refrigeration, *Journal of Alloys and Compounds* **823**, 153810 (2020).

[5] L. Frolova, T. Ryba, P. Diko, V. Kavecansky, O. Milkovic, **A. Dzubinska**, M. Reiffers, Z. Vargova, R. Varga: Smart Shape Memory Actuator Based on Monocrystalline Ni_2FeGa Glass-Coated Microwire, *IEEE Transactions on Magnetics* **54**, 1 – 5 (2018).

[6] L. Frolova, J. Mino, T. Ryba, J. Gamcova, **A. Dzubinska**, M. Reiffers, P. Diko, V. Kavecansky, J. Kravcak, O. Milkovic, Z. Vargova, R. Varga: Novel compositions of Heusler-based glass-coated microwires for practical applications using shape memory effect, *Journal of Alloys and Compounds* **747**, 21 – 25 (2018).

citation: [1] G. Gurau et al.: Structural change in Ni-Fe-Ga magnetic shape memory alloys after severe plastic deformation, *Materials* **12**, 1939 (2019).

citation: [2] D. Peng et al.: Research progress in electroactive polymer materials, *Modern Chemical Industry* **39**, 22 – 26 (2019).

citation: [3] A. Amiror et al.: Multiferroic polymer composite based on Heusler-type magnetic microwires with combined magnetocaloric and magnetoelectric effects, *Journal of Magnetism and Magnetic Materials [online]* ***510****, (2020).*

[7] M. Bouhbou, R. Moubah, **A. Dzubinska**, M. Reiffers, V. Tuyikeze, A. Natik, F. Fraija, H. Lassri: Magnetic, magnetocaloric and critical exponent properties of amorphous $Fe_{67}Y_{33}$ ribbons prepared by melt-spinning technique, *Physica A* **534**, 1 – 9 (2019).

[8] K. Arun, T. P. Rashid, I. Curlik, S. Ilkovic, M. Reiffers, **A. Dzubinska**, R. Nagalakshmi: Magnetism, magnetocaloric and magnetotransport properties of Dy_5NiSi_2 alloy, *Applied Physics A* **125**, 1 – 7 (2019).

[9] K. Arun, T. P. Rashid, I. Curlik, S. Ilkovic, M. Reiffers, **A. Dzubinska**, R. Nagalakshmi: Metamagnetism, Multiple Magnetic Transitions and Wide Temperature Range Magnetocaloric Effect in $Dy_{6.5}Co_2Si_{2.5}$ Alloy, *Journal of Superconductivity and Novel Magnetism* **32**, 1407 – 1414 (2019).

[10] S. Swathi, K. Arun, **A. Dzubinska,** M. Reiffers, R. Nagalakshmi: Systematic investigations on the magnetic properties of moderate heavy Fermion $CeAg_{0.68}Si_{1.32}$ alloy, *Physica B* **575**, 1 – 8 (2019).

[11] K. Arun, S. Swathi, U. D. Remya, **A. Dzubinska,** M. Reiffers, R. Nagalakshmi: Evaluation of critical exponents and magnetocaloric properties in moderate heavy fermion $Mn_{4.5}Ni_{0.5}Sn_3$ alloy, *Journal of Applied Physics* **127**, 1 – 11 (2020).

[12] G. Lamura, I. J. Onuorah, P. Bonfà, S. Sanna, Z. Shermadini, R. Khasanov, J. C. Orain, C. Baines, F. Gastaldo, M. Giovannini, I. Curlík, **A. Dzubinska**, G. Pristas, M. Reiffers, A. Martinelli, C. Ritter, B. Joseph, E. Bauer, R. De Renzi, T. Shiroka: Pressure-induced antiferromagnetic dome in the heavy-fermion $Yb_2Pd_2In_{1-x}Sn_x$ system, *Phys. Rev. B* **101**, 054410 (2020).

[13] K. Arun, T. P. Rashid, M. Reiffers, **A. Dzubinska**, R. Nagalakshmi: Systematic investigations on the magnetic properties of $Gd_3Ni_2In_4$ compound, *Current Applied Physics* **20**, 266 – 271 (2020).